

GAS MIXING IN BEDS OF
FLUIDIZED SOLIDS

by

EDWARD ARCHIBALD MASON

B.S., University of Rochester
(1945)

M.S. in Chemical Engineering Practice
Massachusetts Institute of Technology
(1948)

SUBMITTED IN PARTIAL FULFILLMENT OF THE
REQUIREMENTS FOR THE DEGREE OF
DOCTOR OF SCIENCE

at the

MASSACHUSETTS INSTITUTE OF TECHNOLOGY
(1950)

Signature of Author
Department of Chemical Engineering, May 12, 1950

Certified by . . . / . . . Thesis Supervisor

Chairman, Departmental Committee on Graduate Students

Department of Chemical Engineering
Massachusetts Institute of Technology
Cambridge, Massachusetts

May 12, 1950

Professor Joseph S. Newell
Secretary of the Faculty
Massachusetts Institute of Technology
Cambridge, Massachusetts

Dear Sir:

I take pleasure in submitting this thesis,
entitled "Gas Mixing in Beds of Fluidized Solids" in
partial fulfillment of the requirements for the degree
of Doctor of Science in Chemical Engineering.

Respectfully submitted,

Edward A. Mason

ACKNOWLEDGMENT

The author wishes to express his deep appreciation for the generous suggestions and encouragement given in the course of this work by Professor E. R. Gilliland, who acted as thesis supervisor.

Theses for the Master's Degree by G. C. Sweeney, B. V. Potter, and C. A. Sleicher formed a part of the effort underlying this thesis. The help of S. M. Holbrook and A. E. Bothe in the construction of equipment and of E. M. Berly, B. V. Potter, and A. J. Poynton in operating the apparatus is gratefully acknowledged. The helpful criticism of other graduate students is appreciated.

Financial assistance was provided by the Standard Oil Development Company and the General Electric Company.

TABLE OF CONTENTS

	<u>Page</u>
I SUMMARY	1
II INTRODUCTION	7
A. Purpose	7
B. Other Studies	12
C. Method of Investigation	26
III APPARATUS AND PROCEDURE	30
A. Fluidization Equipment	30
B. Materials	39
C. Gas Sampling and Analysis	45
D. Procedure in Back-Mixing Studies	52
E. Procedure in Residence-Time Studies	54
F. Electrostatic Effects	56
IV RESULTS AND DISCUSSION OF RESULTS	57
A. Back-Mixing Studies	57
1. Experimental Results	57
2. Sampling Problem and Gas Flow Pattern.	86
3. Correlation of Back-Mixing Results	107
B. Residence-Time Studies	123
1. Experimental Results	123
2. Analysis of Experimental Technique	149
3. Effect of Operating Variables: Correlations	160
C. Mechanism of Gas Mixing	196
D. Application of Results	203
1. Effect on Chemical Reaction	203
2. Examination of Chemical Reaction Rate Studies	218
V CONCLUSIONS	224

TABLE OF CONTENTS (CONTINUED)

	<u>Page</u>
VI RECOMMENDATIONS	227
VII APPENDIX	228
A. Details of Apparatus and Procedure	228
1. Helium Injection in Back-Mixing Studies	228
2. Size Analysis of Solids	230
3. Gas Analysis	231
a). Gas Density Balance	231
b). Electric Analyzer	235
B. Derivations	240
1. Sampling Error in Back-Mixing Studies due to Bubbles	240
2. Back-Mixing Derivation	241
3. Probability Derivation of Significance of Residence-Time Data	245
4. Semi-Logarithmic Plotting of Residence-Time Data	250
5. Application of Back-Mixing Results to First Order Chemical Reaction	252
6. Application of Residence-Time Results to First Order Chemical Reaction	258
a). Direct Derivation of Expression for Exit Composition for Piston Flow	258
b). Direct Derivation of Expression for Exit Composition for Perfect Mixing	258
c). Derivation of Residence-Time Expression for Perfect Mixing -- No Chemical Reaction	259
d). Derivation of Expression for Exit composition for Perfect Mixing Using Probability Approach	259
e). Derivation of Expression for Exit Composition Using Experimental Residence-Time Curves	260
7. Application of Residence-Time Results to Second Order Chemical Reaction	263
a). Direct Derivation of Expression for Exit Composition for Piston Flow	263
b). Direct Derivation of Expression for Exit Composition for Perfect Mixing	264
c). Derivation of Expression for Exit Composition Using Experimental Residence-Time Curves	265

TABLE OF CONTENTS (CONTINUED)

	<u>Page</u>
C. Sample Calculations	268
1. Back-Mixing Studies	268
2. Residence-Time Studies	270
3. Densities of Glass Beads	274
4. Calculation of Core and Annular Velocities from Back-Mixing Traverses	275
5. Calculation of Bed Densities, ρ_B	275
D. Summary of Data and Calculated Values	276
1. Back-Mixing Data	276
2. Back-Mixing Data - Semi-Logarithmic Plots	296
3. Solids Concentration	320
4. Residence-Time Data	328
5. Residence-Time Data - Semi-Logarithmic Plots	355
E. Location of Original Data	369
F. Nomenclature	370
G. Literature Citations	372

TABLE OF TABLES

<u>Table</u>	<u>Description</u>	<u>Page</u>
I	Properties of Glass Beads	42
II	Properties of Aerocat Microspheres, MSA . .	43
III	Average Values of C/C_0 for No.11 Glass Beads	59
IV	" " " " " No.13 Glass Beads	62
V	" " " " " Microspheres, H	63
VI	" " " " " Microspheres, D	64
VII	" " " " " Microspheres, E	65
VIII	" " " " " Microspheres, F	66
IX	" " " " " Microspheres, G	67
X	Reproducibility of Sampling	85
XI	Downward Injection of Tracer	88
XII	Effect of Sampling Time on Gas Composition	92
XIII	Void and Solids Sampling	94
XIV	Core and Annular Velocities from Back-Mixing Data	102
XV	Back-Mixing Results	112
XVI	Relative Rates of Gas Flow and Sampling for Residence-Time Studies	145
XVII	Effect of L/D Ratio on Values of S and I .	178
XVIII	Effect of Particle Size on Values of S and I	186
XIX	Maximum Gas Velocities from Residence-Time Data	192
XX	Effect of Residence-Time Distribution on First Order Chemical Reaction	210

TABLE OF TABLES (CONTINUED)

<u>Table</u>	<u>Description</u>	<u>Page</u>
AI	Back-Mixing Data	276
AII	Solids Concentration	320
AIII	Residence-Time Data	329

TABLE OF FIGURES

<u>Figure</u>	<u>Description</u>	<u>Page</u>
1	Gas Mixing Apparatus	32
2	Experimental Apparatus	33
3	Helium Injection Manifold	36
4	Photomicrographs of Glass Beads and Microspheres	41
5	Gas Density Balance	49
6	Apparatus for Gas Analysis	50
7	Sample Traverses - No. 11 Glass Beads	68
8	" " No. 11 Glass Beads	69
9	" " No. 11 Glass Beads	70
10	" " No. 11 Glass Beads	71
11	" " No. 13 Glass Beads	72
12	" " Microspheres, E	73
13	" " Microspheres, D	74
14	" " Microspheres, D	75
15	" " Microspheres, F	76
16	" " Microspheres, G	77
17	" " Microspheres, M2	78
18	Back-Mixing Sampling, R = 0	79
19	" " " R = 1.10 inches	80
20	" " " R = 1.43 inches	81
21	Sampling Error	97
22	Back-Mixing Results - No. 11 Glass Beads	111

TABLE OF FIGURES (CONTINUED)

<u>Figure</u>	<u>Description</u>	<u>Page</u>
23	Effect of C_0 on Back-Mixing	115
24	Variation in E with u_0	117
25	Variation in E with $u_0 \rho_B$	120
26	Residence-Time Results - Fixed Bed and Empty Tube	124
27	Residence-Time Results - No. 7 Glass Beads	125
28	" " " No. 9 Glass Beads	126
29	" " " No.11 Glass Beads	127
30	" " " No.13 Glass Beads	128
31	" " " No.13 Glass Beads	129
32	" " " No.15 Glass Beads	130
33	" " " Microspheres, M2	131
34	" " " Microspheres, M3	132
35	" " " Microspheres, D	133
36	" " " Microspheres, F	134
37	" " " Microspheres, M2	135
38	" " " Microspheres, M3	136
39	" " " Microspheres, M4	137
40	" " " Microspheres, M2	138
41	" " " Microspheres, M3	139
42	Effect of Radius of Sampling	147
43	Effect of Tracer Injection Rate	148
44	Residence-Time Derivation	152

TABLE OF FIGURES (CONTINUED)

<u>Figure</u>	<u>Description</u>	<u>Page</u>
45	Theoretical Residence-Time Curves	157
46	Comparison of Residence-Time Curves	161
47	Residence-Time Results - Fixed Bed and Empty Tube	164
48	Fixed Bed and Empty Tube - Calculated Curve	165
49	Residence-Time Results - Microspheres, M2-70	166
50	Microspheres, M2-70 - Calculated Curve . .	167
51	Residence-Time Results - Microspheres, M3-35L	168
52	Microspheres, M3-35L - Calculated Curve . .	169
53	Microspheres: Effect of Bed Dimensions . . .	174
54	Microspheres: Effect of Bed Dimensions . . .	175
55	Microspheres: Effect of Bed Dimensions . . .	176
56	Variation in S with L/D	179
57	Glass Beads: Effect of Particle Size	181
58	Glass Beads: Effect of Particle Size	182
59	Microspheres: Effect of Particle Size	183
60	Microspheres: Effect of Particle Size	184
61	Microspheres vs. Glass Beads	188
62	Microspheres vs. Glass Beads	189
63	Microspheres vs. Glass Beads	190
64	Effect of Residence-Time on Fraction Con- verted: First Order Reaction	209

TABLE OF FIGURES (CONTINUED)

<u>Figure</u>	<u>Description</u>	<u>Page</u>
65	Effect of Residence-Time on Fraction Converted: Second Order Reaction, Assumed No Mixing	213
A1	Injection and Sampling Details	229
A2	Wiring Diagram: Gas Analyzer	236
A3	Probability Density	245
A4	Semi-Logarithmic Plotting of Residence-Time Data	250
A5	Effect of Back-Mixing on First Order Chem- ical Reaction Rate Constant	255
A6	Effect of Back-Mixing on Fraction of Re- actant Converted in First Order Reaction .	256
A7	Effect of Back-Mixing on Fraction of Re- actant Unconverted in First Order Reaction	257
A8 -A30	Back-Mixing Results - Semi-Logarithmic Plots	297- 319
A31-A37	Pressure Gradients	321- 327
A38-A50	Residence-Time Results - Semi-Logarithmic Plots	356- 368

I SUMMARY

The action of the gases flowing up through beds of fluidized solids usually promotes a high degree of agitation of the solids in the confining reactor. This motion of the solids is highly advantageous in cases where large heat effects are present by preventing localized overheating. However, the solids mixing produces mixing of the gases and, in the case of chemical reactions, this gas mixing causes the products of reaction to be mixed with the reactants thereby decreasing the rate of reaction. Fluidized beds are used both in the laboratory for obtaining information concerning reaction kinetics and, commercially, for chemical production purposes. Knowledge of gas mixing in fluidized beds is of value in interpreting laboratory data and in the rational design of commercial equipment.

The purpose of this thesis has been to investigate the manner and extent of gas mixing in fluidized beds of laboratory size. This work should provide a better understanding of the action of fluidized beds and thus aid in their evaluation.

Two different experimental procedures were employed. In the back-mixing studies, a stream of tracer gas, helium, was injected into the central region of a bed of solids

fluidized by air; gas samples were withdrawn at various radii both above and below the point of injection. These samples were then analyzed for helium content, and in this way the flow of gas through the bed could be followed. In the residence-time studies, streams of helium and air were well mixed in a chamber immediately below the bed of solids; this mixture of about 20% helium in air then passed through the bed fluidizing it. When the concentration of helium was uniform throughout the bed, the helium flow was abruptly stopped, and gas samples were withdrawn at short intervals of time through a probe located at the top of the fluidized bed. It was thereby possible to determine the residence-times of the tracer gas in the bed.

Two transparent Lucite tubes, having inside diameters of 3 inches and 4-1/2 inches, were used as the confining columns during the studies; (see diagrammatic sketch in Figure 1 and photograph in Figure 2). Bed heights of approximately 36 and 70 inches when fluidized were employed; the ratio of bed height to diameter, L/D , varied from 7.8 to 24. All runs were made under conditions of batch operation with the top of the bed lying below the top of the Lucite column. Two different solids were studied. One consisted of various closely sized fractions of spherical glass beads ranging in size from

about 0.003 to 0.018 inches in diameter. The other solid was a microspheroidal cracking catalyst which was screened into sized fractions. (See Figure 4.)

The experimental studies showed that there was definite back-mixing of gas in the beds of fluidized solids, and this mixing of gas in a direction opposite to the direction of net flow was caused by the presence of the finely divided solids. There was a circulation pattern present in which the gases tended to flow rapidly upward in the middle of the bed and slowly downward along the wall. An exchange of gas between these two regions was found to take place.

In general, fluidized beds are characterized by regions of high solid concentration ("dense phase") and low solid concentration ("lean phase"); the "lean phase" consists of bubbles of gas rising through the solids. The transfer of gas between "dense" and "lean" phases through the interstitial spaces between the solid particles tends to be slow. Under certain operating conditions, large differences in gas composition, if created, can exist between the gas at the wall and at the core of the bed. In addition, large differences in composition can exist between the gas in the bubbles and the surrounding "dense phase". Both vertical and horizontal gradients in gas composition can exist in fluidized beds.

The passage of bubbles through the bed and the extent of interstitial gas flow are believed to affect the mixing and residence-times of the gases. The bubbles travel up through the bed at velocities ranging from 4 to 12 times the average gas velocity through the void spaces. Because of these high bubble velocities, gas samples drawn from within fluidized beds are apt to give a faulty impression of the average gas composition at the point of withdrawal.

The flow of gas through the void spaces in the bed was apparently reduced by a decrease in the average particle size or the introduction of solid fines. It is believed that this reduction in gas flow was due to the decrease in the size of the interstitial pores.

It is possible to determine the residence-time distribution of the gas entering a fluidized bed by the method developed in this investigation. The fraction of an entering slug of gas that leaves in any subsequent time interval can be determined from the slope of the experimental residence-time curves (see Figure 33). It was possible to characterize the individual experimental data curves by the magnitude of a single quantity. The experimental technique should prove useful in other mixing studies.

The nature of the gas flow through fluidized beds caused the residence-time history of the gas to resemble that expected from perfect mixing. However, it is believed that the results obtained are due to a stripping action of the bubbles passing through the bed. The concentration differences existing in the beds prove that perfect mixing was not present. The residence-time results, radial concentration gradients and back-mixing prove that the gas flow was not according to piston flow.

The residence-time distribution obtained in fixed beds of solids and in empty tubes closely approximated that to be expected from piston flow.

The residence-time for a given fraction of entering gas was inversely proportional to the gas flow rate. A fixed amount of gas was found to be required to sweep a certain fraction of entering gas out of the bed, regardless of the gas velocity.

An increase in the length-to-diameter ratio, L/D , caused a decrease in the by-passing of gas flowing through the beds. The spread in residence-times was reduced. In view of this, it is recommended that consideration be given to the introduction of baffles in industrial reactors where the effects of gas mixing have been found to be detrimental.

There was a slight trend toward a reduction in the range of residence-times as the average diameter of the particles or the amount of fines was decreased, probably due to increased flow of gas between "dense" and "lean phases."

The results of studies made in fluidized beds concerning chemical reaction kinetics can be significantly affected by the character of the gas mixing in the bed. If the reaction takes place at the solid surface, the concentration of the products of reaction will tend to become high in the dense phase; in general, this will decrease the overall rate of reaction. The use of fluid-beds as a laboratory tool to study reaction mechanisms should be considered as a compromise between the control of temperature and gas mixing.

II. INTRODUCTION

A. Purpose

The past twelve years has seen the development and tremendous growth of the fluidized powder technique as a tool for the chemical industry. While the suspension of solids in fluid streams has been used for years as a method of sizing and transportation, the application of fluidization to the catalytic cracking of petroleum has shown that this method of solid-fluid contact may hold great advantages for certain chemical operations. Today, in addition to its growing use in the cracking of petroleum, it is being considered for the gasification of coal, the synthesis of liquid hydrocarbons by the Fischer-Tropsch process, the burning of lime, the retorting of oilbearing shale, and in many other applications. To date, only gas-solid systems have received more than laboratory attention.

The primary advantage of the fluidized bed over the fixed bed which has led to its utilization is one of temperature control. In a fluid bed, particles of solid are suspended in an upward-moving fluid stream; a high degree of agitation is usually present in the bed, with the result that the solids are in continual motion and circulation throughout the confining vessel. Even with reactions where large heat effects are involved, this

solid motion tends to eliminate formation of "hot-spots" and temperature gradients of large magnitude. Due to the "fluid" character of the solid-gas mixture, which can be caused to flow through pipes, it is possible to add or remove heat from a reactor with comparative ease. Moreover heat transfer coefficients of fluid beds, based on the area of the retaining walls, have been found to be higher than those of fixed beds (35). Another advantage derives from the use of much smaller particles in a fluid bed than in a fixed bed, facilitating better gas to solid contact.

However, there are certain disadvantages in the application of a fluidized technique to chemical reactions. The very motion of the solids that provides for uniformity of temperature undoubtedly causes some mixing of the gaseous constituents. In chemical reactions exhibiting a mechanism of higher than zero order, any mixing of the products and reactants would tend to decrease the overall rate of reaction when carried out under isothermal conditions. Obviously, in industrial use this "back-mixing" effect would be undesirable and for a given conversion would call for modifications in reactor design.

In addition to its use for production purposes by the chemical and petroleum industries, the fluidized technique has been applied as a laboratory tool in the study

of chemical reaction rates and mechanisms. Since reaction rate constants are defined by differential equations, while in practice finite conversion takes place in a fluid bed, the nature of the gas flow through the reactor is of importance for the proper interpretation of experimental results. To obtain the reaction rate constants from the laboratory data, the integrated rate equation must be applied, and therefore any assumptions made upon integration concerning the path of the gas will directly affect the magnitude of the desired constant.

Lacking evidence concerning the character of the gas mixing in fluidized beds, it has been necessary in the past to make certain simplifying assumptions when designing industrial fluidization equipment and when interpreting reaction data obtained from fluid beds. Two obvious assumptions present themselves. First, one could assume that, while the solids are known to be in vigorous motion, the gases pass up through the bed in "piston flow." In this case, it is assumed that there is no back-mixing of the gases, that the composition of the gases at any level in the bed is uniform, and that there is no radial velocity gradient in the gas. Several workers have used this set of assumptions in evaluating reaction experiments conducted in small fluidized beds having large length to diameter ratios (8, 19, 28). Conversely, one

could assume that, due to the rapid mixing of the solids, the gases were completely and instantaneously mixed, i.e., that "perfect" mixing prevailed. Here, the assumption is that the composition of the gases throughout the reaction vessel is uniform and equal to the composition of the exit stream. At least one authority in the field of reaction kinetics holds to this latter view (9).

In all probability, the true facts lie somewhere between these two extreme conditions, and the above assumptions are only applied as a simplification due to lack of pertinent data.

This brief discussion serves to highlight the interest in, and purpose of, this study. Generally speaking, the object of this thesis has been to investigate the manner and extent of gas mixing in beds of fluidized solids with a view to the effect this mixing may have on chemical reactions conducted in such systems. A study of the effect of changes in operating variables has been involved.

The work presented here has been part of an overall program of research conducted at the Massachusetts Institute of Technology studying the fundamental physical behavior of fluidized beds. In addition to an investigation of gas mixing, the program has involved inquiries into the flow characteristics, heat transfer properties,

and solid mixing in beds of fluidized solids.

Before continuing with a consideration of other investigations on fluidized beds, it will be well to describe the visual appearance of such beds and to define several terms which will appear from time to time throughout this presentation.

When fluid flows up through a bed of solid particles at such a rate that the particles remain at rest, one on another, the bed is called "fixed." Starting from the fixed bed conditions, as the flow rate of fluid is increased, a point is reached where the solids lift slightly, "unlocking"; the solids are not in motion and will not sustain a force applied to the surface. This is known as a "quiescent" fluidized bed. Further increase in the flow rate will cause the bed to expand even more, and the solids will exhibit definite, and usually vigorous, motion throughout the vessel. If the particles are individually and uniformly dispersed by an increase in the flow rate, then "particulate" fluidization prevails; this type of bed action is generally exhibited when liquids are used as the supporting fluid. However, if an increase in the flow rate of fluid through the bed causes the appearance of regions of dense and dilute solid concentration as the bed expands, then "aggregative" fluidization is taking place; this is usually found when gases are used as the fluidizing medium.

The appearance of aggregative fluidization is similar to that of a boiling liquid; the regions of dilute solid concentration are bubbles of gas containing very few solid particles and will be called the "lean phase." The surrounding areas of high solid concentration will be referred to as the "dense phase." "Slugging" is a condition in which the bubbles, as they rise, grow in size to the diameter of the confining vessel; masses of particles are forced up the column between the bubbles much in the manner of pistons. When conditions are such that little or no solid is blown from the bed and none added, operation is said to be "batch."

B. Other Studies

This section will deal with the findings of others working in the fields of mixing and of fluidized solids. In addition to covering the limited studies made concerning gas mixing in fluid beds, some of the work done on flow characteristics, heat transfer, mass transfer, reaction rates, and solid mixing in fluidized beds will be discussed where the findings in these fields are pertinent with regard to the study at hand. Most of the articles to be discussed have been published since the initiation of this thesis in February, 1948.

Gas Mixing

Two preliminary studies were made in the field of

gas mixing in beds of fluidized solids prior to the start of the present work. Kennel (12) fluidized a filtrol clay with air in a one-inch glass column; batch operation was used. He injected carbon dioxide, as a tracer, into the middle of the fluid bed and drew samples from points above and below the point of injection through 1/4-inch tubes that were mounted axially. The samples were analyzed for CO₂ content. When the glass column was empty, no CO₂ was found in the gas stream below (i.e., upstream of) the point of injection; on the other hand, when the tube was full of fluidized solid, an appreciable concentration of the tracer was found below the point of injection. This indicated that the back- or down-mixing of the gas was due to the presence of solid. The concentration of tracer was found to decrease as the distance below the injection point increased. The following equation was employed in correlating the results: (See VII Appendix B)

$$\ln \frac{C}{C_0} = - \frac{u_0}{E} (x) \quad (1-II)$$

where C = concentration at distance (x) below the point of injection

C₀ = concentration at x = 0

u₀ = superficial gas velocity

E = eddy or back-mixing diffusivity coefficient

The data were found to be represented fairly well by the

exponential relationship, and Kennel reported that E was a linear function of u_0 and affected by particle size. While his results cannot be extended to quantitative conclusions, Kennel did show that back-mixing of gases does exist in beds of fluidized solids and may be affected by operating variables.

Giborowski (6) conducted similar experiments in a glass tube having an inside diameter of one inch. He correlated his results in the same manner as Kennel (12) and reported that E was independent of the superficial gas velocity and increased with increasing particle size. However, most of his results are open to criticism since the bed height used appears to have been low. When there was enough solid present to have covered the injection point, values of E found by Giborowski compared closely with those of Kennel's work.

Sherwood and Towle (32, 34) studied eddy mixing in empty tubes by injecting CO_2 , as a tracer, from a single injection point mounted axially in air ducts of different diameters. Gas samples were taken at points downstream and analyzed for tracer. Eddy diffusion was considered analogous to molecular diffusion, and the eddy diffusivity, E_m , defined by the following equation:

$$-\frac{dN_A}{d\theta} = E_m \frac{dC_A}{dx}$$

where N_A = mols of A transferred per unit area

θ = time

C_A = concentration of A at distance x

Using Wilson's integration of the resulting differential equation for mass transfer (38), values of E_m were obtained from the experimental method outlined above. Towle reported that E_m ranged from 0.004 to 0.04 ft.²/sec. and varied directly with the Reynolds number based on the diameter of the confining tube; for a constant diameter tube, E_m increased linearly with the superficial velocity. As might be expected from the nature of eddy mixing, the results obtained when hydrogen was used as a tracer checked the CO₂ values of E_m . The values obtained for eddy diffusivity ranged from 27 to 240 times the molecular diffusivity of CO₂ in air, showing that a molecular diffusion plays a minor role in the presence of turbulence. It should be noted that the eddy diffusivity coefficients obtained in this work may be of a different nature than those obtained in the fluidized bed studies, where the eddy diffusivities are obtained from mixing in a direction opposite to the net direction of flow.

Polack (26), using a technique patterned after that of Towle (34), studied eddy mixing in packed beds of solid particles using both air and water, and suitable tracers. For either fluid, E_m was found to increase with the 1.2 power of the Reynolds number based on particle

diameter; this meant that E_m increased with an increase in the superficial velocity. The reported values of E_m for CO_2 in air ranged from 0.0065 to 0.019 ft.²/sec. The values of eddy diffusivity were determined from mixing that occurred downstream of the point of injection, as in the case of Towle.

Flow Properties

Several investigations have been made concerning the flow properties of fluidized beds. One of the most complete is that of Bauer (2), who made both visual and quantitative studies on fluidized beds of small diameter. He confirmed the findings of Walker (36) in reporting that, once the quiescent state has been reached, the pressure drop across a fluidized bed is essentially equal to the weight of solids per unit area. "Excess pressure drop" was defined as the difference between the experimental pressure drop and the weight of solid per unit area; the excess pressure drop was found to increase slightly as the gas rate through the bed was increased, especially when slugging was present. This increase in the pressure drop is probably due to increased friction between the solid particles and the walls of the vessel. In "continuous" beds of fluidized solids, i.e., where solid was continually fed and blown out, Bauer found that the slip velocity, which is the average superficial gas velocity minus the average solid velocity, was independent of

solid concentration and gas and solid feed rates. This also checked previous work done by Walker (36). Using a Lucite column with an internal cross section of 1/2 by 6 inches, Bauer was able to observe the bubbles rising through a bed of solids fluidized with air. At the bottom of the column there were numerous gas bubbles of small diameter, which usually increased in size as they rose through the bed. This growth seemed to be due to gas flowing from one bubble to another through the interstices in the dense phase; some bubbles grew in size while others disappeared. Bauer found that the bubbles grew when the diameter of the fluidized particles was large; but did not when small diameter particles were used. In addition, when a wide size range of particles or a light material was used, small bubbles were present and these did not tend to grow rapidly, if at all, as they rose through the bed. At high gas rates, the size and number of bubbles was mainly a function of the gas rate. He reported that the concentration of solid in the dense phase appeared to be the same as that found in the quiescent bed, and that the increase in bed volume with increasing gas rate resulted from the displacement of the gas bubbles rising through the bed. Visual observation showed that while the bubbles tended to rise in the central region of the bed, the dense phase solids tended to move down along the walls. For particles smaller than

200 mesh and for particles with an effective particle density of less than 100 lbs./ft.³, the fluidization behavior was reported to be independent of the actual diameter.

Bauer (2) also reported on two small experiments by two other workers, Goring and Curran. Using nitrogen under atmospheric pressure and at 75 p.s.i.a., Goring fluidized glass spheres, 0.0061 inches in diameter, at a superficial velocity of 0.4 ft./sec. in a 1.33-inch steel tube. He found that the ratios of experimental pressure drop to the predicted pressure drop based on the weight of solid in the tube were 1.5 and 1.2 for the atmospheric and 75 p.s.i.a. runs, respectively. Since this ratio has been found to increase with slugging, which means greater interstitial flow, these results indicate that the tendency for gas to flow from bubble to bubble decreases as the density of the gas increases. Curran, fluidizing coal with hydrogen, nitrogen, and carbon dioxide, had reported to Bauer that the slugging was greater with the lighter gases.

Connors and Fuchs (7) studied the batch fluidization of filtrol clay with air under reduced pressures and found that the bed expansion obtained for a given superficial gas velocity was independent of the pressure.

Matheson, Herbst, and Holt (20) write that the decrease in overall bed density in a fluidized bed with

increased gas velocity is due to the presence of gas bubbles in the bed and that solid concentration in the dense phase is the same as that in the quiescent bed. Rate of bubble growth was found to increase with increasing particle diameter and particle density as well as with increasing gas velocity. Changes in the gas density or viscosity were found to have minor effects on the quiescent bed density. Experiments were conducted with a modified Stormer viscometer provided with a paddle that turned in a bed of fluidized solids. Thus the "viscosity" of the bed under varying conditions could be measured, and this viscosity, or resistance to an external force, was found to decrease with increasing gas velocity and with the addition of small amounts of fines. Beds of spherical particles were found to be more "viscous" than irregularly shaped materials. The tendency of the bed to slug increased as the bed viscosity increased.

Morse (21) applied a relationship for flow through fixed beds developed by Carman (4) and Kozeny (14) to the interstitial flow in fluidized beds. He concluded that the rate of this gas flow, and hence the rate of bubble growth, should increase with increasing particle density and diameter, with increasing bed height, and with decreasing gas density and viscosity.

Parent, Yagol, and Steiner (22) investigated the

fluidization of several solids with different gases in beds of varying size. They observed that fluidized beds resembled boiling liquids. By adding some red rouge to a bed of white filtrol, the solid mixing was observed to be very rapid. The pressure drop supporting the bed was practically independent of the shape of the column and of the density, viscosity and pressure of the gas.

Other investigators (15, 16, 17, 37) in studying fluidized beds report that their measurements on pressure drop and solid densities were independent of column diameter, total weight of solid, particle shape and gas density. Wilhelm and Kwauk (37) found that they could not obtain particulate fluidization when using air as the supporting gas in spite of trying a wide variety of materials in highly subdivided states.

Ryan (30) employed an X-ray technique to study the concentration gradients of solid in a fluidized bed of square cross section. He found that the average concentration of solids was highest near the walls and lowest in the middle of the column. This coincides with visual observation that the gas bubbles tend to rise in the central portion of a fluid bed.

Heat Transfer

Using a fluidized unit which had the upper section electrically heated and the lower section water-cooled,

Ciborowski (6) investigated the flow pattern of the solid. Two thermocouples were arranged so that the temperature along the center line and the temperature approximately 0.1 inch from the wall could be measured at various levels in the bed. In the lower section of the column, where the wall was water-cooled, the temperature near the wall was found to be higher than at the center, while the temperature of the wall was less than at the center. This difference in temperature between the region near the wall and the center line increased from low values at the bottom of the bed to fairly high values (50°F.) at the top of the cooling section. This indicated that the hot solid from the heated section was flowing down along the wall and upwards in the middle of the bed. This was the first time experimental evidence to support a definite circulation pattern in a fluidized bed had been reported.

Trilling (35) has made a rather extensive study of the heat transfer in small fluidized beds. He found that the heat transfer coefficients to the walls of the vessels in fluidized beds were from 2 to 150 times higher than those which would prevail in empty tubes or fixed beds under the same conditions of superficial velocity and particle diameter to column diameter ratio, D_p/D . He suggested that the increase is due to (1) the solid motion increasing the turbulence of the gas stream

and decreasing both the core resistance and film along the heat transfer surface, and (2), the solid acting as a carrier of heat. He found that radial temperature gradients existed in his apparatus only near the walls of the apparatus, indicating rapid horizontal solid mixing. He reports that the physical dimensions of the equipment did not seem to have any effect on the heat transfer coefficients. The heat transfer coefficients were found to increase with decreasing particle size until the particles were about 170 mesh in size; below this size the trend seemed to disappear.

Leva, Weintraub, and Grummer, (18), working with externally heated fluidized beds made of standard 2 and 4-inch pipe, report that bed height, solid concentration, particle density and vessel diameter all had no significant effect on the heat transfer coefficients obtained.

Mass Transfer

Resnich and White (29) conducted some experiments on mass transfer in fluidized beds by vaporizing naphthalene into air, hydrogen, and carbon dioxide. Very shallow beds, ranging in height from 5/8 to a maximum of 4 inches when fluidized, were employed; nevertheless the partial pressure of naphthalene in the exit stream was usually quite close to the equilibrium vapor pressure for

the temperatures used. The assumption of piston flow was used in evaluating mass transfer coefficients. The presence of two types of fluidization was reported, bubbling and slugging, and it was reported that the "j-factors," defined as

$$j_D = \frac{k_G p_{BM} M_M}{\mu \rho} \left(\frac{\mu_f}{\rho D} \right)^{2/3}$$

where k_G = mass transfer coefficient

p_{BM} = log mean partial pressure of nondiffusing gas in film

M_M = mean molecular weight of the main fluid stream

D = molecular diffusivity

μ = viscosity

ρ = density

increased with gas velocity in the bubbling region, went through a maximum as slugging began, and then decreased with a continued increase in the gas velocity. Due to scatter in the experimental results, this conclusion is not strongly substantiated. It was reported that the mass transfer coefficients increased with increasing gas velocity, throughout the range covered.

Reaction Rate Studies

Paxton, (23), studying the oxidation of carbon, reported regions of localized overheating in a reactor 10 feet tall having an inside diameter of 1.78 inches, an

L/D of 67.5. Slugging occurred in most of the runs he made, and he attributes the local overheating to poor solids mixing.

Solids Mixing

Some very recent work (1, 3, 5) on solids mixing has confirmed the existence of a flow pattern in fluidized beds in which solids tend to flow up the middle and down along the walls of the vessel accompanied by some side-mixing between the two zones. Both the rate of circulation and the agitation of the bed, causing the side-mixing, were found to increase with increasing air velocity. In addition, the circulation increased for a given gas rate when the particle size was decreased. The velocity of solid in the core, or center, of the bed was found to be higher than the superficial gas velocity, while that in the annular region surrounding was less than the superficial gas velocity.

Summary of Literature

In summarizing the information that is now available having bearing on gas mixing in beds of fluidized solids, it is possible to arrive at a few broad conclusions.

Due to the presence of the solids in fluidized beds, back-mixing of the gases does occur. This back-mixing may be affected by such operating variables as gas velocity

and particle size.

Fluidized beds of the gas-solid type resemble boiling liquids, in that they exhibit regions of high and low solid density. The "lean phases" are bubbles of gas rising to the upper surface. The bubbles usually grow in size as they rise, indicating interstitial flow of gas. It is to be expected that the interstitial flow of gas will affect the transfer of gas from bubble to bubble and from dense phase to lean phase, and, therefore, will affect the overall gas mixing. This gas flow within the bed appears to increase with an increase in particle diameter and density, an increase in gas velocity, and a decrease in gas density. Judging from studies on the flow characteristics and heat transfer in such beds, the effect of particle diameter may disappear at small diameters.

A general circulation pattern exists in the flow of solids tending to carry the solid upwards in the middle of the bed and downwards along the walls of the confining vessel. Since the gases mix mainly due to solid motion, and as the pattern of solid flow may be affected by the shape of the vessel, the diameter and bed height may affect gas mixing.

Referring to mixing studies in empty tubes, if the mixing is predominantly due to turbulence, then changes

in the physical properties of any tracer gas used (with the exception of adsorptivity) will probably have little effect on the results obtained.

C. Method of Investigation

In formulating the experimental program, several general methods of attack presented themselves. Since the ultimate purpose of the thesis is, in addition to increasing the general knowledge of fluid-solid systems, to aid in understanding and applying the fluidized technique to chemical operations, determination of the time-place history of the gas molecules as they pass through a fluidized bed could be imagined as the goal of this work. However, as is generally true when speaking of gases, this means a statistical or average study of large groups of gas molecules. Of course, this is a highly idealized goal; nevertheless, it leads to two different experimental techniques. In one the operation of the bed could be altered slightly and probes introduced into the bed to study, from within, what has happened due to the change. In the second method, the bed could be subjected to changes, and the effect of these changes studied wholly from outside the bed. Both of these general approaches were applied in this study and will be described here in general outline.

The internal investigation, to be referred to as the

back-mixing experiment, was a steady-state operation. A bed of solids was fluidized using air as the supporting medium, and a continuous stream of tracer gas was injected through the side of the column about half-way between the top and bottom of the bed. Both a single injection tube, resembling a point source, and a multi-tube arrangement, simulating a plane source, were employed. Arrangements were made so that samples of the gas could be withdrawn at any radius through fine hypodermic tubing at various levels above and below the point of injection. The air and tracer gas, which was helium, were metered before entering the column, and the gas samples were analyzed for helium content. Observations concerning bed action were noted. By taking samples at the various levels, it was possible to determine any longitudinal gradients in helium concentration. Radial sampling permitted examination of any horizontal concentration gradients in the gas. Some gas sampling from dense and lean phases was carried out.

The external studies, called the residence-time experiments, were unsteady-state. A bed of solids was fluidized with a mixture of air and helium, as a tracer, until the composition of the gas throughout the bed was uniform. Then at some given instant, the helium fed to the bottom of the column was turned off; the air continued

to fluidize the bed of solids and acted to dilute and sweep out the original air-helium mixture. At the same instant a stopwatch was started. Thereafter, at definite time intervals, gas samples were withdrawn into gas bottles through a sample tap located just over the top of the fluid bed. The air and helium were metered before entering the column, and the successive gas samples, along with one containing some of the original helium-air mixture, were analyzed for helium content. This experimental technique gave the concentration of helium in the exit stream as a function of time.

It might be expected that the following variables would be pertinent to the mixing of gases in fluidized beds; gas density, velocity, and viscosity; bed height, diameter, and cross section shape; particle diameter, density, shape and porosity; whether the type of fluidization was particulate or aggregative and continuous or batch. Of these, the following have been given some consideration in this investigation: gas velocity; bed height and diameter; particle diameter, density and porosity. All experimental work has been conducted in cylindrical tubes made of transparent Lucite, using air as the fluidizing medium; the operations have all been particulate and batch.

The data obtained give information concerning con-

centration gradients that may exist in fluidized beds, the average time a gas molecule may remain in a fluidized bed, and the effect that variation in operating variables may have. Such information should be of value in the interpretation of reaction rate studies carried out in fluidized beds and in the rational design of industrial reactors.

III. APPARATUS AND PROCEDURE

The experimental work of this thesis has been conducted in two pieces of apparatus; in addition, two different experimental techniques have been employed. Therefore, this section will describe the two pieces of apparatus, the methods of gas analysis, and then the procedures used.

A. Fluidization Equipment

1. Small column

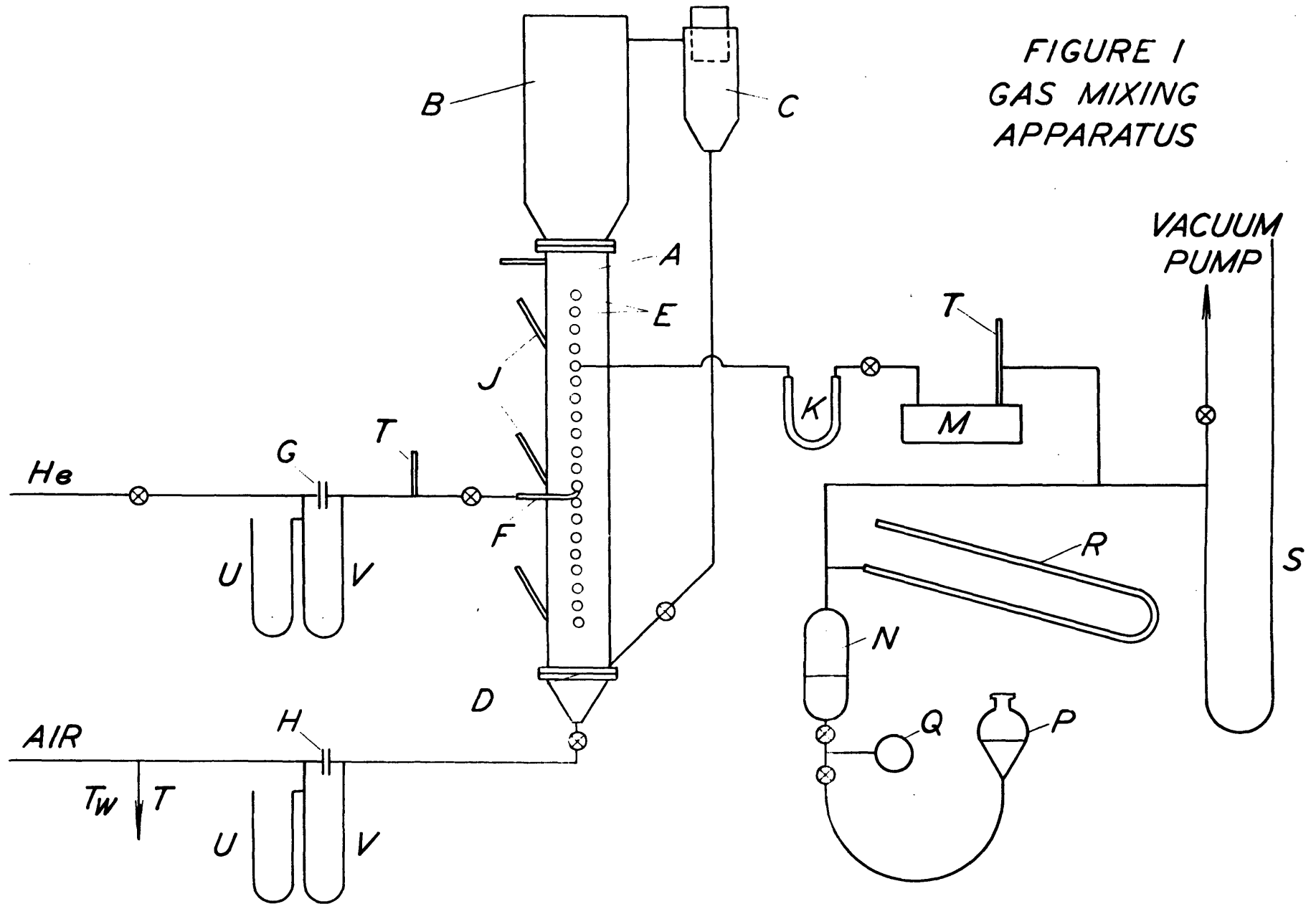
The smaller of the two units consisted of a cylindrical tube of Lucite having an inside diameter of 3 inches and a height of 6 feet; the walls were 1/4 inch thick. A schematic diagram of the apparatus is shown in Figure 1. Figure 2 is a photograph showing the experimental apparatus with the large column in the foreground and the small column to the left. Above the Lucite column was a disengaging section 3 feet high and having a square cross section. It was constructed of Lucite sheets, 1/8 inch thick and 6 inches wide. To this was connected a cyclone separator, which served to remove additional solids from the gas stream before it discharged to the room. These solids were returned to the bottom of the unit through a glass tube one-half inch in diameter. Pressure taps were attached to the side of the column at

FIGURE 1. BACK-MIXING APPARATUS

Key:

- A - Fluidization column
- B - Disengaging section
- C - Cyclone separator
- D - 200 mesh screen
- E - Sampling ports
- F - Injection tube, I.D. = 0.141"
- G - Capillary orifice
- H - Sharp edge orifice
- J - Pressure taps every foot
- K - CaCl₂ drying tube
- M - Gas density balance
- N - Pressure adjustment bottle
- P - Mercury leveling bottle
- Q - Fine adjustment bellows
- R - 5:1 inclined manometer
- S - Absolute manometer
- T - Thermometer
- T_w - Wet-bulb thermometer
- U - Mercury manometer
- V - Water manometer

FIGURE I
GAS MIXING
APPARATUS



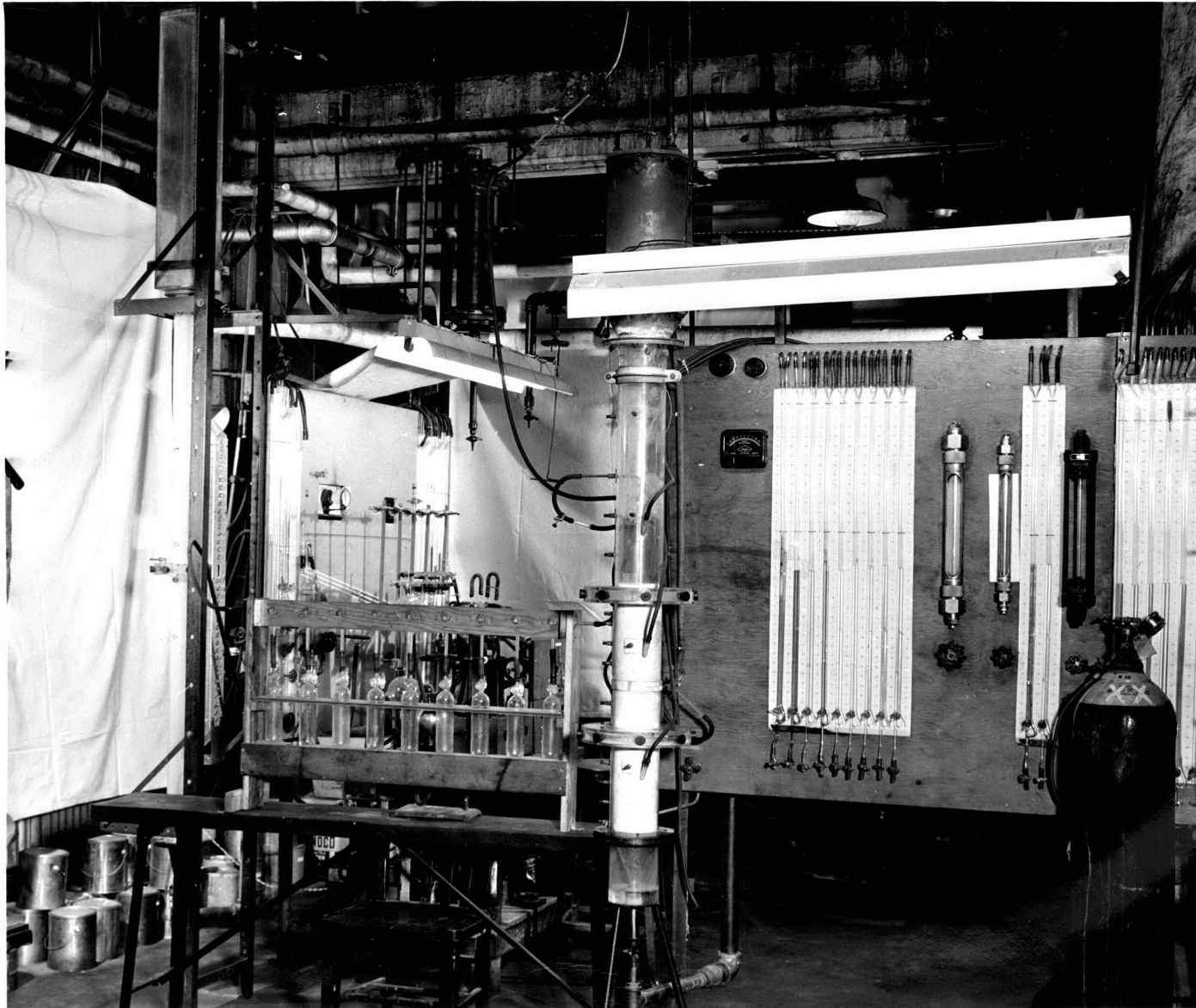


FIGURE 2. EXPERIMENTAL APPARATUS.

intervals of one foot from the bottom; the manometers were equipped with stopcocks in one of the liquid legs so that the pressure fluctuations could be damped.

The fluidizing gas, air in all cases, was introduced into the bottom of the column through a conical section and was distributed by a 200-mesh screen; this screen was supported by heavier wire screening having a spacing of about $1/2$ inch. The air was metered before entering the column by means of an orifice plate having a $1/4$ -inch hole; the plate was mounted in standard $3/4$ -inch pipe. Water and mercury manometers indicated the differential and static pressures. A mercury-filled thermometer indicated gas temperature in the line. The humidity of the air from the compressor was measured by a diaphragm-type gage, or, in some runs, by a wet and dry bulb technique.

According to the experiment that was being conducted, the tracer gas, helium, was admitted to the column in one of several ways. Runs were made in which the helium was injected at a point $3-1/2$ feet from the bottom of the column through a piece of 5-millimeter glass tubing. This tubing was bent at a right angle inside the column so as to inject the gas upwardly in the center of the column. A multi-point injection system was also employed to inject the helium into the fluidized bed. Details of this

are shown in Figure 3. Stainless steel hypodermic tubes projecting through the walls of the column were held in place by means of leather gaskets; these tubes were enclosed in a Lucite manifold to which the helium was fed. (For details of construction, see VII APPENDIX A.) Both of the above methods of tracer injection were used in the back-mixing studies. In the residence-time studies, the helium was introduced into the conical section at the bottom of the column through a piece of 1/4-inch copper tubing soldered to the cone 1/2 inch below the 200-mesh screen. The helium feed rate was measured by means of a capillary orifice made of glass; water and mercury manometers measured the differential and static pressures.

The air and helium orifices for both the small and large units were calibrated using a new dry-test meter made by the American Meter Company (serial number 5373470).

For the back-mixing studies the sampling tube was a 0.075-inch O.D. stainless steel tube soldered axially in a threaded brass rod. By means of a threaded knob on the brass rod, it was possible to position the end of the sample tube accurately to any desired radius. The sample tube projected through holes which were spaced vertically at one-inch intervals in the side of the column. Leather gaskets served to make a gas-tight joint between the sample tube and the Lucite. Plugs were inserted in the

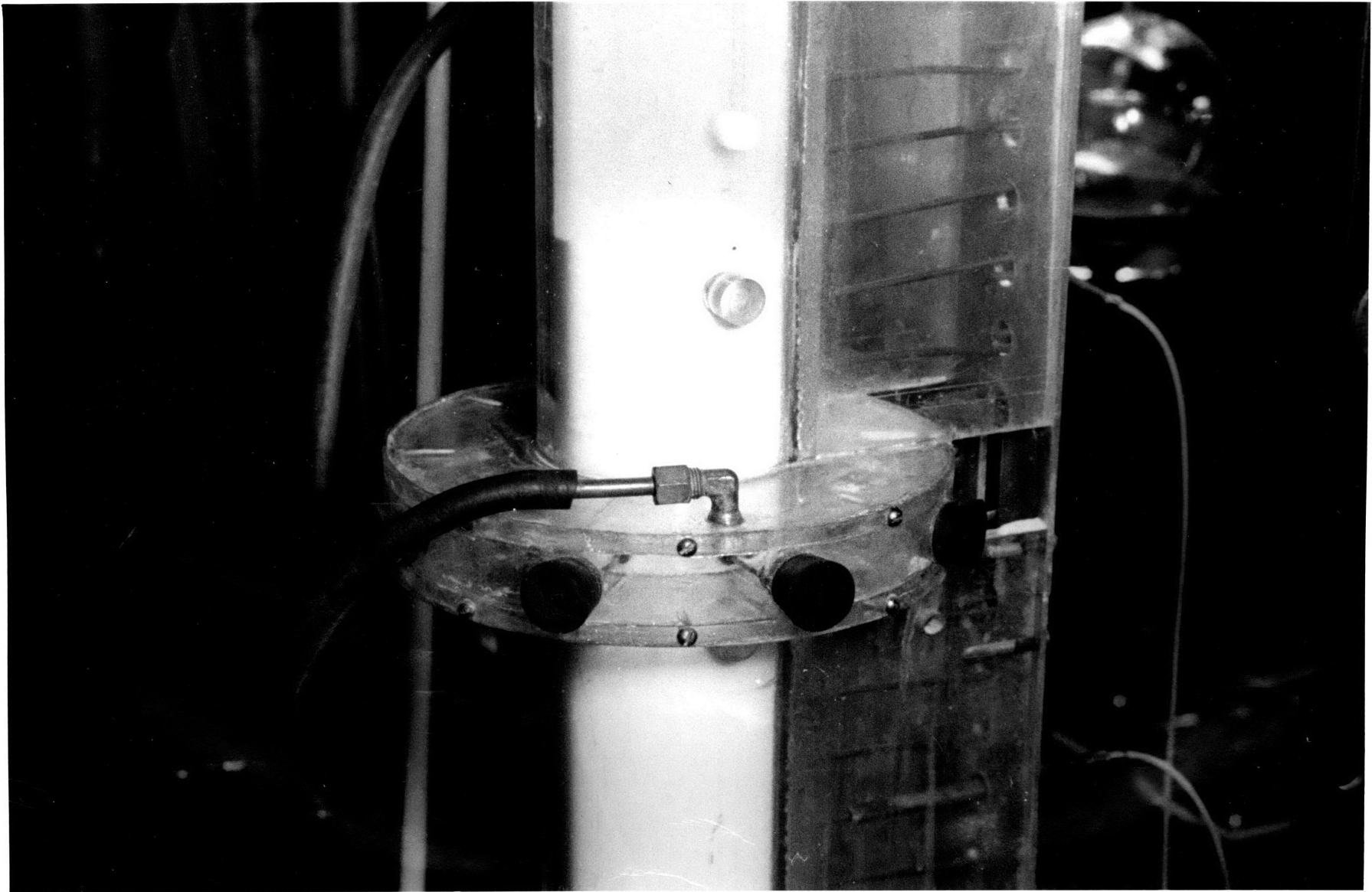


FIGURE 3. HELIUM INJECTION MANIFOLD.

sample holes when not in use. In the residence-time experiment, samples were drawn through a piece of 5-millimeter glass tubing which was bent at right angles inside the column so that the tip pointed down along the axis of the tube. Covering the end of this sample tube was a piece of 320-mesh screen formed into a cylinder and soldered. This solids-filter extended one inch beyond the open end of the sample tube. Samples could be taken at either of two levels; at one, the open end of the sample tube was 37 inches from the screen and at the other, 70 inches.

2. Large column

The large unit was a cylindrical tube of 1/8-inch Lucite having an inside diameter of 4-1/2 inches and a height of 50 inches. Above the column was a disengaging section 18 inches tall having a diameter of 8 inches. As in the small unit, a cyclone separator served to remove additional solids from the gas stream; these solids were returned to the bottom of the column through a 1/2-inch tube. Pressure taps were located below the bottom of the bed and at distances of 0.5, 1.0, 1.5, 2.5, and 3.0 feet from the bottom; these were connected to manometers that had stopcocks in one liquid leg.

The fluidizing air was introduced into the bottom of the column through a conical section. At the base of the

cone, which formed the bottom of the fluid bed, was a 200-mesh stainless steel screen supported by a disc of 0.022-inch perforated brass (the perforations were 24 per inch and 0.021 inches in diameter). A heavy 200-mesh screen was soldered to the inside of the cone 2-3/8 inches from its base. A piece of 1/4-inch copper tubing was soldered through the side of the cone between these two screens; it served to introduce the helium into the air stream in the residence-time studies. The air was metered before entering the column by means of a calibrated rotameter.

As mentioned above, in the residence-time studies, the helium was introduced into the conical section at the bottom of the column. The column was also provided with two Lucite manifolds, similar to the one on the small column, for back-mixing studies. The helium was metered into one of these manifolds by means of a calibrated orifice made of glass capillary tubing.

In the few back-mixing runs made with the large column, the gas samples were withdrawn through a piece of 1/8-inch stainless steel tubing with 0.065-inch I.D. This tubing entered the column through standard 1/8-inch copper tubing fittings that had been reamed out so that the steel tubing could slide through. Brass collars were used to give a gas-tight seal. In the residence-time experiments, the gas samples were taken through a piece of 1/4-inch

copper tubing bent at right angles inside the column so that the open end pointed down along the axis of the Lucite tube. The 320-mesh filter that was used on the small column covered the end of the sample tube, which was 35 inches from the supporting screen.

B. Materials

1. Gases

Air was used as the fluidizing gas in all of the work reported here. The reasons for its choice were convenience and economy. A rotary positive displacement compressor, built by the Beach-Russ Company, capable of delivering up to 110 c.f.m. of air at 7.5 p.s.i.g. supplied the air for both units. The compressor had an oil seal so that the air it delivered was always contaminated by oil; a filter made of a piece of standard 5-inch pipe, flanged at both ends, and packed with glass wool proved quite effective in removing most of the entrained oil. Provision was made to humidify the air, when desired, by injecting steam about 100 pipe diameters upstream from the filter.

Helium was used as the tracer gas in all of the runs made during the course of this work. The primary reason for its choice was to reduce, as far as possible, the part adsorption would have in the gas mixing. In addition, some of the physical properties of helium provide for

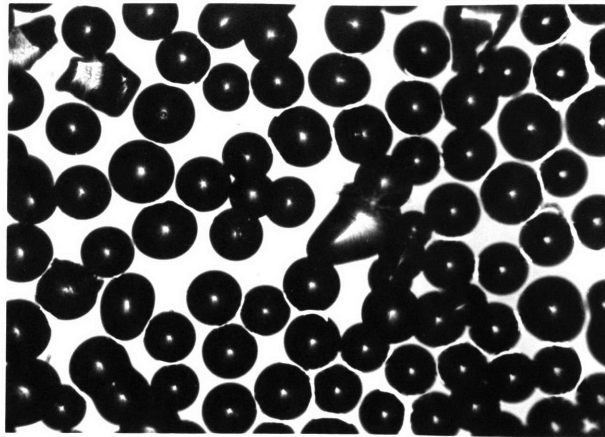
easy analysis of helium-air mixtures. The helium was supplied in 220 cu.ft. cylinders by the Air Reduction Sales Company which obtained it from the U.S. Bureau of Mines. The gas was quoted at a purity of 99.5 + % helium.

2. Solids

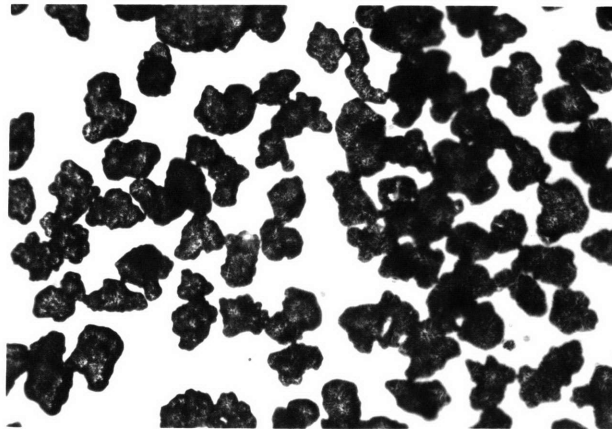
Two different solids were employed in the course of this work: spherical glass beads and a petroleum cracking catalyst referred to as microspheres. The shapes of both types of solids may be seen in Figure 4.

The glass beads were a product of the Minnesota Mining and Manufacturing Company and go under the trade-name of Scotchlite Glass Beads. Their properties are listed in Table I. The average diameters of the closely sized fractions were determined by Trilling (35). He used photographs taken through a microscope fitted with a calibrated eyepiece micrometer; this method was checked by micrometer. The average diameter is the arithmetic average of a group of about 50 particles. The absolute densities were determined by water displacement.

The microspheres were a silica-alumina cracking catalyst manufactured by the American Cyanamid Company. Their properties are listed in Table II. In order to reduce the loss of fines during the course of the work due to elutriation, the raw microspheres were fluidized



No. 11 Glass Beads



Microspheres, M3

FIGURE 4. PHOTOMICROGRAPHS OF
GLASS BEADS AND MICROSPHERES

TABLE IProperties of Glass Beads

Size No.	Diameter		% Devia- tion	Size Analysis	Abs. Density ρ_s , lb./ft. ³
	Inches	Microns			
7	0.0178	452	6	Microphotographs Micrometer	173
9	0.0106	262	7	"	169
11	0.0061	155	7	"	151
13	0.0040	102	6	"	151
15	0.00275	70	12	"	150

TABLE II

Properties of Aerocat Microspheres, MSA

<u>Size Range (microns)</u>	<u>Weight %</u>	<u>Weight Mean Diameter (microns)</u>	<u>Method of Analysis</u>	<u>Abs. Particle Density, ρ_s, (lbs./ft.³)</u>	
<u>Microspheres F, through 150 Mesh</u>					
0-25	2.0	70	Screening and Microscope		
26-50	20.6				
51-75	31.1				
76-105	46.1				
>105	0.2				
	100.0				
<u>Microspheres G, Fines Only</u>					
0-10	8.6	17	Rate of Settling in Water	122 Water displacement	
11-20	65.4				
21-30	21.4				
31-40	4.6				
	100.0				
<u>Microspheres D, Less Fines</u>					
0-25	0	104	Screening and Microscope		
26-50	5.2				
51-75	16.4				
76-100	31.8				
101-125	22.2				
126-150	13.0				
151-175	7.0				
176-200	2.8				
> 200	1.6				
<u>Microspheres M2, 150-200 Mesh</u>					
0-25	0	107	Analysis by Microscope		
26-50	0.4				
51-75	5				
76-100	29				
101-125	52				
126-150	14				
<u>Microspheres M3, 100-150 Mesh</u>					
0-25	0	150	Microscope		
26-50	0				
51-75	1				
76-100	5				
101-125	16				
126-150	33				
151-175	30				
175-200	7				
201-225	4				
226-250	5				

TABLE II (CONTINUED)

<u>Size Range (microns)</u>	<u>Weight %</u>	<u>Weight Mean Diameter (microns)</u>	<u>Method of Analysis</u>	<u>Abs. Particle Density, ρ_s, (lbs./ft.³)</u>
<u>Microspheres M4, 65-100 Mesh</u>				
< 100	0	216	Microscope	
101-125	1			
126-150	4			
151-175	9			
176-200	24			
201-225	24			
226-250	18			
251-275	11			
276-300	9			
<u>Microspheres H</u>				
< 74	9.8	130	Screening	
74-104	19.9			
104-124	15.6			
124-147	18.4			
147-208	34.7			
> 208	1.6			

for about an hour in the small unit at an air velocity of 1.5 ft./sec.; the fines removed in the cyclone were discarded. The solids remaining in the column were then screened into the various size fractions shown. It is interesting to note that the fractions all contain considerable quantities of particles larger than the largest opening in the limiting screen. This illustrates the fact that, while the particles are roughly spherical, many of them are oblong. The size analyses for M2, M3, M4 were made using a microscope fitted with a Filar micrometer eyepiece and converted to weight per cent by assuming the particles to be spherical. (See VII APPENDIX A, for details of method.) The size analyses of the other microspheres are based on the rates of settling through water. The particles are porous and a heat of adsorption was noticed while determining the absolute density by means of water displacement. In view of this, the densities listed may not be the critical ones so far as fluidization is concerned.

C. Gas Sampling and Analysis

1. Gas Sampling

All gas samples were drawn from the columns into previously evacuated spaces. When the gas density balance was used, it and all the accessory apparatus were evacuated before sampling; a valve in the sampling line leading

to the column was closed. In the back-mixing experiments using the thermal conductivity analyzer, the sampling line led to a gas sample bottle which was evacuated for sampling and served to mix the sample before analysis. In both cases, the sampling line was purged several times before the final sample was taken. In the residence-time studies, the sampling line led to nine previously evacuated gas sample bottles. A Cenco Hy-Vac vacuum pump was employed throughout.

A small plug of knitting yarn filled the end of the sampling tube in the back-mixing experiments. This served as a filter to keep solids out of the sampling and analytical equipment. The plug throttled the flow of gas from the column, so that the sampling time was about 30 to 40 seconds.

For the residence-time studies, a rack of nine gas sample bottles connected to a common manifold was used in order to draw successive samples at short intervals of time. Three-way stopcocks were arranged in the manifold so that it was only necessary to turn one stopcock in order to seal off one bottle and divert the flow of gas into the next.

The gas sample line in the residence-time studies was provided with a short piece of glass tubing filled with loosely packed glass wool; this acted as a filter

for any solid which passed through the 320-mesh screen at the end of the sample tube.

One bottle at a time, the gas in each bottle was displaced into the previously evacuated analyzer by means of a mercury-filled leveling bottle which was connected to the bottom of the sample bottles.

2. Gas Density Balance

In the first runs conducted in the small column, the gas samples were analyzed for helium using an Edwards-type gas density balance. In this device (Figure 5), a horizontal beam having a small hollow bulb mounted at one end and a mirror at the other was suspended in a gas-tight chamber. Using a leveling bottle of mercury and an outside reservoir of sample gas, the pressure in the chamber was adjusted until the beam was balanced; the pressure as indicated on an inclined manometer and the temperature inside the chamber were observed. The complete apparatus can be seen in the background of Figure 6 and is shown at the right side of Figure 1. Comparing the results with those obtained for air (known molecular weight), and assuming the perfect gas laws, it was possible to calculate the composition of the helium-air mixtures. A drying tube filled with calcium chloride was used to dry the gases before analysis. This piece of apparatus gave considerable trouble and so was abandoned

FIGURE 5. GAS DENSITY BALANCE**Key:**

- A - Float
- B - Mirror and hairline
- C - 0.001" x 0.012" brass ribbon
- D - Balance arm
- E - Balance platform
- F - Shell
- G - Screw-on caps with glass windows
- H - Balance frame
- J - Check bars
- K - Ribbon clamp
- M - Gas ports

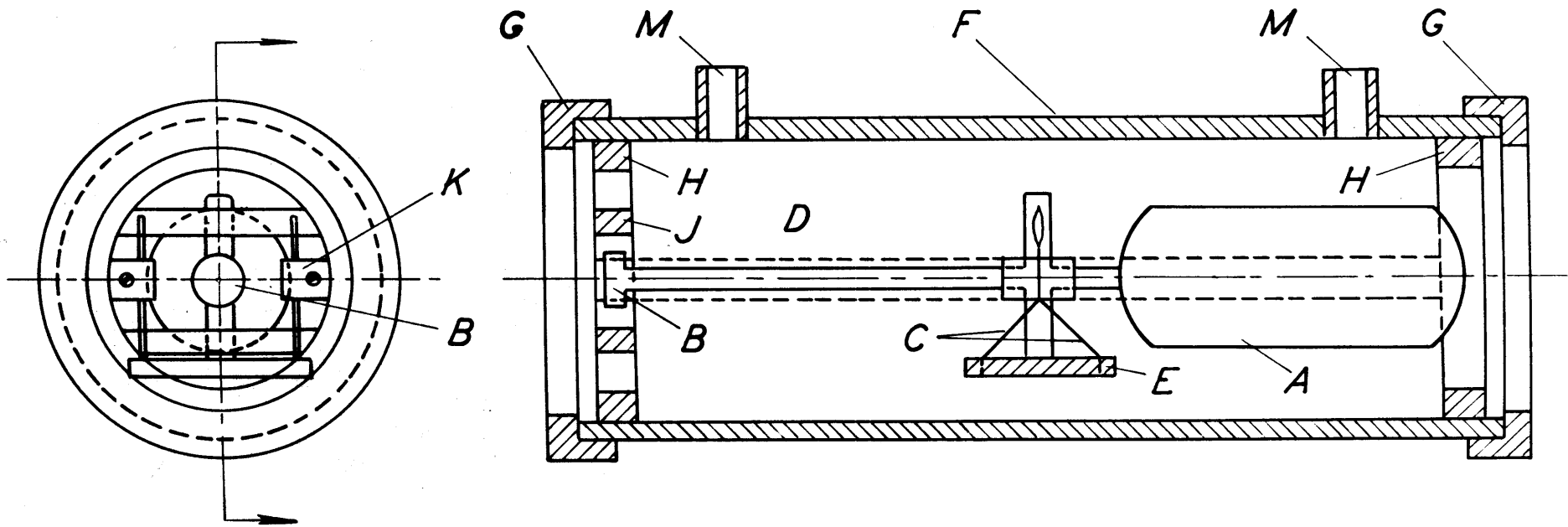


FIGURE 5
GAS DENSITY BALANCE

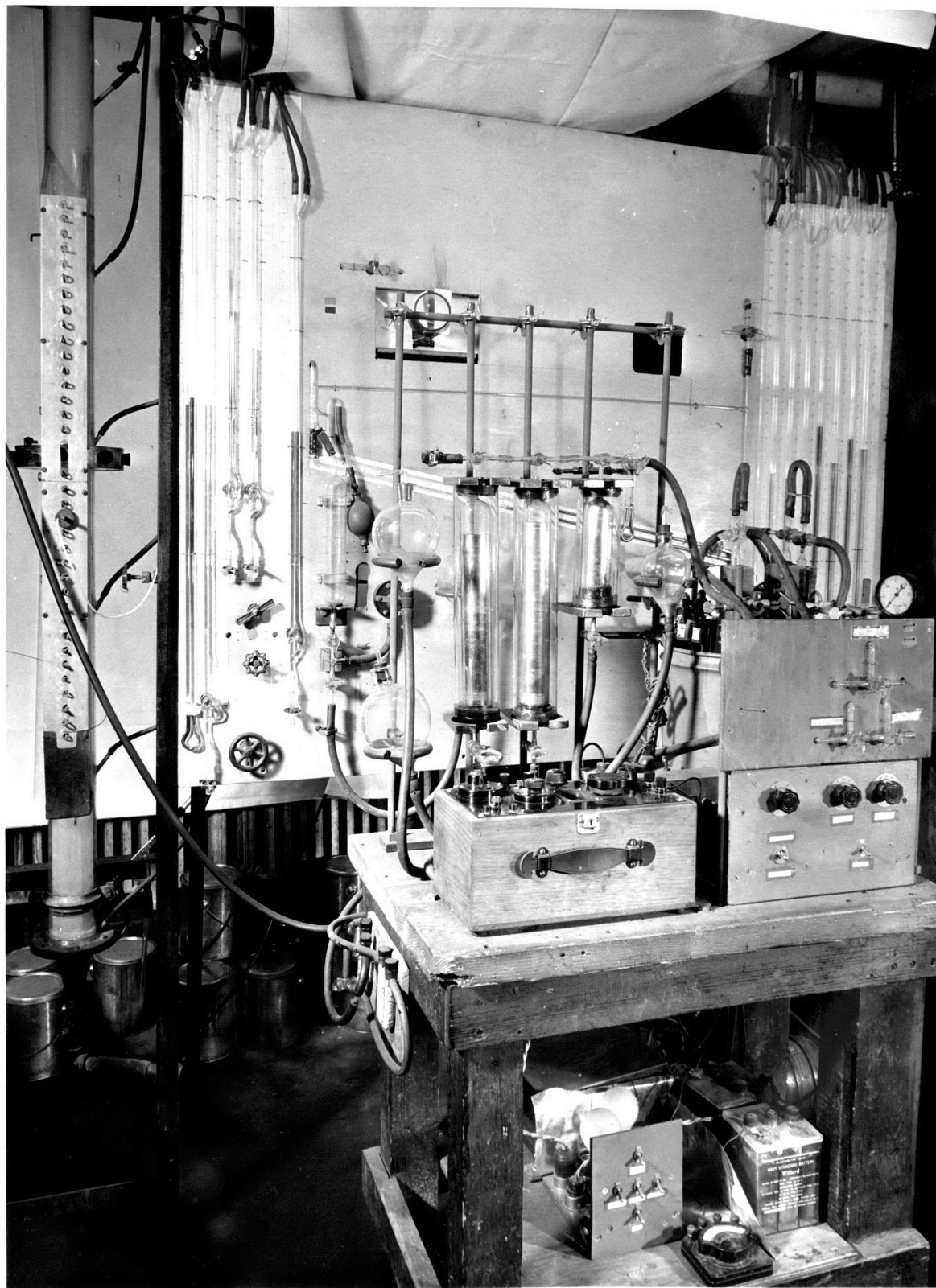


FIGURE 6. APPARATUS FOR GAS ANALYSIS.

in favor of the thermal conductivity analyzer.

3. Thermal Conductivity Analyzer

The bulk of the gas samples taken in the course of this work were analyzed for helium in an electric analyzer (see Figure 6), which took advantage of the difference in the thermal conductivity of helium and of air. A pair of thermal conductivity cells, consisting of platinum wires enclosed in glass, were connected as two of the legs of a Wheatstone Bridge circuit (see VII APPENDIX A for details). The cells were suspended in a constant temperature bath. One cell was used as a standard and was always filled with air; the other cell was used for analyzing the unknown air-helium mixtures. The bridge circuit was operated in unbalance under a constant impressed e.m.f.; the unbalance potential, which was a measure of the helium concentration, was measured by a potentiometer. Drying tubes filled with indicating Drierite (calcium sulfate) served to dry the gas before analysis. A calibration of helium concentration against unbalance e.m.f. was made by repeated subdivision and dilution of a known volume of helium. The analyzer gave trouble-free operation and proved to be much faster in use than the gas density balance.

Each day, before using the electric gas analyzer, the zero-point was checked by drawing fresh air from the

column into both cells to determine any drift. This was to prevent any damage to the circuit from going unnoticed; in the seven-month period in which one calibration was used, the zero-point drifted about 0.1 millivolts, which corresponds to about 0.03% helium and is well within the accuracy desired. Once the zero-point had been checked, the standard cell was sealed from the rest of the sampling and analysis train, while the unknown cell was evacuated in preparation for use.

D. Procedure in Back-Mixing Studies

All of the studies conducted in the course of this work were made using a "batch" fluidized bed. Any small amount of solid that was carried into the cyclone and there separated from the gas stream was returned through a tube leading to the bottom of the bed. This tube was tightly clamped during the course of any run, so that no gas flowed up the tube, bypassing the fluidized bed; the solids were returned between data runs. In the case of the glass beads, there was no solid carryover, and in the case of the microspheres the carryover during a run was less than 0.5% of the total solids present, even in the case of the smallest size fractions.

The back-mixing runs were made in the small column and conducted with the fluidized bed just filling the column. The beds, due to the passage of bubbles and

slugging, fluctuated in height, and the weight of solid in the bed for any given air velocity was adjusted so that at the maximum height of the bed, just a little solid entered the bottom of the disengaging section. This gave an L/D ratio of roughly 24. Once the weight of the solid and the superficial air velocity had been adjusted to the desired conditions, the helium feed to the column was adjusted so that the helium concentration in the exit stream was about 10%.

Meanwhile, the sampling and analytical system was evacuated, so that once steady state had been reached (i.e., helium concentration in the fluidized bed was not a function of time), the sample line was purged and a sample withdrawn from the column to be analyzed. When the gas density balance was used, the helium was turned off after each sample, and the exit concentration of helium was calculated from the air and helium orifice readings. This value was only occasionally checked by actual gas sampling from the cyclone. However, when the thermal conductivity analyzer was employed, the time for analysis was short enough so that the helium could be economically left on between samples; in this case, the exit concentration of helium was determined by sampling and only checked by orifice calculations. In addition to reading the necessary manometers and thermometers for the air

and helium rates, the manometers indicating the static pressures at the various levels in the bed were also observed.

The column, gas lines, sampling and analytical apparatus were checked daily for leaks; the column and gas lines by use of a soap solution, and the sampling apparatus by observing the rise in pressure in the evacuated system on a vacuum gage.

E. Procedure in Residence-Time Studies

Residence-time experiments were carried out in both large and small columns. Bed heights of 37 and 70 inches in the small column and 35 inches in the large column were studied. These heights were the distances from the end of the sampling probe to the supporting screen. The weight of solid in the column for any desired gas velocity was adjusted so that, on the average, the upward fluctuation of the bed carried the top of the bed to the level of the sample probe; occasionally the bed level rose slightly higher.

When the bed level had been adjusted to the proper position, the gas bottles were evacuated and the flow of helium to the conical section at the bottom of the column adjusted to give about 15 to 20% helium in the helium and air mixture. Flow and temperature readings were made, along with observations as to the height and character of

the bed. The sample line was purged just before the samples were to be drawn.

When the concentration of helium was uniform throughout the bed, one sample was drawn. Then one man diverted the flow of helium from the column to the room by means of a three-way stopcock attached to the helium line about 2 inches from the conical section. At the same time, another man started a stop watch, and at the desired time intervals turned the three-way stopcocks on the sampling train so as to divert the sampled gas into one bottle after another. When all samples had been taken, readings of the static pressures in the column were taken, and then samples were analyzed one at a time. The stop watch used in the timing made one revolution every ten seconds, each second being divided into ten parts; it was possible to time the turning of a stopcock to 0.1 second. Experiment had shown that it took about 0.5 seconds for the pressure in one of the evacuated gas sample bottles to reach atmospheric, and therefore all the desired times of sampling were led by 0.2 seconds, e.g., if a sample of gas was desired at 4 seconds after the helium had been turned off, the appropriate valve was turned at 3.8 seconds after the helium had been turned off. By careful operation, it was possible to take samples at one-second intervals, if desired.

The glass wool filter in the sample line was changed after each run, and was loosely packed so that the time of sampling would not be affected.

F. Electrostatic Effects

In dry weather, and particularly with the glass beads, electrostatic effects caused by the fluidization were present. They gave rise to a different type of solid motion than occurred under normal conditions. An effective means of reducing the electrostatic charges was to add one or two cubic centimeters of an "anti-static solution" sold by Forest Products, Inc., of Cambridge, Mass. Humidification of the air also proved effective. In order to note changes in air conditions promoting electrostatic effects, the humidity of the air from the blower was noted for each run.

IV. RESULTS AND DISCUSSION OF RESULTS

A. Back-Mixing Studies

1. Experimental Results

The results of the back-mixing studies are summarized in the following tables:

Table III	No. 11 Glass Beads
Table IV	No. 13 Glass Beads
Table V	Microspheres, H
Table VI	Microspheres, less fines, D
Table VII	Microspheres, on 100 Mesh, E
Table VIII	Microspheres, through 150 Mesh, F
Table IX	Microspheres, fines only, G

The letters given are to identify the various solids. The data in Tables III and V were collected largely by Sweeney (33), and those of Tables IV and VI through IX by Sleicher and Potter (27).

Radial traverses showing concentration gradients are presented in Figures 7 through 17. These include data taken both above and below the point where tracer was injected. The vertical gradients in gas composition are shown for one run at three different radii in Figures 18 through 20, which are representative of other runs. The single tube injector was used in this run.

In the tables, the vertical distance below the point

of injection is reported; positions above the point of injection are indicated by a negative sign (-). The radii of sampling are designated positive if lying on the side through which the sampling tube extended (North) and negative if on the far side (South). The following designations for sampling radii were used.

- R0 - center
- R1 - 0.566 inches
- R2 - 0.980 inches
- R3 - 1.27 inches
- R4 - 1.45 inches
- R5 - 1.10 inches
- R6 - 1.43 inches

R0, R1, R2, and R3 represent centers of equal areas, while R4, R5, and R6 are the correct points for a Gauss 5-point integration (31). At one level, 11 inches above injection, a sampling port is provided for East-West sampling (see Figure 11).

Most of the investigations concerning back-mixing were carried out in the smaller, or 3-inch column. The bed height was adjusted so that the top of the fluidized bed remained slightly below the disengaging section at all times. If the average height of the bed is determined by extrapolating the static pressure gradient up the column to atmospheric pressure, it appears that the top of the

TABLE III

Average Values of C/C_0 for No. 11 Glass BeadsA. Single Tube Injection, 3-inch Column

Air Velocity: (ft./sec.)		0.6	0.9	1.2	1.8
C_0		16.5%	16.5%	9.2%	9.2%
Sample Position					
V	H				
-12	R0	1.61	1.35	1.84	1.93
-12	R5	1.47	1.15	1.20	0.98
-12	R6	1.58	1.17	1.23	0.89
-10	R0	1.76			
-10	R5	1.65			
-10	R6	1.71			
- 9	R0		1.45	2.06	2.07
- 9	R5		1.08	1.04	0.77
- 9	R6		1.16	1.00	0.84
- 8	R0	1.75			
- 8	R5	1.46			
- 8	R6	1.67			
- 6	R0	1.88	~1.72	2.58	2.42
- 6	R5	1.38	0.90	1.08	0.67
- 6	R6	1.35	0.98	0.97	0.81
- 4	R0	>2.00		3.14	
- 4	R5	1.17		0.72	
- 4	R6	1.37		0.82	
- 3	R0		>1.72		2.94
- 3	R5		0.60		0.51
- 3	R6		0.66		0.60
- 2	R0	>1.94		3.31	
- 2	+ 1/4	>1.95			
- 2	+ 1/2	1.76			
- 2	+ 3/4	1.23			
- 2	+ 7/8	0.91			
- 2	R5	0.84		0.65	
- 2	1-1/8	0.91			
- 2	1-1/4	0.74			
- 2	1-3/8	0.83			
- 2	R6	0.95			
- 2	1-1/2	0.90		0.74	
0	R5				0.33
0	R6				0.45
2	R0	0.20	0.27	0.29	0.25
2	+ 1/4		0.24	0.31	0.26
2	+ 1/2	0.19	0.22	0.34	0.26
2	+ 3/4		0.26	0.39	0.29
2	+ 1		0.20	0.39	0.27

TABLE III (CONTINUED)

Air Velocity: (ft./sec.)		0.6	0.9	1.2	1.8
C _o		16.5%	16.5%	9.2%	9.2%
<u>Sample Position</u>					
V	H				
2	R5	0.23	0.26	0.24	0.28
2	+1-1/4		0.26	0.35	0.28
2	R6	0.16	0.33	0.39	0.34
2	+1-1/2		0.33	0.52	0.48
3	R0	0.18			
3	R5	0.17			
3	R6	0.12			
4	R0	0.11	0.20	0.20	0.26
4	R5	0.10	0.22	0.22	0.24
4	R6	0.06	0.29	0.37	0.28
6	R0	0.03	0.10	0.24	0.26
6	R0			0.11	
6	1/4		0.11	0.23	0.28
6	1/2		0.10	0.23	0.28
6	3/4		0.11	0.20	0.28
6	1		0.11	0.22	0.26
6	R5	0.03	0.10	0.12	0.23
6	1-1/4		0.13	0.20	0.24
6	R6	0.03	0.16	0.16	0.24
6	1-1/2		0.17	0.37	0.35
6	- 1/2				0.27
8	R0	0.006	0.05	0.10	0.19
8	R5	0.006	0.09	0.11	0.13
8	R6	0.006	0.10	0.14	0.15
10	R0	0.006	0.06	0.13	0.15
10	R5	0.006	0.05	0.14	0.15
10	R6		0.07	0.14	0.15
12	R0		0.01	0.10	0.14
12	R5		0.01	0.10	0.14
12	R6		0.00	0.13	0.14
15	R0		0.00	0.05	0.13
15	R5		0.00	0.07	0.10
15	R6		0.00	0.04	0.11
18	R0			0.01	0.11
18	R5			0.02	0.10
18	R6			0.03	0.12
21	R0			0.00	0.04
21	R5			0.008	0.05
21	R6			0.008	0.03
24	R0				0.01
24	R5				0.02
24	R6				0.03

TABLE III (CONTINUED)

Average Values of C/C₀ for No. 11 Glass BeadsB. Single Point Injection at 12 inches below that of Table III-A, 3-inch column

Air Velocity:		1.5ft./sec.
C ₀		9.5%
<u>Sample Position</u>		
V	H	
-24	R0	1.48
-24	1/2	1.43
-24	3/4	1.40
-24	1	1.30
-24	1-1/4	1.34
-24	1-1/2	1.45
-16	R0	1.78
-16	- 1/2	1.59
-16	- 1	1.39
-16	- 1-1/4	1.48
-16	1/2	1.70
-16	1	1.43
-16	1-1/4	1.54
-16	1-1/2	1.62
-12	R0	2.04
-10	R0	2.00
-10	R5	1.47
-10	R6	1.34
- 8	R0	2.31
- 8	R5	1.29
- 8	R6	1.14
- 6	R0	>2.26
2	R0	0.41
2	R5	0.41
2	R6	0.48
4	R0	0.40
4	R5	0.44
6	R0	0.24
6	R2	0.26
8	R0	0.21
10	R0	0.18
12	R0	0.11

TABLE IV
Average Values of C/C₀ for No. 13 Glass Beads
12 Tube Injection, 3-inch Column

Air Velocity (ft./sec.):	0.4	0.6	0.9	1.2
Sample Numbers:	298-313	250-268	123-147	317-326
C ₀	10.2%	7.8%	8.4%	4.9%
<u>Sample Position</u>				
V	H			
2	R0		1.24	
4	R0	0.80	1.02	0.97
5	R0	0.55		1.20
6	R0	0.48	0.83	0.95
7	R0	0.39		1.17
8	R0	0.24	0.64	0.56
10	R0	0.07	0.41	0.46
12	R0	0.004	0.21	0.36
14	R0		0.098	0.19
16	R0			0.21
18	R0			0.14
-11	R0			1.39
-11	R1			1.40
-11	R2			1.54
-11	R3			1.40
			(Sample No. 239-249)	
6	R0			0.62*
6	R1			0.67
6	R2			0.47
6	R3			0.58
6	R4			0.57
14	R0		0.098	0.15
14	R1		0.090	0.12
14	R2		0.064	0.10
14	R3		0.048	0.12
14	R4		0.090	0.17

*Note: This value disagrees strongly with that for the same sample position shown higher up in the column of the table. The two samples were taken under similar conditions but on different occasions and no explanation is known.

Sample Position gives: (1) Inches below injection level
 (2) Radius at which taken

TABLE V

Average Values of C/C_0 for Microspheres, H,
Single Tube Injection, 3-inch Column

Air Velocity (ft./sec.)	1.7	1.7		
C_0	8.5%	8.5%		
<u>Sample Position</u>		<u>Sample Position</u>		
V	H	V H		
-12	RO	1.21	6 +1/2	0.30
-12	+1	1.08	6 +3/4	0.23
-10	RO	1.42	6 +1	0.28
-10	+1	1.11	6 +1-1/4	0.31
- 8	RO	1.53	8 RO	0.21
- 8	+1	1.01	8 +1	0.22
- 6	RO	1.60	8 -1	0.24
- 6	+1	0.92	10 RO	0.17
- 4	RO	2.13	10 +1	0.17
- 4	+1	0.78	12 RO	0.14
- 2	+1	0.64	12 +1	0.13
- 2	-1	0.78	12 -1	0.15
0	+1	0.50	14 RO	0.10
2	RO	0.30	14 +1	0.10
2	+1	0.40	16 RO	0.10
4	RO	0.24	16 +1	0.08
4	+1	0.36	20 RO	0.04
6	RO	0.22	24 RO	0.02
6	-1	0.23	24 +1	0.02
6	+1/4	0.23		

TABLE VI

Average Values of C/C₀ for Microspheres, D, less Fines
12 Tube Injection, 3-inch Column

Air Velocity: (ft./sec.)		0.4	0.6	0.9	1.2
Sample Numbers:		361-384	385-408 467-486	409-436	437-466
C ₀		10.3%	7.4%, 8.0%	5.45%, 4.8%	3.6%
<u>Sample Position:</u>					
4	R0	0.68	0.71	0.51	0.42
6	R0	0.60	0.50	0.43	0.34
8	R0	0.47	0.43	0.35	0.30
10	R0	0.36	0.30	0.33	0.24
12	R0	0.30	0.23	0.21	0.18
14	R0	0.23	0.18	0.16	0.15
16	R0	0.18	0.16	0.12	0.11
18	R0	0.19	0.13	0.088	-
-11	R0	1.01	1.07	1.04	1.08
-11	R1	1.06	1.06	1.07	1.05
-11	R2	1.06	1.10	1.02	1.09
-11	R3	1.03	1.06	1.07	1.03
-11	R4		1.04	1.02	1.04
-11	average	1.04	1.07	1.05	1.06
- 6	R0	1.19			
- 6	R1	1.11			
- 6	R2	1.09			
- 6	R3	1.06			
- 6	R4	1.05			
6	R0	0.66	0.60	0.43	0.34
6	R1	0.72	0.63	0.43	0.45
6	R2	0.87	0.81	0.70	0.46
6	R3	1.21	0.79	0.75	0.61
6	R4	1.40	0.84	0.73	0.71
12	R0	0.30	0.22	0.26	0.16
12	R1	0.28	0.27	0.23	0.23
12	R2	0.43	0.44	0.37	0.27
12	R3	0.54	0.50	0.42	0.32
12	R4	0.52	0.47	0.36	0.38

Sample Position gives: (1) Inches below injection level
(2) Radius at which taken

TABLE VII

Average Values of C/C_0 for Microspheres, E,
Retained on 100 Mesh

12 Tube Injection, 3-inch Column

Air Velocity (ft./sec.):	0.4	0.6	0.9	1.2
Sample Numbers:	487-524	525-543	544-564	565-579
C_0	10.8%	8.3%	5.8%	4.5%
<u>Sample Position</u>				
4 R0	0.45	0.57	0.60	0.50
5 R0	0.21	0.46	0.50	
6 R0	0.14	0.30	0.43	0.41
7 R0	0.12	0.24	0.33	
8 R0	0.066	0.18	0.30	0.34
9 R0		0.15	0.27	
10 R0		0.11	0.20	0.29
12 R0			0.074	0.23
14 R0				0.099
-11 R0	1.01	1.01	1.10	1.13
-11 R1	1.05	1.00	1.12	1.16
-11 R2	1.06	1.03	1.18	1.21
-11 R3	1.10	1.09	1.13	1.27
-11 R4	1.05	1.12	1.16	1.18
-11 average	1.05	1.03	1.14	1.17

Sample Position gives: (1) Inches below injection level
 (2) Radius at which taken

TABLE VIII
Average Values of C/C₀ for Microspheres, F,
through 150 Mesh, less Fines
12 Tube Injection, 3-inch Column

Air Velocity: (ft./sec.)	0.4	0.6	0.9	1.2
Sample Numbers:	580-593	594-607 784-800	608-621	622-636
C ₀	10.6%	7.3%	5.1%	3.8%

Sample Position

1 R0		0.79		
1 R1		1.12		
1 R2		1.50		
1 R3				
1 R4		1.89		
1 -R1		0.92		
1 -R2		1.09		
1 -R3		1.49		
1 -R4		1.60		
2 R0		0.74		
4 R0	0.84	0.68	0.63	0.58
6 R0	0.725	0.545	0.47	0.465
8 R0	0.505	0.50	0.38	0.345
10 R0	0.43	0.33	0.31	0.345
12 R0	0.31	0.37	0.25	0.265
14 R0	0.26	0.22	0.18	0.195
16 R0	0.245	0.23	0.155	0.16
18 R0	0.177	0.167	0.15	0.12
-11 R0	1.01	1.065	1.05	1.05
-11 R1	1.04	1.015	1.10	1.04
-11 R2	1.075	1.045	1.08	1.08
-11 R3	1.07	1.025	1.05	1.08
-11 R4	1.03	1.035	1.03	1.08

Various Helium Rates with Air Velocity of 0.9 ft./sec.

C ₀ :	3.48%	5.0%	7.3%	10.1%
<u>Sample Position</u>				
4 R0	0.56	0.60	0.45	
6 R0	0.42	0.47	0.425	
8 R0	0.39	0.37	0.35	0.285
10 R0	0.33	0.30	0.29	
12 R0	0.23	0.25	0.225	
14 R0	0.205	0.18	0.21	0.17
16 R0		0.16	0.15	
18 R0		0.15	0.087	

Sample Position gives: (1) Inches below injection level
(2) Radius at which taken

TABLE IX

Average Values of C/C_0 for Microspheres, G, Fines Only12-Tube Injection - 3-inch Column

Air Velocity (ft./sec.)	0.4	0.6	0.9	1.2
Sample Numbers:	751-761	762-768	769-784	No runs made
C_0	10.6%	6.9%	7.65%	

Sample Position

4	RO	0.29	0.23	0.235
5	RO	0.24	0.195	0.20
6	RO	0.17	0.14	0.14
7	RO	0.17	0.12	0.11
8	RO	0.127	0.105	0.086
9	RO	0.104	0.084	0.078
10	RO	0.086		
-11	RO	0.98		0.98
-11	R1			0.99
-11	R2	0.97		0.98
-11	R3	0.97		

Sample Position gives: (1) Inches below injection level
(2) Radius at which taken

FIGURE 7
SAMPLE TRAVERSES
SINGLE TUBE INJECTION

NO. 11 GLASS BEADS

$u_0 = 0.6 \text{ ft./sec.}$

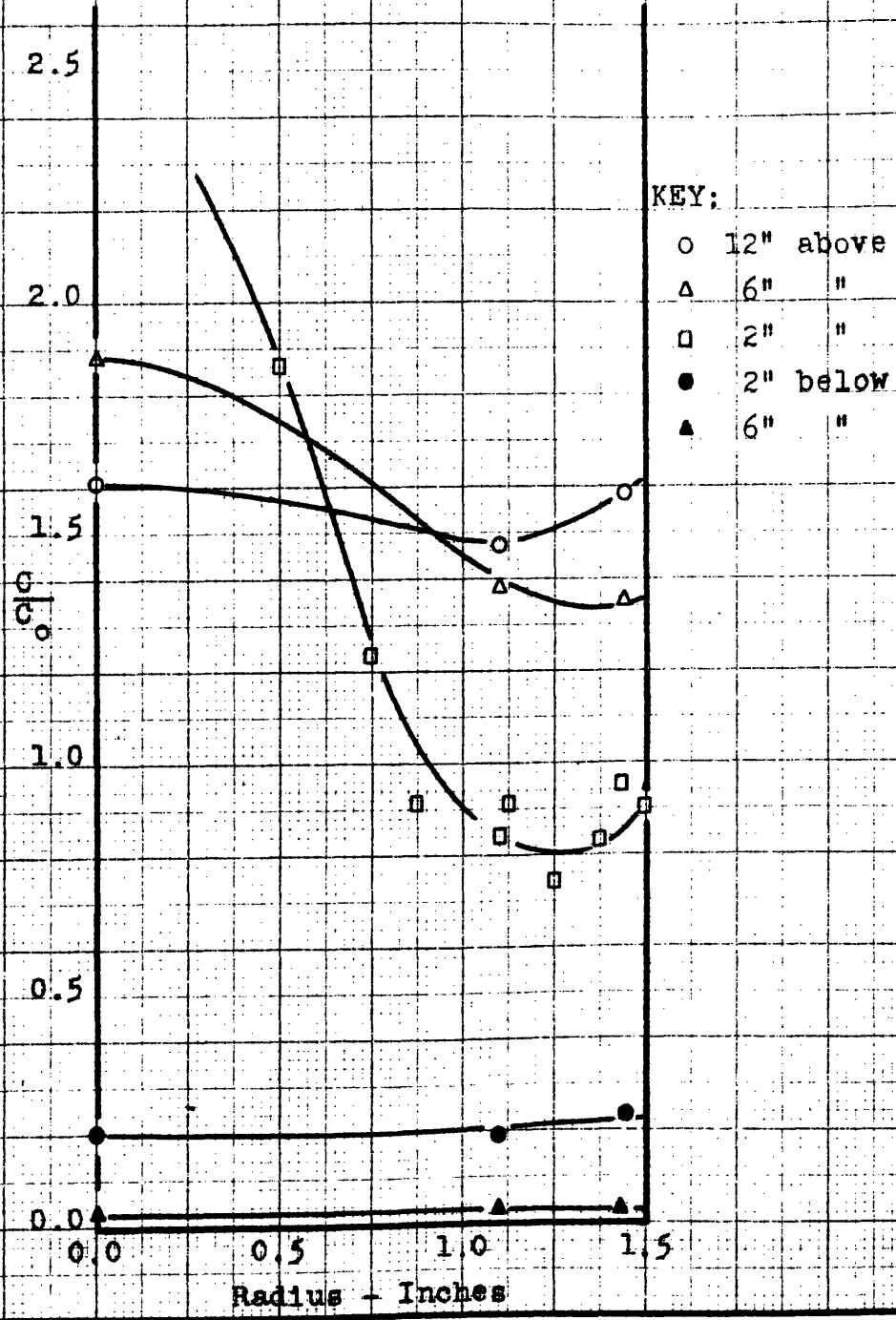


FIGURE 8
SAMPLE TRAVERSES
SINGLE TUBE INJECTION
NO. 11 GLASS BEADS
 $u_0 = 0.9 \text{ ft./sec.}$

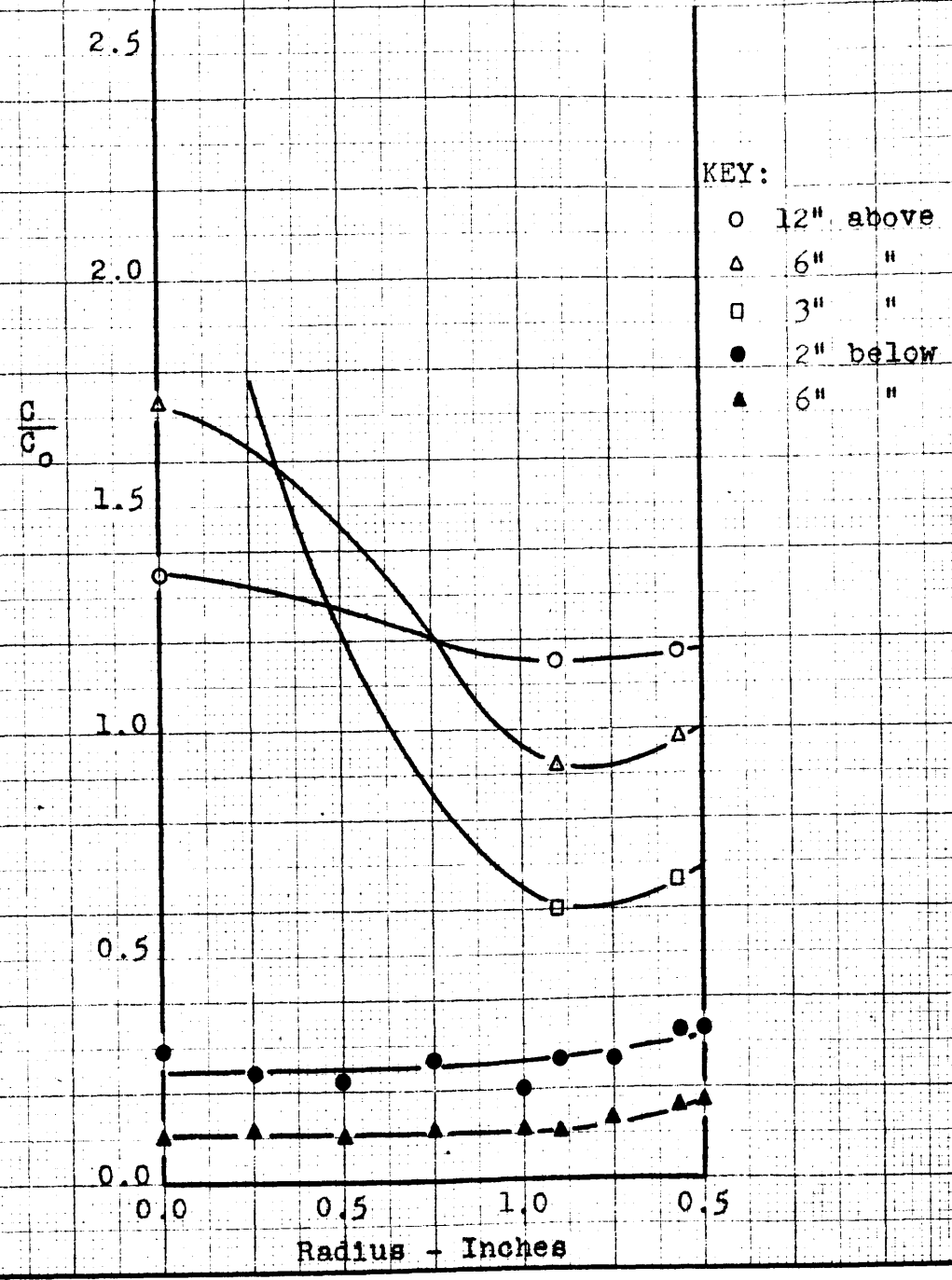


FIGURE 9
NO. 11 GLASS BEADS
SAMPLE TRAVERSES
SINGLE TUBE INJECTION

$u_o = 1.16$ ft./sec.

- KEY:
- 12" above
 - △ 6" "
 - 2" "
 - 2" below
 - ▲ 6" "

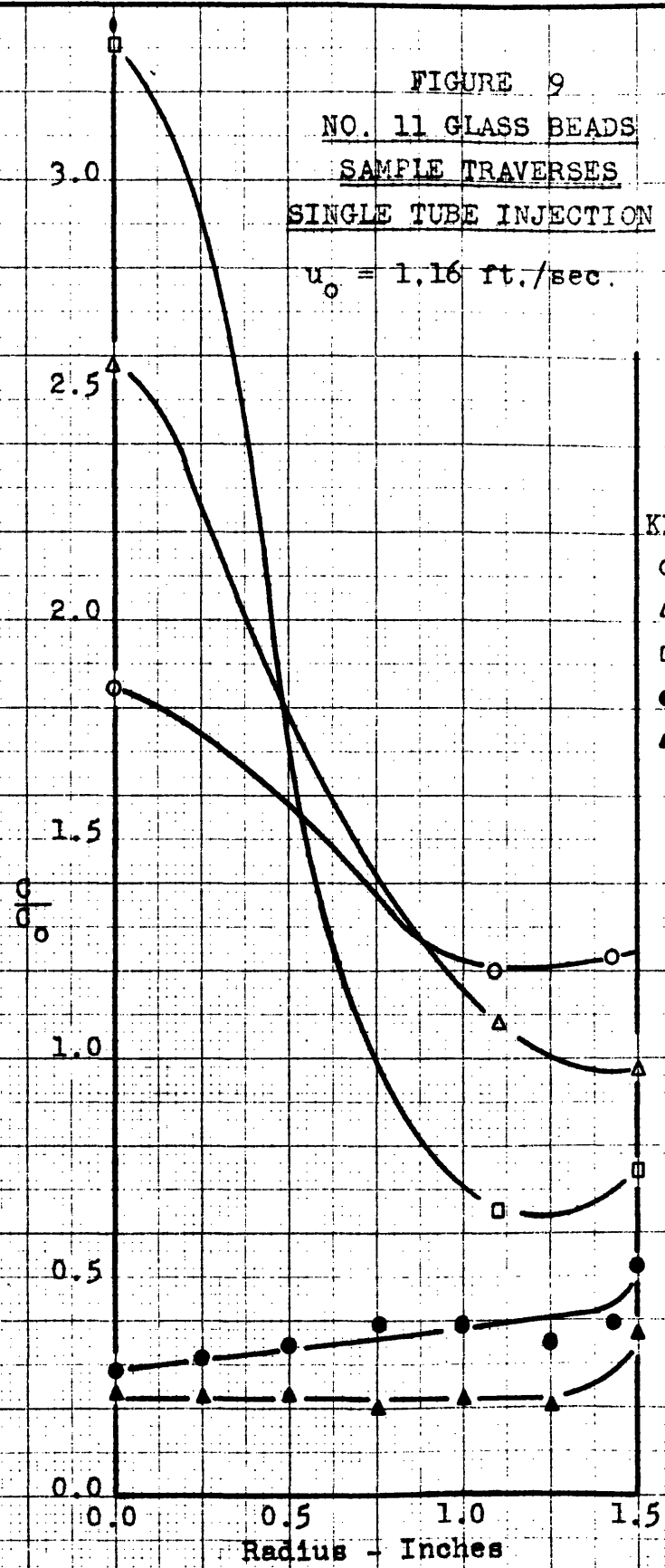
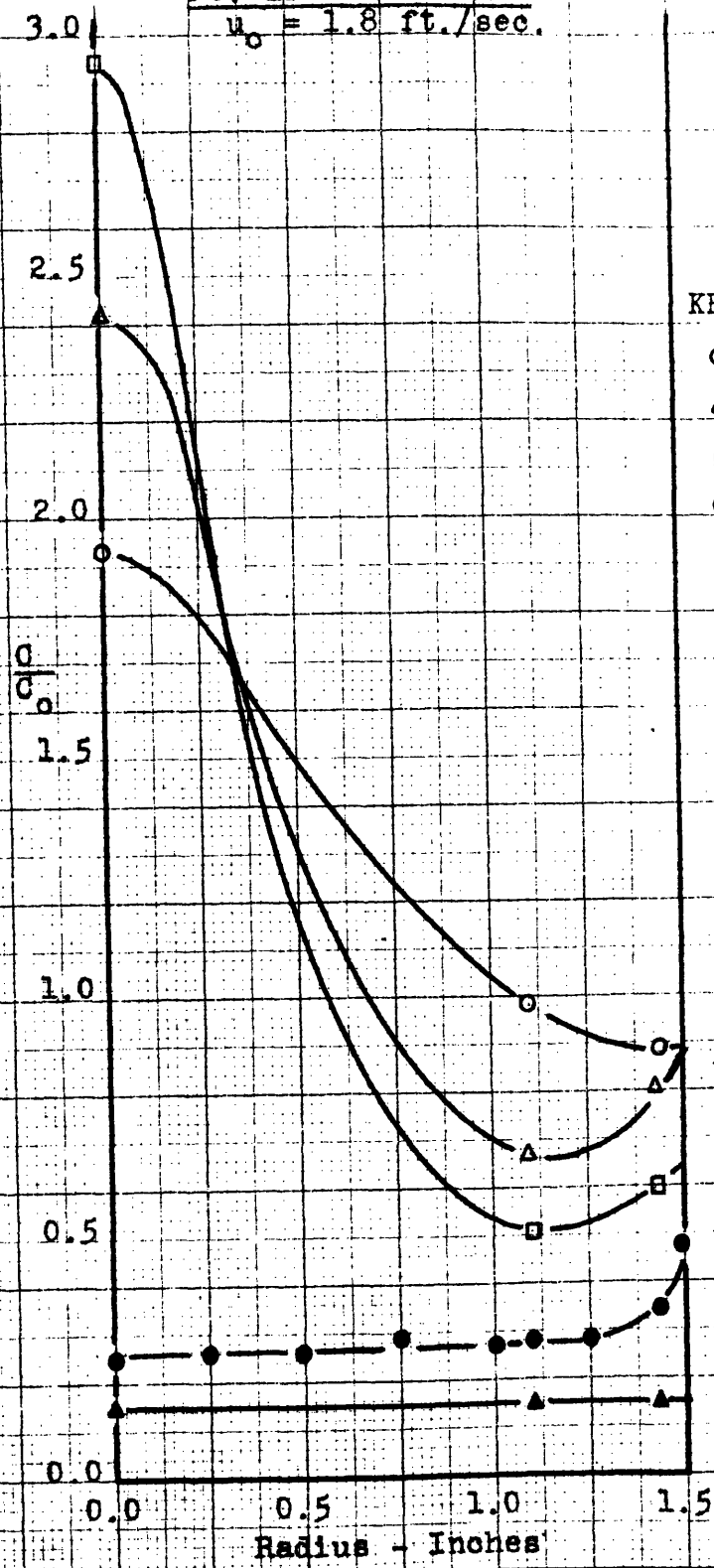


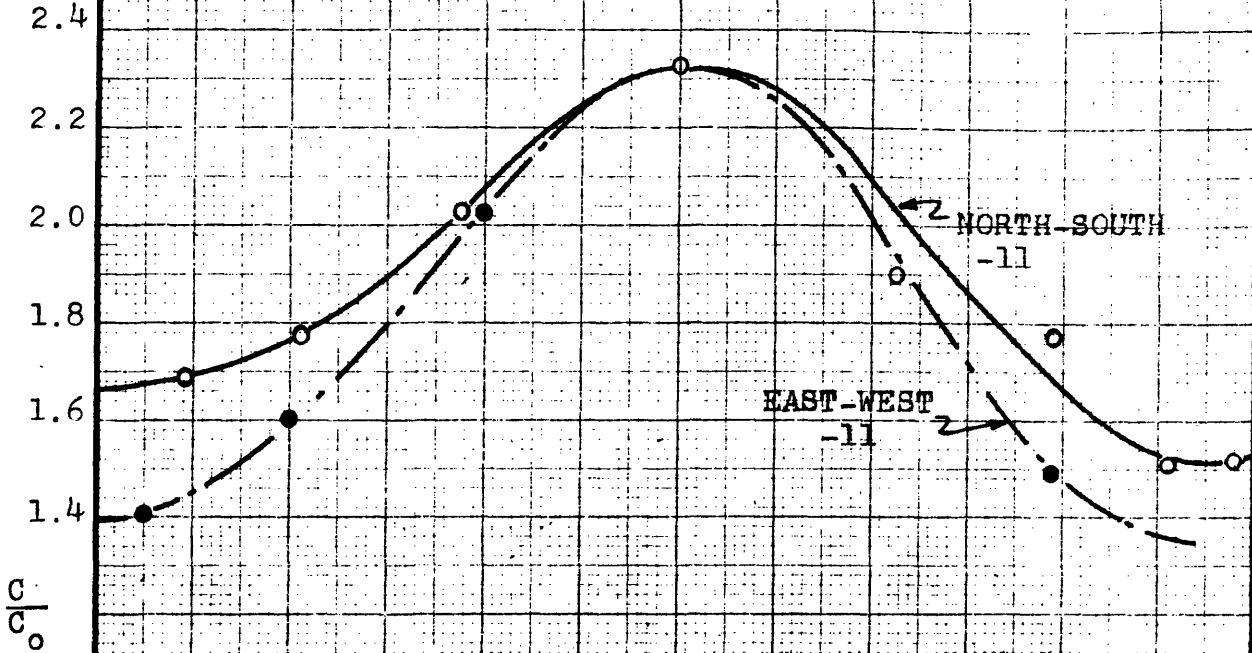
FIGURE 10
 SAMPLE TRAVERSES
 SINGLE TUBE INJECTION
 NO. 11 GLASS BEADS
 $u_0 = 1.8$ ft./sec.



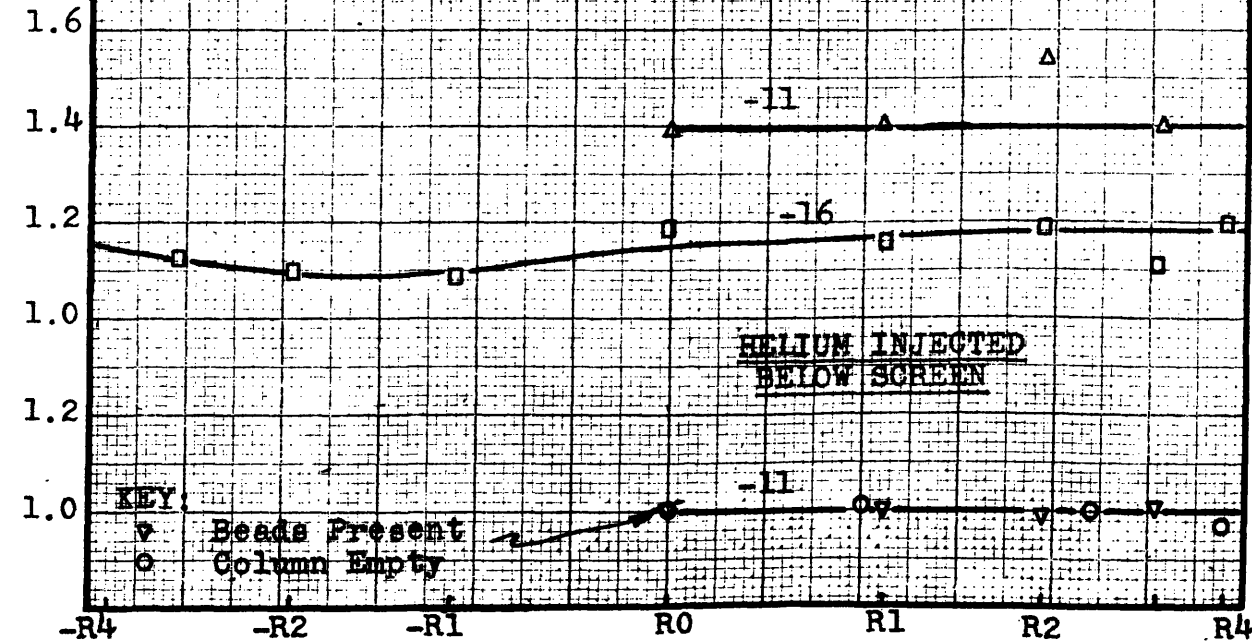
KEY:
 ○ 12" above
 △ 6" "
 ◻ 3" "
 ● 2" below
 ▲ 10" "

FIGURE 11
 NO. 13 GLASS BEADS
 SAMPLE TRAVERSES

SINGLE POINT INJECTION



12-POINT INJECTION



KEY:
 ▽ Beads Present
 ○ Column Empty

HELIUM INJECTED
 BELOW SCREEN

FIGURE 12

MICROSPHERES, ON 100 MESH, E

SAMPLE TRAVERSES

(11 IN. ABOVE INJECTION LEVEL)

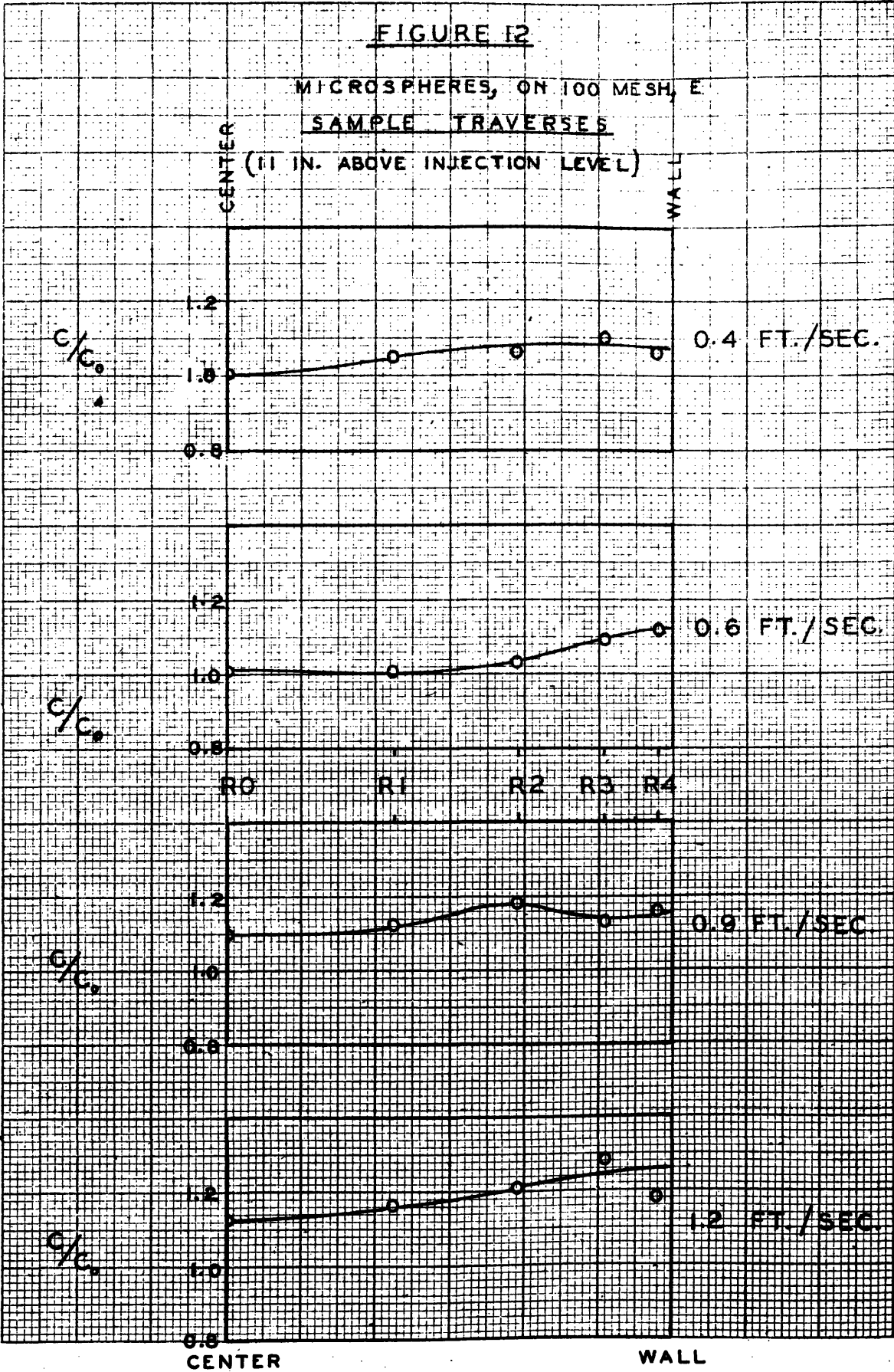


FIGURE 13

MICROSPHERES, LESS FINES, D

SAMPLE TRAVERSES

(NO. ON CURVE IS INCHES BELOW INJECTION LEVEL)

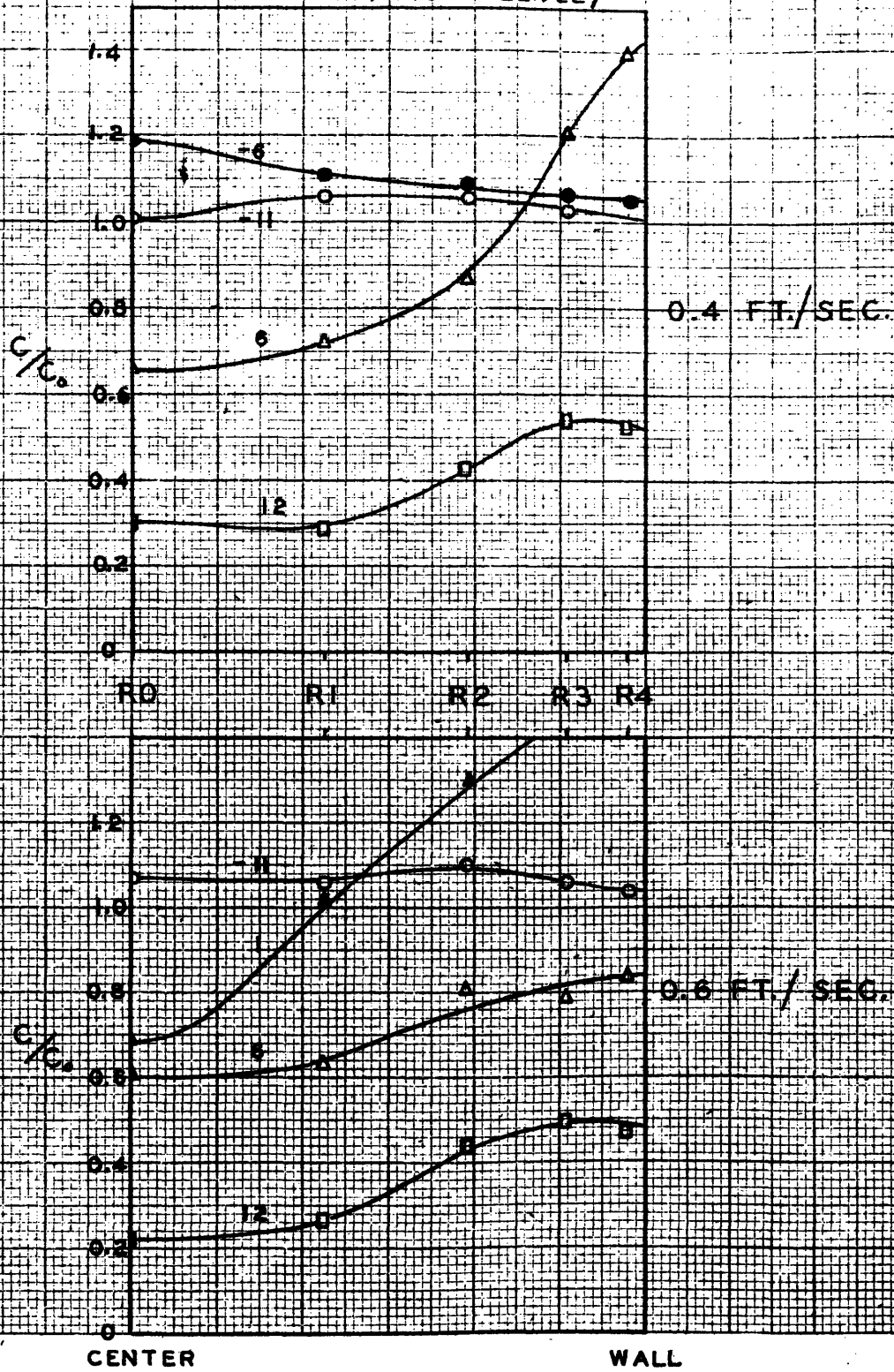
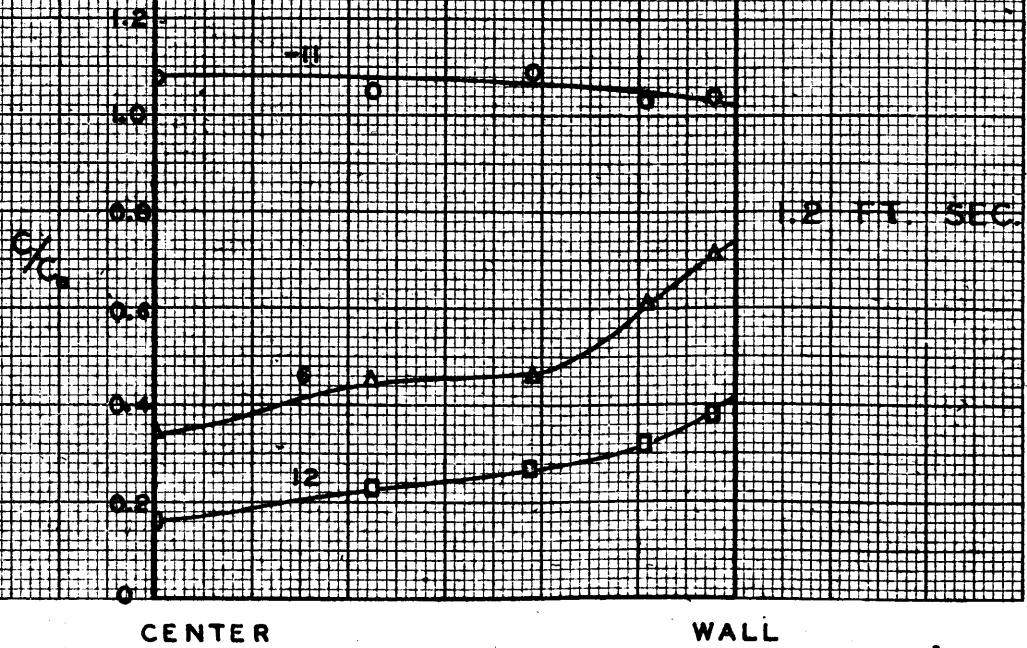
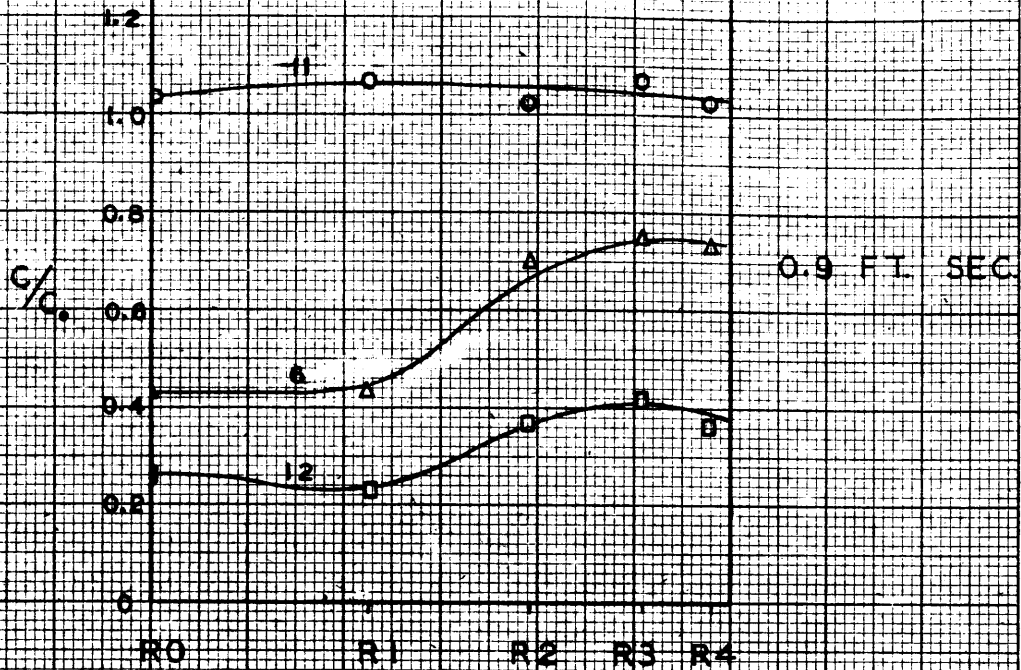


FIGURE 14

MICROSPHERES, LESS FINES, D
SAMPLE TRAVERSES

(NO. ON CURVE IS INCHES
BELOW INJECTION LEVEL)



CENTER

WALL

FIGURE 15

MICROSPHERES, THROUGH 150 MESH, F
SAMPLE TRAVERSES

(NO. ON CURVE IS INCHES
 BELOW INJECTION LEVEL)

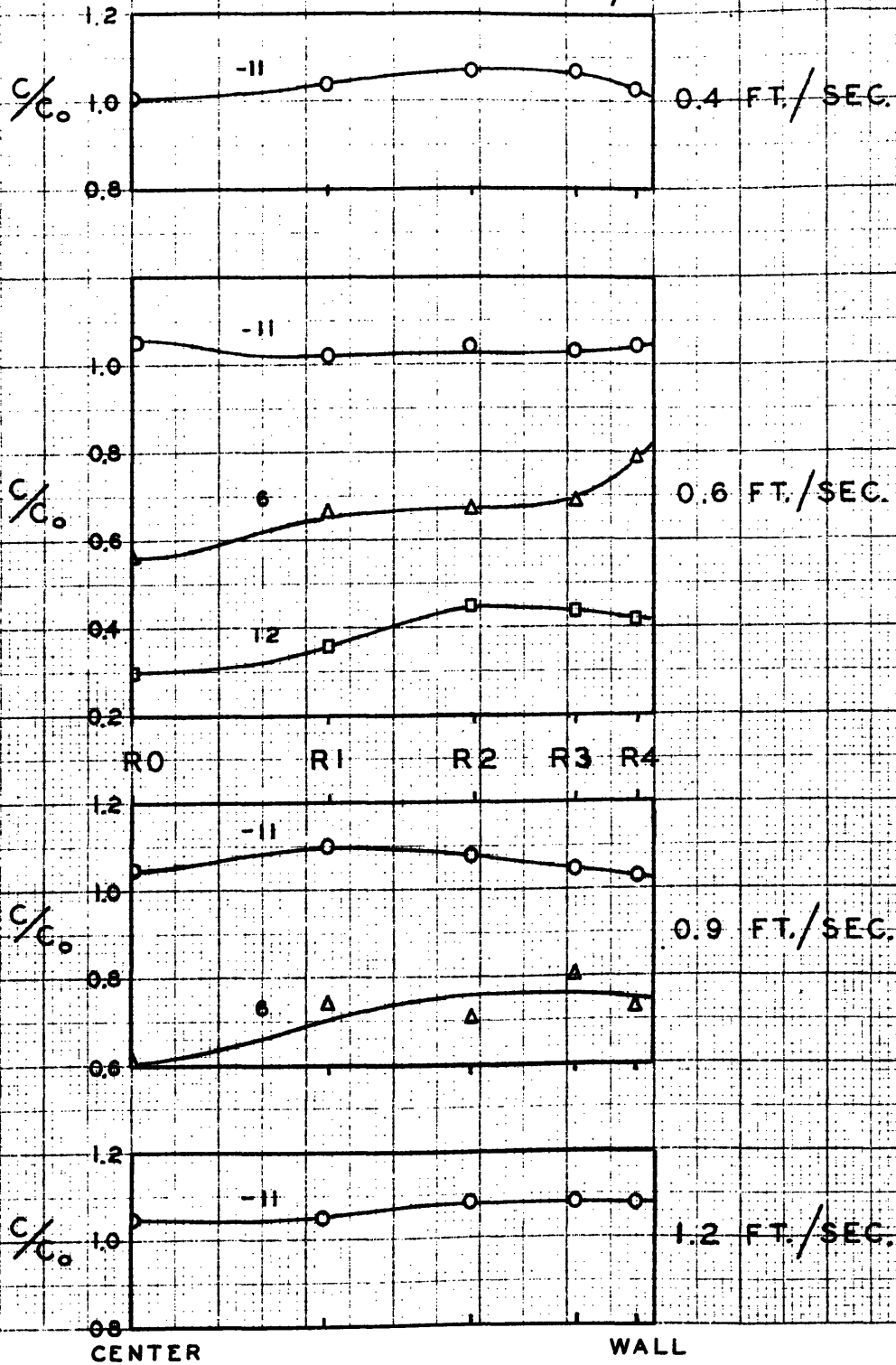


FIGURE 16

MICROSPHERES, FINES ONLY, G

SAMPLE TRAVERSES

(11 IN. ABOVE INJECTION LEVEL)

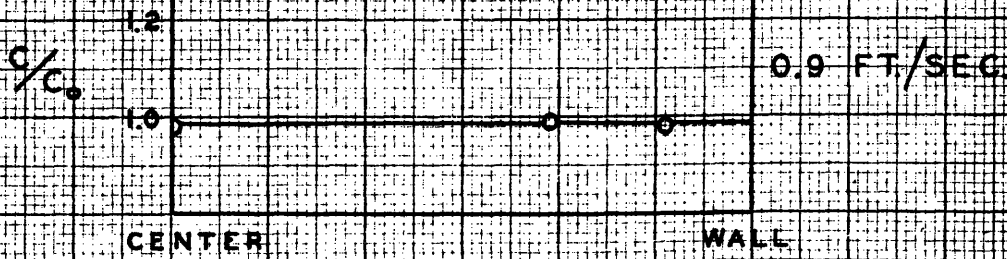
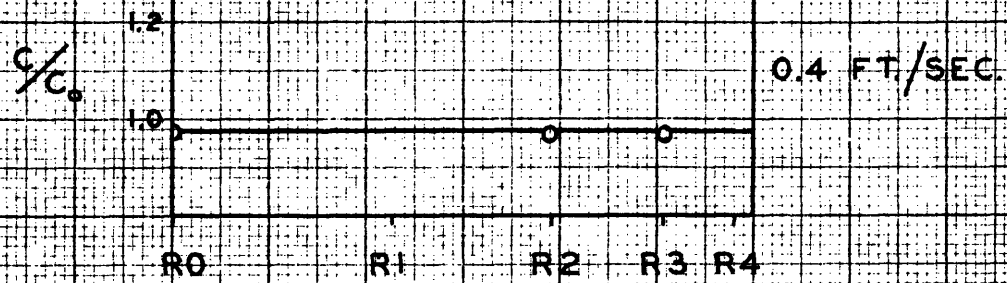


FIGURE 17

MICROSPHERES, M2, 150-200 MESH

$u_0 = 0.4$ ft./sec.

SAMPLE TRAVERSES

12-TUBE INJECTION

4-1/2-INCH COLUMN

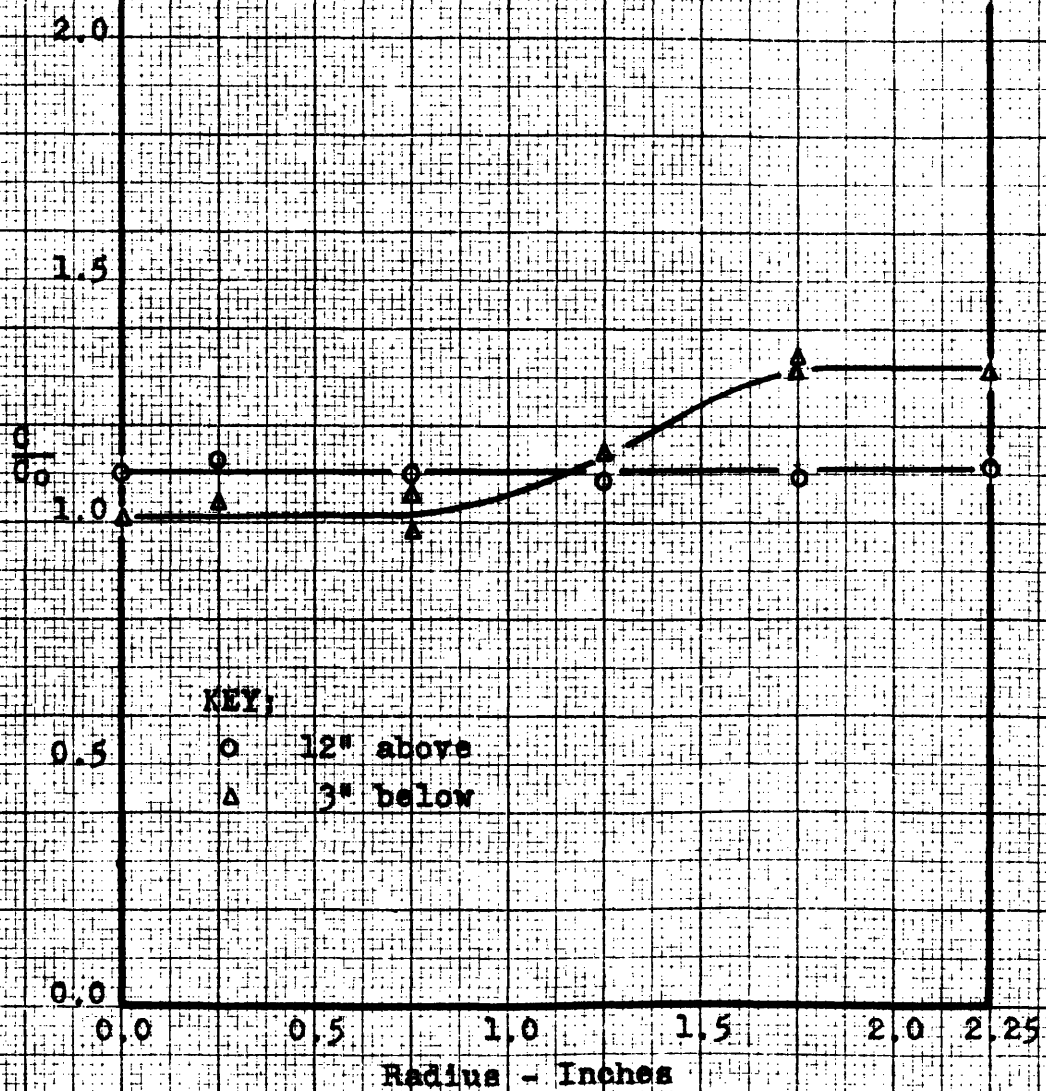


FIGURE 18
BACK-MIXING SAMPLING
NO. 11 GLASS BEADS
 $u_0 = 1.2 \text{ ft./sec.}$
Samples at $R = 0$

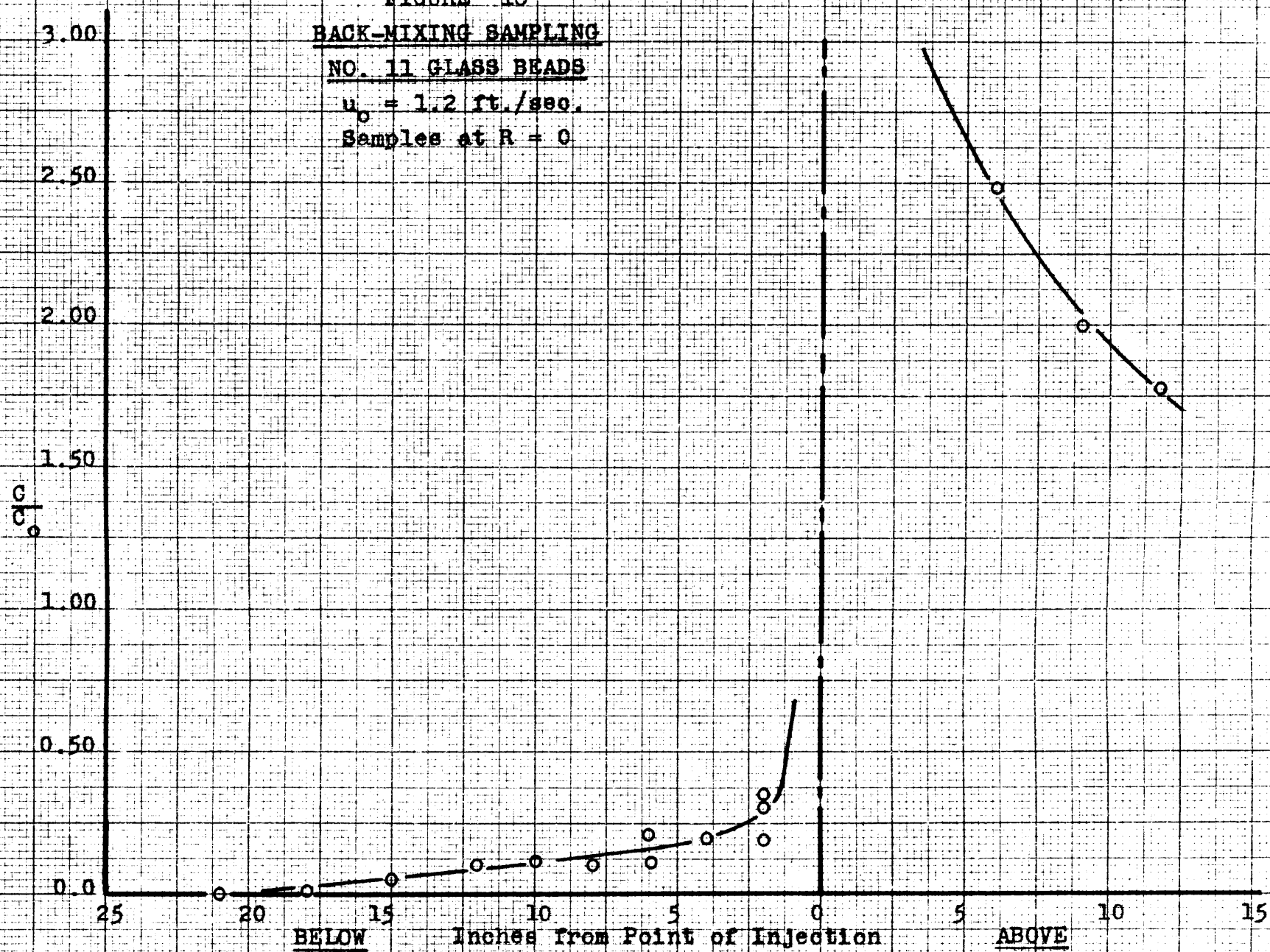


FIGURE 19

BACK-MIXING SAMPLING

NO. 11 GLASS BEADS

$u_o = 1.2$ ft./sec.

Samples at $R = 1.10$ inches

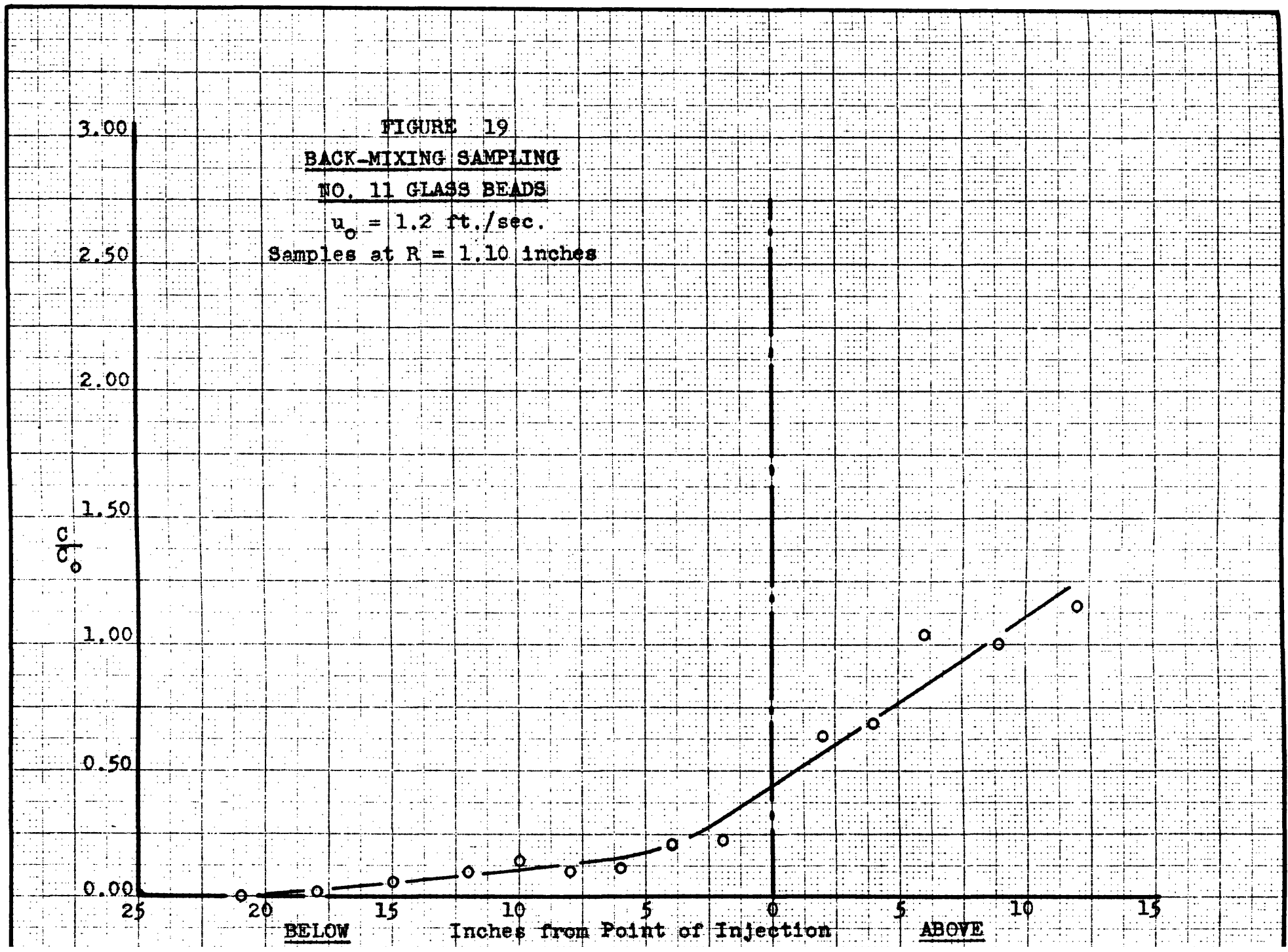
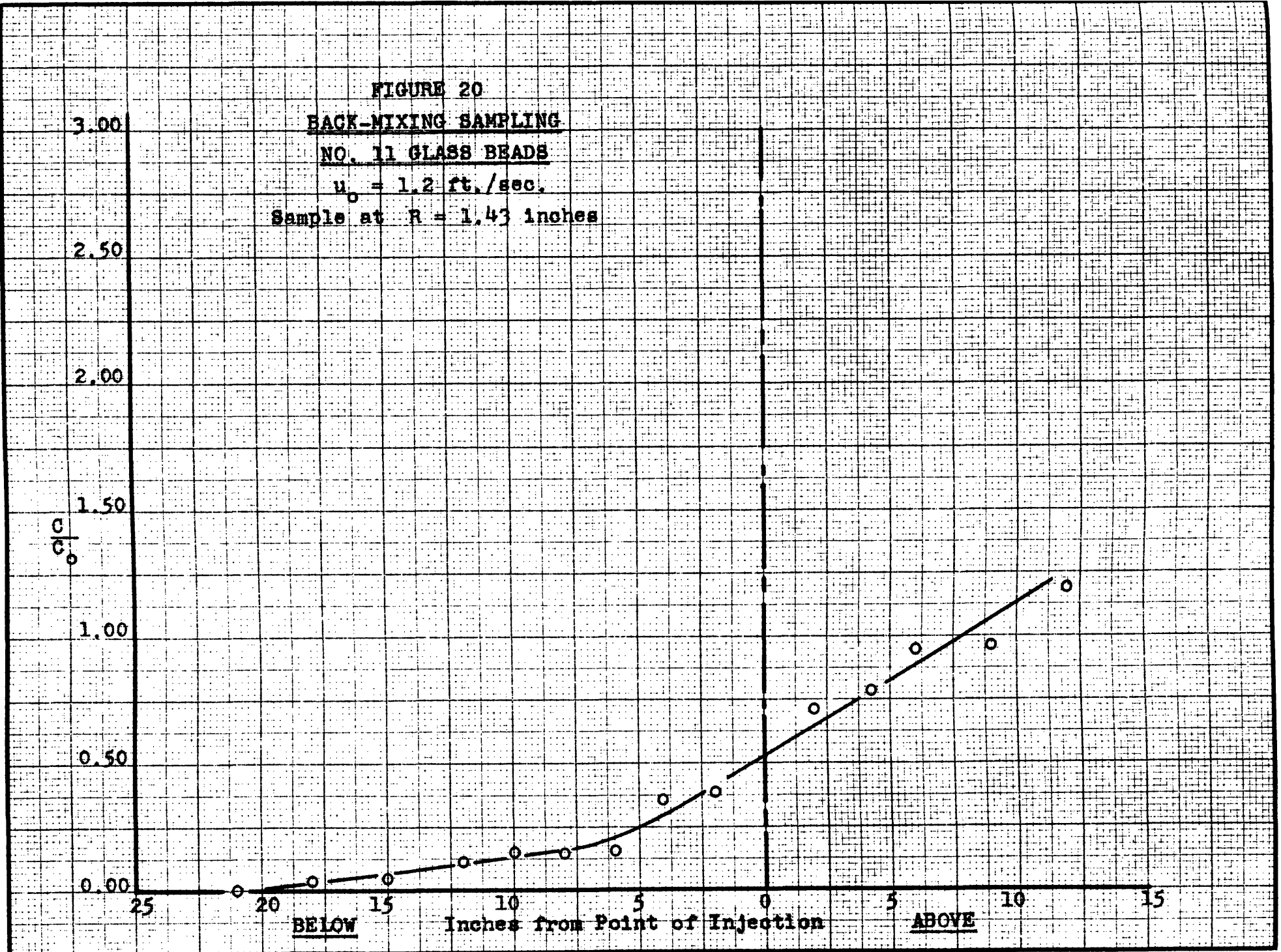


FIGURE 20
BACK-MIXING SAMPLING
NO. 11 GLASS BEADS
 $u_0 = 1.2$ ft./sec.
Sample at $R = 1.43$ inches

3.00
2.50
2.00
1.50
 $\frac{c}{c_0}$
1.00
0.50
0.00

25 20 15 10 5 0 5 10 15
BELOW Inches from Point of Injection ABOVE



bed ranged from 4-1/2 to 5-1/2 feet in height (see VII APPENDIX D). This corresponds to a length to diameter ratio, L/D , of about 20.

Since it was desired to study the physical mixing of the gases in fluidized-solids beds, helium was used exclusively as a tracer. Helium, with its extremely low adsorptivity (10) should reduce the effects of adsorption to a minimum.

All the plots shown express the gas composition as the ratio of the concentration, C , existing at some point to the concentration, C_0 , in the exit stream; this dimensionless ratio, C/C_0 , was used to eliminate the effects of minor variations in C_0 .

Calculation and Reliability of Results

In the results listed in Tables III and V, the values of C are the analyses of the gas samples obtained using the gas density balance; C_0 represents the calculated composition of the gas leaving the cyclone based on the helium and air orifice readings. The details of the method of calculation are shown in VII APPENDIX C. An error analysis of one run (see VII APPENDIX C) showed that the maximum error in C_0 was about 1/2 of 1% of helium and in C was about the same, giving a maximum error in C/C_0 of 9%. This value is probably high compared to the average error but does suggest that there may be some

scatter due only to errors introduced in taking readings.

The data listed in Tables IV and VI through IX are based entirely on gas analyses performed in the electric analyzer. C is the analysis of the gas from the point being studied and C_0 is based on the analysis of a sample of gas drawn from the cyclone separator: this latter value was checked by the stoichiometric value based on the orifice readings. Using the electric analyzer, it was possible to determine the composition of a gas sample to within about 0.05% helium; for the sample in the error analysis cited above, the error in C/C_0 would be about 0.5%. Thus, it was felt that analysis of the exit gas by the electric analyzer would provide a more reliable basis for C_0 than the orifice calculations.

When traverses were made, symmetry of mixing about the axis of the column was assumed, and in most cases samples were only taken along one-half a diameter. A few traverses were made across the whole diameter and are presented in Figure 11 which shows that this was a reasonable assumption.

Since small diameter tubing was used for the injection of the tracer gas, the superficial velocity of the gas leaving the tube was considerably higher than

the superficial velocity of the air in the column. In the single glass tube (0.141 inches I.D.), which directed the tracer upwards along the axis of the Lucite tube, the superficial velocity of the helium ranged from 50 to 80 ft./sec. as compared to superficial air velocities of 0.6 to 1.8 ft./sec. In the 12-point injection system, the total cross section area for flow of the 12 steel tubes (0.065 inches I.D.) was 2.55 times that of the single glass tube, and, in addition, use of the electric analyzer permitted the use of lower values of C_0 . Therefore, for a given air velocity, the injection velocity of the tracer in the multi-tubular arrangement was one-third, or less, that of the single tube. In the 12-tube system, the helium was injected in a plane perpendicular to the axis of the column. When the helium was not flowing, there was no noticeable change in the character of fluidization; when the helium was being injected into the bed, the only change noticed was that large slugs were generally broken as they passed the injection level.

Due to the plug of wool in the end of the sampling tube, the time of sampling in most cases was about 30 seconds. No attempt was made to keep the time constant from sample to sample. Instead the sample was drawn until the pressure in the sampling train was substantially

atmospheric; this time varied slightly from sample to sample. In general, the reproducibility obtained in repeat samples was good and this was taken to mean that the sampling time was sufficient to smooth out any fluctuations in gas composition that might occur over short intervals. The following table shows a few cases of repeated samples:

TABLE X
Reproducibility of Sampling

Solids	u_o (ft./sec.)	Sample Position		C/C _o
		V	H	
Microspheres, D	0.4	12	RO	0.30, 0.26 0.26, 0.26
	0.9	12	RO	0.21, 0.26
	1.2	12	RO	0.15, 0.27 0.16, 0.17
No. 13 Glass Beads	0.4	8	RO	0.15, 0.30 0.26, 0.24

Usually, repeat samples gave analyses agreeing within about 10 to 15%. In cases where the sample was judged to be inconsistent with the composition of samples taken from positions near by, at least two repeat samples were taken as a check.

Spherical glass beads and petroleum cracking microspheres were the only solids employed in these gas mixing

studies. Preliminary work on filtrol clay and finely divided anthracite coal (100 to 200 Mesh) showed that the losses due to elutriation amounted to about 10% of the total charge in 1/2 hour; this could not be considered batch operation. In addition, fines from both these materials plugged the sample filter completely, preventing gas withdrawal.

2. Sampling Problem and Gas Flow Pattern

Figures 18, 19, and 20 show the vertical gradients in gas composition occurring when the single point injection system was employed. Figure 18 gives the composition of the gas along the axis of the tube at points above and below the point of injection. As would be expected, the concentration immediately above the injection is very high and then falls off farther up the column as the center stream becomes mixed with the surrounding gas. Below the point of injection, helium is detectable for over a foot, indicating that there is considerable back-mixing of the gases. Figures 19 and 20 show similar data taken at distances of 1.10 and 1.43 inches from the center of the 3-inch I.D. column. Below the injection level, these figures show trends similar to that of Figure 18, but above this point the trends are reversed. Considering the system employed, these differences are to be expected.

The data presented in Figures 7, 8, 9, 11, and 12, concerning concentration gradients across a fluidized bed above the level of injection, require examination. As indicated in Figures 18, 19, and 20, the concentration at the center of the tube just above the level of injection is very high, decreasing at greater radii. It can be seen that the concentration gradient goes through a minimum at some point between the center of the tube and the wall. However, the interesting point is that at higher levels in the bed, the concentration of tracer at every point across the bed appears to be significantly greater than the exit concentration; C/C_0 averages about 1.5 to 1.8. Some explanation is required for this apparent violation of a material balance.

Analysis of samples of gas taken from the cyclone separator agreed with the calculated exit composition within 1 or 2%. Thus, consideration of leaks and faulty analysis as an explanation of the anomaly was eliminated.

Several different possible causes of the irregularity were investigated and the results of these studies will be presented in the following paragraphs. Recycling of helium within the bed, due to adsorption of helium on the solids, was deemed unlikely considering the low adsorptivity of helium compared to oxygen and nitrogen and

the nature of the glass beads used.

The effect caused by disturbance of the flow pattern within the bed by the upward injection of the tracer through the single injection tube was studied. The position of the injection tube was reversed, so that the tracer was injected downward along the axis of the tube. The results of this experiment are shown in the following table:

TABLE XI

Downward Injection of Tracer

No. 13 Glass Beads
 $u_0 = 0.9$ ft./sec.

Position		$\frac{C}{C_0}$
V	H	
-11	R0	1.64
-11	-R1	1.91
-11	-R2	1.47
-11	-R3	1.46
-11	R1	1.96
-11	R2	1.41
-11	R3	1.49
-11	R4	1.46

Use of the 12-point injection system with No. 13 Glass Beads gave a flatter concentration profile than did the single tube (see Figure 11), but at 11 inches above the injection level, C/C_0 was still 1.40. It would be expected that these three different methods of injection would alter the flow pattern differently, and yet the average values of C/C_0 above the point of injection re-

mained approximately the same for all three. Therefore, it is felt that disturbance of the flow pattern was probably not the primary source of error in C/C_0 .

Explanations based on faulty sampling were next explored. Due to the differences in the molecular weights of helium and the principal constituents of air, it was conceivable that the small sampling tube, with its tightly packed wool filter, would lead to barrier diffusion, and hence to selective sampling of helium. To check this, the sample probe was placed in a test-tube filled with glass beads. The test-tube was then lowered into the cyclone, where the gas composition was known to agree with the orifice readings. Two samples were taken and the values of C/C_0 were 1.01 and 0.98; on this basis the barrier diffusion explanation was rejected.

Figure 11 shows that the average tracer concentration obtained at a level 11 inches above the plane of the 12-point injection was slightly less than that of the single tube injector, and that the average value of C/C_0 had dropped from 1.40 at 11 inches above, to about 1.16, 16 inches above the twelve steel tubes. In another experiment tracer was injected into the air stream below the 200-mesh screen in the conical section at the bottom of the Lucite column. Figure 11 shows the result-

ing composition traverses for the cases when glass beads were present and when the column was empty. These findings indicate that the composition of a gas sample withdrawn from within a fluidized bed depended on how well the gases at the point of withdrawal were mixed. When the gases were well mixed by introduction into the cone below the screen before entering the bed, no discrepancy between gas analyses and a material balance was noticed; when more time was allowed for mixing, by withdrawing the sample farther from the injection level, less discrepancy was present. From these results, it appeared that the gases in the fluid bed were not of uniform composition at any particular point, and that this variation in composition was in some way responsible for the anomalous results obtained with internal sampling.

Two possibilities were immediately evident. It was conceivable that the gas was being drawn from the region near the axis of the column (where the concentration of helium was highest) even in cases where the end of the sample tube was near the wall. This would happen if there was little gas flow through the solid in this region under normal conditions. The second possibility was based on the difference in the density of helium and air and the finding that there apparently were regions

where these two gases were not well mixed. If air and helium are subjected to the same pressure drop over a certain path under conditions of turbulent flow then the helium will flow faster than the air due to its lower density. There was probably a slight pressure gradient in the bed in the vicinity of the tip of the probe during sampling. (It was estimated from the time of sampling that the sample tube draws gas from a distance of about 3 mm. from its tip.) Thus, there was a possibility that a sample drawn from non-uniform mixtures of helium and air would give an analysis of the tracer higher than the average composition in the bed at the point of sampling. Both of these potentialities were investigated by varying the rate of sampling; if either of these explanations were correct, lower values of C/C_0 should have resulted with decreasing sampling rates. The results of these tests are shown in Table XII which indicates that the value of C/C_0 did not decrease as the rate of sampling was decreased.

In order to find out if there were momentary differences in gas composition at any point in a fluidized bed, samples of gas were taken preferentially from regions of dense solid phase and lean solid phase. In brief, the method consisted of pinching the small tube leading from the sample probe with a pair of pliers until

TABLE XII

Effect of Sampling Time on Gas Composition

No. 13 Glass Beads, A
 $u_0 = 0.9$ ft./sec.
 Single Glass Injection Tube, pointed upward

<u>Sampling Time</u>		<u>Values of C/C₀</u>		
		<u>38-40 sec.</u>	<u>380 sec.</u>	<u>540 sec.</u>
<u>Sampling Position</u>				
-11	R1	2.04		2.38
		1.92		2.30
		2.13		
		2.18		
		2.13		
		Ave. 2.08		Ave. 2.34
-11	R2	2.36	2.14	
		2.43	2.21	
		Ave. 2.40	Ave. 2.18	

a bubble (region of "lean" phase) passed by; the tube was released while the bubble surrounded the tip of the probe and was pinched again as the bubble passed on. The same technique was employed to draw samples from the dense phase. This method was admittedly crude, and the analyses of the samples represent the gas composition of several bubbles or regions of high solids density. Nevertheless, the analyses should tend toward the gas composition of the dense and lean phases; the results of such sampling are presented in Table XIII. The concentration of tracer in the lean phase or bubbles, was in every case found to be less than that in the dense phase and in the normal sample. The helium concentration in the dense phase was approximately the same as in the normal sample: in the cases where any significant difference between these two existed, the dense phase sample gave a higher concentration of tracer than did the normal sample. Due to the crude sampling technique, the actual differences in gas composition are believed to be greater than those obtained.

Such selective sampling was only feasible with the glass beads and large microspheres. Fluidization of these solids gave large bubbles and slugging, while with finer microspheres the bubbles were so small as to render impossible selective sampling by the technique described

TABLE XIII

Void and Solids SamplingValues of C/C_0

A. No. 13 Glass Beads, Single Point Injection, Sample Numbers 159-170.

Air Velocity (ft./sec.)	Sample Position		Normal Sample	Lean Phase Sample:	Dense Phase Sample:
0.9	-11	R2	2.14	1.34	1.50
	-11	R2	2.36	1.32	3.15
	-11	R2	2.21		2.04
	-11	R2	2.43		
			Ave. <u>2.28</u>	Ave. <u>1.33</u>	Ave. <u>2.23</u>
0.9	-11	R4	1.52	0.92	
	-11	R4		0.80	
			Ave. <u>1.52</u>	Ave. <u>0.86</u>	

B. No. 13 Glass Beads, 12-point Injection System, Sample Numbers 313-5, 273-90, 320-26.

Air Velocity (ft./sec.)	Sample Position		Normal Sample	Lean Phase Sample:	Dense Phase Sample:
0.4	5	RO	0.55	0.37	
	5	RO		0.27	
			Ave. <u>0.55</u>	Ave. <u>0.32</u>	
0.6	10	RO	0.44	0.19, 0.16	0.61, 0.53
	10	RO	0.38	0.22, 0.18	0.56, 0.75
	10	RO		0.18	0.78, 0.73
	10	RO			0.40, 0.39
			Ave. <u>0.41</u>	Ave. <u>0.18</u>	Ave. <u>0.59</u>
1.2	10	RO	<u>0.89</u>	<u>0.65</u>	<u>0.95</u>
1.6	10	RO	0.95	0.67	0.96
	10	RO	0.69	0.22	
			Ave. <u>0.82</u>	Ave. <u>0.45</u>	Ave. <u>0.96</u>

TABLE XIII (CONTINUED)

C. Microspheres on 100-Mesh, Sample Numbers 496-573

Air Velocity (ft./sec.)	Sample Position	Normal Sample	Lean Phase	Dense Phase
0.4	6 RO	0.12, 0.16 0.18, 0.11 0.06, 0.12 0.14, 0.19 Ave. <u>0.135</u>	0.14 0.11 Ave. <u>0.125</u>	0.16 Ave. <u>0.16</u>
0.9	6 RO	0.43 0.46 0.37 0.36 0.30 Ave. <u>0.38</u>	0.176 0.26 Ave. <u>0.22</u>	
1.2	8 RO	0.34 Ave. <u>0.34</u>	0.30 0.24 Ave. <u>0.27</u>	0.32 Ave. <u>0.32</u>

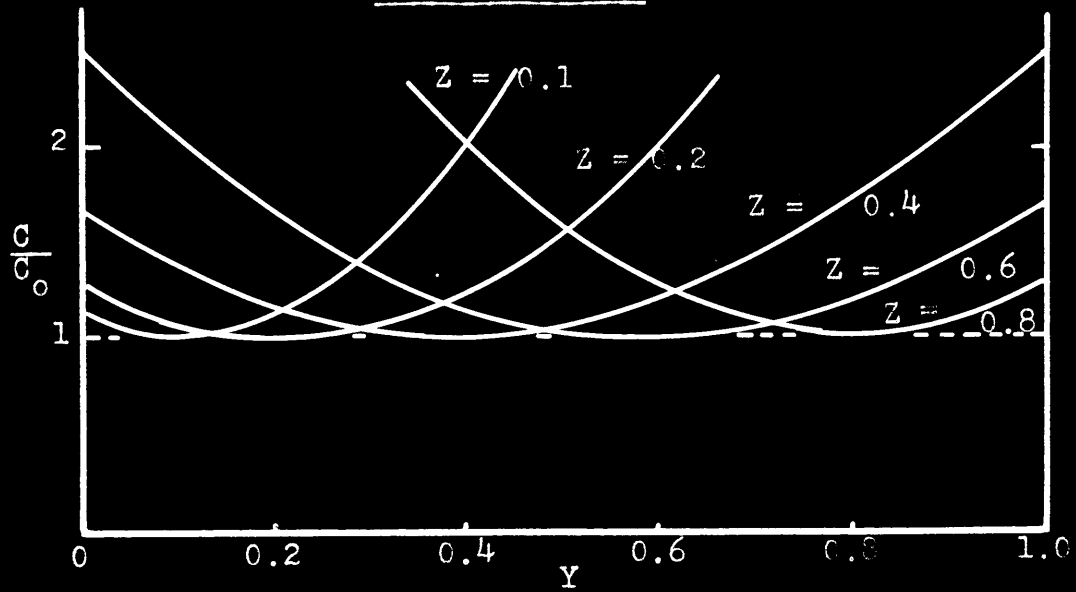
above.

With this knowledge that differences in gas composition in the dense and lean phases can, and do, exist, it can be shown that gas samples drawn from within a fluidized bed may not represent the average composition of all the gas passing the sample probe. Let the fraction of the bed occupied by the lean phase be called "Y", and the fraction of the total gas (tracer and air) flowing through the lean phase be "Z"; the fraction of a normal sample drawn from the lean phase is assumed to equal Y. Then for a normal sample drawn from above the injection level,

$$\frac{C}{C_0} = \frac{Y^2}{Z} + \frac{(1-Y)^2}{(1-Z)} \quad (1-IV)$$

(See VII APPENDIX B.) This equation is plotted in Figure 21, which shows that only when $Y=Z$ does C/C_0 equal unity above the point of injection; in all other cases where no gas transfer occurs between dense and lean phases, the value of C/C_0 is greater than unity. While no exact information concerning the values of Y and Z are available, if the gas in the bubbles rises faster than that in the dense phase, as seems probable, then Z is greater than Y, and any normal samples withdrawn from above the point of injection would be in error if the transfer of gas between dense and lean phases is slow.

FIGURE 21
SAMPLING ERROR



While the proof presented does not apply directly to regions below the point of injection, consideration of the experimental technique and bed action indicates that when sampling error is present above the point of injection it is also present below the point of injection.

In the mixing experiments, there undoubtedly was some transfer of gas between dense to lean phases, and such transfer would reduce the error due to sampling. However, it is believed that this sampling error is inherent to fluidized beds and is the cause of the anomaly concerning values of C/C_0 above the point of injection. Furthermore, the fact that the results do indicate this type of error, coupled with the actual dense and lean phase sampling, is taken to mean that significant differences in gas composition between dense and lean phases, once created, can exist in fluidized beds. This is of importance not only in the studies of gas mixing but also is pertinent to chemical reaction studies carried out in fluidized beds.

Gas Flow Pattern

Before continuing with an examination of the effect of this sampling error on gas mixing studies, it will be necessary to discuss the evidence concerning the gas flow pattern found in fluidized beds.

The radial concentration gradients presented in Figures 7 through 15 lead to the conclusion that there was a definite flow pattern of the gas. The curves indicate that the probable flow of gas was upward in the center of the bed and downward along the walls, with varying amounts of side-mixing between these two zones.

Visual examination of fluid beds shows that the motion of the solids is downward at the walls, and hence upward in the middle, but this would not necessarily entail any significant downflow of gas. If, however, this were the gas pattern, then it would be expected that immediately above the point of injection, the concentration of tracer would be high and gradually decrease on mixing with the surrounding gas. Thus, there would be a relatively high concentration of tracer at all levels above the injector, and the gas along the wall would be flowing downward giving a high concentration of tracer in the gas at the wall below the injection level. Figures 7 through 10, which set forth results obtained with No. 11 glass beads, show that below the point of injection the concentration profile was quite flat in the central portion, rising slightly near the walls. This would indicate that there was flow of gas from the region adjacent to the wall, and that the transfer of gas was

relatively rapid. However, in the figures showing the microsphere data, much steeper gradients are found between the center and the wall at levels below the plane of injection, implying a much slower transfer of gas from the walls to the center. This picture of gas flow agrees with the work of Ciborowski (6) on solid mixing.

Additional information concerning the error due to sampling can be obtained from a calculation of the gas velocities required along the wall and in the core of the bed in order to maintain the concentration profiles observed below the point of injection. This involves the use of the circulation pattern described above as the mechanism of gas mixing. If it is assumed that a region of upflow and a region of downflow exist, and that the gas velocity and composition across both of these core and annular spaces are uniform, then it is possible to estimate the core and annular velocities by using the following equations:

$$\frac{u_C}{u_o} = \frac{2.25 C_A}{R_C^2 (C_A - C_C)} \quad (2-IV)$$

$$\frac{u_A}{u_o} = \frac{2.25 C_C}{(2.25 - R_C^2)(C_A - C_C)} \quad (3-IV)$$

where R_C = assumed radius of core, inches, and subscripts A and C refer to the annulus and core, respectively. (See VII APPENDIX C.) The effect of the assumed values for the radius of the core, R_C , can be seen in these two equations. For reasonable values of R_C , which can be estimated from Figures 13, 14, and 15, the ratio of u_A/u_0 is fairly insensitive to changes in R_C , while the ratio of u_C/u_0 is quite sensitive to changes in the assumed value of R_C .

Core and annular velocities, based on Figures 13, 14, and 15, are presented in Table XIV. To show the effect of R_C , two different values were used for each run. The presence of the solids has been neglected in calculating these values.

All of the values of u_A/u_0 , representing the ratio of the annular velocity to the superficial velocity, seem high. Visual timing of pieces of coal in beds of microspheres places the down-velocity of solids near the wall at about one-half the superficial air velocity; this is in general agreement with the values reported by Carlsmith and Freund (3) in their studies on solids mixing. If the ratio of u_A/u_0 for the gases is assumed to be one-half, the material balance fixes the ratio of u_C/u_0 at 5.5 for R_C equal to 0.75 and at 13 for R_C equal to 0.5 regardless of the gas composition, again showing

TABLE XIV

Core and Annular Velocities from Back-Mixing Data

(Based On Figures 13, 14 and 15)

Solid	u_o ft./sec.	Vertical Position of Traverse	Assumed Radius of Core Inches	u_C	u_A	$\frac{u_C}{u_o}$	$\frac{u_A}{u_o}$	
Microspheres, D less fines	0.4	6	0.5	6.7	0.39	17	1.0	
		12	0.5	6.2	0.38	15	0.9	
		Ave		6.4	0.38	16	1.0	
			6	0.75	3.0	0.46	7.5	1.2
			12	0.75	3.0	0.46	7.5	1.2
			Ave		3.0	0.46	7.5	1.2
Microspheres, D less fines	0.6	6	0.5	19	1.7	32	3.0	
		12	0.5	9.6	0.53	16	1.0	
		Ave		15	1.1	24	2.0	
			6	0.75	8.4	2.0	14.0	3.3
			12	0.75	4.3	0.63	7.2	1.0
			Ave		6.8	1.3	10.6	2.2
Microspheres, D less fines	0.9	6	0.5	19	1.4	21	1.5	
		12	0.6	13	1.5	15	1.7	
		Ave		16	1.4	18	1.6	
			6	0.85	6.6	1.8	7.3	2.0
			12	0.85	6.8	1.9	7.5	2.1
			Ave		6.7	1.8	7.4	2.0

TABLE XIV (CONTINUED)

Solid	u_o ft./sec.	Vertical Position of Traverse	Assumed Radius of Core Inches	u_C	u_A	$\frac{u_C}{u_o}$	$\frac{u_A}{u_o}$
Microspheres, D less fines	1.2	6	0.6	14	1.3	12	1.1
		12	0.6	12	0.9	11	0.8
		Ave		13	1.1	12	0.9
		6		8.1	1.5	6.8	1.3
		12		6.9	1.1	5.7	0.9
		Ave		7.5	1.3	6.2	1.1
Microspheres, F thru 150-mesh	0.6	6	0.5	18	1.6	30	2.6
		12	0.5	16	1.4	27	2.2
		Ave		17	1.5	28	2.4
		6	0.8	7.0	2.0	12	3.3
		12	0.75	7.2	1.6	12	2.7
		Ave		7.1	1.8	12	3.0
Microspheres, F thru 150-mesh	0.9	6	0.4	60	3.6	67	4.0
		6	0.6	27	4.0	30	4.4

that the value chosen for R_C has a large effect on the ratio u_C/u_o . Some of the values for the ratio of core velocity to superficial velocity, u_C/u_o , agree with the ratios of maximum core velocity to superficial velocity obtained in the residence-time studies (see Table XIX).

Admittedly, the assumptions used in calculating the values given in Table XIV simplify the picture greatly and do not allow for rapid local eddies which might account partially for the high values obtained. However, a very likely explanation for the high calculated velocities is that of sampling error. If the transfer between dense and lean phases is slow, the samples withdrawn from the column will give high values for the gas composition. The error will be largest in the core where the majority of the bubbles rise; a small error in the concentration of gas in the core would account for the high velocities derived from the traverses. This interpretation is supported by the sharp concentration gradients that were obtained below the point of injection, which indicate that the flow of gas from wall to center is slow with the microspheres. Therefore, the presence of some sampling error in the data seems likely. This conclusion is not contradicted by the fact that average values of C/C_o above the point

of injection are close to unity, since the 12 jets of tracer tend to distribute the helium across the whole bed eliminating large differences in tracer concentration.

Eleven inches above the point of injection, the values of C/C_0 obtained for Microspheres, G, were almost unity (see Figure 16). The fluidization of this size cut was very smooth; the top of the bed hardly fluctuated at all, and only very small bubbles, about 1/4-inch in diameter, or smaller, were evident. These moved around in a much more random fashion than did the bubbles in the other sizes of microspheres or in the glass beads. It may well be that the sampling error with these very small microspheres was negligible due to the unusual action of the bed.

Consideration of the sampling problem seems to indicate two factors that should have an influence on the error introduced on withdrawal of gas. One is the size and number of bubbles passing through the bed; the other is transfer of gas between the dense and lean phases. If the number of bubbles is decreased, then it seems likely that Z will approach Y, reducing the error, and as the size of the bubbles decreases, the area for exchange of gas between the two phases increases for a given fraction of lean phase in the bed, tending to

reduce sampling error. As the size of the particles decreases and the amount of fines increases, the interstitial spaces between particles decrease in size, and this probably decreases the flow of gas between the two phases, fostering differences in concentrations and so increasing the error due to sampling. It is obvious that the larger the difference in concentration of tracer in dense and lean phases, the greater will be the magnitude of the sampling error; with identical gas composition in both phases, there would be no error due to sampling.

The possibility of errors in the data due to sampling does place doubt on any quantitative conclusions to be drawn. Nevertheless, the data do show certain trends from which valid qualitative conclusions may be drawn. Recognition of the error that may be present to a greater or less degree in the experimental data does not nullify any comparison of the relative magnitudes of the gas compositions measured.

Several qualitative conclusions based on the internal gas mixing studies are of interest. There is definite back-mixing of gases in fluidized beds. The experimental evidence points to a definite flow pattern of the gas, consisting of flow up the middle of the bed and flow down along the walls; superimposed on this pattern is a

varying degree of side-mixing of the gases between the two zones. Based on the findings with microspheres and glass beads, it appears that this transfer decreases as the particle size decreases and the amount of fines increases. The transfer of gas through the interstices of fluidized beds can be quite slow, so that concentration differences between dense and lean phases, once established, can be maintained. It is therefore possible for appreciable concentration gradients to exist in the gases at a given level in a fluidized bed. Due to the bubbling action, withdrawal of gas from within the bed may lead to samples that do not represent the average composition of the gas passing the sample probe. A study of bubble action and the development of a method for accurately sampling from dense and lean phases should lead to a better understanding of the mixing of gases in fluidized beds.

3. Correlation of Back-Mixing Results

There is definite evidence in the data obtained during the back-mixing studies indicating vertical gradients in gas concentration in fluidized beds. A method for predicting these vertical concentration gradients would be of value in the application of the fluidized technique to chemical problems. However, if the method is based on an empirical correlation of the data collected

by normal internal sampling, any use of the correlations must be tempered by an appreciation of the errors inherent to them and of the flow pattern in the beds.

In order to correlate the down-mixing data, an attempt was made to fit them to an eddy diffusivity type of equation

$$\frac{dN_A}{d\theta} = -E \frac{dC}{dx} \quad (4-IV)$$

where N_A = quantity of gas "A" transferred per unit area

C = concentration

θ = time

E = eddy, or down-mixing, diffusivity

x = distance

Using the experimental technique described earlier, the system comes to steady state, where the amount of tracer carried down the column by mixing is equal to that carried up by the net flow of gas. In order to integrate Equation (4-IV) under these conditions, two assumptions must be made: (1) the gas velocity and concentration of tracer are uniform across any cross section, and (2) the eddy diffusivity is constant. While the validity of these assumptions is doubtful, especially the first, the resulting value of E should be an indication

of the average down-mixing. Integration of the equation and substitution of the following boundary conditions:

$$\text{at } x = 0, \quad C = C_0 \quad (5-IV)$$

$$\text{at } x = L_1, \quad C = 0 \quad (6-IV)$$

where L_1 = distance to bottom of bed,
results in

$$\frac{C}{C_0} = \frac{\exp\left(-\frac{u_0 x}{E}\right) - \exp\left(-\frac{u_0 L_1}{E}\right)}{1 - \exp\left(-\frac{u_0 L_1}{E}\right)} \quad (7-IV)$$

(See VII APPENDIX B.)

It follows that

$$\frac{d(\ln C/C_0)}{dx} = -\frac{u_0/E}{1 - \exp\left(-\frac{u_0(L-x)}{E}\right)} \quad (8-IV)$$

For sufficiently large values of u_0/E and/or where x is small compared to L , (8-IV) reduces to

$$\frac{d(\ln C/C_0)}{dx} = -\frac{u_0}{E} \quad (9-IV)$$

or

$$\ln \frac{C}{C_0} = -\frac{u_0}{E} (x) \quad (10-IV)$$

Equations (9-IV) and (10-IV) can be obtained from (4-IV) by substituting the boundary condition

$$\text{at } x = \infty, \quad C = 0 \quad (11-IV)$$

for (6-IV). This substitution can only be justified if

deep beds are being considered. Kennel (12) employed this latter approach.

These relationships are tested by plotting the logarithm of the concentration ratio as a function of the distance below the injection point. Only data taken at least two inches below the injector are considered. If the data fit the simplified equation (10-IV), a straight line should result having a slope of $-u_0/E$, while if the data are characterized by (7-IV), a curved line concave downward should result. The value of u_0/E can be determined from the slope of this curved line at $C/C_0 = 0$ ($x = 0$), utilizing equation (8-IV).

As an example, Figure 22 gives the results of a study made with No. 11 glass beads at an air velocity of 0.9 ft./sec. with the single tube injector. (The graphs of the other runs will be found in VII APPENDIX D.) Data are shown for three different radii, and within the scatter of the data a single line is characteristic of the three sets. The slope of the line, representing u_0/E , is 2.5 reciprocal feet. The values of E obtained in the other runs are given in Table XV. Also included in this table are the values found by Kennel (12) and Ciborowski (6) in the course of their studies. All of these values have been obtained using the method of equation (9-IV); in some runs a slight tendency toward

FIGURE 22

BACK-MIXING RESULTS

NO. 11 GLASS BEADS

$u_0 = 0.9 \text{ ft./sec.}$

$u_0/E = 2.5 \text{ ft.}^{-1}$

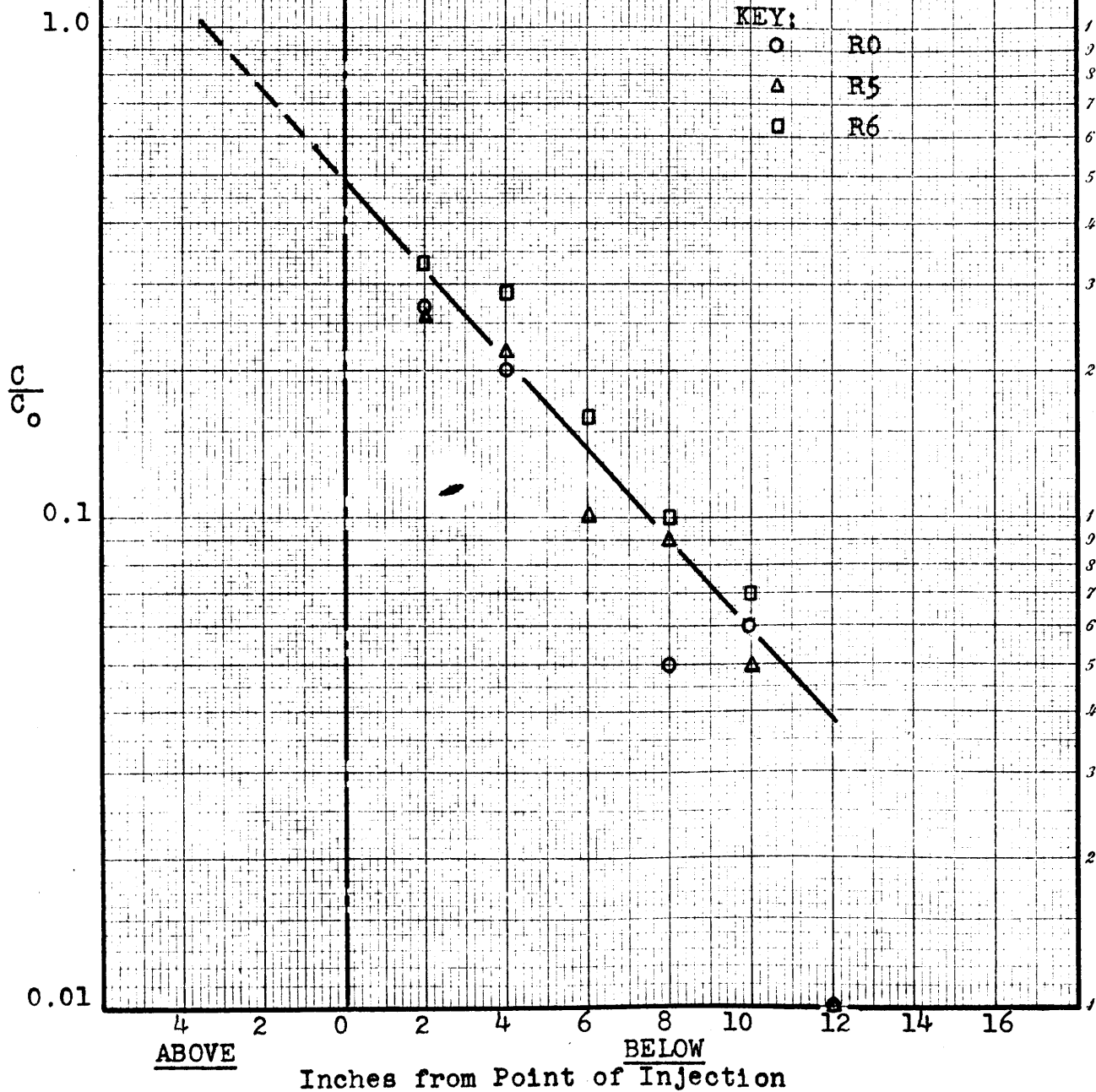


TABLE XV
BACK-MIXING DATA

Investigator	Fluidizing System	Type	Size Tyler Mesh	Mean D_p micron	Charge lb.	ρ_B $\frac{\text{lb.}}{\text{ft.}^3}$	u_o $\frac{\text{ft.}}{\text{sec.}}$	u_o/E 1 ft.	E $\frac{\text{ft.}^2}{\text{sec.}}$	$u_o \rho_B$
(6)	Air-CO ₂	Filtrol	65-100	147-208	0.33		1.35	2.19	0.62	
(6)	"	"	100-200	74-147	0.33		1.35	2.46	0.55	
(6)	"	"	200-270	53-74	0.33		1.35	2.62	0.52	
(12)	"	"	60%	60%	0.33		0.5	3.44	0.15	
(12)	"	"	100-200	74-147	-		0.5	2.44	0.21	
(12)	"	"	+30%	+30%	-		0.5	2.91	0.17	
(12)	"	"	thru 325	less than	-		1.0	2.44	0.39	
(12)	"	"	"	44	-		1.5	2.04	0.74	
(12)	"	"	"	"	0.33		1.5	2.07	0.73	
(12)	"	"	"	"	-		1.5	1.82	0.82	
(12)	"	"	"	"	0.33		2.0	2.44	0.82	
(12)	"	"	"	"	-		2.5	2.36	1.06	
(12)	"	"	Thru 200		0.33		1.0	4.40	0.23	
(12)	"	"	100-200		0.33		1.0	4.25	0.24	
(33)	Air-He	Microspheres H		130	4.5	20.2	1.7	1.25	1.36	34.4
(33)	"	Glass Beads No. 11		155	17.2	75.8	0.6	5.0	0.12	45.5
(33)	"	"	"	"	14.3	64.9	0.9	2.5	0.36	58.4
(33)	"	"	"	"	13.2	60.8	1.2	1.6	0.75	73.0
Author	"	"	"	"	-	68.5	1.5	1.7	0.88	103
(33)	"	"	"	"	13.0	50.0	1.8	1.1	1.64	90

TABLE XV (CONTINUED)

Investigator	Fluid-izing System	Type	Mean D_p micron	Charge lb.	ρ_B $\frac{\text{lb.}}{\text{ft.}^3}$	u_o $\frac{\text{ft.}}{\text{sec.}}$	u_o/E 1/ft.	E $\frac{\text{ft.}^2}{\text{sec.}}$	$u_o\rho_B$
(27)	Air-He	Glass Beads, No. 13	102	17.8	71.5	0.4	3.46	0.12	28.6
(27)	"	" " "		14.9	72	0.6	2.71	0.22	43.2
(27)	"	" " "		13.4	69	0.9	1.65	0.55	62.0
(27)	"	" " "		12.4		1.2	1.42	0.85	
(27)	"	Microspheres D	104	7.1	25.9	0.4	1.38	0.29	10.4
(27)	"	" D		6.25	23.2	0.6	1.41	0.41	13.9
(27)	"	" D		5.6	22.3	0.9	1.47	0.61	20.1
(27)	"	" D		5.3	21.2	1.2	1.31	0.92	25.4
(27)	"	Microspheres E	Greater than	7.3	28.3	0.4	4.68	0.085	11.3
(27)	"	" E		6.7		0.6	3.28	0.18	
(27)	"	" E	147	5.6	23.3	0.9	2.13	0.42	21.0
(27)	"	" E		4.9	23.3	1.2	2.40	0.50	28.0
(27)	"	Microspheres F	70	7.4	27.1	0.4	1.33	0.30	10.9
(27)	"	" F		7.4	24.1	0.6	1.28	0.47	14.5
(27)	"	" F		5.8	23.2	0.9	1.28	0.70	20.9
(27)	"	" F		5.4	21.3	1.2	1.31	0.92	25.6
(27)	"	Microspheres G	17	4.6	15.3	0.4	2.44	0.16	6.1
(27)	"	" G			13.9	0.6	2.44	0.25	8.4
(27)	"	" G			10.4	0.9	2.84	0.32	10.4

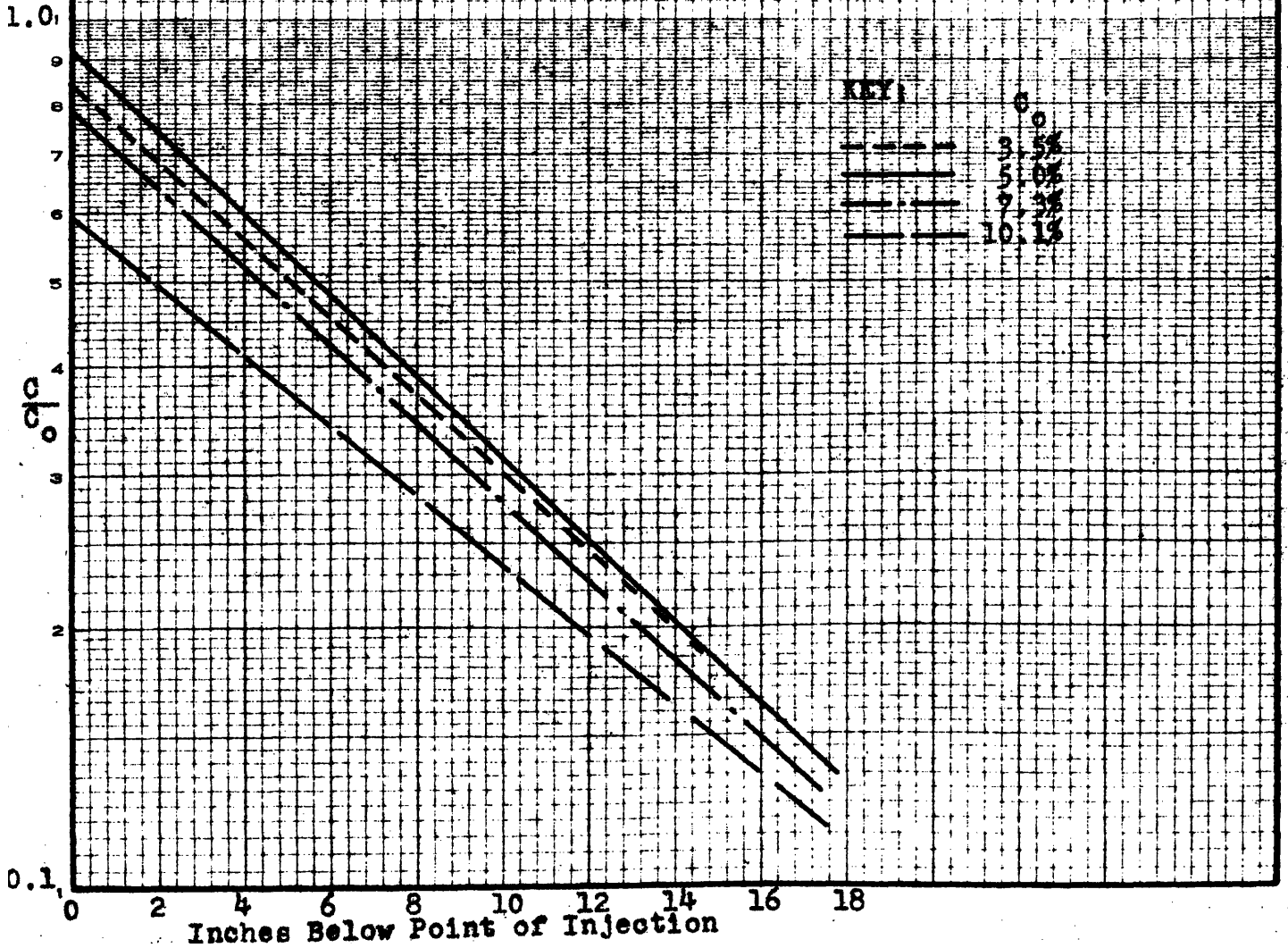
curvature was displayed by the experimental points, especially with the samples taken farthest from the point of injection (high values of x). In these cases the samples taken at high values of x were disregarded and straight lines drawn through the rest of the points. Since the slopes were greater than unity and L was 2-1/2 feet, the error introduced on setting u_0/E equal to the slope, instead of using equation (8-IV) at $x = 0$, was always less than 5%; the accuracy in the data points will not permit estimation of the slopes with this degree of certainty, so that no significant error is introduced by disregarding the points at high values of x . In general, the values were obtained from plots of the axial concentration gradients.

The values of C/C_0 extrapolated to $x = 0$ was found to vary from run to run, and in an attempt to find the explanation, several runs were made with constant air velocity under conditions of varying rates of helium injection. These were made with Microspheres, F, and the data are summarized in Figure 23 (see VII APPENDIX D for data points). It can be seen that the increase in helium rate did not change the slope of the line, u_0/E , significantly, but did tend to shift the intercept at $x = 0$ to lower values of C/C_0 . The intercept at $x = 0$ was less than unity in all the single tube runs.

FIGURE 23

EFFECT OF C_0 ON DOWN MIXING

Microspheres, F
 $u_p = 0.9$ ft./sec.

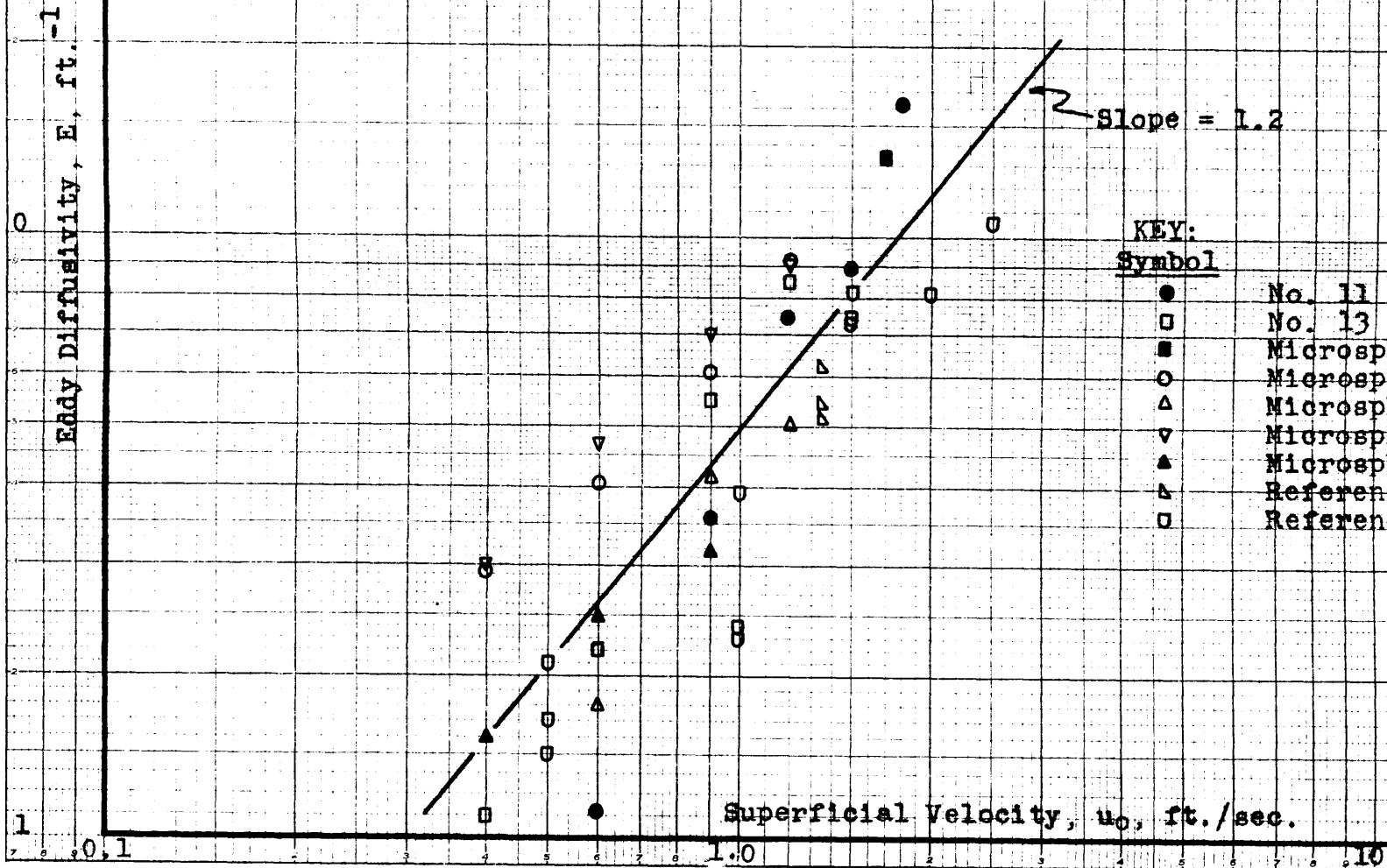


In some runs, at low velocities with the multi-point injector, the intercept at $x = 0$ is greater than unity, and this is attributed to errors introduced through sampling and to extrapolation of the data into the injection zone. Since the intercepts at $x = 0$ are dependent on the arbitrary helium rate, no attempt has been made to introduce any correction for the intercept in the derived equations, or to develop any correlation concerning these intercepts.

Examination of Table XV does not reveal any striking trend in the value of the eddy diffusivity with particle size. If the data for different sizes are compared at constant velocity, Microspheres D and F, having mean sizes of 105 to 70 microns, respectively, exhibit about the same values for E; these are larger than the values of E for Microspheres G, which have a mean diameter of 17 microns. On the other hand, the opposite tendency is revealed when the information on the glass beads is examined, where it appears that E increases with decreasing particle size.

Figure 24 presents the data of all investigators by plotting the eddy diffusivity against the superficial air velocity. It is possible to draw reasonably straight lines through the data of several of the different solids used; these lines would be of varying slope. However, in

FIGURE 24
VARIATION IN E WITH u_0



view of the errors known to occur in sampling, an extended probing of the data hardly seems justified. It does appear that the eddy diffusivity increases with the superficial velocity. For the purpose of order of magnitude results, the dimensional equation

$$E = 0.5 (u_0)^{1.2} \quad (12-IV)$$

is reasonably representative of all the data. This is not meant to imply that E is a function of superficial velocity only. Since bed density decreases with increasing gas velocity, the eddy diffusivity can not increase indefinitely with u_0 .

Towle (34) working in empty tubes found that the eddy diffusivity was a linear function of the Reynolds number, based on tube diameter, and Polack (26) found the eddy diffusivity of packed beds varied with the Reynolds number raised to the 1.2 power, using the particle diameter as the size variable.

If a correlation based on the Reynolds analogy is expected to apply to fluidized beds, the problem concerning the pertinent variables is raised. A choice between the properties of the supporting fluid alone and those of the fluid bed, including solids, must be made; a consistent approach would seem the most sensible. If the Reynolds number based on the tube diameter, gas

velocity, density and viscosity is used, the experimental data would appear as in Figure 24, as all the reliable work was conducted in a 3-inch tube using atmospheric air.

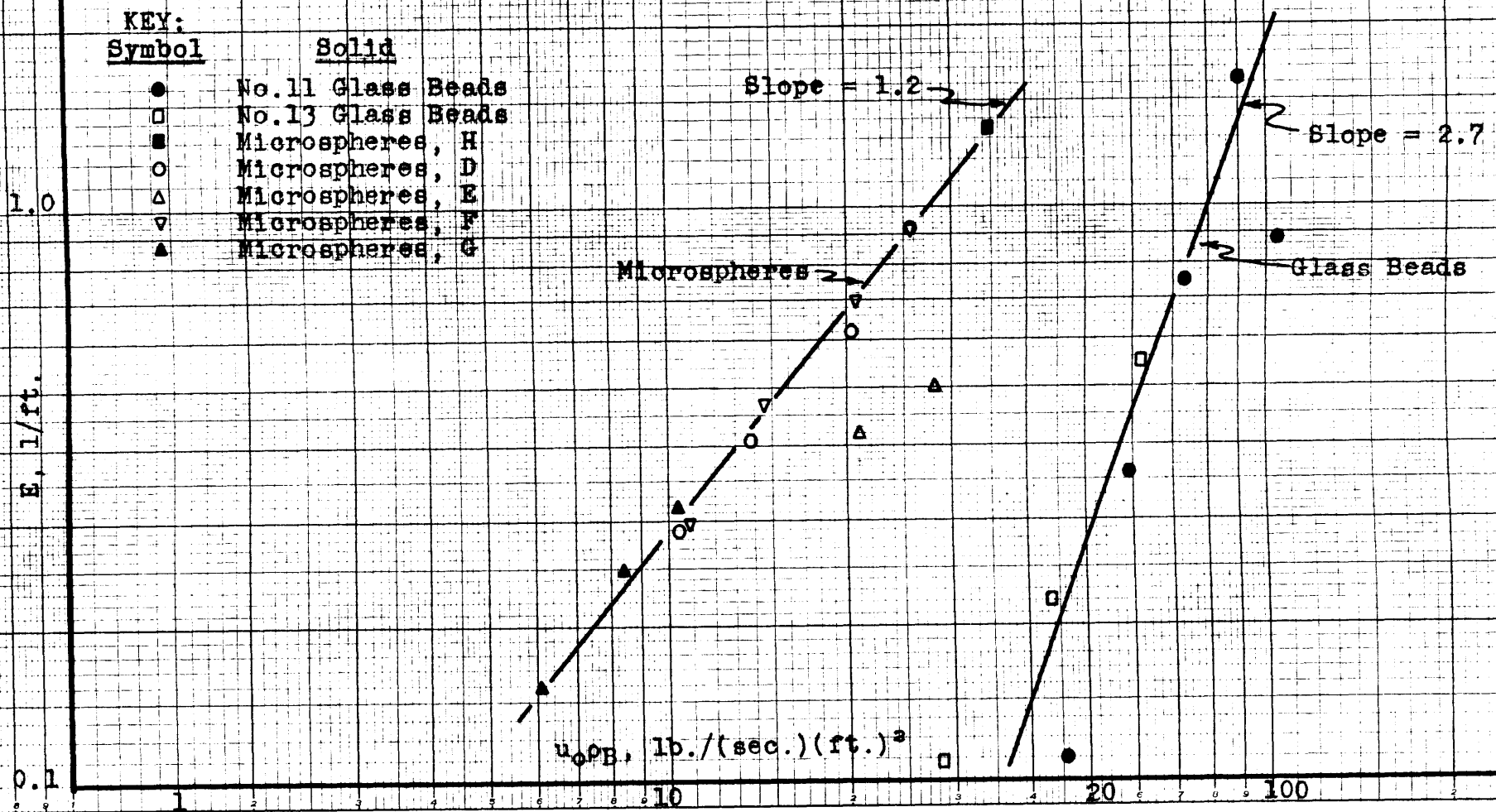
Since the mixing of gases in fluidized beds is primarily due to the presence of the solids, use of the properties of the fluid bed might be indicated. The diameter of the particles would seem to be important as it appears to have bearing on the rate of gas flow through the interstices; the diameter of the bed may also have an effect due to its influence on the solid circulation pattern. The solids density of the fluidized bed should be important, since it is a measure of the porosity of the bed. The viscosity of the bed appears to be a measure of the slugging tendency of the bed (20). In batch beds, the gas velocity should have an influence on the gas mixing, since increasing gas velocity promotes more and larger bubbles (2) and increases the solid circulation rate (3). The net solids velocity in batch beds is zero.

Figure 25 shows the data of this investigation plotted as the eddy diffusivity, E , against the product of the superficial gas velocity times the bed density, $u_0 \rho_B$. It is evident that such a plot separates the data obtained with microspheres and glass beads. However, all the data

FIGURE 25
VARIATION IN E WITH $u_o \rho_B$

KEY:

Symbol	Solid
●	No. 11 Glass Beads
□	No. 13 Glass Beads
■	Microspheres, H
○	Microspheres, D
△	Microspheres, E
▽	Microspheres, F
▲	Microspheres, G



on microspheres, with the exception of the largest diameter fraction, E, can be represented by a straight line having a slope of 1.2. A straight line having a slope of 2.7 has been drawn through the results obtained with glass beads; the scatter is worse than with the microspheres.

This method of plotting was chosen since quantitative information concerning the viscosity of the beds is not available, and inclusion of the particle diameter in the abscissa product would separate the data. However, it appears that these two factors, if included to form a Reynolds grouping, might act to offset each other and even bring the data of the two solids together. With the exception of the "E" fraction, the microspheres gave a bubbling type of fluidization, while the "E" cut and the glass beads slugged. Matheson, et.al., (20), report that spherical particles and slugging beds exhibited higher viscosities than irregular shaped particles and bubbling beds, and the viscosity was found to increase with increasing particle size. They also report that the viscosity decreased rapidly with increasing gas velocity. If these findings apply to the present data, inclusion of the particle diameter and bed viscosity in a Reynolds group would tend to bring the data of the two solids together. In-

formation concerning the viscosities of fluidized beds and the effect of viscosity on bubble formation and growth would be of value in checking this hypothesis.

It bears repeating that these correlations are based on gas samples which do not represent the average composition of all the gas passing the point of sampling, and hence it is recommended that the use of the plots and empirical relationships presented be judicious.

The significance of these findings on back-mixing in relation to the use of fluidized beds in chemical reactors will be discussed in a subsequent section.

B. Residence-Time Studies

1. Experimental Results

The results of the residence-time studies are presented in summary form in Figures 26 through 41. Data obtained for different sizes of microspheres and glass beads, under conditions of varying superficial gas velocity, and bed height and diameter are shown. The tabulated data may be found in VII APPENDIX D.

The following code has been used to number the various runs: Type of Solids-Bed Dimensions-Superficial Velocity. The types of solids are classified in III PROCEDURE. Bed dimensions are designated as 37, 70, or 35L, standing for bed heights of 37 or 70 inches in the 3-inch column, or a bed of 35 inches in the 4-1/2-inch column, respectively, (L denotes larger column). The following letters are used to denote superficial velocities:

A = 0.4 ft./sec.	D = 1.0 ft./sec.
B = 0.6 ft./sec.	E = 1.2 ft./sec.
C = 0.8 ft./sec.	F = 1.4 ft./sec.

As an example of the method of designation, M2-35L-C would represent a run made with Microspheres, 2, in the 4-1/2-inch column with a bed height of 35 inches, under a superficial gas velocity of 0.8 ft./sec.

FIGURE 26
FIXED BED AND EMPTY TUBE

Runs	u_0	Q	V	Area
○ 7-37-A	0.38	1.12	0.059	
△ 7-35L-A	0.38	2.53	0.130	0.96
□ 0-35L-A	0.40	2.68	0.322	

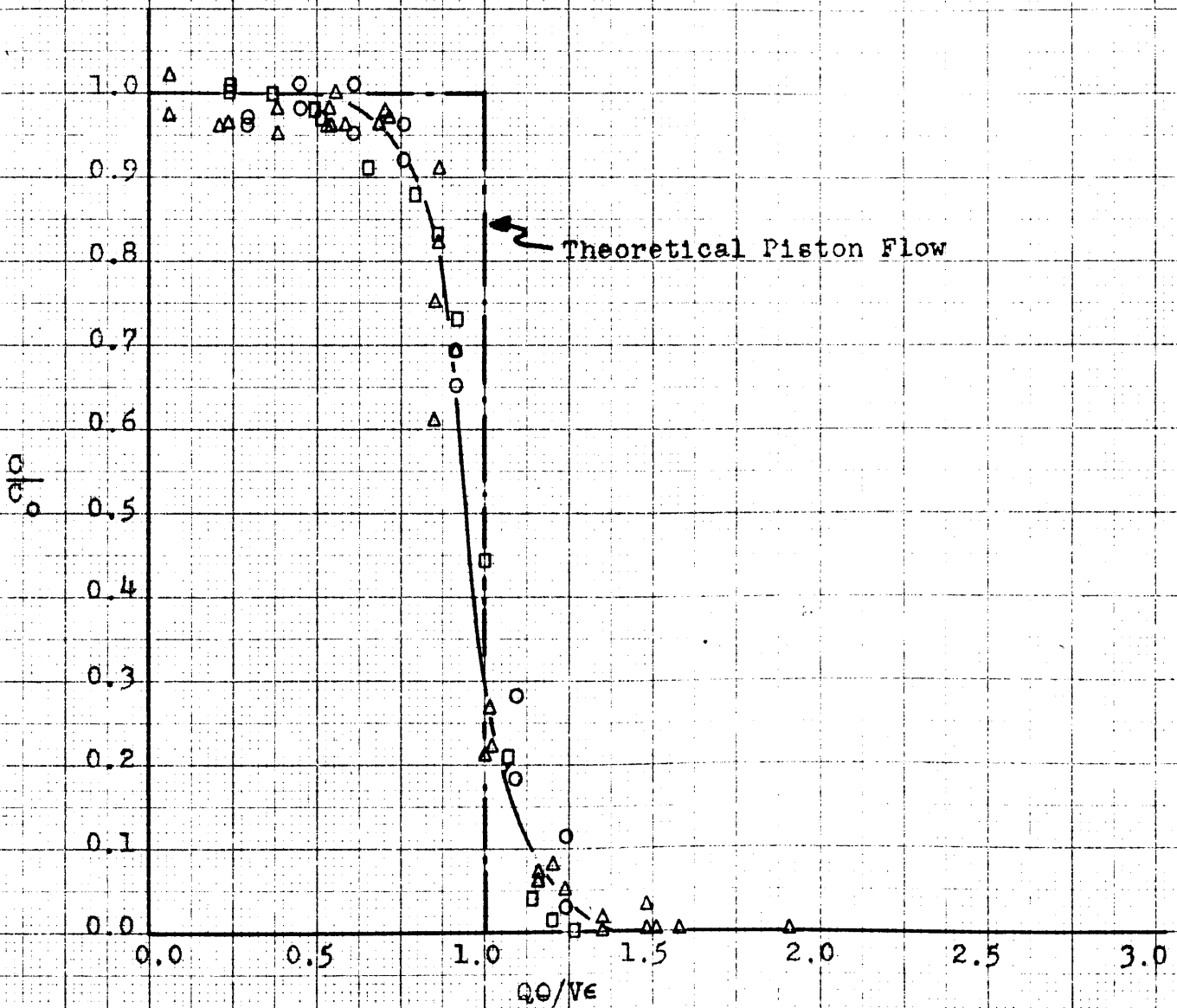


FIGURE 27
NO. 7 GLASS BEADS

	Runs	u_0	Q	V	Area
○	7-37-A	0.38	1.12	0.059	0.99
△	7-37-C	0.77	2.24	0.069	
□	7-37-D	0.94	2.76	0.079	
x	7-37-E	1.14	3.36	0.084	0.93
+	7-37-F	1.32	3.86	0.091	

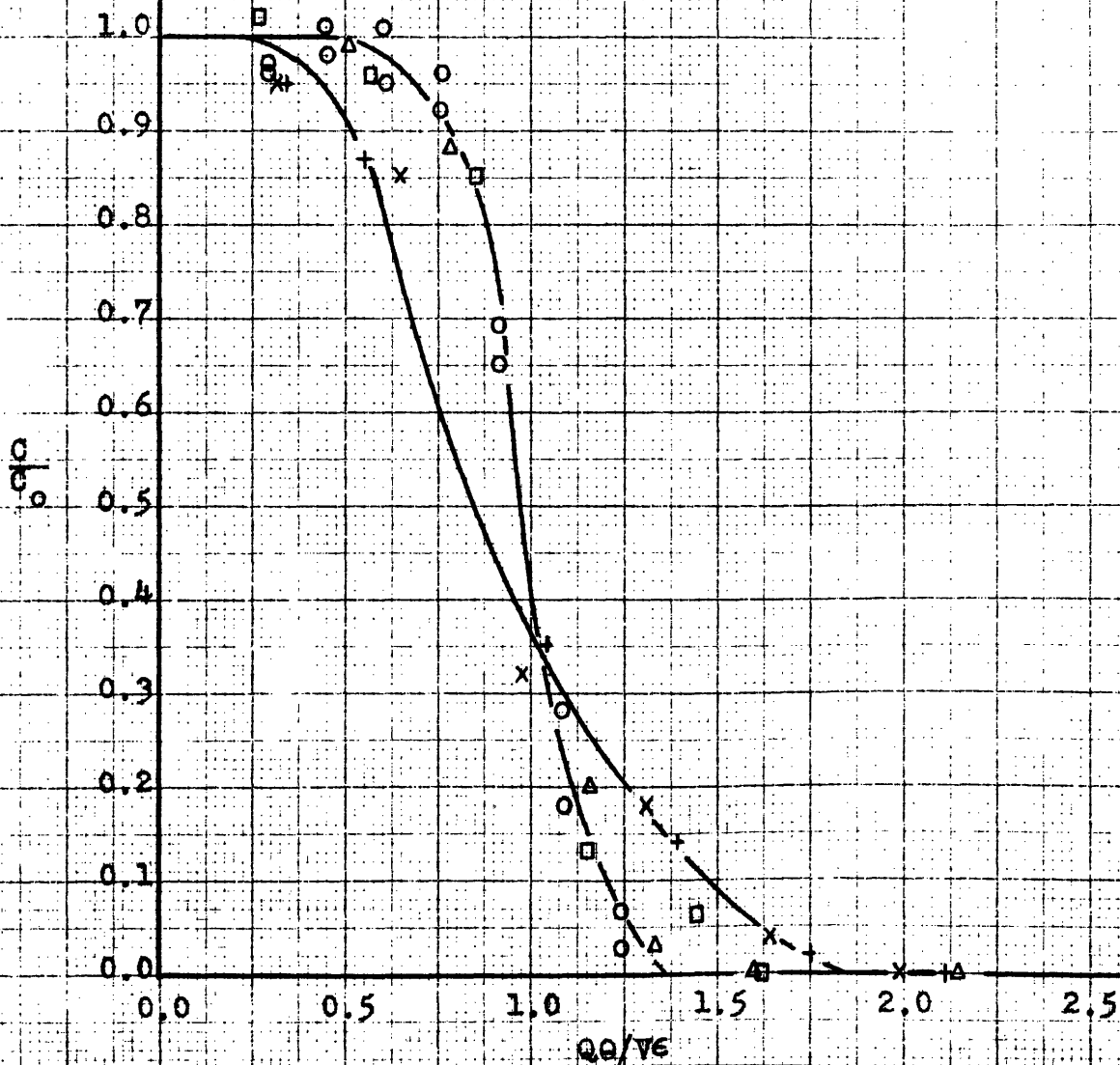


FIGURE 28

NO. 9 GLASS BEADS

Runs	u_0	q	v	Area
○ 9-37-A	0.37	1.10	0.074	
▽ 9-37-B	0.57	1.66	0.086	0.97
△ 9-37-C	0.78	2.27	0.099	

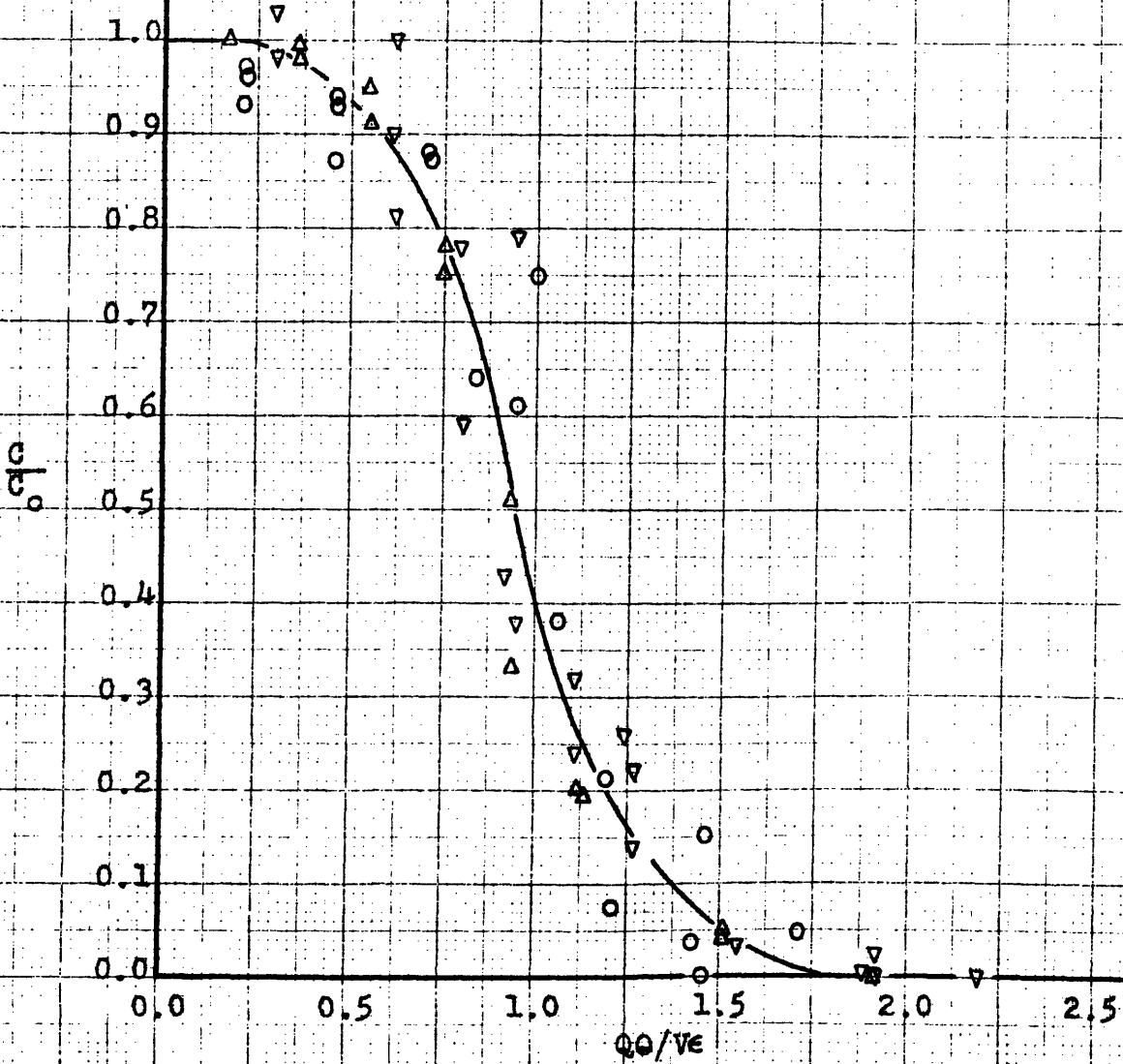


FIGURE 29
 NO. 11 GLASS BEADS

	Runs	u_o	q	v	Area
○	11-37-A	0.39	1.14	0.089	
▽	11-37-B	0.58	1.72	0.100	1.00
△	11-37-C	0.78	2.29	0.107	

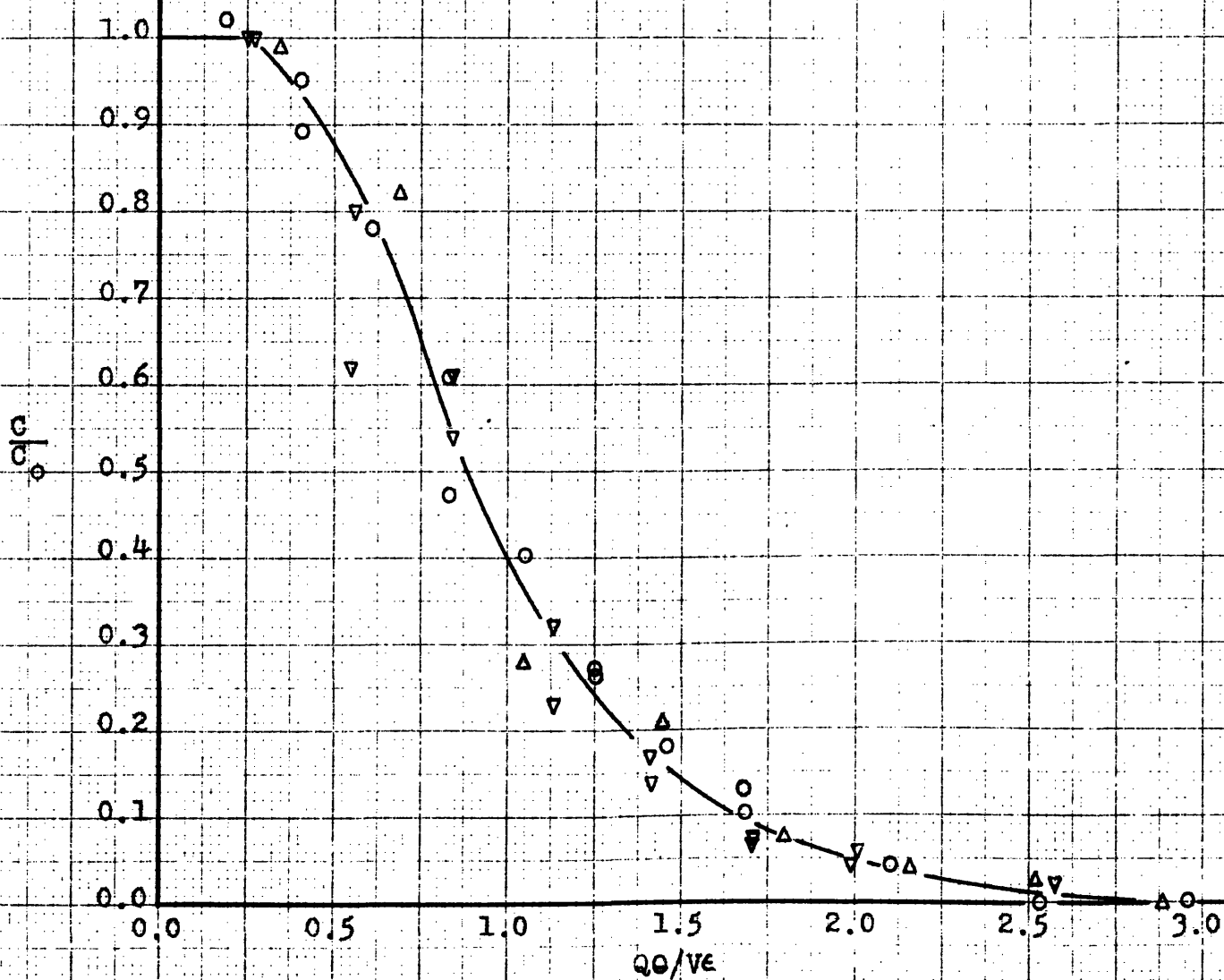


FIGURE 30
NO. 13 GLASS BEADS

	Runs	u_0	Q	V	Area
○	13-37-A	0.39	1.14	0.091	0.93
▽	13-37-B	0.59	1.74	0.101	
△	13-37-C	0.79	2.32	0.107	
□	13-37-D	1.00	2.94	0.111	

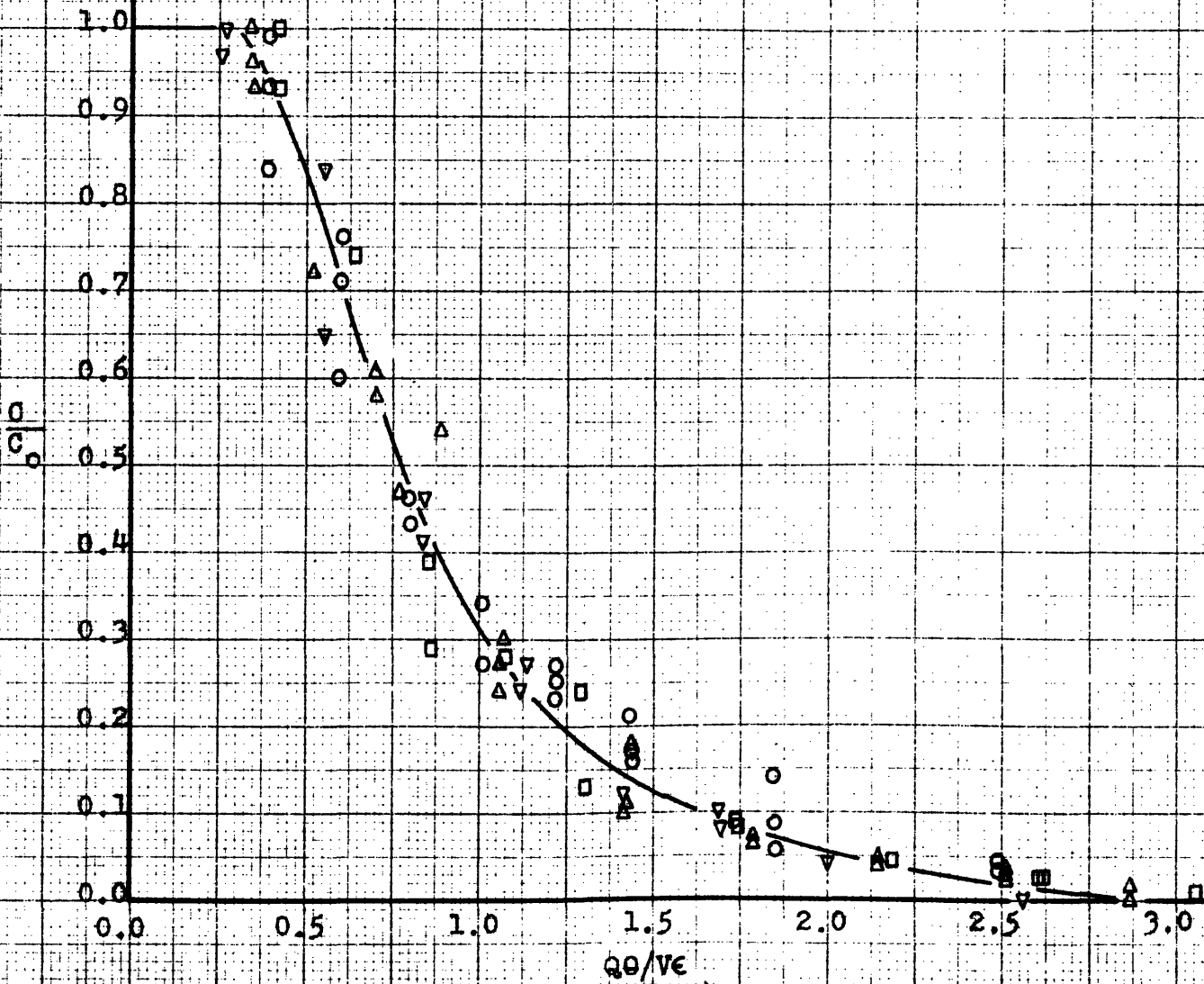


FIGURE 31
NO. 13 GLASS BEADS

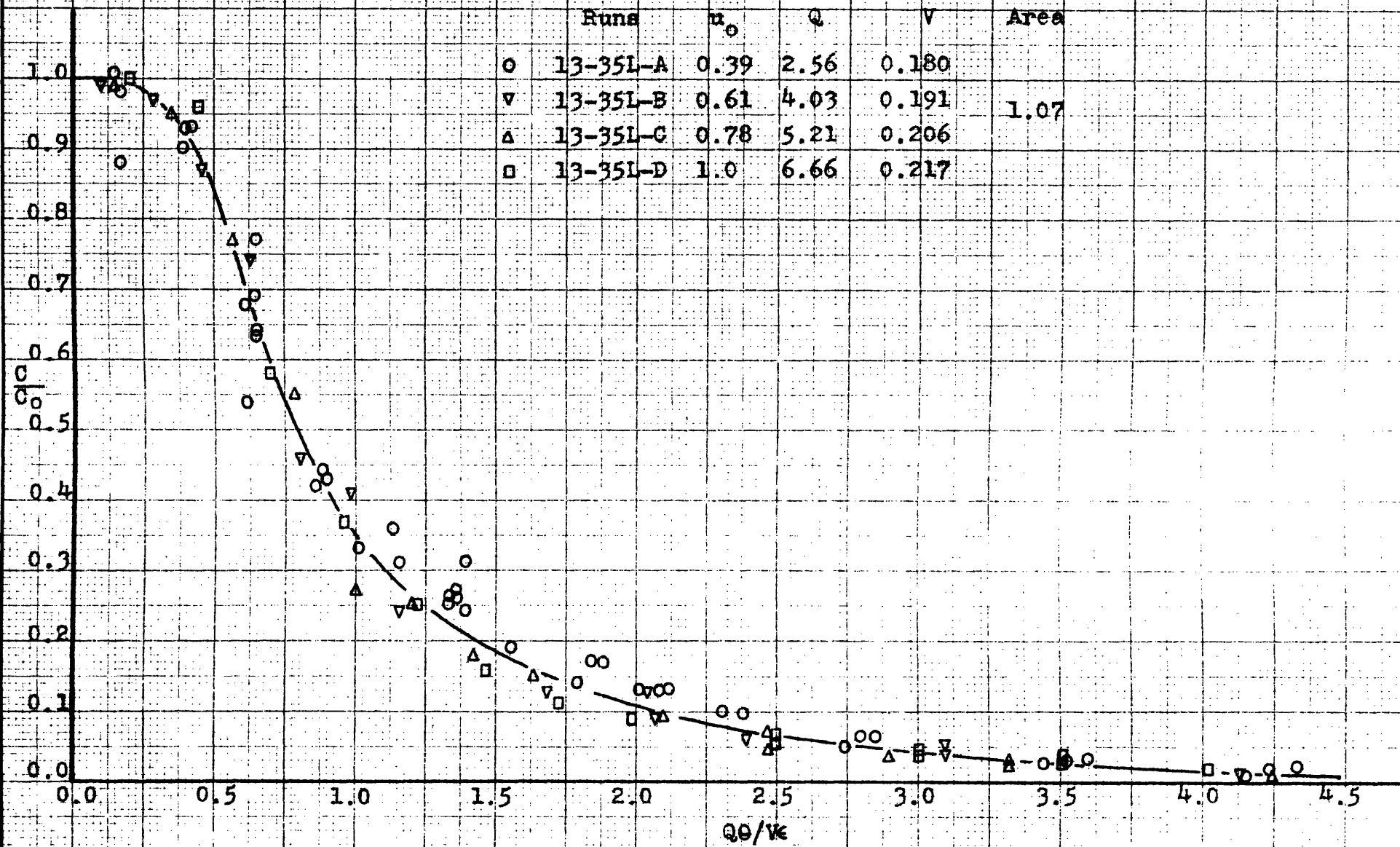


FIGURE 32
NO. 15 GLASS BEADS

	Runs	u_0	Q	V	Area
○	15-35L-A	0.44	2.91	0.182	
▽	15-35L-B	0.61	4.02	0.190	1.07
□	15-35L-D	1.00	6.66	0.203	

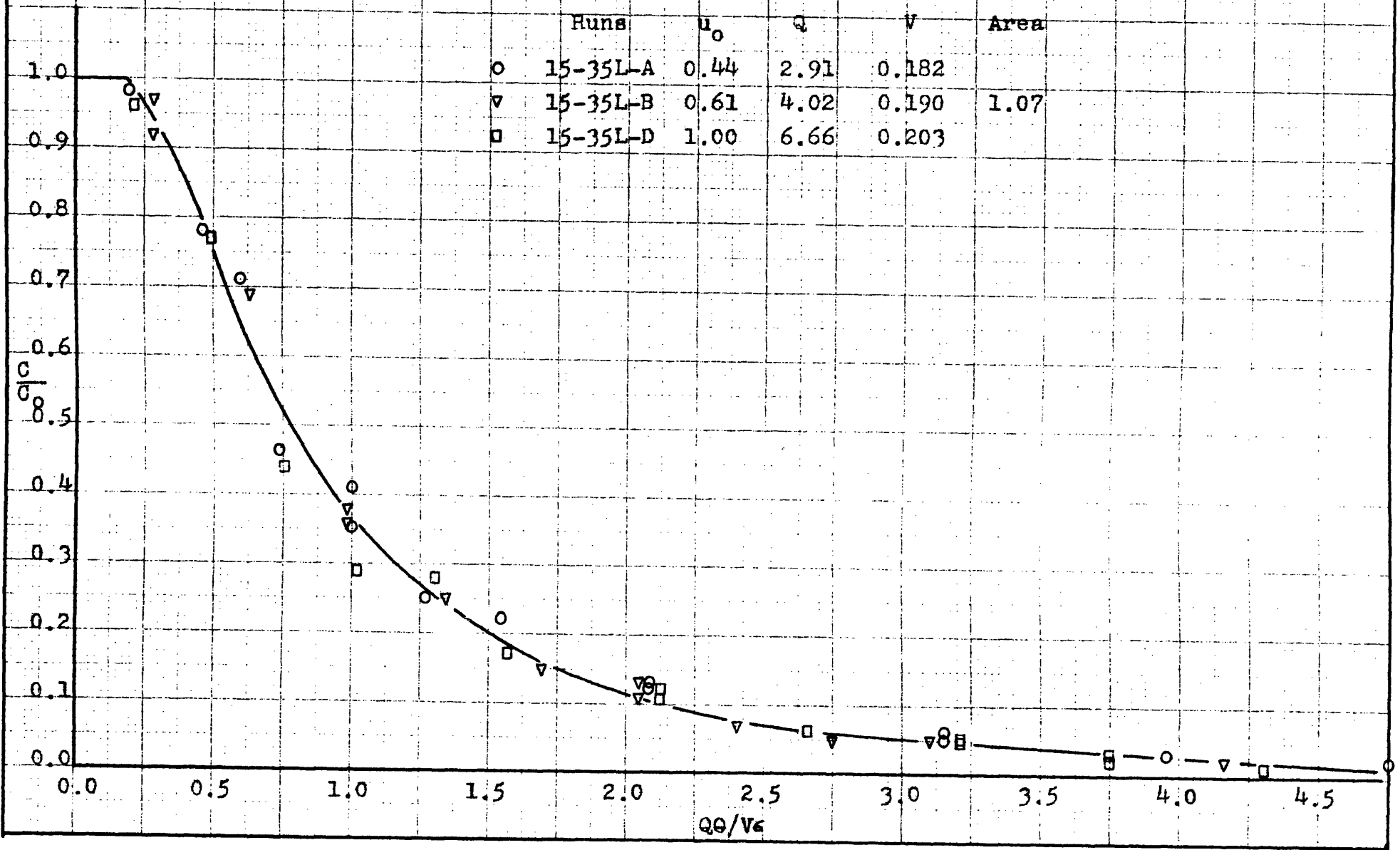


FIGURE 33

MICROSPHERES, M2

Runs	u_o	Q	V	Area
○ M2-70-A	0.38	1.13	0.231	0.99
△ M2-70-B	0.78	2.32	0.244	1.0

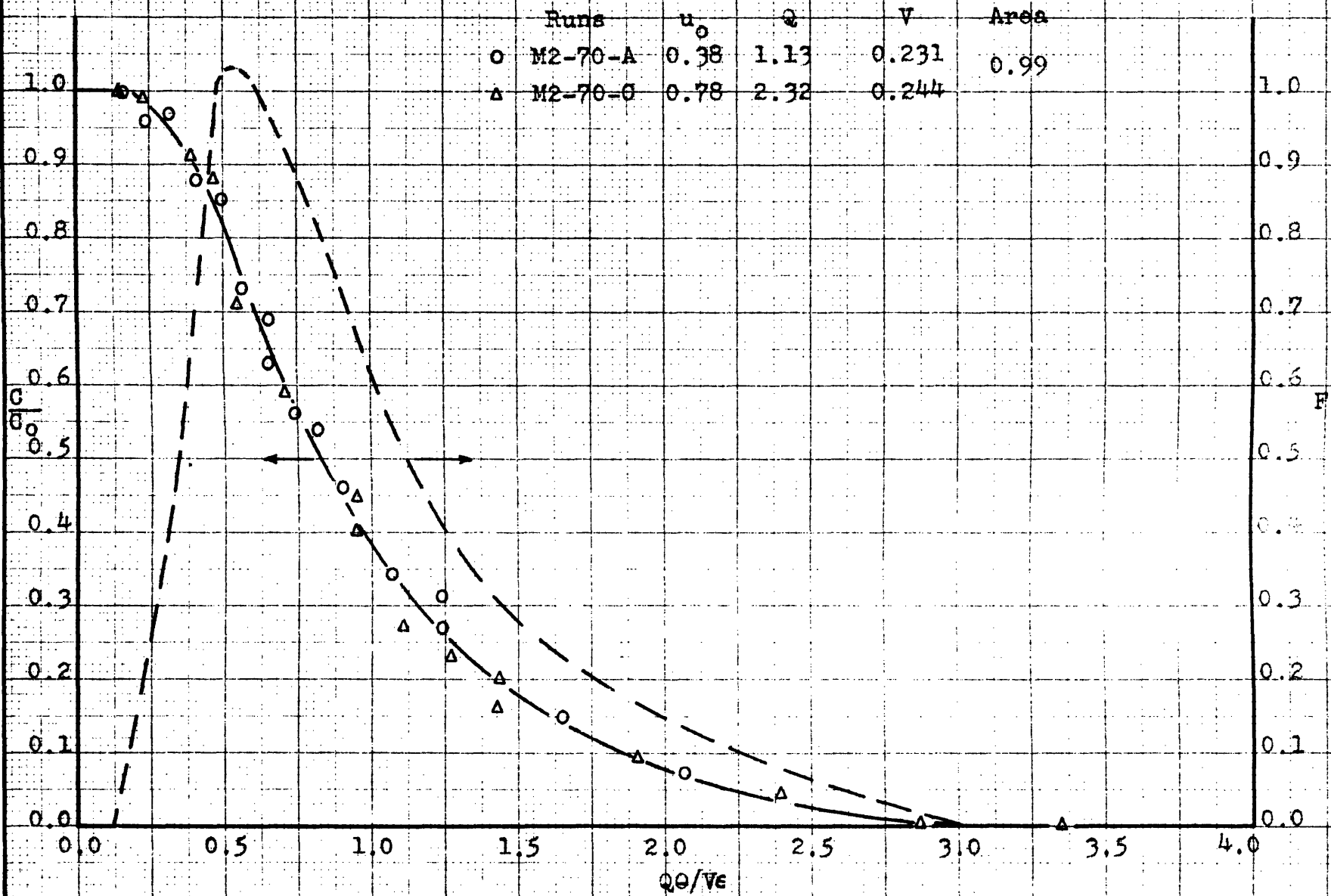


FIGURE 34
MICROSPHERES, M3

	Runs	u_0	Q	V	Area
○	M3-70-A	0.39	1.16	0.233	1.01
▽	M3-70-B	0.58	1.71	0.248	

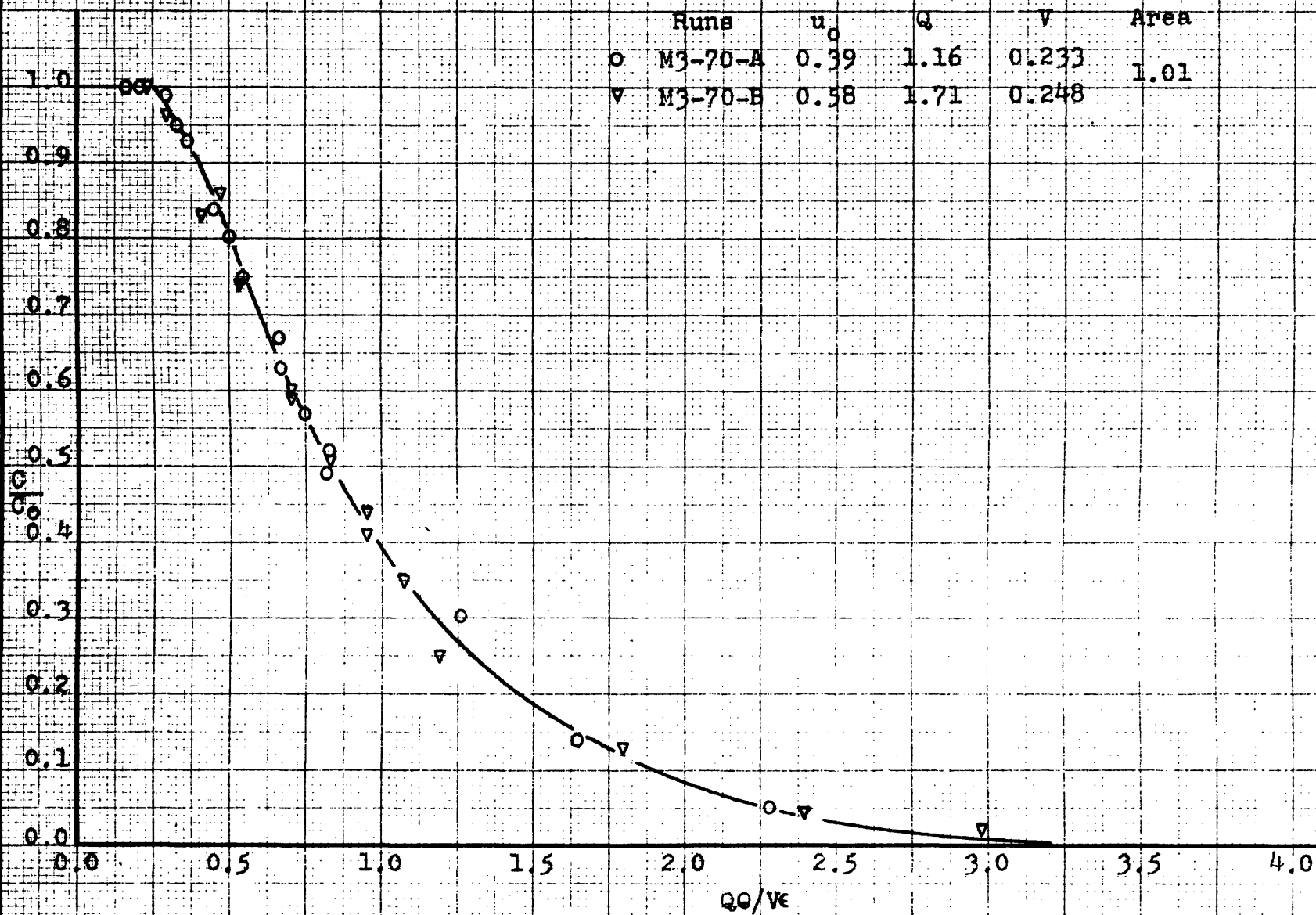


FIGURE 35
MICROSPHERES, D

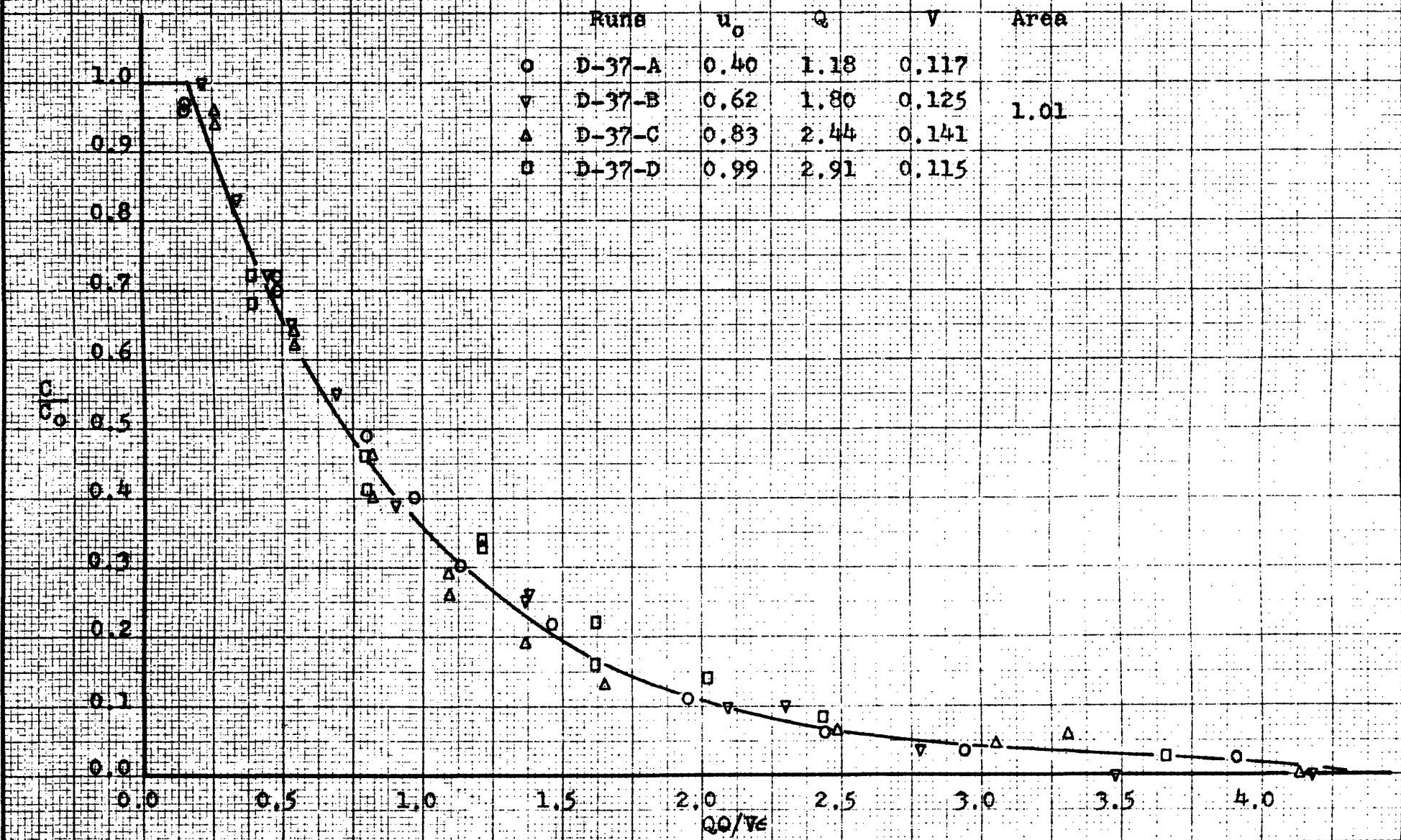


FIGURE 36
MICROSPHERES F

Runs	u_0	Q	V	Area
○ F-37-A	0.40	1.18	0.115	0.99
▽ F-37-B	0.61	1.77	0.116	
△ F-37-C	0.82	2.41	0.117	
□ F-37-D	1.02	3.01	0.106	

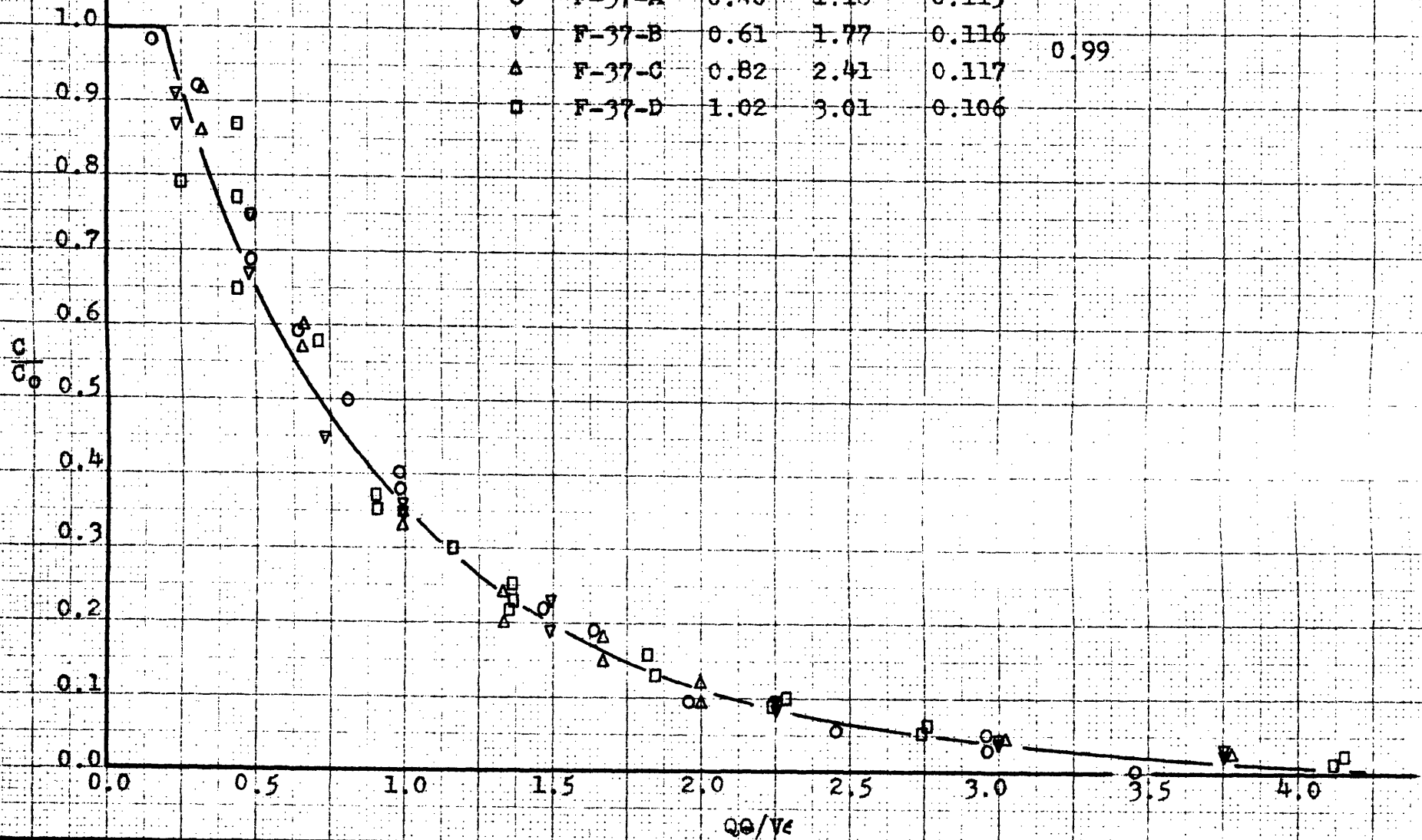


FIGURE 37
MICROSPHERES, M2

	Runs	u_o	Q	V	Area
○	M2-37-A	0.40	1.18	0.124	
▽	M2-37-B	0.61	1.81	0.136	0.99
△	M2-37-C	0.81	2.37	0.132	

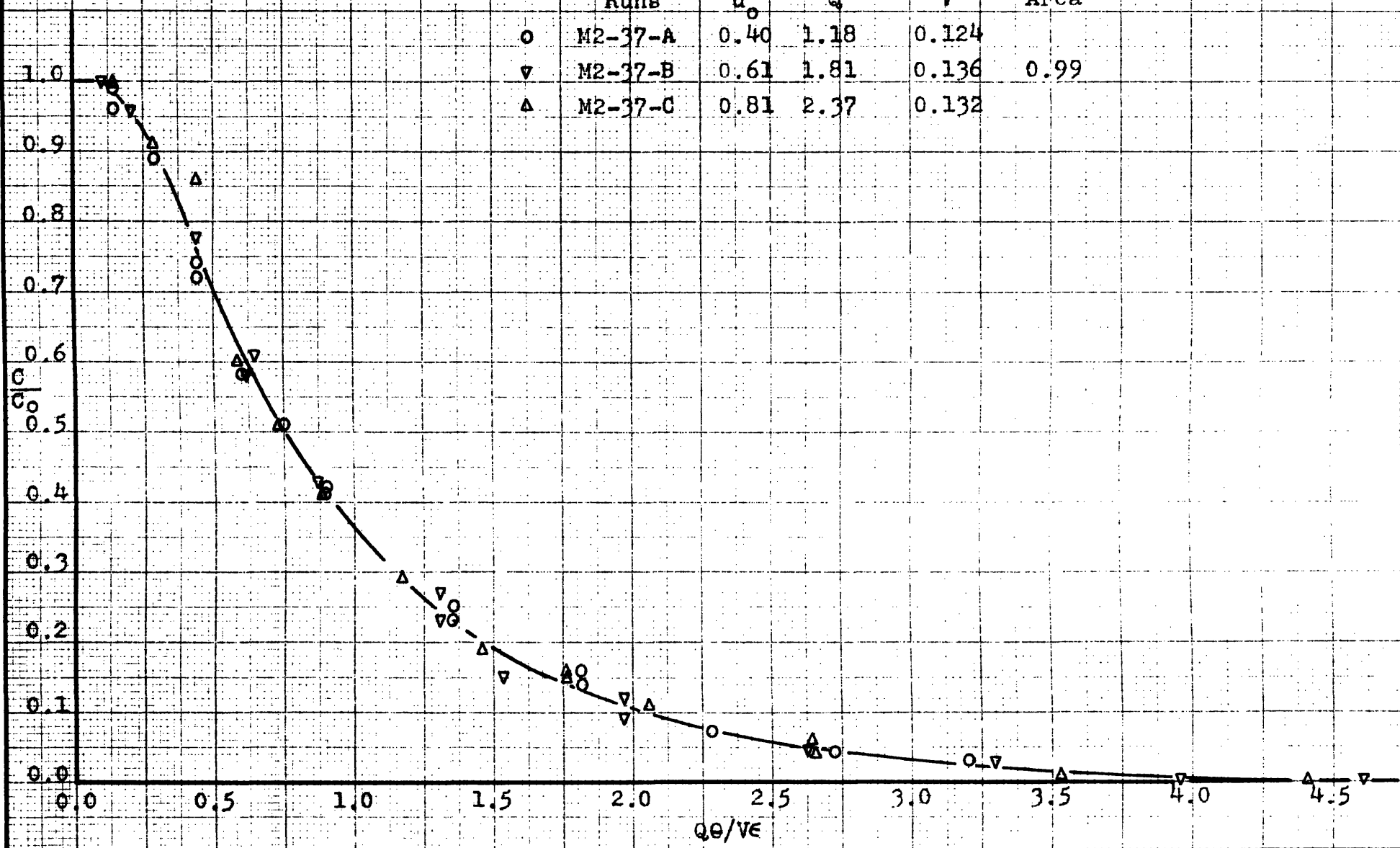


FIGURE 38
MICROSPHERES, M3

	Runs	u_0	Q	V	Area
○	M3-37-A	0.40	1.18	0.123	
▽	M3-37-B	0.60	1.77	0.128	1.00
△	M3-37-C	0.81	2.36	0.132	

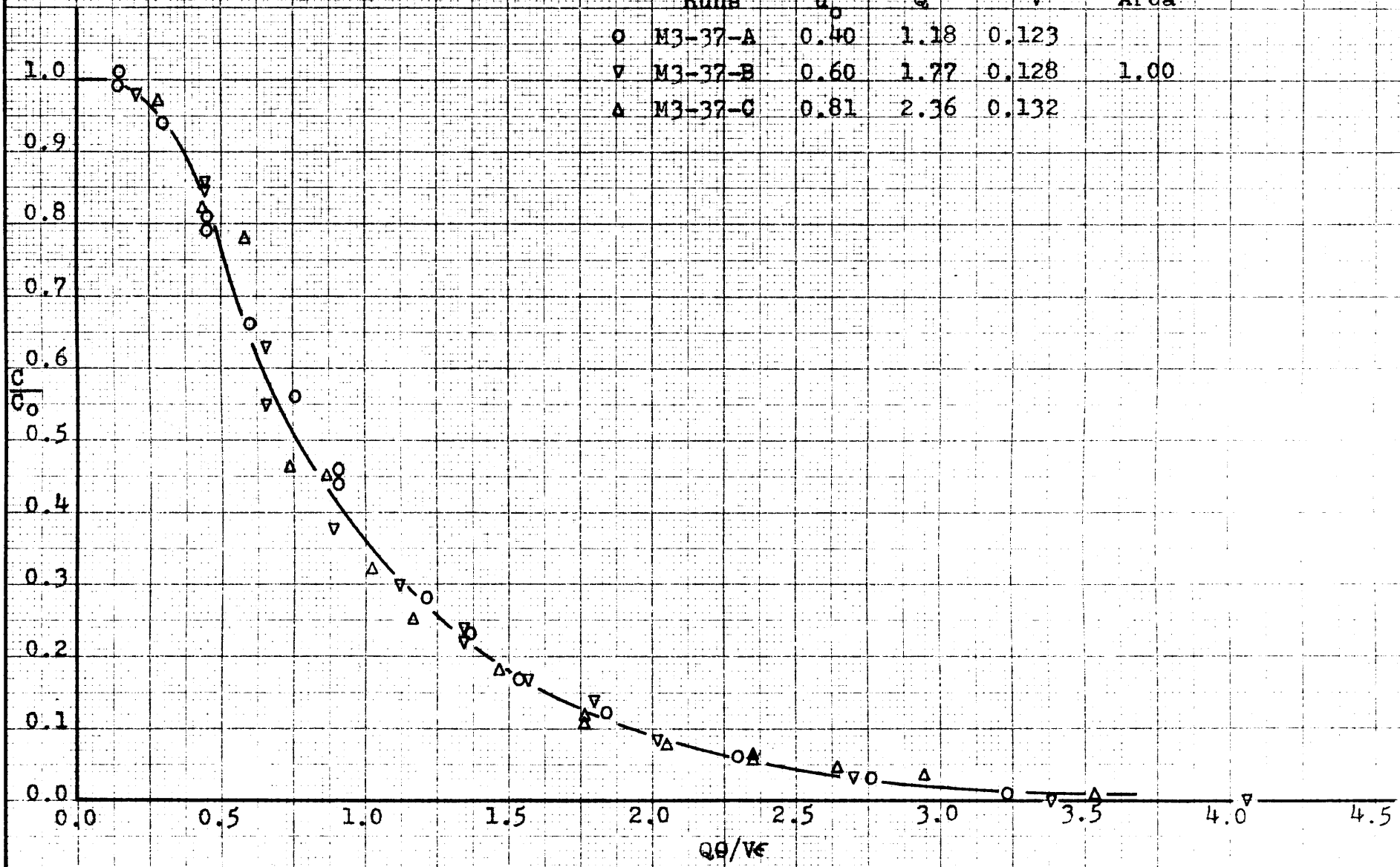


FIGURE 39
MICROSPHERES, M4

Runs	σ_0	ξ	γ	Area
o M4-37-A	0.42	1.23	0.126	1.00
Δ M4-37-B	0.60	1.77	0.126	

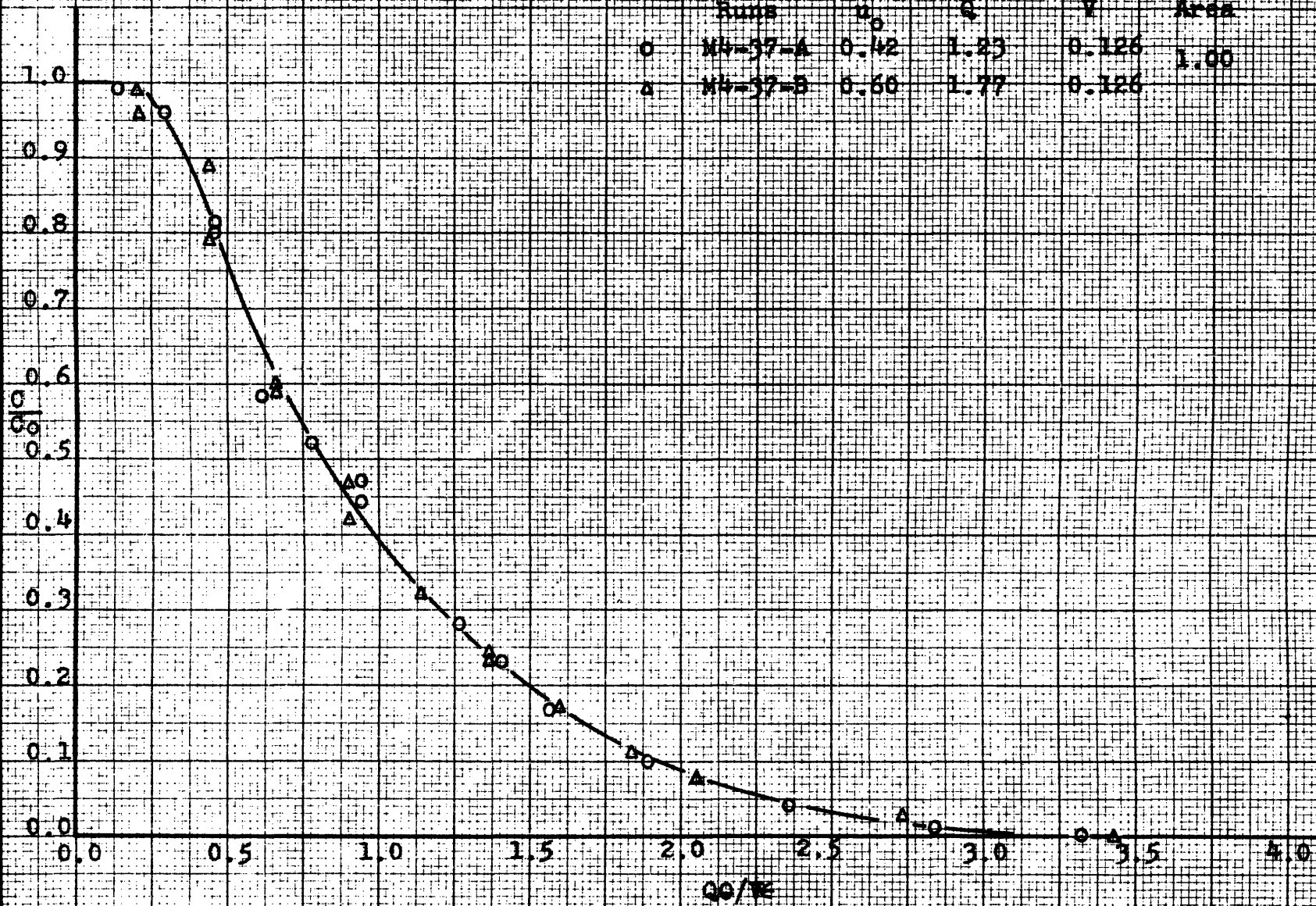


FIGURE 40
MICROSPHERES, M2

	Runs	u_0	Q	V	Area
○	M2-351-A	0.41	2.74	0.274	
△	M2-351-B	0.62	4.14	0.278	0.99
□	M2-351-C	0.83	5.47	0.299	
▽	M2-351-D	1.03	6.85	0.256	

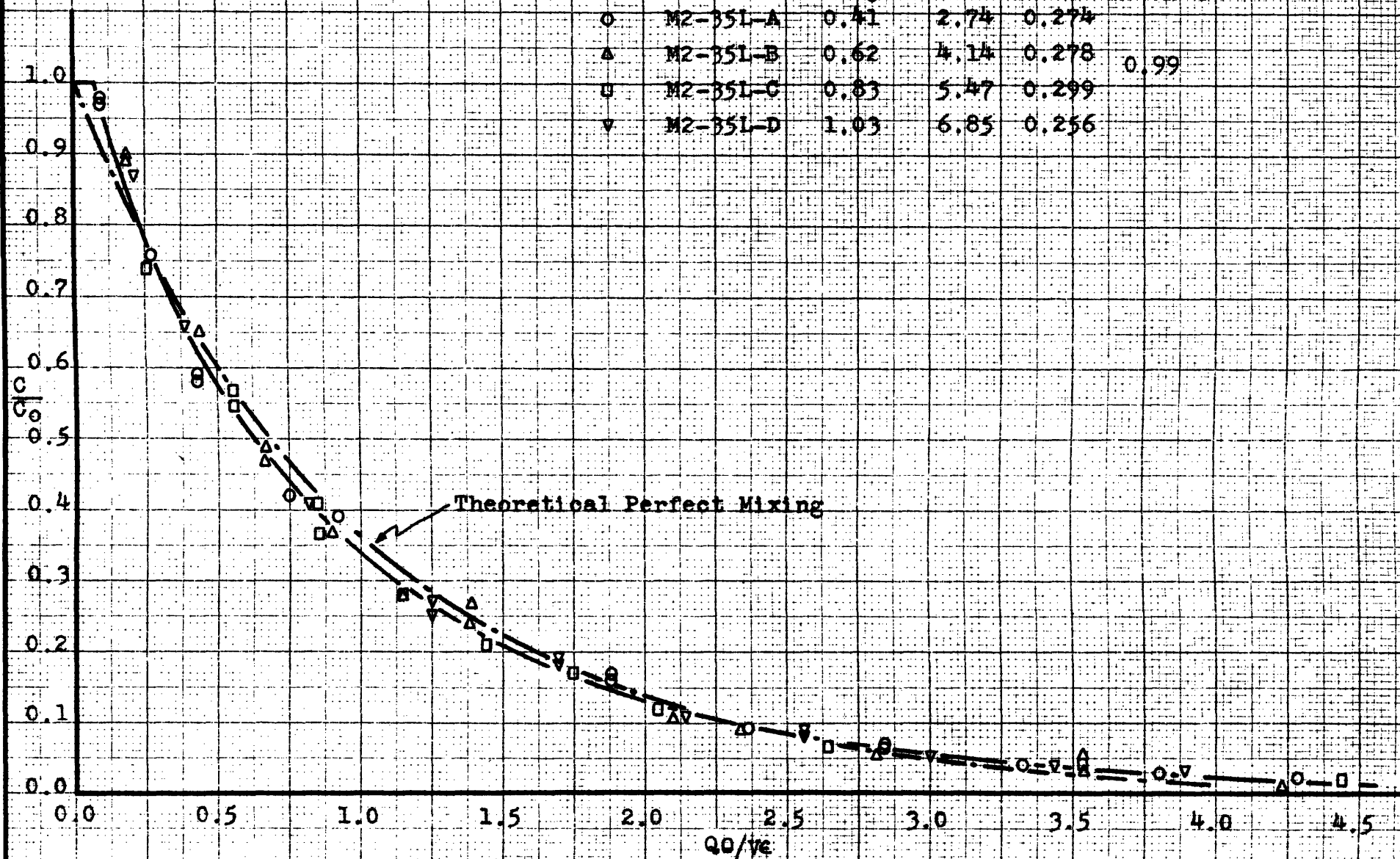
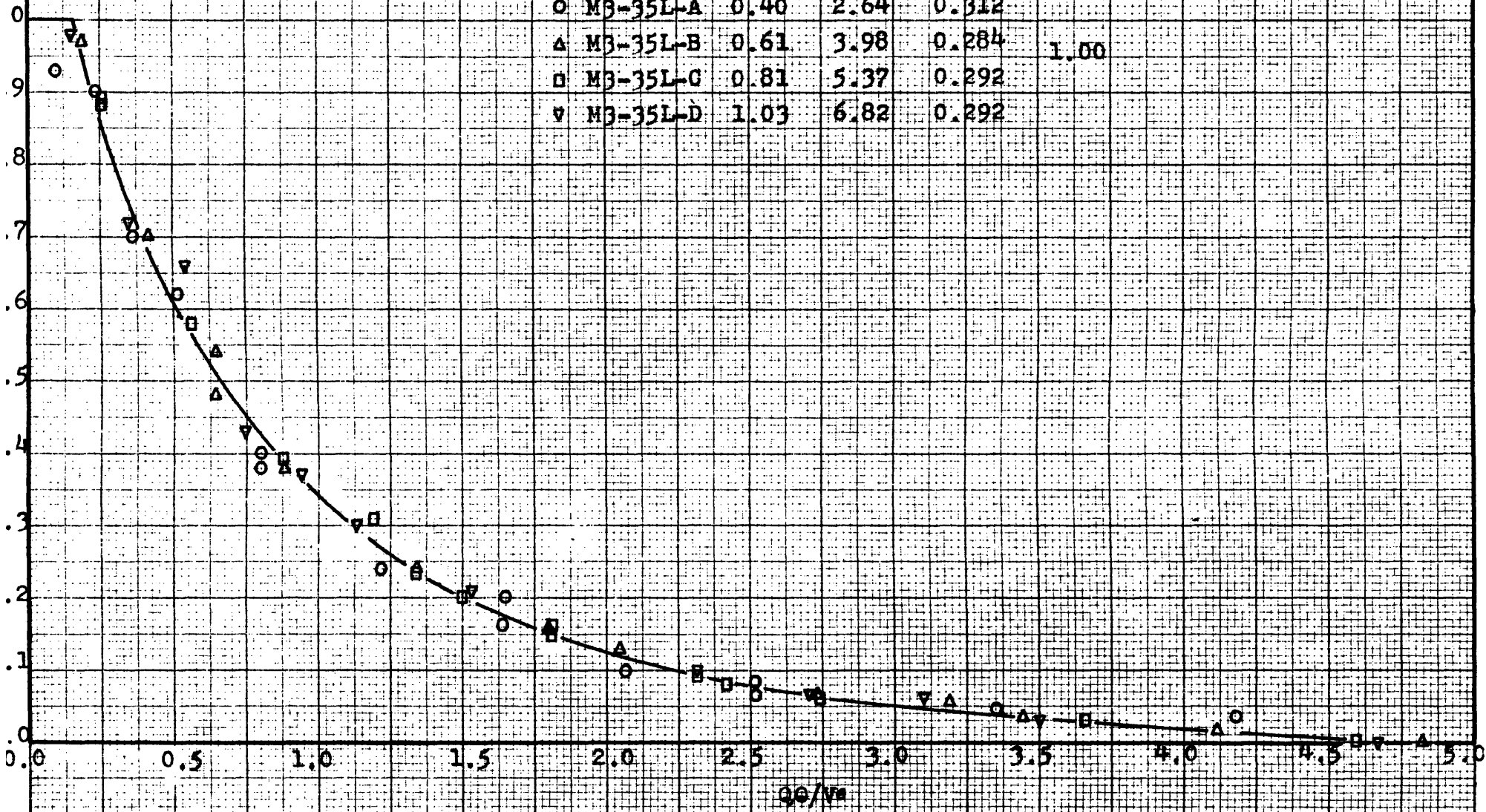


FIGURE 41
MICROSPHERES, M3

Runs	u_o	Q	V	Area
○ M3-35L-A	0.40	2.64	0.312	
△ M3-35L-B	0.61	3.98	0.284	1.00
□ M3-35L-C	0.81	5.37	0.292	
▽ M3-35L-D	1.03	6.82	0.292	



All of the data are plotted with C/C_0 as ordinate and the group $Q\theta/V\epsilon$, as abscissa. For the residence-time experiments the symbols have the following meanings:

C = concentration of tracer in gas leaving bed at time θ

C_0 = initial concentration of tracer in bed:
time $\theta = 0$

Q = volumetric flow rate, ft.³/min.

θ = time since first "fresh" gas entered bed

V = total volume of fluidized bed

ϵ = fraction voids

"Fresh" gas is gas that enters the bottom of the bed after the last tracer has entered: time $\theta > 0$.

Consideration will show that the group, C/C_0 , denotes the concentration in the exit stream of the original helium-air mixture at time θ . Thus, it is possible to consider the original mixture of helium in air (usually around 16% helium) as a homogeneous gas that can be detected in the presence of air. When tracer gas is mentioned in the following discussion, reference is being made to this helium-air mixture that was present at time zero, i.e., before the helium was turned off. Pure helium was not used as the tracer since it was felt that the switch from pure helium to air might cause a significant change in the manner of fluidization. As a consequence of this technique, the concentration of "fresh"

gas in the exit stream at any time is denoted by the quantity $1-C/C_0$.

The product of the total bed volume, V , and the fraction voids, ϵ , equals the void, or gas, volume of the fluidized bed. Thus, $Q\theta/V\epsilon$, represents the number of volumes of gas equal to the void volume of the bed, that have left (or entered) the bed since time equal to zero. By removing time as a variable this method of plotting places runs made with different size beds and different gas velocities on a comparable basis.

Calculation and Reliability of Results

It was necessary to take into account the tracer gas that was in the conical distributing section below the fluidized bed. Since the stop watch was started when the valve on the helium line was turned off, there was an interval of time before the tracer present in the cone was swept out and "fresh" gas flowed into the bottom of the bed, which ideally was the "zero time." The time elapsed since the valve was turned, as recorded on the stop watch (called time θ^*), was corrected during calculation of the results by subtracting the volume of the tracer in the cone from the total volume of gas that had flowed into the bed since $\theta^* = 0$. This volume was taken as the volume of the mixing chamber between the two mesh screens in the cone; the subtraction of this

volume as a means for obtaining θ from θ^* involves the assumption that the gases in the conical section are swept into the bed in piston flow. The presence of the wire screens of 200 mesh in the diverging section should provide a reasonable flat velocity profile in the mixing space, and so, the assumption of piston flow appears reasonable.

The volumetric flow rate, Q , is reported at the temperature in the air line feeding the column and at the average static pressure in the fluid bed.

Two different methods for determining the value of V_G were employed. In the case of the glass beads, the absolute density of the beads was determined by water displacement; knowing the total volume of the bed and the weight of solids in the bed, it was then possible to calculate the void volume, independent of any of the gas sample data.

However, in the case of the microspheres, which are porous, it was not known whether the volume given by water displacement was the correct one to use for the purposes of gas flow; a heat of adsorption was noticed on wetting of the microspheres. It was not known whether either the water or tracer gas filled the pores of the particles. Therefore, it was decided to determine the void volume by using the following relationship, which

is a material balance on the tracer.

$$\int_0^{\infty} \frac{C}{C_0} d(Q\theta) = V\epsilon \quad (13-IV)$$

For the microspheres, the values of C/C_0 were plotted against values of $Q\theta$, and the area under the resulting curve, representing the void, or gas, volume of the bed, was obtained by graphical integration using a planimeter. This quantity, $V\epsilon$, was then divided into all the experimental values of $Q\theta$ to give the desired group, $Q\theta/V\epsilon$. Having obtained $V\epsilon$ in such a manner, it should be possible to determine the value of ρ_g from a knowledge of the bed volume and the weight of solids. Comparison of the values of ρ_g obtained for different runs would then provide a check on the experimental procedure and graphical integration. However, since the fraction of voids in beds of microspheres is generally around 0.8, a fractional error in determining $V\epsilon$ results in a large fractional error in the calculated absolute density of the particles. This method did not provide a reasonable check of the experimental data in the case of the microspheres; the calculated fraction voids gave a better indication of reliability.

The data obtained using the glass beads were checked for inconsistencies by use of the following equation:

$$\int_0^{\infty} \frac{C}{C_0} d\left(\frac{Q\theta}{V\epsilon}\right) = 1.0 \quad (14-IV)$$

which is a consequence of the truth of equation (13-IV). The values of $Q\theta/V\epsilon$ used were obtained directly from flow rates and the known absolute densities of the non-porous beads. The area under the experimented curves was determined using a planimeter and indicated good reliability for the experimental technique employed, in spite of the opportunity present for experimental errors. The areas obtained with the glass beads were generally within 5% of unity. This result promotes increased confidence in the method of calculation used with the microspheres, where no good independent check of the experimental procedure was available.

Perhaps the largest potential source for experimental error lies in the establishment of an accurate zero time. It was necessary for one operator to turn off the helium, while another started the stop watch and then turned the stopcocks for sampling. Apparently the method of counting aloud up to the zero time and the reflexes of the operators were good; no difference in results were noticed when the positions of the operators were reversed or in the many cases when different operators were employed for either task.

About 0.5 seconds were required to draw a gas

sample, and therefore the analyses reported represent the average composition over that period. Since the time of sampling was known, the bottles were opened 0.2 seconds before the indicated time of sampling in order to have this indicated time coincide with the average time of the sample.

Figure 11 shows radial concentration traverses made across the column, during the course of the down-mixing studies, when the helium was injected into the conical section below the bed, and indicates that the helium and air were well mixed before entering the fluid bed.

The rate of sampling was approximately 1.0 ft.³/min. The following table shows the ratio of the air rate, Q , passing any cross section, to the sampling rate (the air rate into the bed equals the rate of gas flow from the bed).

TABLE XVI

Relative Rates of Gas Flow and Sampling

For Residence-Time Studies

$S = \text{sampling rate} = 1.0 \text{ ft.}^3/\text{min.}$

<u>Gas Velocity, u_0</u> <u>ft./sec.</u>	<u>3-inch</u> <u>Column</u>	<u>Q/S</u>	<u>4-1/2-inch</u> <u>Column</u>
A 0.4	1.2		2.6
B 0.6	1.8		4.0
C 0.8	2.4		5.3
D 1.0	2.9		6.6

The sampling rate can be seen to be less than the total gas flow for all velocities. However, the sampling is definitely not isokinetic, and gas is drawn from an area larger than the end of the sampling tube.

Figure 42 shows the results obtained with the sampling probe located at the top of the bed at different radii in the column. In all of the other data, the end of the sampling probe, which points downward, was located at the top of the bed at the axis of the column. No significant difference was found when the radial position of sampling was shifted.

In order to keep the experimental technique as simple as possible, with the hope that this would reduce the difficulties of operation, the air rate was left undisturbed when the helium was turned off. Since the helium rate was small compared to the air rate, the effect on bed operation of stopping the flow of helium should be small. The top of the bed dropped slightly immediately after the helium was turned off; this observation gives reliability to the use of the inlet air rate as the measure of the exit gas rate. To confirm the validity of the experimental approach, several runs were made with varying rates of helium injection (see Figure 43). If the decrease in the total flow rate had

FIGURE 42
EFFECT OF RADIUS OF SAMPLING

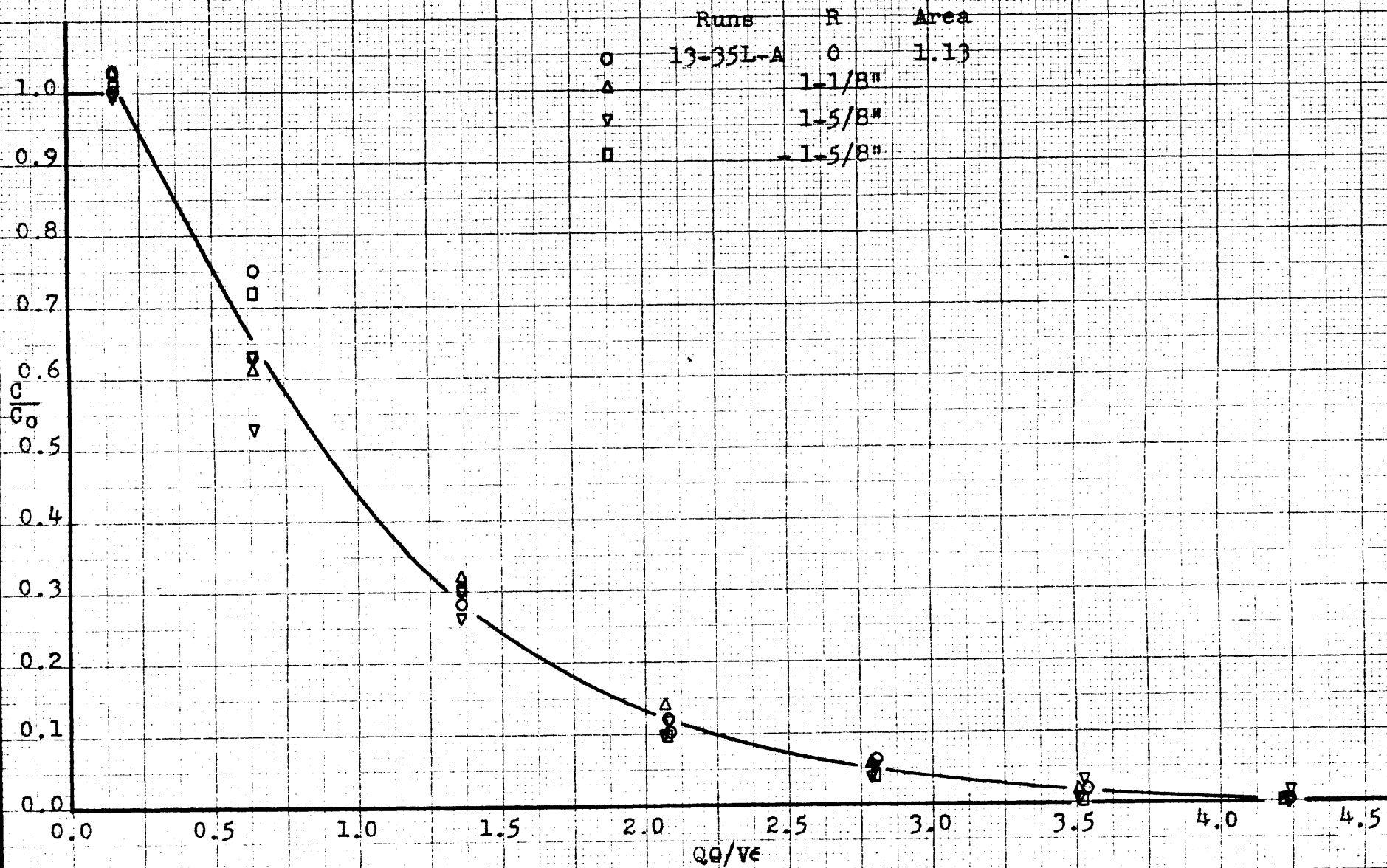
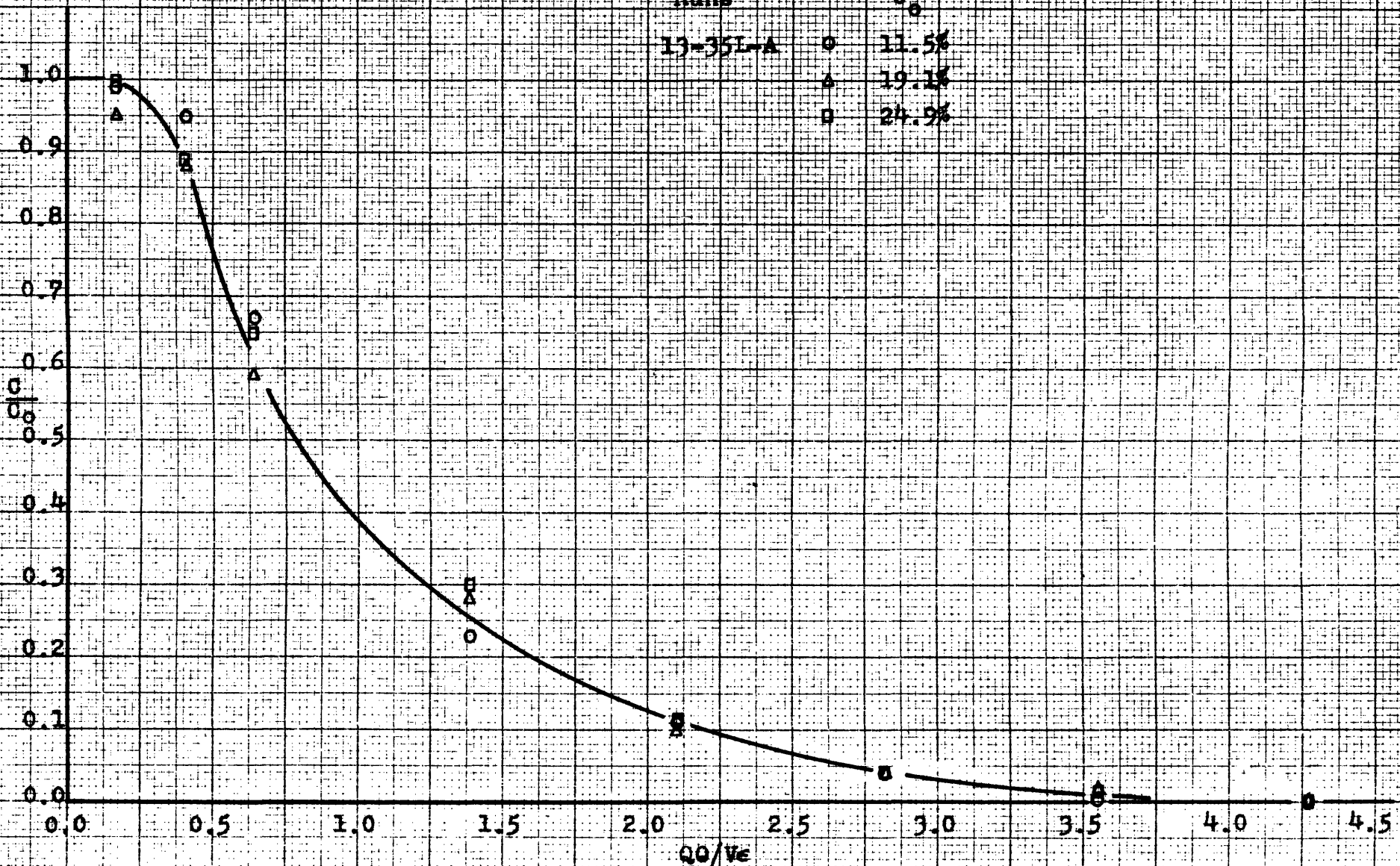


FIGURE 43

EFFECT OF TRACER INJECTION RATE

Runs	θ
13-35L-A	11.5%
	19.1%
	24.9%



an effect on the residence-time results, changing the helium rate should have drawn attention to it. In Figure 43, no effect of stopping the flow of helium is evident for the flow rates used in these studies.

2. Analysis of Experimental Technique

The advantage of the technique of sampling used in the residence-time studies over that used in the back-mixing investigation is in the elimination of the sampling error caused by the two "phases" present in aggregative fluidization. Since the gases are sampled after they leave the bed, their analysis should represent the average composition of the gases with greater accuracy. This means that the results of the residence-time studies should be more quantitatively reliable than those of the down-mixing experiments.

However, the information to be obtained from external sampling is limited by the very nature of the technique employed. Only knowledge concerning the time that the gases remain in the apparatus is obtained; nothing is disclosed concerning the concentration gradients existing in the bed, and only limited information concerning the mechanism of gas flow through the beds is acquired. It is possible to compare the experimental results with those to be expected from a definite type of gas mixing, but such a comparison can not definitely

establish the true pattern of gas flow.

The concentration of tracer in the exit stream, C/C_0 , is employed in the figures presented in the Results section in order to permit a graphical check on the reliability of any run. However, interest is centered in observing the flow of fresh gas through the bed. The fresh gas is known to have entered either at, or after, some definite time, and thus the concentration of fresh gas in the exit stream is of more utility than that of the tracer. Therefore, it should be remembered that the concentration of fresh gas in the exit stream at any time θ , or at $Q\theta/V\epsilon$, is equal to $1-C/C_0$; this is obtained by subtracting the given ordinates from unity.

In addition to the direct observations which can be made of the experimental data, a mathematical consideration of the experimental technique reveals that the curves contain additional information of considerable value. The experimental curves show that piston-type flow is not occurring in fluidized beds, but, rather that the exit gas is composed of gas molecules that have been in residence in the bed for varying periods of time; this is evident from the fact that both tracer gas and fresh gas are found in the exit stream at certain times. From this, it follows that the individual mole-

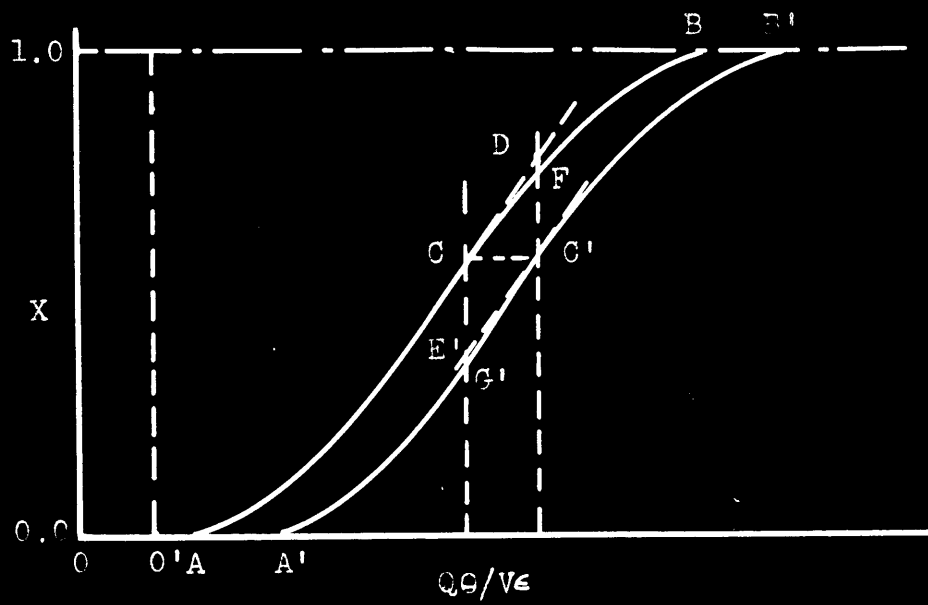
cules in any slug of gas that enters a fluidized bed have various residence times. Knowledge of these residence times and the variables that affect them is of importance in the application of fluidization to chemical operations. The residence-time technique developed in the course of this study provides a means for obtaining such information.

In developing the proof underlying the methods used in interpreting the experimental data, a graphical approach will be used. The same result can be obtained by employing a probability concept (see VII APPENDIX B). It was desired to determine how long any fraction of a unit of entering gas remains in a fluidized bed and the rate at which this fraction leaves the bed. The problem was to obtain this information concerning an element of entering gas from a study of the concentration-time gradient of a tracer gas in the exit gas stream.

Figure 44 is useful in following the derivation. (See following page.)

$X = 1 - C/C_0$ = the concentration of "fresh" gas in the exit stream, where "fresh gas" is gas which enters after $\theta = 0$.

FIGURE 44
RESIDENCE-TIME DERIVATION



$$\int_0^{\frac{Q\theta}{V\epsilon}} X \, d \frac{Q\theta}{V\epsilon} = \text{number of void volumes, } V\epsilon, \text{ of "fresh" (15-IV)}$$

gas that entered after $\theta = 0$ and have
left by $Q\theta/V\epsilon$

= area under curve OACB out to $Q\theta/V\epsilon$

Curve O'A'C'B' is curve OACB displaced by $d(Q\theta/V\epsilon)$
to the right.

$$\int_0^{\frac{Q\theta}{V\epsilon}} X \, d \frac{Q\theta}{V\epsilon} = \text{number of } V\epsilon \text{ of "fresh" gas that enter- (16-IV)}$$

ed after $\theta = 0$ and have left by $Q\theta/V\epsilon$

= area under curve O'A'C'B' out to $Q\theta/V\epsilon$.

Therefore, the area between curves OACB and O'A'C'B' out to any $Q\theta/V\epsilon$ represents the amount of "fresh" gas that entered during the $d(Q\theta/V\epsilon)$ immediately after $Q\theta/V\epsilon = 0$ and has left the bed by the $Q\theta/V\epsilon$ in question.

CC' also represents a $d(Q\theta/V\epsilon)$ of the same size as the entering slug, and therefore the area CFC'G' represents the quantity of "fresh" gas which entered in the $d(Q\theta/V\epsilon)$ following $Q\theta/V\epsilon = 0$ and left in the $d(Q\theta/V\epsilon)$ following $Q\theta/V\epsilon = C$.

Neglecting differentials of higher order, the
slope at C = slope at C' = $\frac{d X}{d \left(\frac{Q\theta}{V\epsilon} \right)}$ (17-IV)

and the area CDC'E' = area CFC'G' = CC' times C'D

$$= \frac{d X}{d \left(\frac{Q\theta}{V\epsilon} \right)} \cdot d \left(\frac{Q\theta}{V\epsilon} \right) \cdot d \left(\frac{Q\theta}{V\epsilon} \right) \quad (18-IV)$$

= amount of fresh gas that enters
in the first $d(Q\theta/V\epsilon)$ and leaves
in the $d(Q\theta/V\epsilon)$ following $Q\theta/V\epsilon = C$.

$$\frac{\frac{d X}{d\left(\frac{Q\theta}{V\epsilon}\right)} \cdot d\left(\frac{Q\theta}{V\epsilon}\right) \cdot d\left(\frac{Q\theta}{V\epsilon}\right)}{d\left(\frac{Q\theta}{V\epsilon}\right)} = \text{the fraction of the gas that} \quad (19-IV)$$

entered in the first $d(Q\theta/V\epsilon)$ that
leaves in the $d(Q\theta/V\epsilon)$ following C .

The desired function, F , is the fraction of an entering differential quantity that leaves per unit of gas, as a function of the total gas leaving.

$$\text{Therefore, } F = \frac{\frac{d X}{d\left(\frac{Q\theta}{V\epsilon}\right)} \cdot d\left(\frac{Q\theta}{V\epsilon}\right) \cdot d\left(\frac{Q\theta}{V\epsilon}\right)}{d\left(\frac{Q\theta}{V\epsilon}\right) \cdot d\left(\frac{Q\theta}{V\epsilon}\right)} \quad (20-IV)$$

$$= \frac{d X}{d\left(\frac{Q\theta}{V\epsilon}\right)} = \text{slope at } C \quad (21-IV)$$

$$= \frac{-d \frac{C}{C_0}}{d\left(\frac{Q\theta}{V\epsilon}\right)} = \text{negative of the slope} \quad (22-IV)$$

of the experimental
data curves.

F is a function of $Q\theta/V\epsilon$. It should be realized that F is not a fraction, but can vary in magnitude from zero to infinity.

$$\int_M^N F d(Q\theta/V\epsilon) = \text{fraction of entering gas which} \quad (23\text{-IV})$$

leaves between $Q\theta/V\epsilon = M$ and N .

$$\int_M^N \frac{dX}{d\left(\frac{Q\theta}{V\epsilon}\right)} d\left(\frac{Q\theta}{V\epsilon}\right) = \int_M^N dX = (X)_N - (X)_M =$$

$$= \left(\frac{C}{C_0}\right)_M - \left(\frac{C}{C_0}\right)_N \quad (24\text{-IV})$$

Therefore C/C_0 at $Q\theta/V\epsilon =$ the fraction of entering gas that remains for time θ or longer.

Consideration will show that Equation (23-IV) also represents the probability that an entering gas molecule will remain in the bed for a time equal to M but leave before time equal to N . Therefore F can be considered to be the probability density.

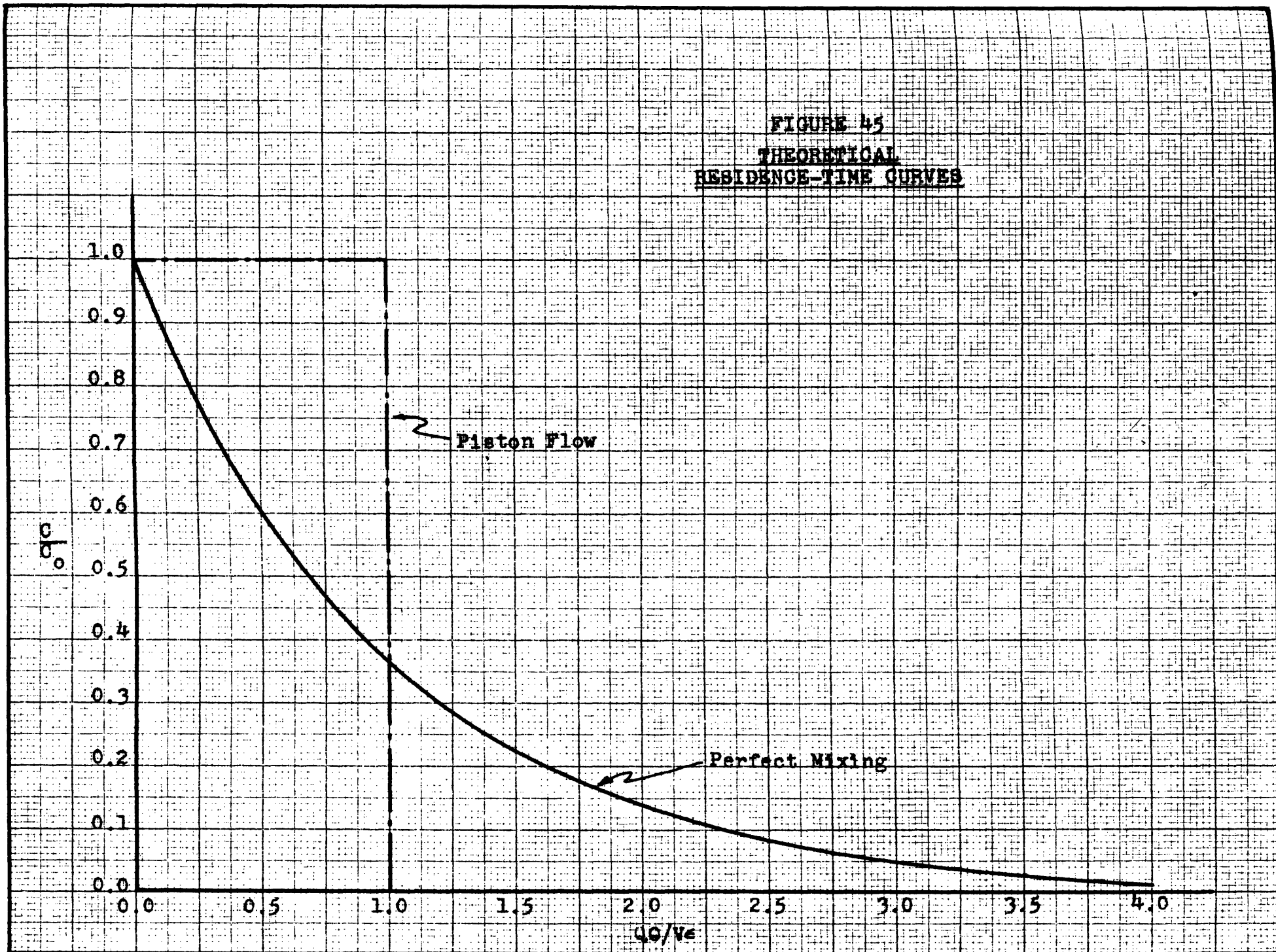
Application of these relationships involves the assumption that the flow of the gases in fluidized beds is reproducible, i.e., that each slug of entering gas will have a fractional residence-time history identical to that of every other slug of entering gas. The reproducibility of experimental runs which were repeated under the same operating conditions supports this assumption.

In summary, the probability that a molecule will remain in a fluidized bed, operated at definite conditions, any definite period of time and then leave can

be determined from the slope of the experimental curves. That period of time is defined as the residence-time. In addition, the ordinate, $1-C/C_0$, at any θ represents the fraction of an entering slug of gas that has left the bed by a time equal to θ after the slug entered the bed. Consequently, the quantity, $(C/C_0)_1 - (C/C_0)_2$ represents the fraction of a slug of gas that leaves, or has left the bed after the slug has been in the bed for a time at least equal to θ_1 but less than θ_2 . For illustration, the probability function, F , is presented for Runs M2-70-All in Figure 33.

Realizing the significance of the graphical method employed to present the results of the experimental work, it is of interest to consider the curves to be expected if piston flow or perfect mixing were to occur. The theoretical curves for these two cases are shown in Figure 45. The piston flow case would result in a horizontal line at a C/C_0 ordinate of unity until one void volume of gas had passed through the bed; then the ordinate would drop instantly to a value of zero and remain equal to zero. The residence-time of a gas molecule for the case of piston flow is the time it takes for one void volume of gas to flow through the bed, i.e., $\theta = V\epsilon/Q$. The significance of the quantity, $1-C/C_0$, with regard to the fraction of an entering slug that remains

FIGURE 45
THEORETICAL
RESIDENCE-TIME CURVES



a given period of time agrees with the concept of piston flow.

For the case of perfect mixing, data fitting the equation

$$C/C_0 = \exp(-Q\theta/V\epsilon) \quad (26-IV)$$

would be expected (see VII APPENDIX B); this is the equation shown in Figure 45. The derivative of $(1-C/C_0)$ at any value of $Q\theta/V\epsilon$, which represents the probability density, F , (see Equation 21-IV), is equal to $\exp(-Q\theta/V\epsilon)$; this is identical with the integral curve plotted. This identity of the data curve and probability curve only holds for the case of perfect mixing. Any ordinate on the theoretical C/C_0 curve for perfect mixing represents the fraction of entering gas that remains in the bed longer than θ time. For example, by the time one void volume of gas has passed through the bed after a given slug entered the bed, only 0.368 of that given slug will remain in the bed. This example illustrates the utility of plotting the curves against $Q\theta/V\epsilon$ as the abscissa. In the cases of perfect mixing and piston flow the probability function for a given residence-time changes with variation in the flow rate, size of the bed, and type of particles used, while the probability function for a given number of void volumes of gas passing through the

bed is constant regardless of operating conditions.

In the following discussion of the curves which were experimentally determined, comparison will be made with the results that would be expected if either piston flow or perfect mixing had taken place under the same operating conditions. Such a comparison should not be taken to mean that these were necessarily the mechanisms of mixing actually existing. If the data agree exactly with those expected from piston flow, then piston flow surely must have been occurring in the fluid bed; no other practical flow pattern would give the identical results.

However, it is possible that data similar to those to be expected from perfect mixing can be obtained from some other mechanism of gas flow through fluidized beds. One such possible mechanism is analogous to the stripping action of bubbles flowing up through a liquid bath. The stream of bubbles rising through fluid beds could conceivably give a perfect mixing curve by stripping the tracer from the dense phase. Other mechanisms may also give results similar to perfect mixing.

Before considering the experimental data, it should be pointed out that the method developed in this thesis and outlined above can be applied to other types of mixing chambers. It would be especially suited for obtaining

the residence-times to be expected in liquid agitators, because the volume change accompanying chemical reactions in liquids is usually negligible; the mathematical interpretation of the data would have greater application in the mixing of liquids than it does with gases, where many reactions are accompanied by large changes in volume.

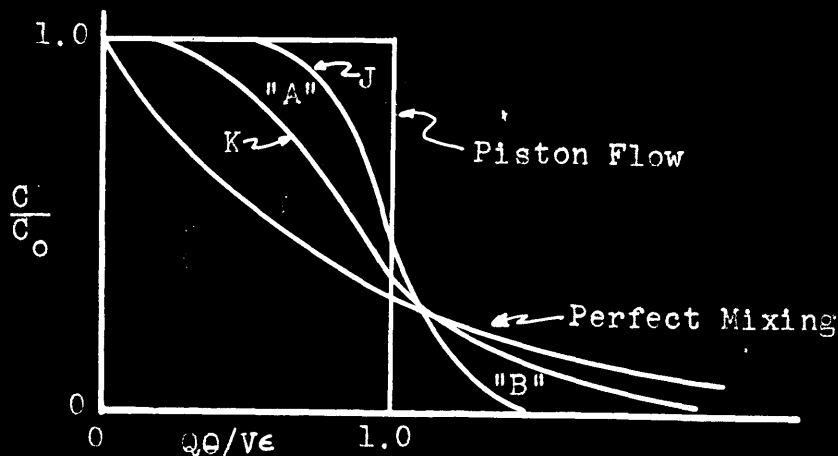
3. Effect of Operating Variables: Correlations

Two methods have been employed for comparing the effects of such operating variables as superficial velocity, bed size, and particle characteristics, on the residence-times.

The first is merely one of visually comparing the shapes of the resulting residence-time curves when shown on rectangular coordinates. The mathematical significance of the shape of these curves is utilized in making this visual comparison.

Figure 46 will be used to illustrate a few comments on the validity of any differences shown between the data taken under varying operating conditions. The theoretical curves for piston flow and perfect mixing and two curves typical of Figures 26 through 41 are shown. From a material balance, Equation 14-IV, it is evident that if one set of operating conditions, designated J,

FIGURE 46
COMPARISON OF RESIDENCE-TIME CURVES



gives results that approach those of piston flow more closely than the results of another set of operating conditions, K, then the experimental points of run J must both lie above those of K in the region marked "A" on Figure 46 and lie below in the region marked "B". The converse applies for perfect mixing. If the experimental points do not conform to both of these conditions, then no definite difference in the residence-times has been established that could not be explained on the basis of experimental error.

The second method used in examining the experimental data was prompted by the shape of the experimental curves shown in Figures 26 through 41. Many of these graphs

resemble exponential curves displaced from the zero abscissa, suggesting an exponential, or semi-logarithmic, presentation of the data. If the data can be represented by an exponential relationship, the logarithm of C/C_0 plotted as ordinate against the group, $Q\theta/V\epsilon$, as abscissa, should yield a straight line with slope represented by $-S$. The value of $Q\theta/V\epsilon$ at C/C_0 equal to unity will be designated by the letter "I." The equation of such a line is

$$\ln C/C_0 = -S(Q\theta/V\epsilon - I) \quad (27-IV)$$

If the experimental results can be represented by an expression of this form, then it can be shown from a material balance that

$$I = \frac{S - 1}{S} \quad (28-IV)$$

(see VII APPENDIX B) and, therefore, the data for any one set of operating conditions could be characterized by the value of S , which is the absolute value of the slope of the data when plotted on semi-logarithmic coordinates. The value of S increases from unity for perfect mixing to infinity for piston flow, while I increases from zero to unity.

In order to test this method of plotting, the data of Figures 26 through 41 were plotted on semi-logarithmic coordinate paper. As examples of this method, Figures

47, 49, and 51 are presented showing the data for several different runs. The data can be represented by straight lines, which are characterized by a slope, S , and an intercept, I . (See VII APPENDIX D for other plots.) In Figures 48, 50, and 52 values of C/C_0 calculated from the slopes of Figures 47, 49, and 51 are shown; the experimental data are those shown in Figures 26, 33, and 41. The agreement between calculated and experimental values is good, indicating that it is possible to characterize the experimental results for any run by the value of S .

The experimental results will now be discussed using the two methods of analysis that have been described.

Fixed Bed and Empty Tube

Figure 26 shows the experimental data obtained for runs made under fixed-bed conditions with No. 7 glass beads in both the 3-inch and 4-1/2-inch columns; a run made with the empty 4-1/2-inch tube is also shown. Within the accuracy of the data, one line is representative of the three runs. As would be expected, the shape of the curve closely resembles that anticipated from piston flow of the gas. The rather good agreement between the experimental residence-time data for the fixed bed and the theoretical curve for piston flow in-

FIGURE 47
FIXED BED AND EMPTY TUBE

Runs	u_o	$S = 8.4$
○ 7-37-A	0.38	$I = 0.85$
△ 7-35L-A	0.38	
□ 0-37-A	0.40	

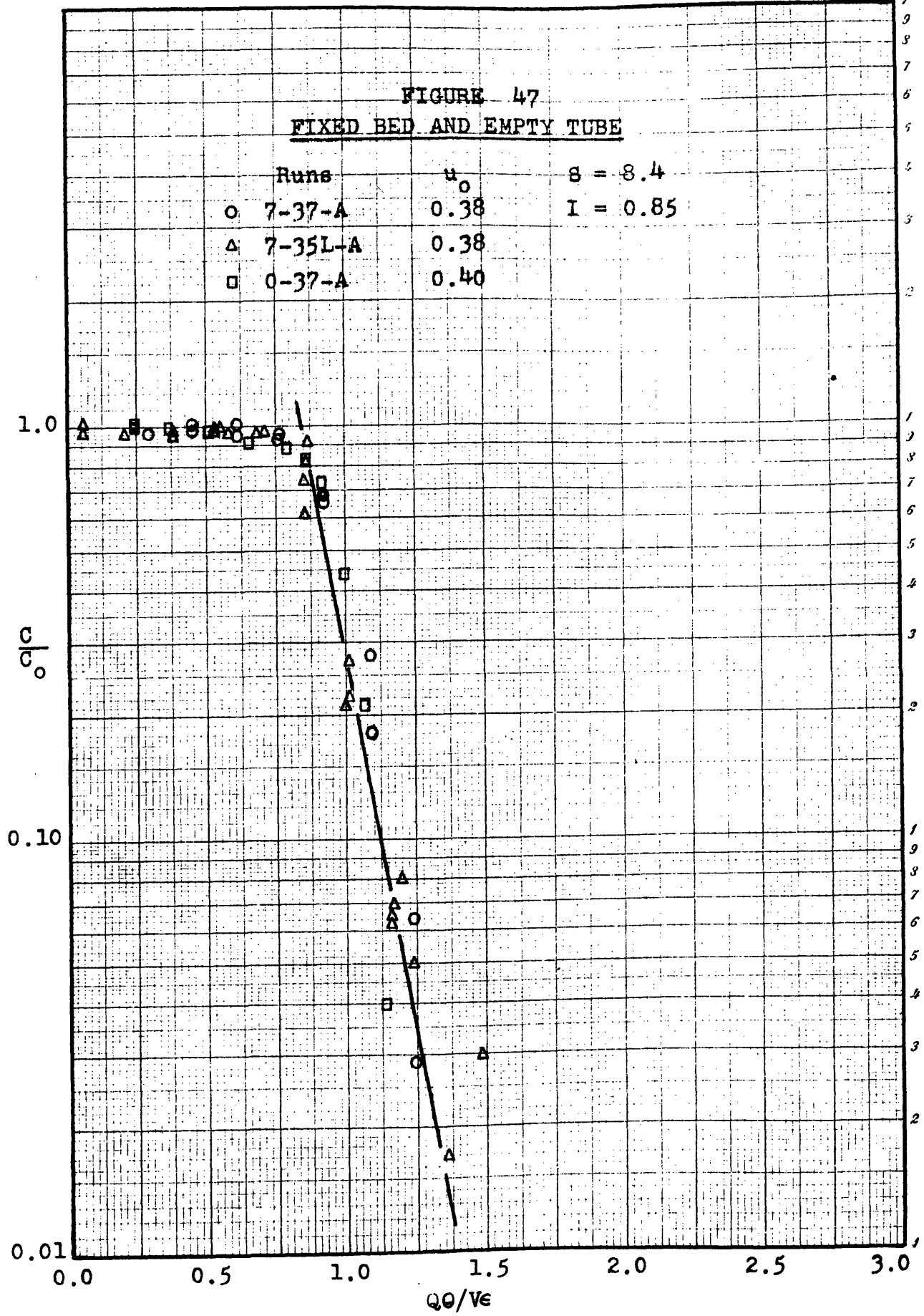


FIGURE 48

FIXED BED AND EMPTY TUBE: CALCULATED

S = +8.4 Points - Experimental

I = 0.85 Curve - Calculated

See Figure 26

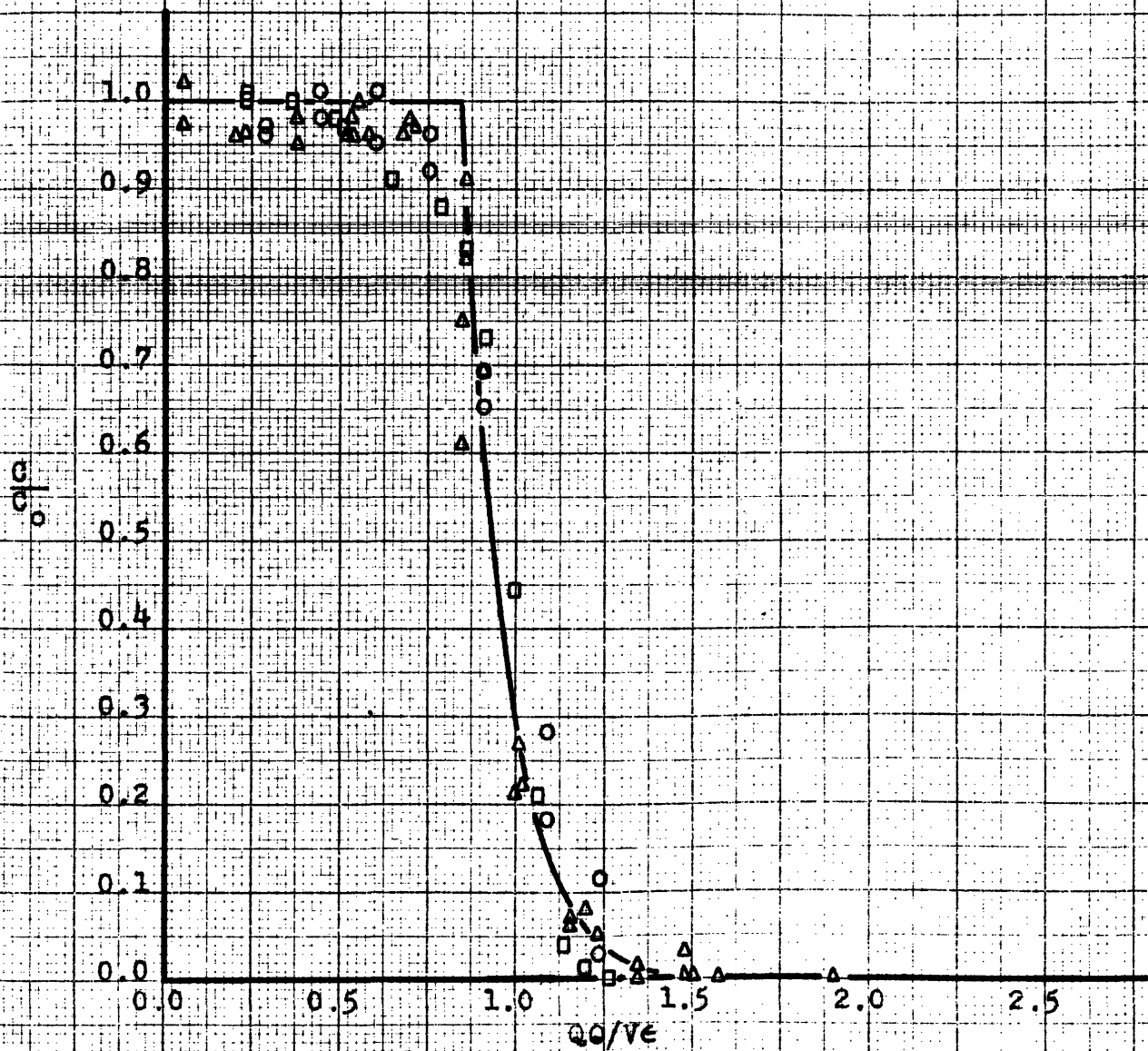


FIGURE 49

MICROSPHERES, M2

Runs	u_0	
○ M2-70-A	0.98	$S = 1.54$
△ M2-70-C	0.78	$I = 0.37$

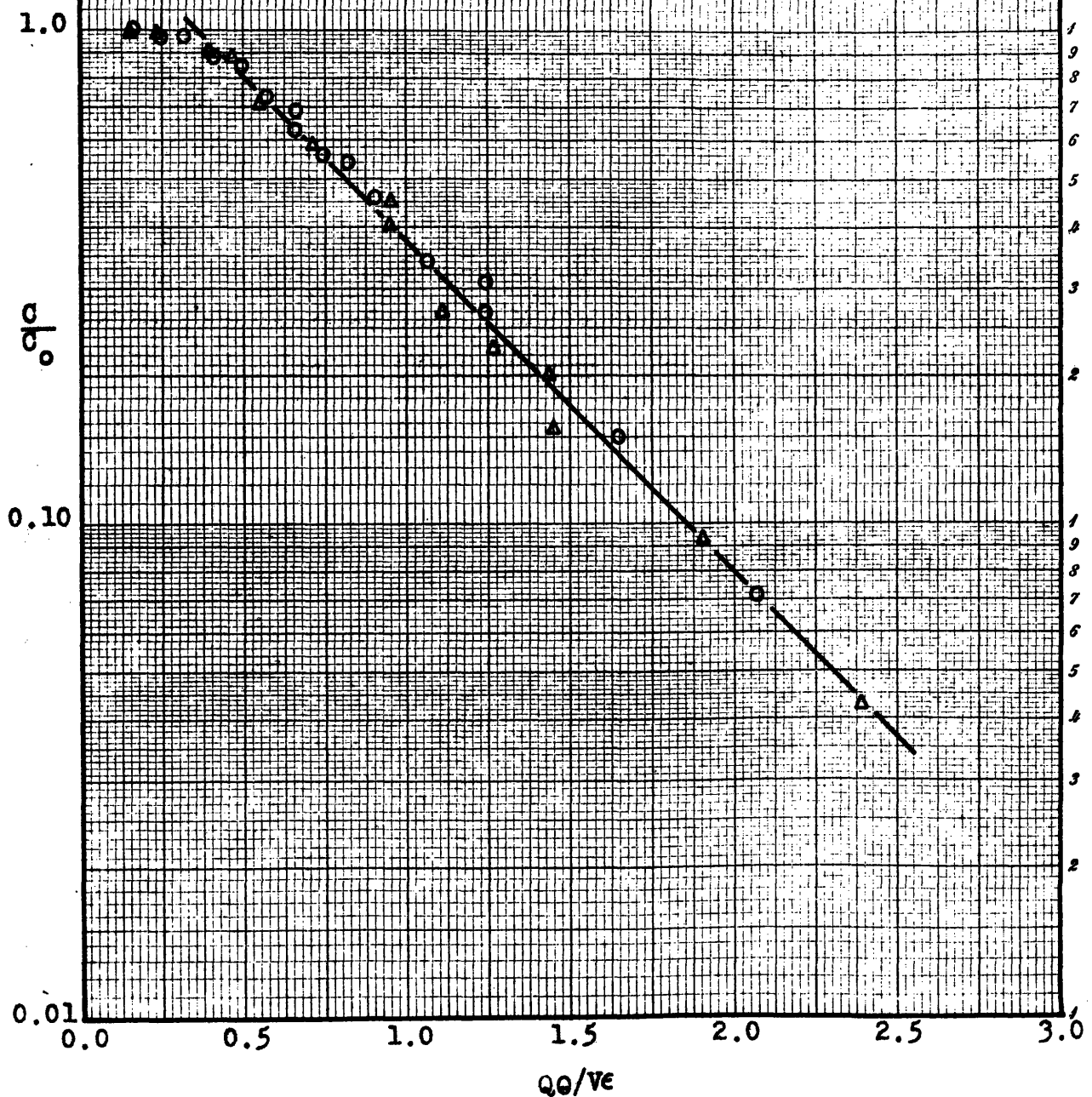


FIGURE 50

MICROSPHERES, M2-70: CALCULATED

$S = 1.54$ Points - Experimental

$I = 0.37$ Curve - Calculated

See Figure 33

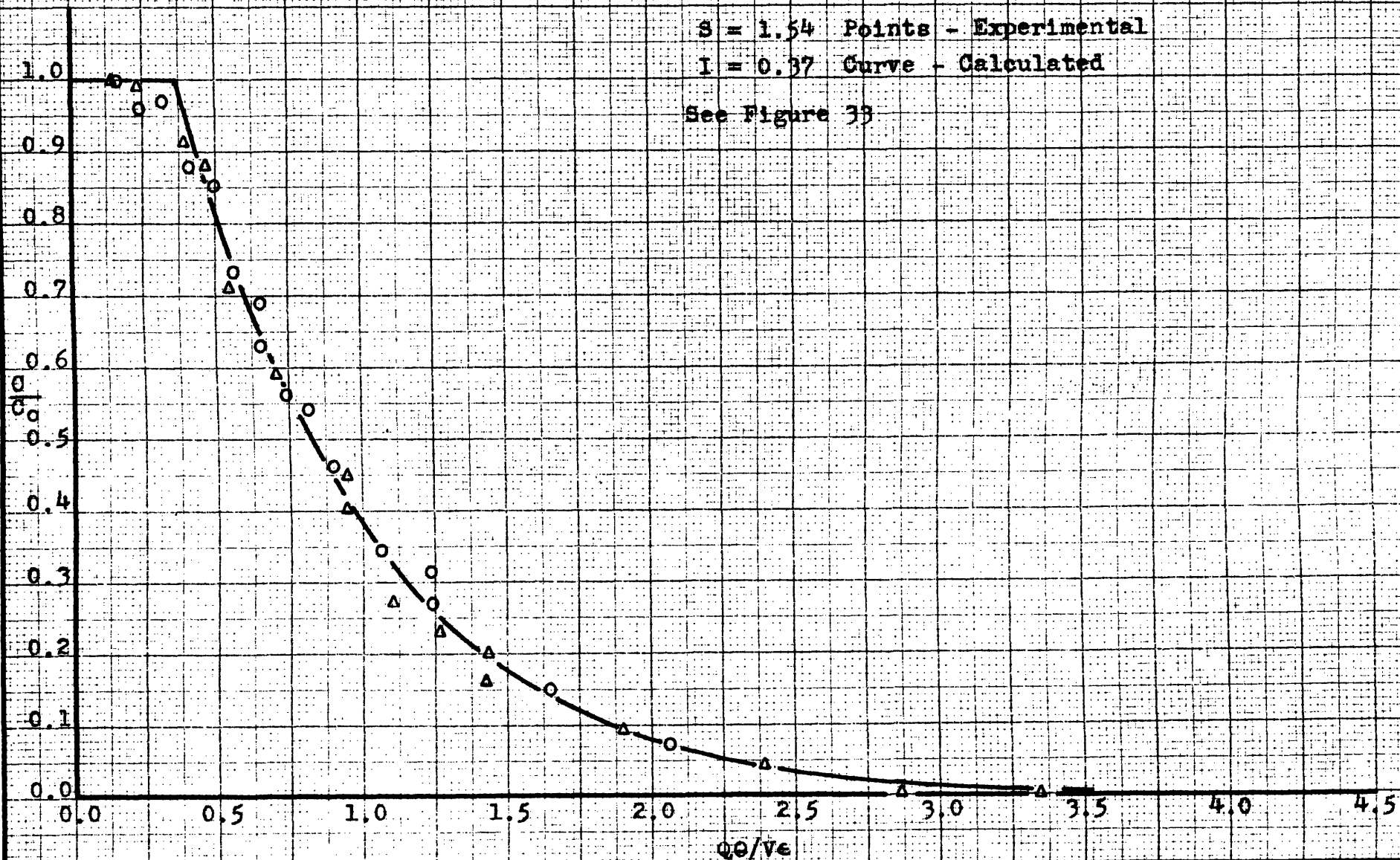


FIGURE 51
 MICROSPHERES, M3-35L

Runs	v_0
○ M3-35L-A	0.40
▽ M3-35L-B	0.61
△ M3-35L-C	0.81
□ M3-35L-D	1.03

$\sigma = 1.05$
 $I = 0.03$

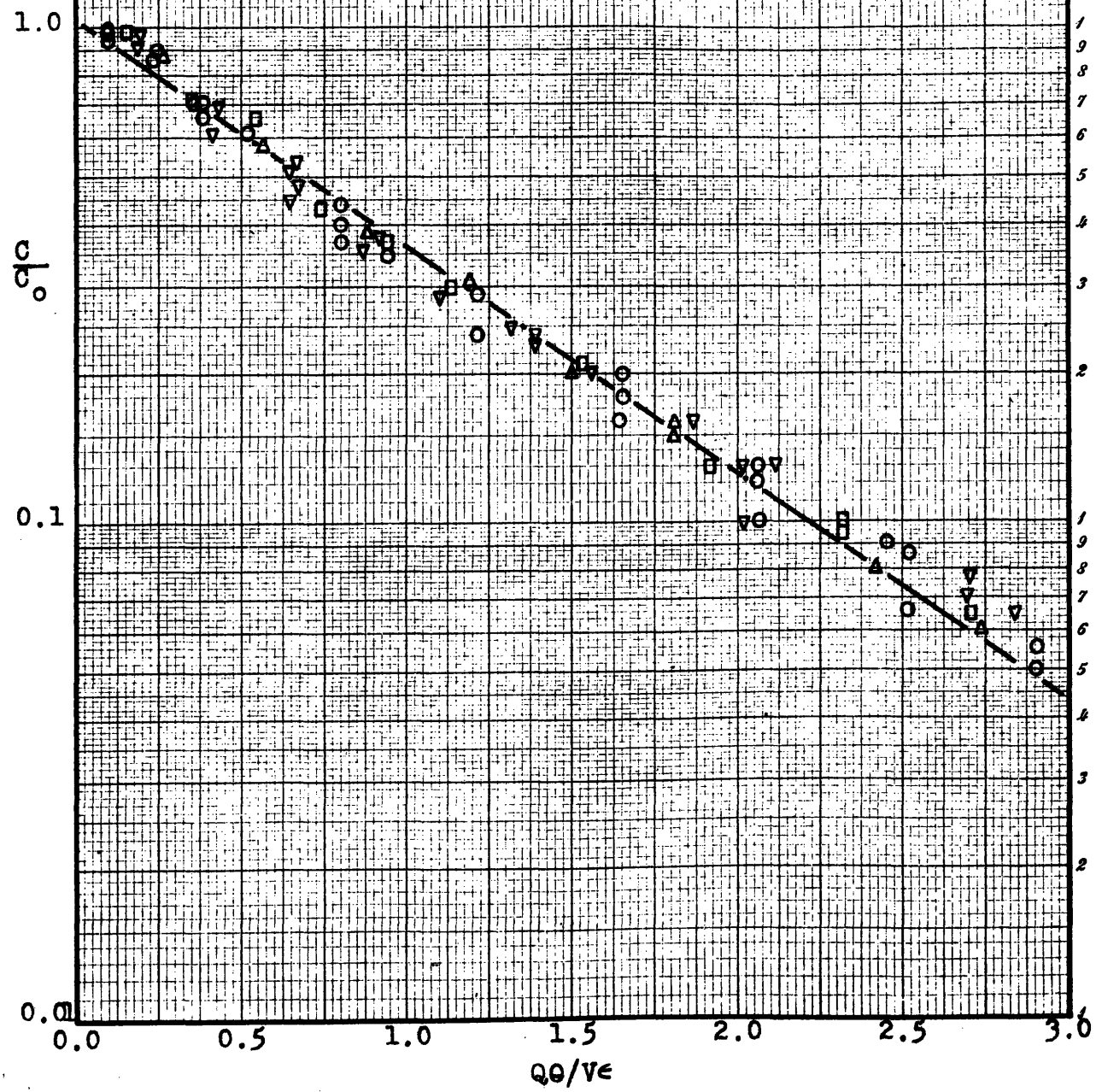


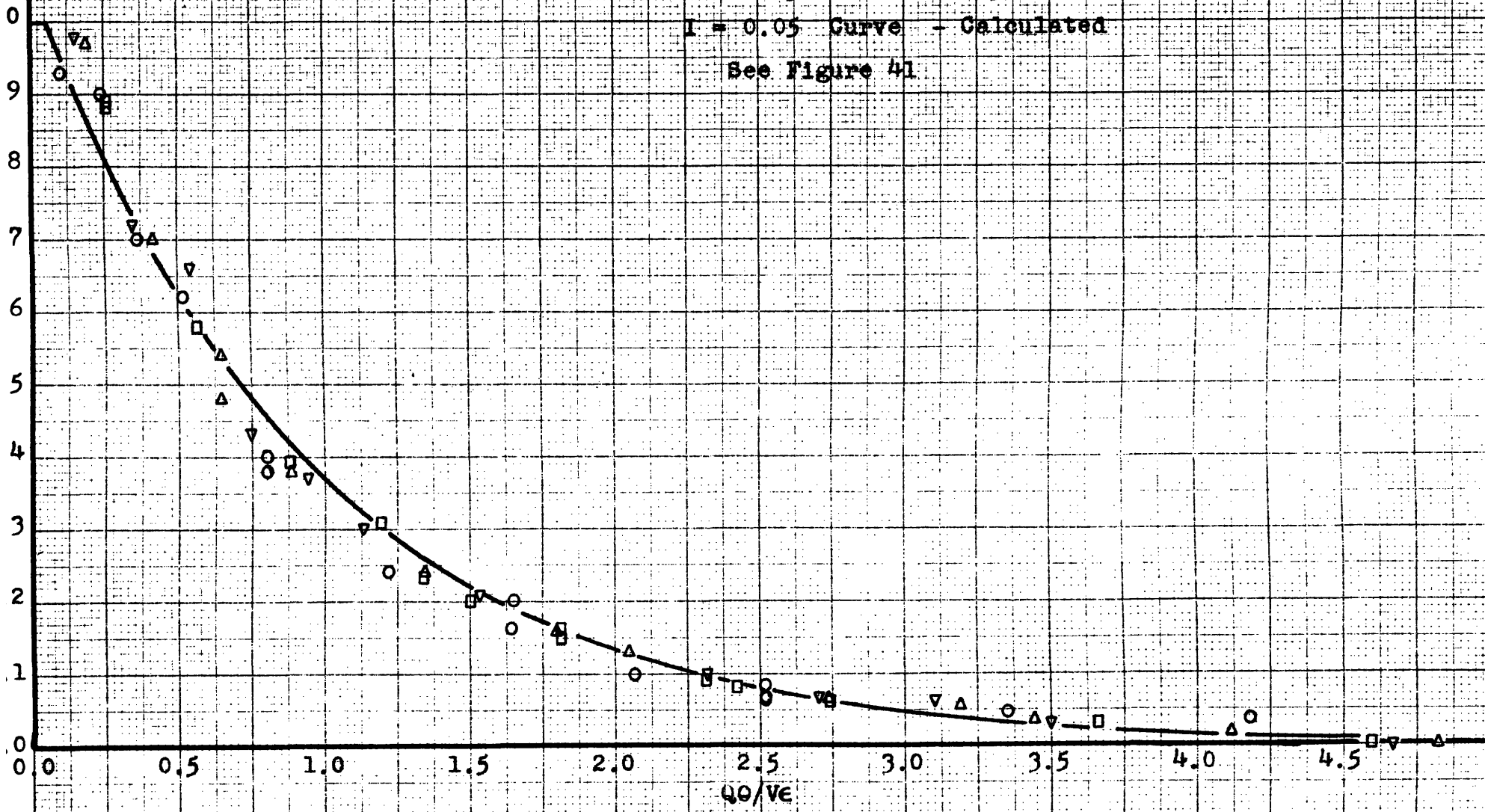
FIGURE 52

MICROSPHERES, M3-35L; CALCULATED

$S = 1.05$ Points - Experimental

$I = 0.05$ Curve - Calculated

See Figure 41



icates that the experimental procedure is valid.

It is of interest to notice that the first "fresh" gas appears at the top of the bed at a value of Q_0/V_0 approximately equal to one-half. For the empty column, this indicates that the ratio of maximum velocity to superficial velocity, u_m/u_0 , is about two. This is the value to be expected if laminar flow were present. While the Reynolds number for the flow during the empty tube run is 900, also indicating laminar flow, it seems doubtful that a parabolic velocity distribution would have been fully developed in the short L/D of 7.8. However, it does appear that the velocity distribution in empty tubes precludes true piston flow.

The ratio of the maximum velocity to the average velocity through the interstices of the fixed bed, u_m/u , is also two. The possibility of a parabolic velocity distribution across the fixed bed seems unlikely, but the evidence presented in Figure 26 suggests the presence of a velocity gradient which causes the flow in fixed beds to differ slightly from piston flow.

Effect of Superficial Gas Velocity

Figures 27 through 41 give the results of runs made under conditions of varying superficial air velo-

city. Each graph presents the runs made for a given solid and bed size at various gas velocities. Within the spread of the experimental data, no dissimilarity can be determined in the residence-time curves for fluid beds of given solids and bed dimensions under conditions of different gas velocities. In most runs the scatter in the experimental points is quite limited. The velocity range covered was from 0.4 ft./sec. to 1.0 ft./sec.

In Figure 27, the results obtained with the two highest gas velocities resemble the theoretical results of perfect mixing more than do the lower velocities used. However, in these experiments with the No. 7 glass beads, which were the largest solids used, the bed was not fluidized at the lower velocities. Only for the two highest velocities was there definite evidence of vigorous solid motion: in fact, slugging conditions were present. For the lower velocities, the bed was fixed or quiescent. The data collected for the two fluidizing velocities are best represented by a single line.

The conclusion that superficial gas velocity has no effect on the residence-time curves, when they are plotted on a void volume basis, can be checked by an examination of the semi-logarithmic plots to be found

in Figures 47, 49, 51, and in VII APPENDIX D. This method of plotting does not cause any separation of the data points for various velocities and one value of S is characteristic of all the runs made with fixed particle and bed size.

The only case where there seems to be any difference in the residence-time curves with a change in gas velocity appears in Figure 31 and the corresponding semi-log plot, which present Runs 13-35L-A, B, C, D. Here at large values of Q_0/V_0 , the points for Run A, 0.4 ft./sec., are higher than the values for the other runs. However, the data at low values of Q_0/V_0 for Run A do not lie below those of the other runs. In addition, the area under the curve presented in Figure 31 is 1.07, compared to the expected value of 1.00; drawing a line through the data of Run A would give a still greater area. Therefore, it is felt that the data for Run A contain a small error of unknown origin and do not actually indicate a different residence-time history.

It should be stressed that the comparison that has been made concerning the residence-time histories given by varying gas velocities has been made on a void-volume basis. From the experimental results, the probability that a molecule, or a certain fraction of

the entering gas, will remain a given time obviously decreases as the gas velocity increases. The residence-time for a given fraction of entering gas is inversely proportional to the gas velocity. However, the probability of a given fraction of entering gas remaining in the bed until a certain number of void volumes of gas have left the bed is independent of the superficial gas velocity. A definite amount of gas is required to "sweep out" any fraction of entering gas, regardless of the rate at which the gas flows through the fluid-bed.

Length-to-Diameter Ratio

Since no effect of gas velocity on the residence-time curves was observed, the composite plots showing all the velocities studied for a given condition of particle or bed size will be utilized in arriving at conclusions concerning the effect of variation in particle and bed size.

Figures 53, 54, and 55 are designed to show the change in the residence-time curves with increasing L/D . Figures 54 and 55 show the experimental curves for two solids, M2 and M3, at values of L/D of 7.8, 12.3, and 23.3. The lines shown were traced from the curves through the experimental points (see Figures 33, 34, 37, 38, 40, and 41). In order to show that

FIGURE 53

MICROSPHERES: EFFECT OF BED DIMENSIONS

$u_o = 0.4$ ft./sec.

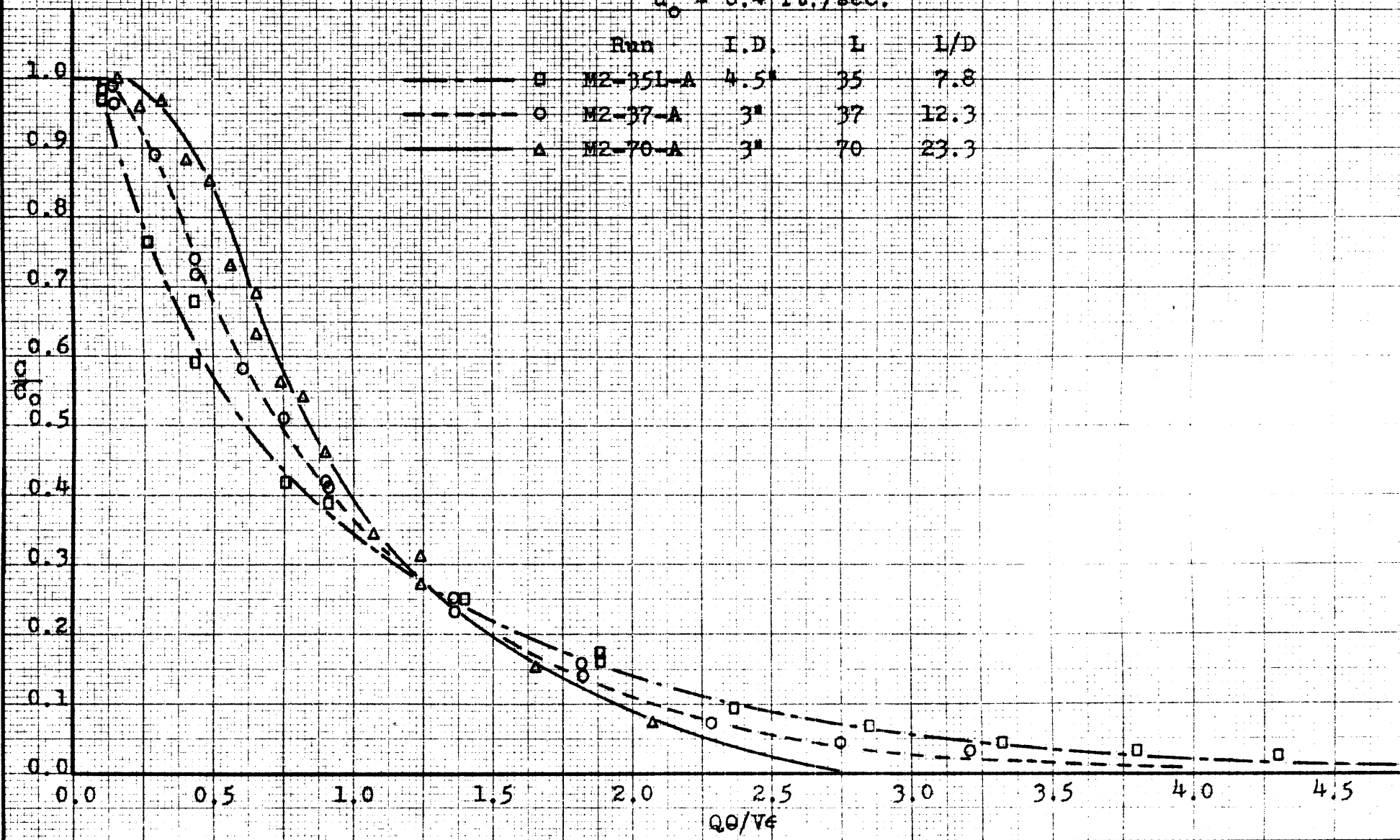


FIGURE 54

MICROSPHERES: EFFECT OF BED DIMENSIONS

Runs	I.D.	L	L/D	Area
M2-35L-A11	4.5"	35"	7.8	0.99
M2-37-A11	3"	37"	12.3	0.99
M2-70-A11	3"	70"	23.3	0.99

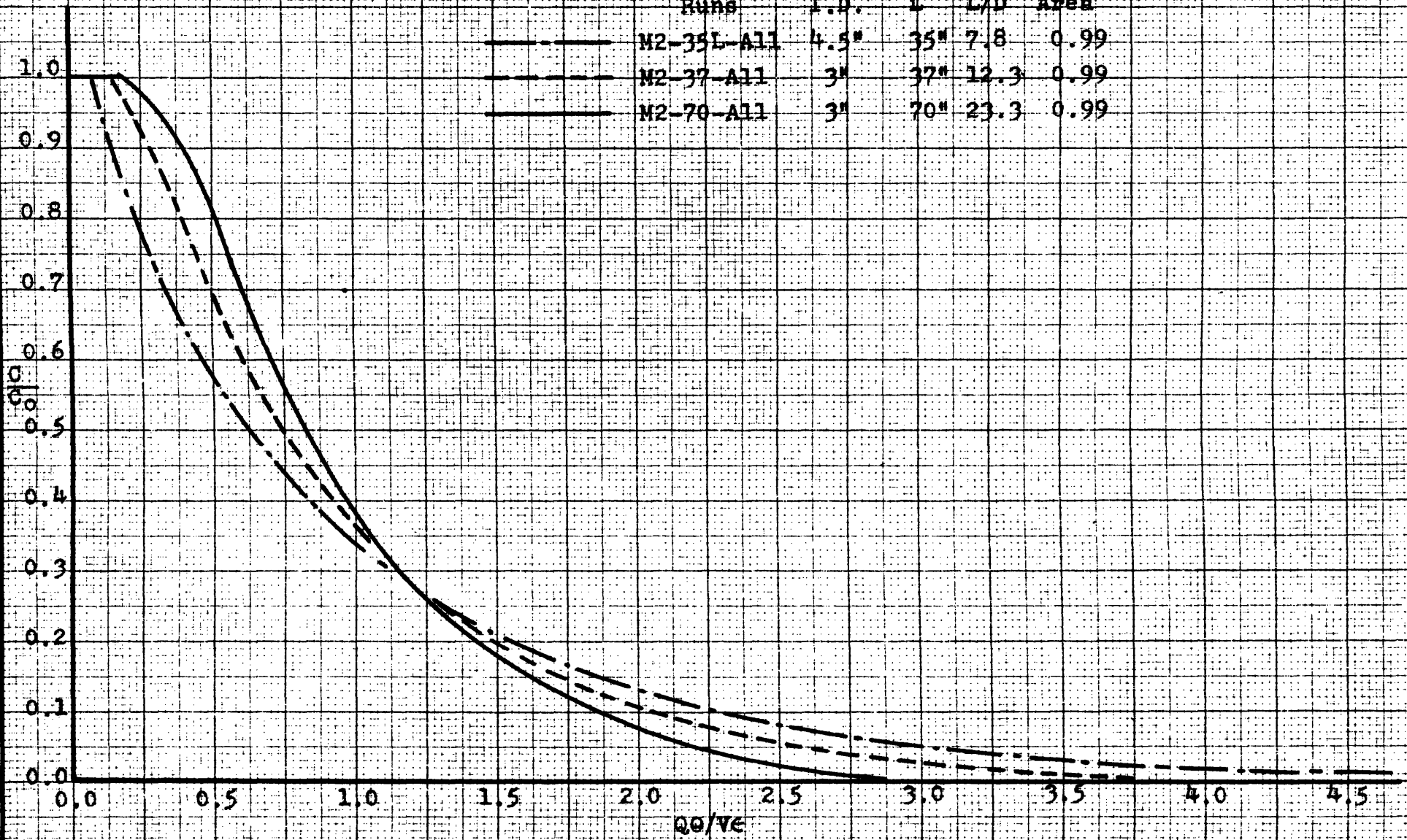
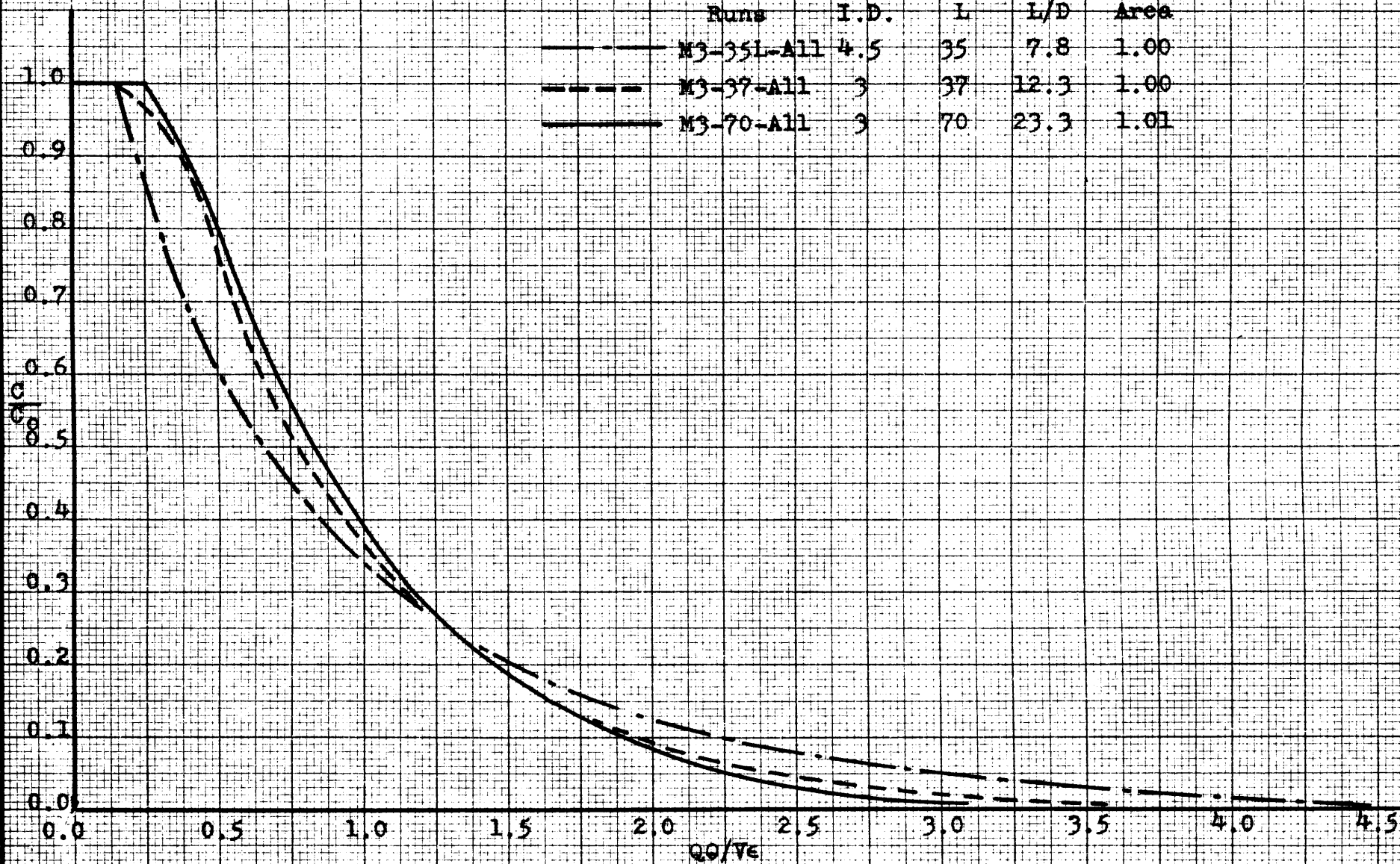


FIGURE 55

MICROSPHERES; EFFECT OF BED DIMENSIONS

Runs	I.D.	L	L/D	Area
M3-35L-A11	4.5	35	7.8	1.00
M3-37-A11	3	37	12.3	1.00
M3-70-A11	3	70	23.3	1.01



the differences between the curves are significant, Figure 53 gives the data of runs made with M2 solids at an air velocity of 0.4 ft./sec. for the three values of L/D employed.

Table XVII presents the values of S and I for the runs shown in Figures 54 and 55. In addition, values of $(S-1)/S$ are given to show the good agreement between the value of I obtained from the experimental intercept and calculated from the slope of the line (see Equation (26-V)).

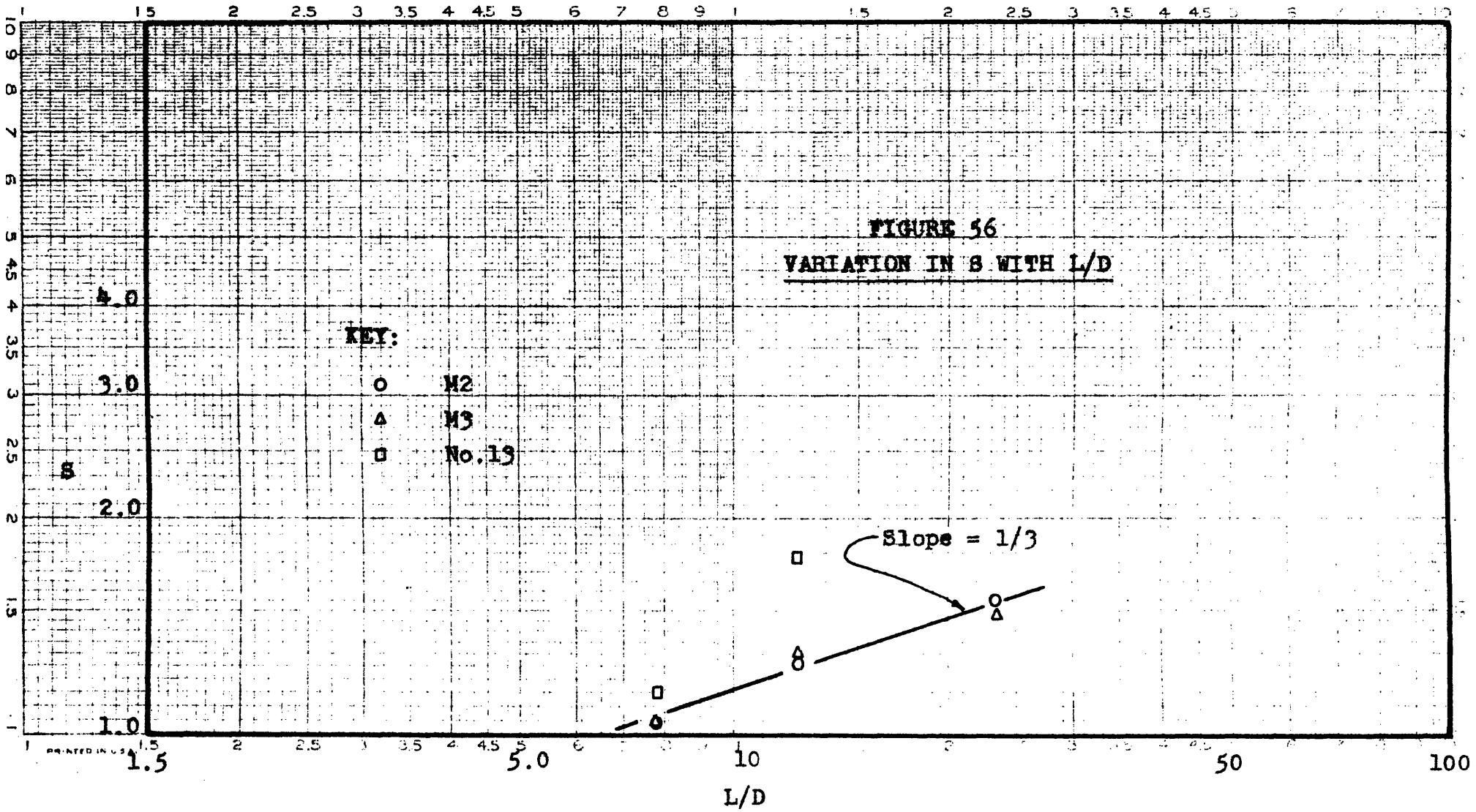
Both visual comparison of the differences between the experimental curves, and the increasing values of S in Table XVII indicate a tendency toward the piston flow results as the L/D increases. The same trend holds as the bed height is increased or the diameter decreased. Figure 56 shows S as a function of L/D on logarithmic coordinates. Within the accuracy of the slopes, a single line characterized the data of both sizes of microspheres used in this experiment. The equation of the line through the experimental points is

$$S = 0.54 (L/D)^{1/3} \quad (29-IV)$$

Obviously, this equation can not be used for extrapolation to low values of L/D. The range of residence-times is higher with beds of low L/D than with high L/D.

TABLE XVIIEffect of L/D Ratio on Values of S and I

Run	L/D	S	I	$\frac{S-1}{S}$	
M2-35L-A11	7.8	1.04	0.01	0.038	
M2-37-A11	12.3	1.25	0.17	0.20	
M2-70-A11	23.3	1.54	0.37	0.35	
M3-35L-A11	7.8	1.05	0.03	0.048	
M3-37-A11	12.3	1.32	0.22	0.24	
M3-70-A11	23.3	1.47	0.36	0.32	
13-35L-A11	7.8	1.15	0.28	0.30	Area = 1.07
13-37-A11	12.3	1.77	0.38	0.44	Area = 0.93



For a given bed height gas velocity and solid, the minimum residence-time is least and the maximum residence-time is greatest for the fluid beds with low values of L/D .

Only two sets of data on glass beads are available for comparison on an L/D basis. These are 13-37-All and 13-35L-All. As shown in Table XVII, the integral area of the data for these two sets of values both vary by 7% from the expected area; one area is high and the other low. Correction of this discrepancy would increase the slope of 13-35L-All and decrease the slope of 13-37-All. The result would be that the values of S would lie above those for the microspheres, but might conceivably have the same power function of L/D . Since the experimental data of the No. 13 beads have the slight discrepancy mentioned, nothing quantitative can be said concerning the variation in the value of S with increasing L/D for glass beads.

Particle Size

Figures 57, 58, 59, and 60 have been prepared to show the effect of particle size on the residence-time curves. Figure 57 shows the data for the runs made with all sizes of glass beads in the 3-inch column with a bed height of 37 inches and a superficial velocity

FIGURE 57

GLASS BEADS: EFFECT OF PARTICLE SIZE

	Runs	u_0
○	7-37-A	0.38
▽	9-37-A	0.37
△	11-37-A	0.39
□	13-37-A	0.39

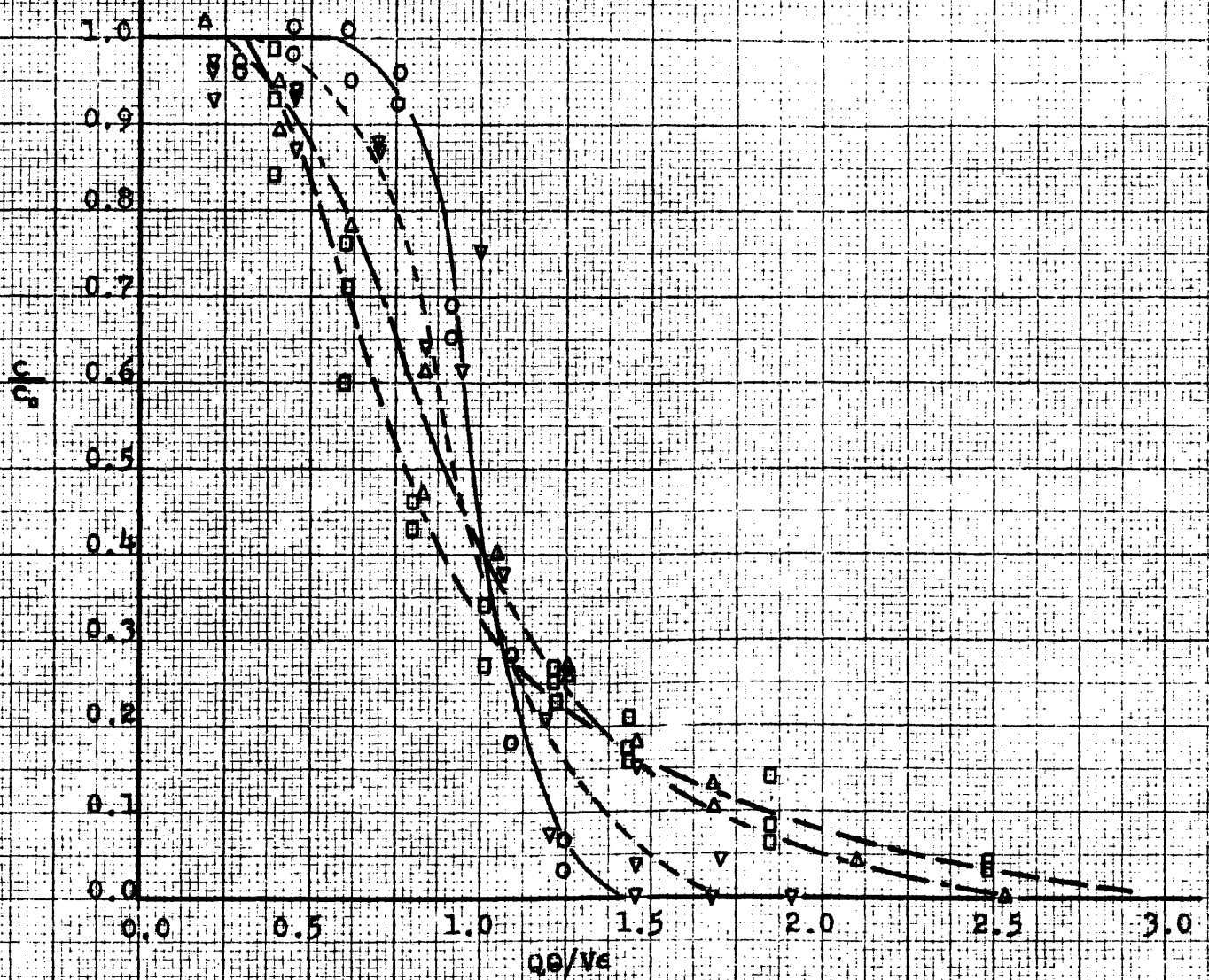


FIGURE 58

GLASS BEADS: EFFECT OF PARTICLE SIZE

	Runs	Area
-----	7-37-All	0.93
————	9-37-All	0.97
-----	11-37-All	1.00
————	13-37-All	0.93

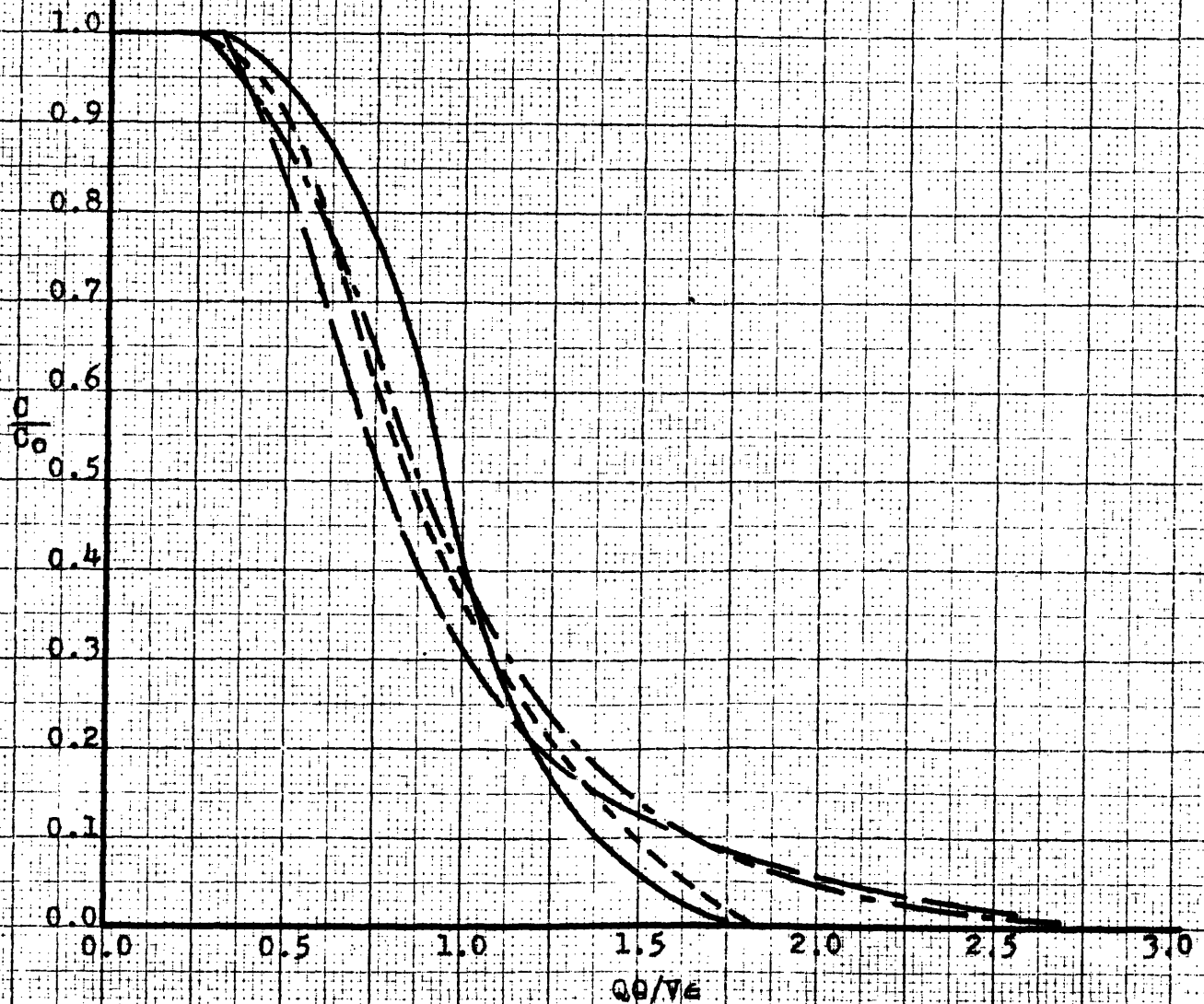


FIGURE 59

MICROSPHERES: EFFECT OF PARTICLE SIZE

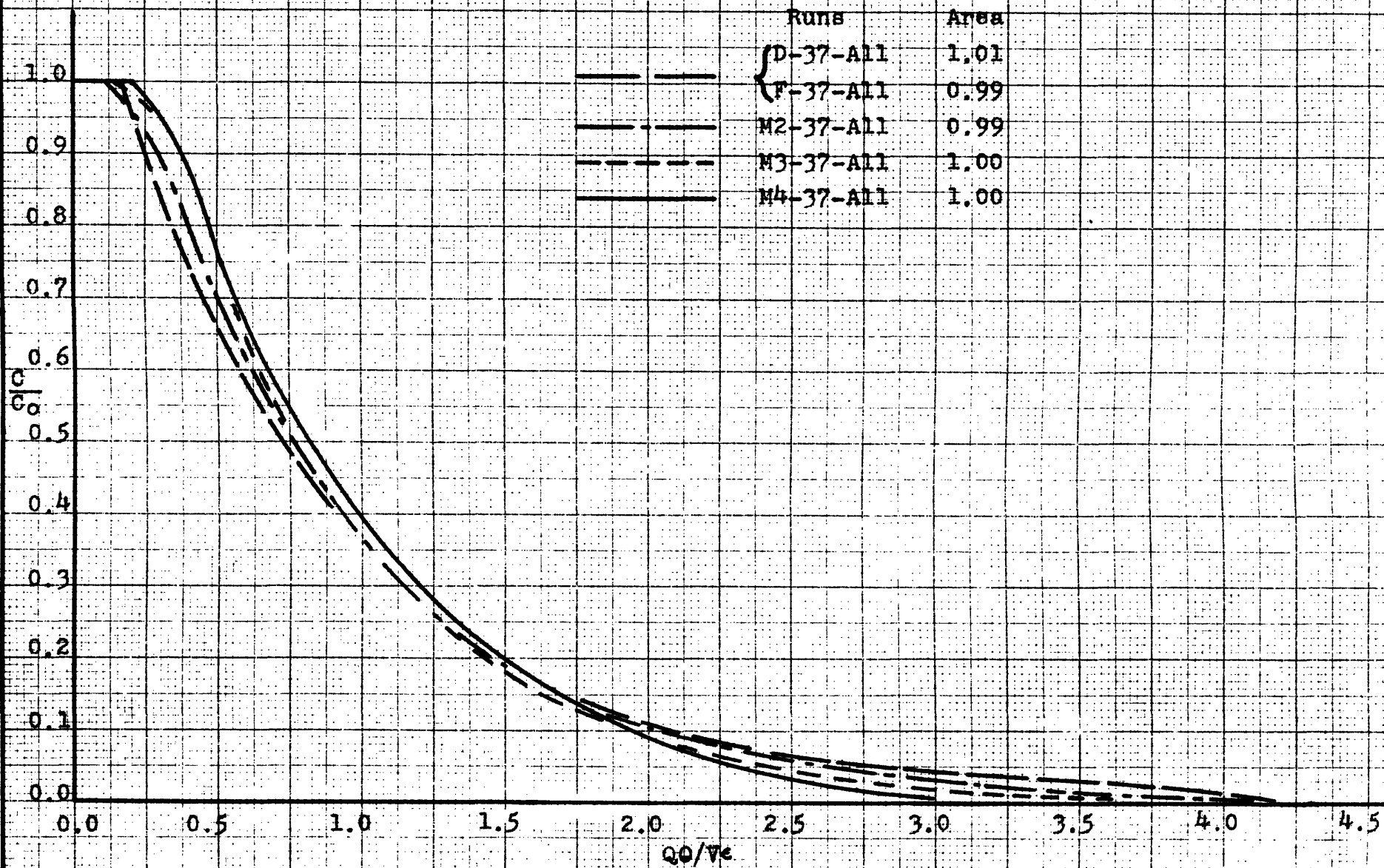
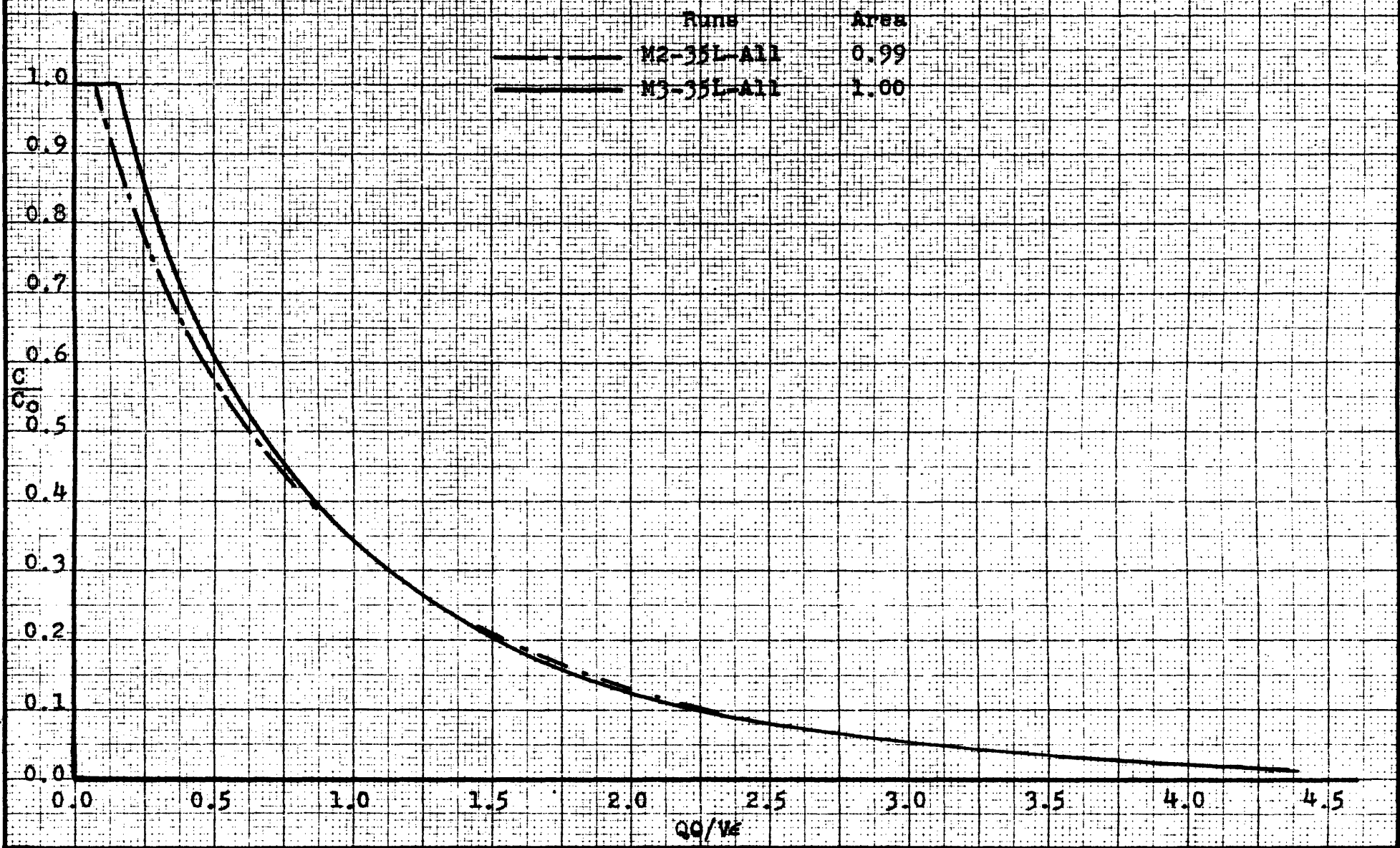


FIGURE 60
MICROSPHERES: EFFECT OF PARTICLE SIZE



of 0.4 ft./sec. (7, 9, 11, 13, -37-A). In spite of the experimental scatter of the points, there appears to be a slight trend toward the piston flow results as the particle size increases.

The curves presented in Figures 58, 59, and 60 are tracings of the curves through the data points for the runs listed. Figure 58, which gives the composite curves of all the velocities for the four sizes of glass beads, indicates a slight trend toward the piston flow case as the particle diameter is increased. The line shown for the No. 7 glass beads does not agree and in addition any trend is well within the scatter of the data (see Figures 27, 28, 29, and 30).

The curves for the runs made with the five size fractions of microspheres are traced on Figure 59. Sizes D and F contain a much higher percentage of fines than do the other three sizes; even though the weight mean diameter of size D is about the same as M2, D has about 22% smaller than 75 microns while M2 has only about 6%. Thus, if the experimental scatter is ignored, it appears that solids having a larger mean diameter or a smaller amount of fines give results that tend toward the piston flow case. Table XVIII gives the values of S and I obtained from the semi-logarithmic plots of the composite curves. In most cases, a slight

TABLE XVIIIEffect of Particle Size on Values of S and I

<u>Run</u>	<u>Mean D_p micron</u>	<u>S</u>	<u>I</u>
D-37-A11	104	1.20	0.15
F-37-A11	70	1.22	0.16
M2-37-A11	107	1.25	0.17
M3-37-A11	150	1.32	0.22
M4-37-A11	216	1.44	0.33
M2-70-A11	107	1.54	0.37
M3-70-A11	150	1.47	0.36
M2-35L-A11	107	1.04	0.01
M3-35L-A11	150	1.05	0.03
13-37-A11	102	1.77	0.38
11-37-A11	155	1.95	0.48
9-37-A11	262	3.7	0.77
7-37-A11	452	2.4	0.56
15-35L-A11	70	1.20	0.22
13-35L-A11	102	1.15	0.28

Area = 1.07

trend can be seen toward piston flow results with increasing D_p .

This discussion has ignored the experimental scatter, which if considered for any one example would not permit the conclusion that increasing particle size may cause a slight decrease in the range of residence-times. However, when the best curves through the individual data runs practically all show this slight tendency, there is a likelihood that such a trend does exist. Obviously, this tentative conclusion can not be rigorously defended, but is only suggested until more accurate information becomes available. Any trend toward the piston flow type of results that stems from increasing particle size or decreasing amounts of fines is certainly small for the sizes studied, compared with the general shape of the residence-time curves.

Type of Solids

Figures 61, 62, and 63 compare the results obtained with microspheres and glass beads of approximately the same size. The glass beads were closely sized in comparison to the microspheres, and gave results which were more like the piston flow results. Whether this was due to the absence of fines in the glass beads or due to the porosity of the microspheres

FIGURE 61
MICROSPHERES VS. GLASS BEADS

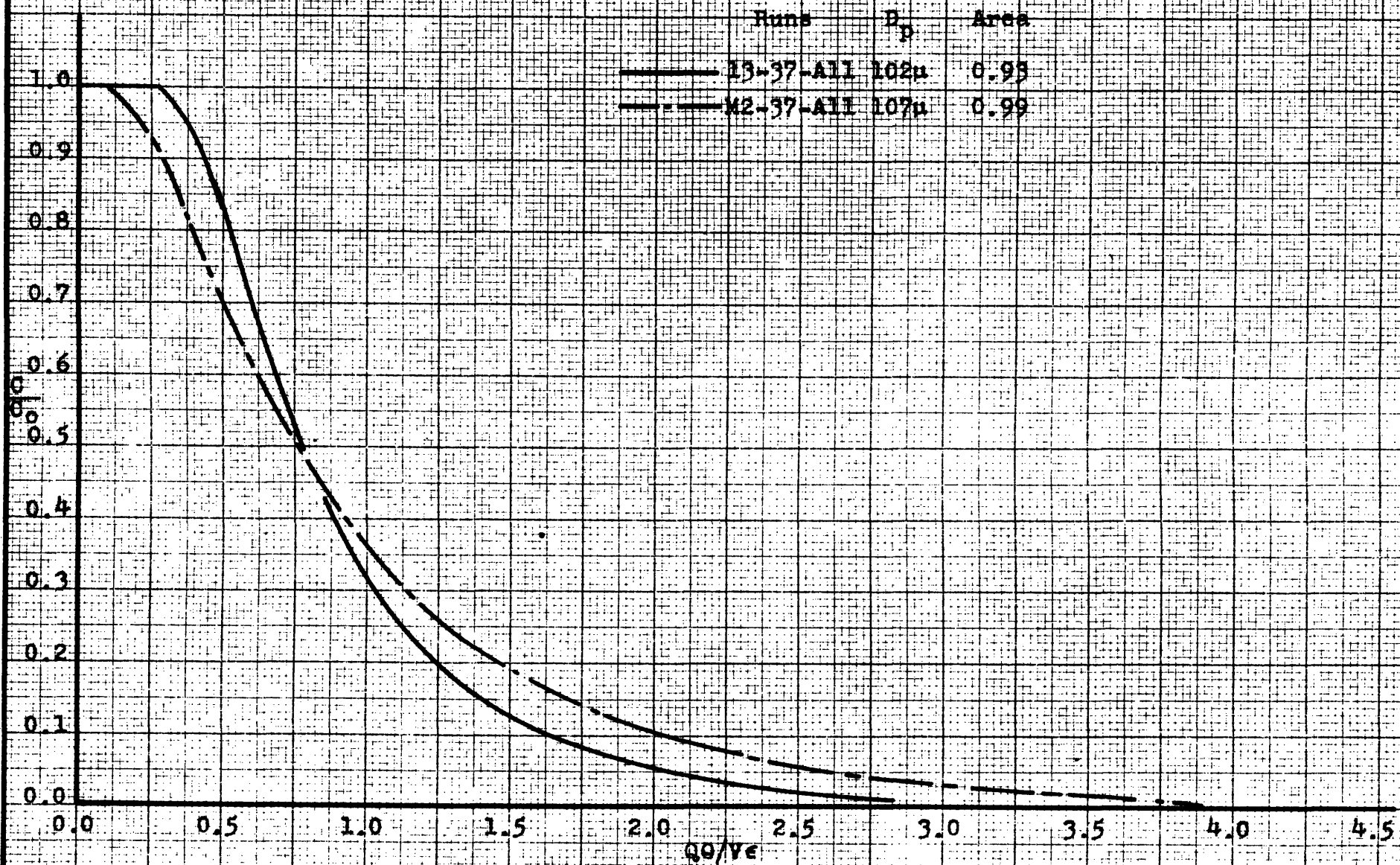


FIGURE 62
MICROSPHERES VS. GLASS BEADS

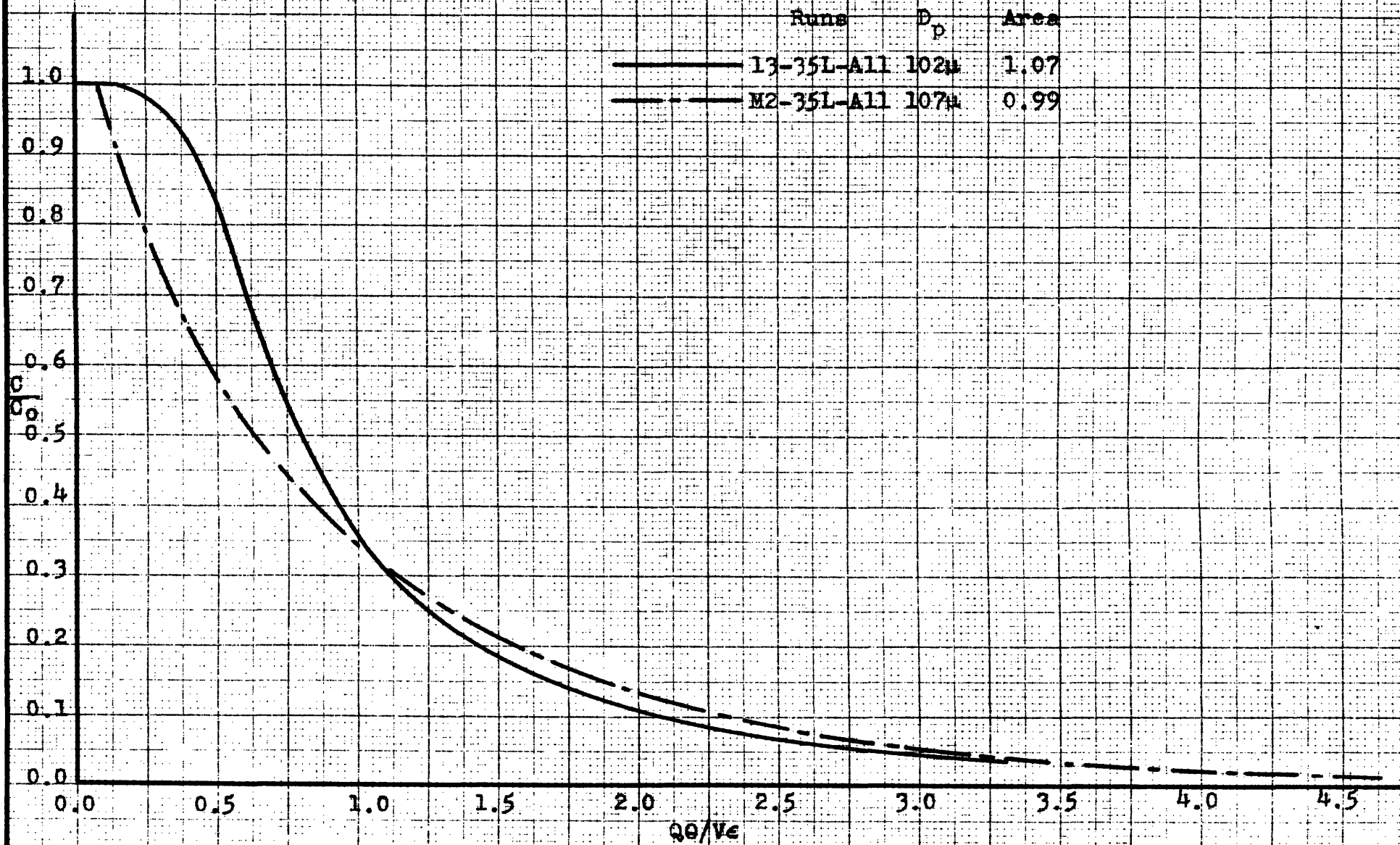
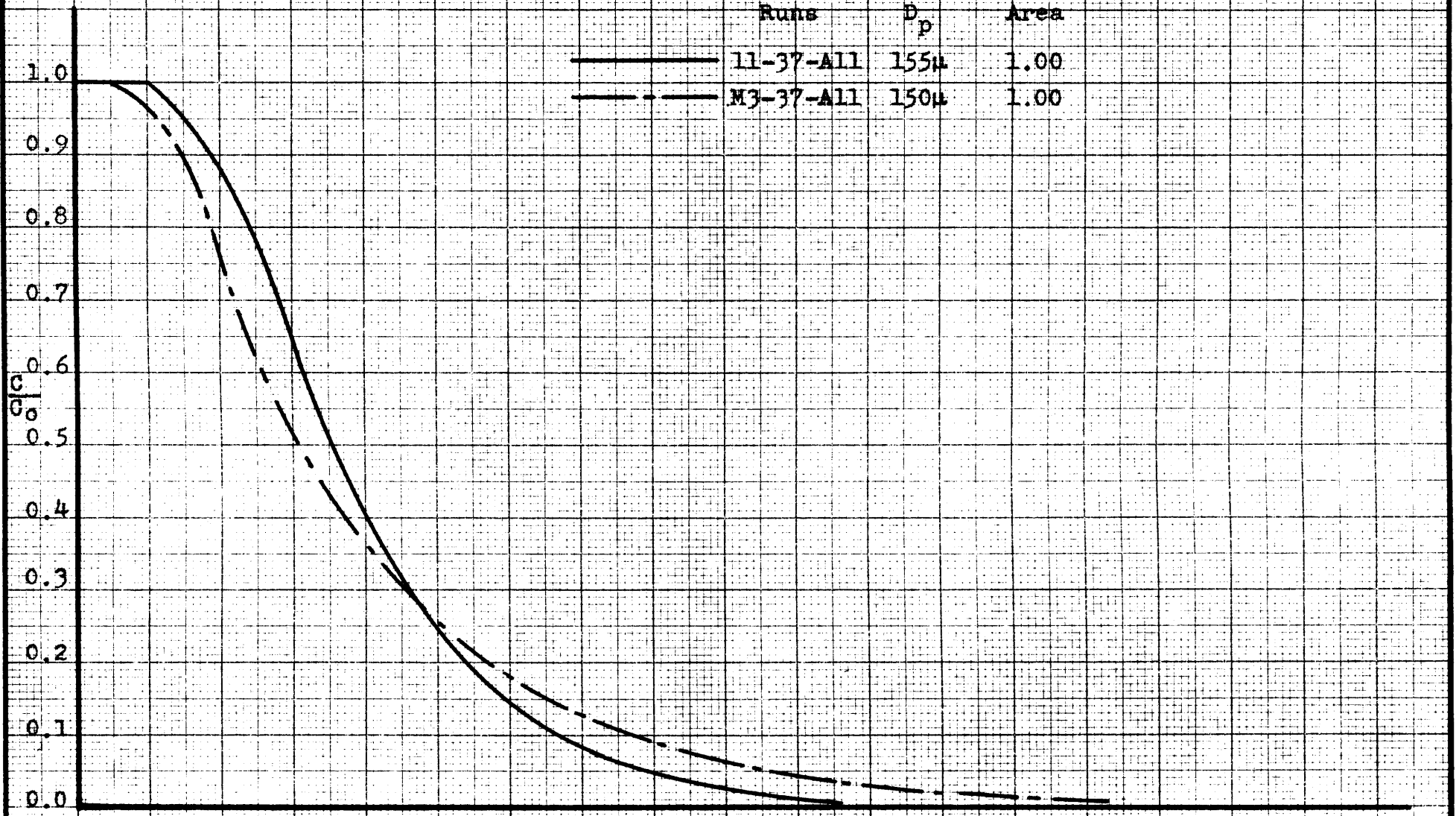


FIGURE 63

MICROSPHERES VS. GLASS BEADS

Runs	D _p	Area
11-37-All	155 μ	1.00
M3-37-All	150 μ	1.00



cannot be determined. If much of the tracer filled the pores of the microspheres, more gas would be required to strip this tracer than is necessary merely to sweep away the tracer filling the interstices between particles.

Bubble Velocities

The point where fresh gas first appears at the top of the bed is an indication of the maximum gas velocity through the bed. In Table XIX may be found the maximum velocities for all the residence-time runs made in the course of this work. These values are calculated from the value of Q_0/V_0 at the point where the value of C/C_0 first drops from unity. In most cases, this point is fixed by graphical interpolation of the data and, therefore, is not exact. Because fresh gas appears in the exit stream at values of Q_0/V_0 that are quite low, an error of small magnitude in determining these values will cause large variations in the value of the maximum velocity, u_m .

It is believed that these maximum velocities are an indication of the maximum velocity of the bubbles formed after the fresh gas entered the bed. Most of the experimental curves appear to fall away slowly from the C/C_0 ordinate of unity at first; this may indicate that there are variations in the speed of the

TABLE XIX

Maximum Gas Velocities from Residence-Time Data

Run	Q ft. ³ /min.	$V\epsilon$ ft. ³	ϵ	u_0 ft./sec.	$\frac{Q\theta}{V\epsilon}$ for mini- mum time	u_{max} ft./sec.	$\frac{u_M}{u_0}$	$\frac{u_M}{u}$
7-37-A	1.12	0.059	0.39	0.38	0.5	1.95	5.1	2
7-37-C	2.24	0.069	0.46	0.77	0.5	3.3	4.3	2
7-37-D	2.76	0.079	0.52	0.94	0.5	3.6	3.8	2
7-37-E	3.36	0.084	0.56	1.14	0.2	10.2	8.9	5
7-37-F	3.86	0.091	0.60	1.32	0.2	11	8.3	5
9-37-A	1.10	0.074	0.49	0.37	0.2	3.8	10.2	5
9-37-B	1.66	0.086	0.57	0.57	0.2	5.0	8.8	5
9-37-C	2.27	0.099	0.655	0.78	0.2	6.0	7.6	5
11-37-A	1.14	0.089	0.59	0.39	0.25	2.6	6.8	4
11-37-B	1.72	0.100	0.66	0.58	0.25	3.5	6.1	4
11-37-C	2.29	0.107	0.71	0.78	0.25	4.4	5.6	4
13-37-A	1.14	0.091	0.60	0.39	0.28	2.3	6.0	3.6
13-37-B	1.74	0.101	0.67	0.59	0.28	3.1	5.3	3.6
13-37-C	2.32	0.107	0.71	0.79	0.28	4.0	5.0	3.6
13-37-D	2.94	0.111	0.74	1.00	0.28	4.8	4.8	3.6
13-35L-A	2.56	0.180	0.56	0.39	0.15	4.6	11.9	6.7
13-35L-B	4.03	0.191	0.594	0.61	0.15	6.9	11	6.7
13-35L-C	5.21	0.206	0.64	0.78	0.15	8.1	10	6.7
13-35L-D	6.66	0.217	0.67	1.0	0.15	10	10	6.7
15-35L-A	2.91	0.182	0.565	0.44	0.18	4.3	9.8	5.6
15-35L-B	4.02	0.190	0.58	0.61	0.18	5.8	9.6	5.6
15-35L-D	6.66	0.203	0.63	1.0	0.18	8.8	8.8	5.6
0-35L-A	2.68	0.322	1.00	0.40	0.5	0.8	2	2
7-35L-A	2.53	0.130	0.40	0.38	0.5	1.9	5	2
M2-70-A	1.13	0.231	0.81	0.38	0.18	2.6	6.9	5.6
M2-70-C	2.32	0.244	0.85	0.78	0.18	5.1	6.5	5.6

TABLE XIX (CONTINUED)

Run	Q ft. ³ /min.	$V\epsilon$ ft. ³	ϵ	u_o ft./sec.	$\frac{Q\theta}{V\epsilon}$ for mini- mum time	u_{max} ft./sec.	$\frac{u_M}{u_o}$	$\frac{u_M}{u}$
M3-70-A	1.16	0.233	0.81	0.39	0.25	1.9	4.9	4
M3-70-B	1.71	0.248	0.87	0.58	0.25	2.7	4.6	4
D-37-A	1.18	0.117	0.79	0.40	0.17	3.0	7.4	5.9
D-37-B	1.80	0.125	0.83	0.62	0.17	4.4	7.1	5.9
D-37-C	2.44	0.141	0.93	0.83	0.17	5.2	6.3	5.9
D-37-D	2.91	0.115	0.76	0.99	0.17	7.6	7.7	5.9
F-37-A	1.18	0.115	0.76	0.40	0.19	2.8	6.9	5.3
F-37-B	1.77	0.116	0.77	0.61	0.19	4.2	6.8	5.3
F-37-C	2.41	0.117	0.78	0.82	0.19	5.5	6.7	5.3
F-37-D	3.01	0.106	0.70	1.02	0.19	7.7	7.5	5.3
M2-37-A	1.18	0.124	0.82	0.40	0.11	4.4	11	9.1
M2-37-B	1.81	0.136	0.90	0.61	0.11	6.2	10	9.1
M2-37-C	2.37	0.132	0.87	0.81	0.11	8.5	10	9.1
M3-37-A	1.18	0.123	0.81	0.40	0.13	3.8	9.5	7.7
M3-37-B	1.77	0.128	0.85	0.60	0.13	5.4	9.0	7.7
M3-37-C	2.36	0.132	0.87	0.81	0.13	7.2	8.8	7.7
M4-37-A	1.23	0.126	0.83	0.42	0.18	2.8	6.7	5.6
M4-37-B	1.77	0.126	0.83	0.60	0.18	4.0	6.7	5.6
M2-35L-A	2.74	0.274	0.85	0.41	0.08	6.0	15	12.5
M2-35L-B	4.14	0.278	0.86	0.62	0.08	9.0	15	12.5
M2-35L-C	5.47	0.299	0.93	0.83	0.08	11	13	12.5
M2-35L-D	6.85	0.256	0.80	1.03	0.08	16	16	12.5
M3-35L-A	2.64	0.312	0.97	0.40	0.16	2.6	6.5	6.2
M3-35L-B	3.98	0.284	0.88	0.61	0.16	4.3	7.1	6.2
M3-35L-C	5.37	0.292	0.91	0.81	0.16	5.6	6.9	6.2
M3-35L-D	6.82	0.292	0.91	1.03	0.16	7.1	6.9	6.2

individual bubbles, i.e., a few bubbles formed after the helium was shut off may reach the top before the main stream of such bubbles.

With the microspheres, the ratio of maximum velocity to superficial velocity, u_m/u_o , and the ratio of maximum velocity to the average gas velocity through the solids, u_m/u , decreases with increasing particle size, while the opposite trend is noticed with the calculated ratios for the glass beads. This apparent contradiction is probably an indication of the errors which are introduced on estimation of the minimum Q_0/V_0 .

For the fluidized beds, the values of u_m/u_o ranged from about 5 to 15 and those of u_m/u from about 4 to 12. While the values of these ratios cannot be depended upon for quantitative accuracy, the fact that they are all considerably greater than unity does indicate that there are velocity gradients of large magnitude in fluidized beds.

It is possible to arrive at approximate values for the upward velocities of the solids in fluidized beds from the work of Carlsmith and Freund (3). This work was conducted at much lower gas velocities (0.024 to 0.079 ft./sec.) than employed in this study. The ratio of maximum solid velocity in the core to the

superficial gas velocity ranged from about 1.5 to 6.0. The fact that these values are lower than those found for the maximum velocity of the gas can be attributed to the slip of the solid through the gas stream and perhaps somewhat to the lower superficial velocities employed.

C. Mechanism of Gas Mixing

Perhaps the most interesting observation to be made from the residence-time curves is their general similarity with the perfect mixing curve. With the exception of the fixed bed runs and the fluidized beds of No. 7 and 9 glass beads, (the two largest sizes), the experimental residence-time curves bear a close resemblance with that expected if perfect mixing were to occur. This is especially true with the smaller sizes of microspheres.

However, inspection of the back-mixing data in Tables III through IX and the graphs showing concentration profiles definitely eliminates serious consideration of a completely random type of mixing and any approach to perfect mixing. Perfect mixing implies that there are no concentration gradients, either radial or vertical, in the bed. The large vertical and radial concentration gradients found in the back-mixing studies show that perfect mixing is not present, or even approached, in fluidized beds. This leads to the conclusion that some other type of gas flow produced both the results of the back-mixing and residence-time studies.

The experimental data of both the back-mixing and residence-time studies also rule out the possibility of

piston flow. The horizontal gradients in gas composition, the back-mixing, as well as the variation in residence-times all are contrary to the nature of piston flow.

The visual action of the bed and the experimental data indicate the importance of the bubbles which flow through fluidized beds. It is suggested that the mixing of gases in fluidized beds is in large measure due to the presence of these bubbles.

Visual evidence of fluid-bed action showed that the bubbles tended to rise in the center, or core, of the small beds studied. During the down-mixing studies the concentration of tracer gas was found to be lower in the core than in the surrounding annulus. Experimental findings indicate that there is downflow of gas at the walls of the confining tube due to the downflow of solids in this region; this means that the gas introduced at the bottom of the bed must of necessity flow up the core of the bed.

In the beds of fluidized solids studied in this work, there was no appreciable circulation of the solid in the bed at the quiescent state; it was only when bubbles began to flow through the bed that the vigorous solid agitation which generally characterizes fluidized beds took place. Studies on the mixing of solids (3,5)

have shown that the circulation pattern in the solid is the same as has been suggested for the gas flow, i.e., up the middle and down along the walls of the vessel. These studies have also shown that the rate of circulation, or solid turnover, is increased as the velocity is increased. Bauer (2) suggests that an increase in the velocity causes a higher fraction of the total gas to flow through the bed in the form of bubbles. As the gas flow rate is increased, the bubbles increase in size until finally slugging conditions are reached.

The sampling for tracer gas in regions of dense and lean solid density showed that large differences in composition can exist between the gas in the bubbles and the gas in the surrounding dense phase.

These various experimental observations suggest a stripping role for the bubbles in fluidized beds. The following discussion is a description of the proposed stripping action the bubbles may play in gas mixing; this picture of gas flow gives a satisfactory explanation of the experimental findings.

Fresh gas entering the bed tends to flow up the core in the form of bubbles. There is a certain amount of gas interchange between the bubbles and the dense phase; some of the fresh gas flows into the dense phase, while

some of the gas that was in the dense phase flows into the bubble and so rises in the column. In the case of the residence-time studies, this gas from the dense phase is at first wholly tracer gas so that the concentration in the bubbles can reach a high value by the time the bubble leaves the bed. The concentration of tracer in the dense phase decreases as the bubbles flow by, and hence the concentration of tracer in the bubbles decreases as they reach the top of the bed. Since it takes a definite time for a bubble to flow from the bottom to the top of the bed, the concentration of tracer in the gas leaving the bed remains constant until the first bubble originally formed of fresh gas does reach the top. In addition to the gas rising in the bubbles, there is also some gas flow up through the dense phase.

In the down-mixing experiments, the gas composition reached steady state in the regions near the wall and core because of the circulation pattern of the solid. This downflow of solid along the wall continually brought more tracer to the lower part of the column. As this solid flowed down along the wall, the gas that it contained was gradually stripped and replaced by gas flowing from the rising bubbles.

The fact that the time required for all of the tracer to be stripped from the column is less with the glass beads than with the microspheres is taken to mean that the transfer of gas between bubbles and dense phase is more rapid with glass beads than with microspheres and that the bubbles flow slower through the beads. This conclusion is confirmed by the concentration traverses made during the down-mixing studies; the difference in concentration between the core and annulus was much less with the glass beads than with the microspheres.

Morse (21) uses the relationships developed by Carman (4) and Kozeny (14) for packed beds to predict that the interstitial flow through the dense phase will decrease as the particle size and density decrease and the bed height decreases. The indication of lower gas transfer from bubble to dense phase in the microspheres than in the glass beads is readily explained on the basis of the lower density of the microspheres and the presence of fines tending to fill the interstitial spaces; both of these factors would tend to decrease the gas flow through the solid.

Predictions for gas flow in fluid-beds, which are based on fixed bed correlations, are a considerable simplification of the actual gas flow. In fluid-beds,

the solid itself moves, so that in addition to the flow of gas through the interstitial spaces, the transport of the gas by solid mixing must also be considered.

In addition, the difference in the fluidization behavior is probably pertinent in comparing the microspheres with the glass beads. The glass beads were slugging in most of the runs made, while the microspheres were not. In slugging, the gas can do a much more complete job of stripping tracer gas from the solid, since the solid is forced up the column in the form of pistons bridging from across the column; when these slugs break there is opportunity for very good mixing between the gas that was in the dense phase and that in the lean phase. After mixing thus, the gas moves on up the column in a slug again. Thus, a slugging bed may be very much like one mixing chamber on top of another where the gas flows in piston fashion for a short distance up the column and then is thoroughly mixed with surrounding gas, only to flow on further before again being well mixed with the surrounding gas.

The variation in residence-times found in fluidized beds can also be explained entirely on the basis of radial velocity gradients involving no gas mixing. However, such a picture does not allow for the downflow of gas along the walls of the column or recognize the differ-

ences in gas composition found in regions of dense and lean phase. While it is believed that there is a large radial velocity gradient in fluidized beds, with high upward gas velocities in the central region of the bed and lower downward gas velocities near the wall, the action of the rising bubbles can not be overlooked.

In an attempt to predict the residence-time curves mathematically, several different sets of assumptions concerning the nature of the gas flow and the stripping action were made and the appropriate differential equations solved. However, none of this work gave the desired results. The physical system involved appears to be quite complicated and hence does not lend itself readily to a mathematical analysis.

D. Application of Results

1. Effect on Chemical Reaction

Back-mixing or variation in the residence-times of the gases undergoing chemical reaction in fluidized beds will have several effects. The products will tend to mix with the reactants, thus decreasing the overall rate of reaction; in addition, longer residence-times will increase the likelihood of secondary reactions. Such secondary reactions will decrease the conversion to the desired product and may cause fouling of the catalyst, as well as causing poor product quality.

The reduction of reaction rate due to mixing of the gases depends on the reaction mechanism and on the relative rates of reaction and mixing. Thus, for a zero-order reaction, mixing would have no effect, but would be detrimental for reactions of higher order in that it dilutes the reactants with the products.

The concept of an eddy-type mixing, which was developed to correlate the back-mixing results, can be mathematically combined with the appropriate reaction rate expression to show the effect that back-mixing would have in decreasing the overall conversion. The case for first order gas reactions occurring without change in volume has been integrated and comparison made between the cases

of reaction with and without mixing. (See VII APPENDIX B 5.)

However, this approach to the question of gas mixing and chemical reaction suffers for two reasons. One is the lack of accurate data from which the necessary values of the eddy diffusion coefficients, E , may be predicted; this is caused by the error which is inherent to internal sampling. But perhaps fully as important as this lack of quantitative information is the unrealistic assumptions that must be made in the application of such eddy diffusion coefficients. The gas velocity and composition are assumed to be uniform at any cross section as well as the value of E . Implicit in the use of the back-mixing correlation is the assumption that the spread in the residence-times for the gas molecules in any entering slug of gas will be less than is actually the case. As an illustration, when E is zero, use of the eddy diffusion picture with a flat velocity profile gives the residence-time curve that is associated with piston flow. If it is recognized that the bubbles of gas rising through the bed actually travel at a velocity over five times the superficial velocity, then a fairly wide variation in the residence-times is realized. The eddy diffusion picture does not even predict the residence-time curves correctly for parabolic

flow, which would be expected for laminar flow in an empty tube. The foregoing argument has been simplified by assuming the case where E is zero, but the same reasoning concerning the effect of velocity profile on residence-times applies where E is not zero.

Therefore, the eddy-diffusion approach would be expected to give a faulty picture of the effect of gas mixing on chemical reactions carried out in fluid-beds.

Direct quantitative application of the residence-time technique to the problem is limited to the case of first order chemical reaction, for which the conversion is only dependent on the time of contact. The rates of higher order reactions depend on the concentration of reactants. This point may be illustrated by an examination of the differential rate expressions for the cases of first and second order reactions:

$$\text{first order,} \quad - \frac{dn}{d\theta} = kn \quad (30\text{-IV})$$

$$\text{second order,} \quad - \frac{dn}{d\theta} = kn \frac{n}{v} \quad (31\text{-IV})$$

where,

n = mols of reactant present at time θ

k = appropriate first or second order rate constant

v = total volume associated with n mols of gas.

Equation (30-IV) shows that only the quantity of reactants affects the rate for first order reactions, while with

second order reactions a concentration term, n/v , is present in the rate-determining expression.

For any reaction, the quantity, $1-C/C_0$, represents the fraction of the reactants that have been converted in time θ . The term, $F d(Q\theta/V\epsilon)$, represents the fraction of the entering stream of gas that remains in a fluidized bed for time equal to θ and leaves before $\theta+d\theta$. Multiplication of these two terms results in an expression for the fraction of the gas leaving a fluidized bed that has reacted:

$$1 - C_f/C_0 = \int_0^{\infty} (1-C/C_0) F d(Q\theta/V\epsilon) \quad (32-IV)$$

where

C_f = concentration of reactants leaving reactor

C_0 = concentration of reactants entering reactor.

Equation (32-IV) is general for reactions of all orders, and the problem is that of evaluating the term $1-C/C_0$.

The fraction of reactants converted by a first order reaction occurring without change in volume is (see VII APPENDIX B):

$$1 - C_f/C_0 = \int_0^{\infty} [1 - \exp(-k\theta)] F d(Q\theta/V\epsilon) \quad (33-IV)$$

The value of F is obtained by taking the slope of the experimental residence-time curve at various values of $Q\theta/V\epsilon$, (see equation 22-IV), and the fraction converted

is then obtained from equation (33-IV) by graphical integration.

If the experimental gas mixing data can be represented by the empirical method of equation (27-IV), the fraction converted can be obtained from (see VII APPENDIX B):

$$1 - C_f/C_o = 1 - \frac{\exp \left[- \frac{V\epsilon k(S-1)}{QS} \right]}{1 + \frac{V\epsilon k}{QS}} \quad (34-IV)$$

where

S = the slope of the residence-time data when plotted on semi-logarithmic coordinates.

The value obtained for the fraction converted for any set of operating conditions in the fluid-bed and any assumed value for k can be compared with the fraction converted calculated assuming perfect mixing or piston flow. The equations used for these two cases are as follows (see VII APPENDIX B):

Perfect Mixing:

$$1 - C_f/C_o = 1 - \frac{1}{1 + \frac{V\epsilon k}{Q}} \quad (35-IV)$$

Piston Flow:

$$1 - C_f/C_o = 1 - \exp \left[- \frac{V\epsilon k}{Q} \right] \quad (36-IV)$$

Attention is called to the presence of the group, $V\epsilon k/Q$, in the last three equations. For small values of k ,

equations (35-IV) and (36-IV) reduce to the same form; the effect of mixing decreases as conversion decreases.

The effect of different residence-time distributions on the fraction converted in a first order reaction can be seen in Figure 64. The ratio of the fraction converted for various values of S , characterizing the residence-time curves, to the fraction converted under conditions of piston flow (C_f^* is the exit concentration of reactants under conditions of piston flow) is plotted as a function of the group kV/Q . k is the reaction rate constant for a first order gas reaction occurring without change in volume. The effect of mixing can be seen to decrease as the value of S increases, and, in addition, the effect of mixing on the fraction converted is seen to decrease under conditions of both high and low conversion.

Table XX compares the fraction converted for the experimental mixing conditions with those of perfect mixing and piston flow. A specific reaction rate, k , of 0.2 sec.^{-1} and flow conditions found with Microspheres, 2, were employed. For Runs M2-70-A and C, comparison is made between the graphical method and the slope method of calculating the fraction converted. The agreement is quite good, especially when the possible errors in drawing slopes, smoothing of the curves, and graphical inte-

FIGURE 64

EFFECT OF RESIDENCE-TIME
ON FRACTION CONVERTED; FIRST ORDER REACTION

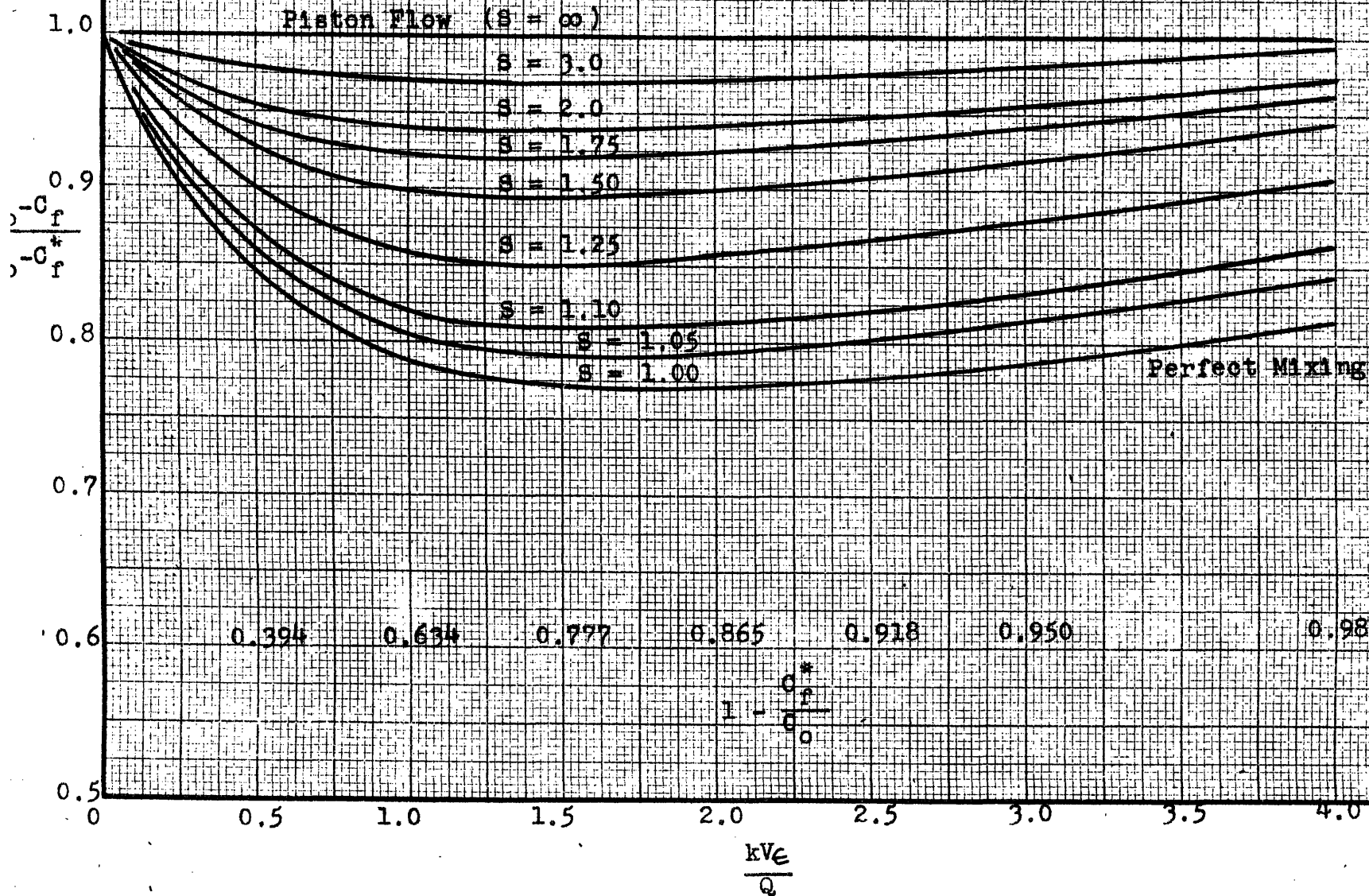


TABLE XX

EFFECT OF RESIDENCE-TIME DISTRIBUTION
ON FIRST ORDER CHEMICAL REACTION

Run	k sec ⁻¹	kV Q	Fraction Converted			
			Graphical Integration Eq. (33-IV) 1-C _f /C _o	"S" Method 1-C _f /C _o	Perfect Mixing 1-C _f /C _o	Piston Flow 1-C _f /C _o
M2-70-A	0.2	2.45	0.81	0.836	0.710	0.914
M2-70-C	0.2	1.26	0.63	0.646	0.557	0.716
M2-37-A	0.2	1.26		0.613	0.558	0.716
M2-37-B	0.2	0.902		0.516	0.475	0.595
M2-37-C	0.2	0.666		0.430	0.400	0.487
M2-35L-A	0.2	1.20		0.555	0.545	0.698
M2-35L-B	0.2	0.805		0.455	0.446	0.553
M2-35L-C	0.2	0.656		0.403	0.395	0.481
M2-35L-D	0.2	0.448		0.314	0.309	0.361

gration are considered. As predicted from the residence-time data itself, the experimental conditions approach those of perfect mixing, especially at low values of L/D . In fact, with an L/D of 7.8, no significant difference exists between the experimental fraction converted for the cases of experimental flow and perfect mixing.

Since the residence-time studies did not give definite information concerning the nature of the gas flow through fluidized beds, it is necessary to make an assumption concerning the concentration gradients in a reactor before the experimental results can be applied to reactions of higher than first order. It was desired to obtain the limits on the fraction of reactants converted in a second order reaction carried out in a fluidized bed under the conditions of the experimentally determined residence-time distributions. None of the experimental distributions were found to differ more from piston flow than does perfect mixing. The lower limit would be that of complete mixing of the gases in the reactor in which the composition throughout the bed would be uniform. The upper limit should be fixed by assuming that the gas passes through the bed in slugs between which there is no mixing; however, the molecules of gas in these slugs are assumed to have varying times of residence in the bed conforming to the experimental mixing results. Any mixing

of the gases in the bed will give a conversion lower than that predicted by this latter assumption.

Figure 65 shows the effect of varying residence-time distributions on the fraction converted in a second order gas reaction under the assumed conditions of no mixing between slugs of gas. The reaction is assumed to cause no change in the volume of the gas stream. The ratio of the fraction converted with variation in the residence-times of the molecules in any slug of gas to the fraction converted by piston flow is shown as a function of the group $kV\epsilon C_0/Q$. The lines are based on the following equations (see VII APPENDIX B 7):

for experimental residence-time distributions,

$$1 - C_f/C_0 = 1 - \frac{SQ}{kV\epsilon C_0} \exp \left[\frac{SQ}{kV\epsilon C_0} + s - 1 \right] \int_0^{\infty} \frac{\exp(-t)}{t} dt \quad (37-IV)$$

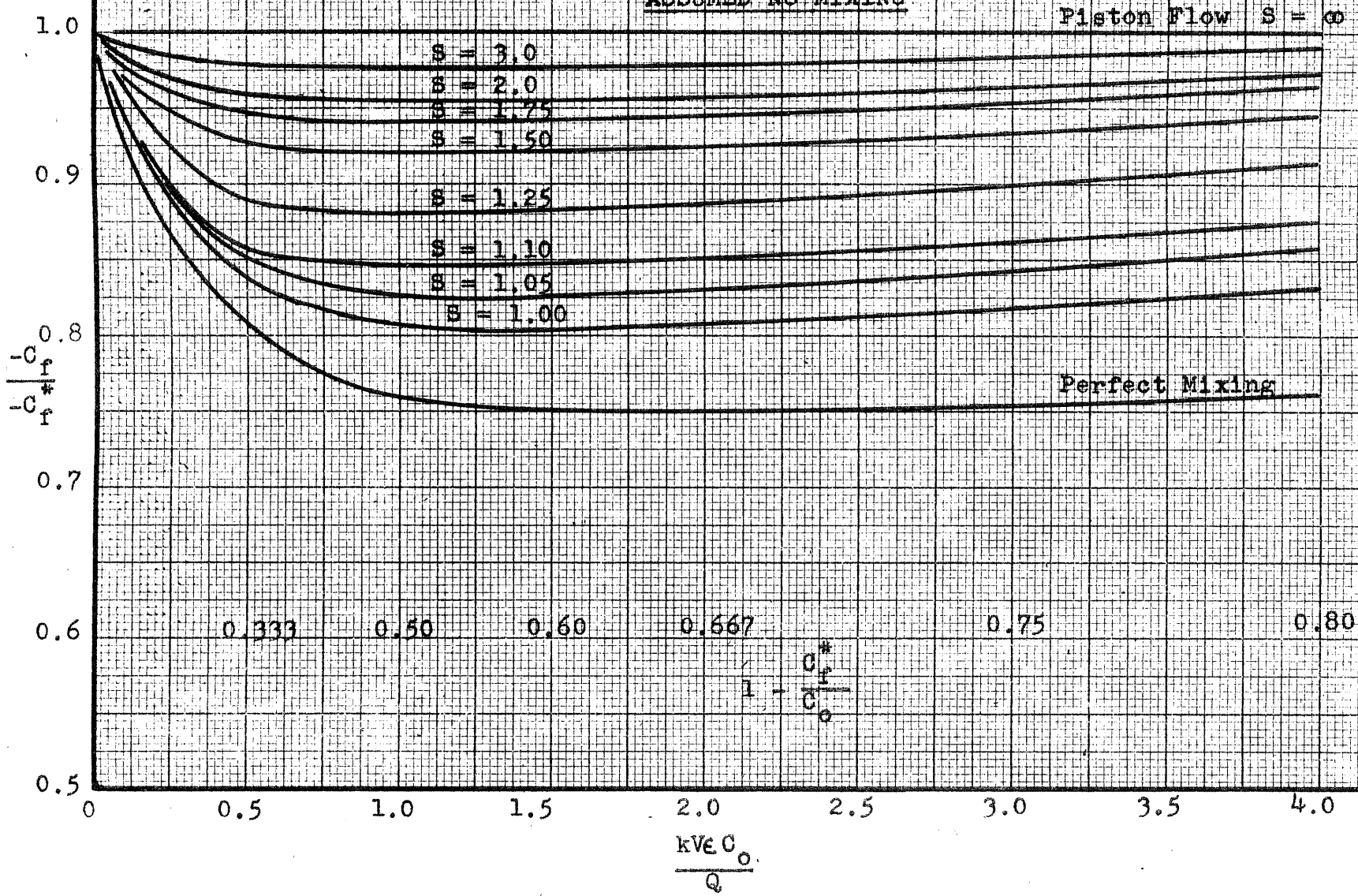
$$\left[\frac{SQ}{kV\epsilon C_0} + s - 1 \right]$$

where values of the integral are tabulated in Jahnke and Emde (11);

for piston flow,

$$1 - C_f/C_0 = 1 - \frac{1}{1 + \frac{kV\epsilon C_0}{Q}} \quad (38-IV)$$

FIGURE 65
EFFECT OF RESIDENCE-TIME
ON FRACTION CONVERTED: SECOND ORDER REACTION
ASSUMED NO MIXING



and for perfect mixing,

$$1 - C_f/C_o = 1 - \frac{-1 + \sqrt{1 + \frac{4kV_e C_o}{Q}}}{\frac{2kV_e C_o}{Q}} \quad (39-IV)$$

As the range of residence-times decreases, (i.e., as the value of S increases), the fraction converted approaches that expected from piston flow. The effect of residence-time distribution is seen to decrease at both high and low conversions. It is interesting to note that for the case of perfect-mixing residence-times, $S = 1$, but no mixing, the conversion is higher than for perfect mixing, showing that both mixing and residence-time affect conversion.

The actual gas flow through fluid-beds that approximates perfect mixing results is far from the defined perfect mixing. There are probably definite concentration gradients existing in the fluid-beds undergoing chemical reaction, and products once formed in the dense phase tend to remain there due to the slow transfer of gas between dense and lean phases. This causes the concentration of products to build up in the dense phase where most of the catalyzed or gas-solid reaction would take place, and thus the overall conversion is decreased.

In the use of fluid-beds as a laboratory tool for studies of reaction kinetics, it is important that the

mechanism of gas flow be accurately known if the results of the studies are to be reliable. Because an increase in gas velocity reduces the overall conversion, the possible magnitude of the effect of mixing on conversion is reduced. Hence it seems advisable to conduct the laboratory studies of chemical reaction rates in fluid-beds at reasonably high velocities, and thus to reduce the effect of undetermined gas mixing and by-passing. In addition, since beds of high L/D give a lower range in the residence-times, it is advisable to use beds of high L/D in the laboratory.

Both of these recommendations will tend to promote slugging conditions, which may interfere with the desired degree of temperature control. The primary advantage of the fluid-bed is one of temperature control and uniformity; however, gas mixing acts somewhat to offset this advantage when the fluidized technique is employed in the laboratory. The use of the fluidized bed for laboratory studies of reaction kinetics must be considered as a compromise between the effects of temperature variation and gas mixing.

Since the bubbles flowing through fluid-beds play an important part in the gas mixing, it is recommended that studies be made concerning the factors affecting bubble formation and growth in beds of fluidized solids.

Such information should be of value in scaling up laboratory or pilot-plant information during the design of industrial reactors. At present, the information presented in this study of gas mixing cannot be reliably extrapolated to the size of industrial reactors, which are of much larger diameter and have smaller ratios of length to diameter. The walls of such large reactors probably do not have as large an effect on the solid circulation as do those of the columns used in this thesis, where in many cases the diameter of the column was only slightly larger than the diameter of the bubbles, if at all larger.

However, it is expected that a significant increase in the L/D of the fluid-beds used in industry would decrease the range of residence-times. Such a reduction in the range of residence-times should permit closer quality control of the product and decrease undesirable secondary reactions. It is therefore suggested that the introduction of baffles into large reactors be considered where there is evidence of undesirable gas mixing. The possible effect of such baffles on temperature control and the possible need for a new gas distributing arrangement should be realized. Baffles would permit the use of a single reactor (as opposed to a battery of parallel reactors of small

diameter) and thus retain its operating advantages.

The use of fluidized beds for reactors of industrial size does not suffer from gas mixing and variation in residence-times in the same manner that the laboratory use does. Industrial reactors are built for production, and the availability of uniform temperature control and ease of handling of large quantities of solids present advantages in the use of fluidized beds that offset the disadvantages of gas mixing.

The findings of this thesis also have bearing on studies of mass transfer rates made in fluidized beds. It should be realized that the gas surrounding the particles in the dense phase probably has a much lower driving force for mass transfer than is indicated by an average gas sample. In the studies carried out to date (13, 29), the assumption of piston flow has been made in correlating the results; average driving forces have been used. However, in both investigations, the average composition of the exit stream was either very close to, or equal to, the equilibrium concentration for the transfer material. The work of this thesis indicates that the concentration in the dense phase tends to be higher than in the lean phase; therefore it appears likely that equilibrium conditions were approached in the dense phase in both studies mentioned, and that the mass transfer co-

efficients calculated using average gas compositions are low. In studying mass transfer in fluidized beds, consideration must be given to possible radial variations in the driving force.

2. Examination of Chemical Reaction Rate Studies

It is interesting to examine the results of studies on the reduction of carbon dioxide with carbon carried out by McBride (19) and Goring (8) who employed fluidized beds and by Wu (39) who used a single layer of particles evenly distributed on a metal screen. These studies permit comparison of chemical reaction rates obtained in fixed and fluidized beds.

McBride and Goring fluidized coke in stainless steel tubes having dimensions of 1.78 inches I.D. by 7 feet high and 1.38 inches I.D. by 8 feet high, respectively. The units were externally heated. Various mixtures of CO_2 , CO , and N_2 were metered before being introduced into the bottom of the column. Analyses were made of the exit gas and of the coke used to obtain the rate of conversion.

Wu supported a single layer of coke particles on a wire screen. Mixtures of CO_2 and CO were caused to flow up through the screen and, since there was negligible conversion of the gas, the partial pressure of CO_2 at all points in the bed was equal to the inlet pressure. The

rate of reaction was followed by the loss in the weight of the coke particles over a known time.

The effect of CO in retarding the rate of reaction was studied by varying the concentration of CO in the inlet stream of CO₂. All three workers reported that CO had a strong retarding effect on the conversion of CO₂ to CO. While coke from the same shipment was used in all the experiments, Wu found the retarding effect to be much greater than that observed by McBride.

The three investigators utilized a Langmuir-type equation to correlate the reaction rate data obtained:

$$-\frac{dn_{\text{CO}_2}}{dW} = \frac{K_1 P_{\text{CO}_2}}{1 + K_2 P_{\text{CO}} + K_3 P_{\text{CO}_2}} \quad (40\text{-IV})$$

where

n_{CO_2} = flow rate of CO₂ passing any point in bed

W = weight of carbon in the bed

P = partial pressure of indicated gas

Because the fluid-beds caused an appreciable conversion, it was necessary for McBride and Goring to integrate Equation (40-IV). In order to do this, they assumed conditions of piston flow in the gas, i.e., that there was no vertical mixing of the gases and that radial mixing was instantaneous and complete. Since the conversion was negligible with Wu's thin fixed bed, it was not necessary for him to integrate the equation or make any

assumptions concerning the gas flow.

In runs in which only pure CO_2 was fed to the reacting coke, the values of the specific reaction rates calculated from the work of Wu are of the order of five times those of McBride and Goring. In addition, this difference between the reaction rates obtained in the thin fixed bed and the fluidized beds increased as the temperature of reaction was increased.

These findings can be explained by the effect of gas mixing in fluidized beds. The gases leaving the top of a fluid bed are composed of gas that is emerging from both the dense and lean phases. The gas samples taken from the exit stream by McBride and Goring represent the average composition of all the gas leaving the bed. However, the work of this thesis has shown that the transfer of gas from dense to lean phases may, under certain operating conditions, be quite slow and large concentration differences between the gas in the two phases, once created, can exist. In the work of McBride and Goring, the CO_2 entering the bottom of the column probably flowed upwards in bubbles or slugs (due to the small column diameter, it seems likely that slugging occurred in these fluid-beds). Some of this gas diffused into the dense phase and reacted with the carbon to form CO. This CO was not immediately

swept out of the solid, but, due to the slow transfer of gas to and from the bubbles, the concentration of CO in the dense phase rose to a high value and because of its retarding effect decreased the rate of reaction. There would also be some reaction of CO₂ with the carbon surrounding the bubbles, but the rates are reported on the basis of the total amount of carbon in the bed, and most of the solid was probably surrounded by a high concentration of the retarding CO.

The use of the piston flow assumptions in the integration of the Langmuir equation did not consider these concentration gradients. The partial pressure of CO₂ in the exit stream was assumed to represent a uniform partial pressure at the top of the bed. Use of this exit gas analysis meant that the partial pressure of CO₂, which determines the "driving force" in the reaction, was thought to be higher than it actually was in the dense phase, where most of the reaction would be expected to occur. Because of the low actual partial pressure of CO₂ in the gas surrounding the bulk of the coke, the specific reaction rates calculated for a given average pressure of CO₂ were less for the fluid-bed than for the thin fixed bed.

Since he did not appreciate how high the concentration of CO was in the dense phase, McBride obtained an

erroneous impression of the retarding effect of CO. He did not realize that the rate measured in fluid-beds for the pure CO₂ (at inlet) runs was already retarded by the high partial pressure of CO in the gas surrounding the coke. This explains the higher retardation effect reported by Wu.

The effect of the range of residence-times of the CO would be increased as the temperature level increased. All three studies showed that the rate of reaction was increased by a rise in temperature. The generation of CO in the dense phase would be more rapid at high temperature, and, hence, if the rate of gas transfer from the dense phase were the same, the effect of mixing, in decreasing the rate of reaction, would be larger at high temperature than at low.

The constants of Equation (40-IV) obtained by McBride and Wu differed considerably over the range of temperature investigated, and this would ordinarily be taken as an indication of a different mechanism of reaction. Since the same type of coke was used to study the identical reaction, a different reaction mechanism is highly unlikely.

This analysis serves to confirm the conclusions of the preceding section that the action of gas flow and mixing in fluid-beds may give an erroneous picture

of both the mechanism and the true rate of a chemical reaction. Therefore, use of the fluidized technique to study chemical reactions must be accompanied by a realization that the character of the fluid-bed itself may have a significant influence on the results obtained. It is necessary to appreciate that a compromise is being made in order to obtain the temperature control inherent to the fluid-bed. The scale-up of laboratory data obtained in fluid-beds must take cognizance of the uncertainties present in the laboratory data and in the use of the large reactor due to the mixing of the gases.

V CONCLUSIONS

Within the range of variables covered in the experimental work, it is possible to arrive at the following conclusions:

1. There is definite back-mixing of the gases in beds of fluidized solids. This mixing of gases in a direction opposite to the direction of net flow is caused by the presence of finely divided solids.

2. A circulation pattern is present in fluidized beds. The gases tend to flow rapidly upward in the middle of the beds and slowly downward along the walls. There is radial exchange of gas between these two regions.

3. The transfer of gas through the interstitial spaces between solid particles in the bed tends to be slow. Under certain operating conditions, large differences in composition, if created, can exist between the gas at the wall and at the core of the bed. In addition, large differences in composition can exist between the gas in the bubbles, or "lean phase," and the surrounding "dense phase," where the solid density is high. Both vertical and horizontal gradients in gas composition can exist in fluidized-beds.

4. The passage of bubbles through the bed and the extent of interstitial gas flow affect the mixing and residence-time of the gases. The bubbles travel up

through the bed at velocities considerably higher than either the superficial velocity or the average velocity through the void space. The flow of gas through the void spaces is apparently reduced by a decrease in the average particle size of the introduction of solid fines. It is believed that this reduction in gas flow is due to the decrease in the size of the interstitial pores.

5. It is possible to determine the residence-time history of the gas entering a fluidized bed by the method developed in this investigation. The general method should prove to be of value in studying mixing problems in other systems.

6. The nature of the gas flow through fluidized-beds caused the residence-time history of the gas to resemble that expected from perfect mixing. However, it is believed that the results obtained are due to a stripping action of the bubbles passing through the bed. The concentration differences existing in the beds prove that perfect mixing was not obtained.

7. The residence-time for a given fraction of entering gas was found to be inversely proportional to the gas flow rate. A fixed amount of gas was required to sweep a certain fraction of entering gas out of the bed, regardless of the gas velocity.

8. An increase in the length-to-diameter ratio,

L/D, caused a decrease in the by-passing of gas flowing through the beds. The range in residence-times is reduced toward the results expected from piston flow.

9. There was a slight trend toward a reduction in the range of residence-times as the average diameter of the particles or the amount of fines was decreased, probably due to increased flow of gas between "dense" and "lean phases."

10. The results of studies made in fluidized beds concerning chemical reaction kinetics can be significantly affected by the character of the gas mixing in the bed. If the reaction takes place at the solid surface, the concentration of the products of reaction will tend to become high in the dense phase; in general this will decrease the overall rate of reaction. The use of fluid-beds as a laboratory tool to study reaction mechanisms should be considered as a compromise between the control of temperature and gas mixing.

11. The variation in gas velocity occurring across a fluidized bed precludes true piston flow.

12. Gas samples taken from within fluidized beds are apt to give a faulty impression of the average gas composition at the point of withdrawal.

VI RECOMMENDATIONS

1. When the fluidized technique is used as a laboratory tool for studying chemical reactions, the possible introduction of errors due to gas mixing should be recognized. It is recommended that beds of high L/D and relatively high gas velocities be used in order to reduce by-passing and conversion.

2. Where the effects of gas-mixing promote undesirable secondary reactions in industrial reactors, it is recommended that consideration be given to the introduction of baffles in the beds.

3. It is recommended that the experimental method developed during the residence-time studies be applied to other mixing problems.

4. A study on the nature of the bubbles in fluidized beds is recommended. This study should attempt to determine the factors affecting bubble formation, size and growth, and include a study of interstitial gas flow.

VII APPENDIX

VII. APPENDIX

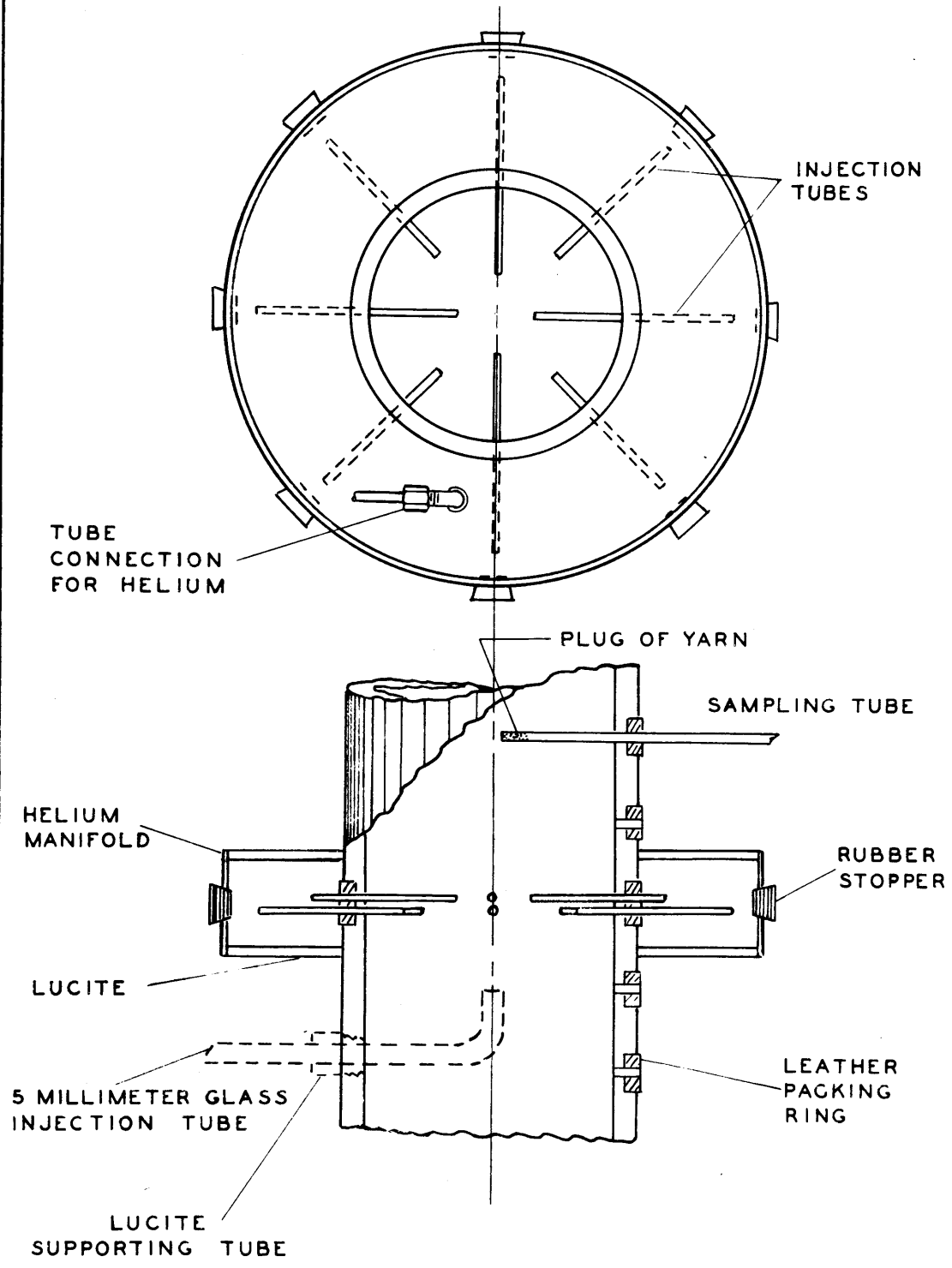
A. Details of Apparatus and Procedure

1. Helium Injection in Back-Mixing Studies

The single-point injection system consisted of a piece of five-millimeter glass tubing. This tubing was bent at right angles so that generally the end of the tube pointed upwards along the axis of the tube. During most of the data runs, the open end of the tube was 40-1/2 inches from the metal screen at the bottom of the column. Provision was made so that the end of the tube could also be placed six and twelve inches below this point, i.e., at 34-1/2 and 28-1/2 inches above the screen.

Figure A1 shows the details of the multi-point injection system used on the three-inch column. The injection tubes were made of stainless steel having an inside diameter of 0.065 inches and an outside diameter of 0.075 inches; the tubes were 1-7/8 inches long. The tubes entered the column through leather gaskets, which permitted the position of the tubes to be altered while maintaining a gas-tight seal. Four of the tubes injected at a radius of 1/2 inch and eight at a radius of one inch. An annular manifold made of sheet Lucite surrounded the column at the injection level. Helium was fed to the manifold through a quarter-inch tubing fitting; the gas was thus distributed among the twelve tubes. In

FIGURE A1
INJECTION AND SAMPLING DETAILS



HALF SCALE

order to prevent the passage of solid particles from the column through the tubes into the helium manifold, an equal length of copper wire was inserted in each tube. The area available for gas flow was thus reduced and therefore the gas velocity increased. For the same reason, provision was made for the injection of air into the manifold should it become necessary to stop the flow of helium. The injection tubes were accessible for adjustment or cleaning through holes in the periphery of the manifold; these holes were closed by rubber stoppers.

Injection manifolds were installed on the 4-1/2 inch column at heights of 10 and 24 inches above the supporting screen. The construction of these manifolds was similar to that on the 3-inch column, but the tubes used were 2-3/4 inches long and had an inside diameter of 0.075 inches and an outside diameter of 0.10 inches.

2. Size Analysis of Solids

The sizes of the glass beads were determined by Trilling (35), who measured about fifty of each size of bead on microphotograph; the sizes reported are the arithmetic average of the beads measured. The diameters found in this manner were checked by measuring a few beads with a micrometer.

The size distribution of microspheres M2, M3, and M4 were determined by measuring about 100 particles

using a microscope fitted with a Filar micrometer eyepiece. A small sample of microspheres was placed on a glass slide. This slide was moved across the field of the microscope by a moveable stage until about 100 particles had been counted. The particles were only measured in one direction, thus assuming that they would be arranged in a random manner on the slide. In order to calculate the size analysis on a weight basis, the particles were assumed to be spherical and to have a constant density.

3. Gas Analysis

a). Gas Density Balance

Figures 1, 5, and 6 show the Edwards-type gas density balance and its accessory equipment. (In Figure 6 the balance, manometers, and pressure adjustment equipment are shown on the panel board in the background.) This apparatus depends on the difference in the density, or molecular weight, of gases in order to effect an analysis of two-component systems.

The balance itself is shown in Figure 5. A horizontal beam, D, was suspended in gas-tight metal cylinder, F. At one end of the beam was a hollow copper float, A, and at the other end a small mirror, B, was mounted vertically and faced away from the float. At both ends of the cylindrical shell, F, were removable metal caps, G, in the center of which were glass windows.

By lining up the cross hair which was located on the mirror with a similar cross hair located on one window, it was possible to balance the beam reproducibly. The beam and float could be balanced by gas of one and only one density; thus, by varying the pressure of the surrounding gas, it was possible to balance the beam in gases of different average molecular weights. The pressure required to balance the arm was determined with a gas of known composition, such as air. Then, it was possible to determine the concentration of helium in an unknown mixture of helium and air if the pressure and temperature required to balance the beam in the mixture were determined. The perfect gas laws were assumed in calculating the composition of the unknown sample.

On the right side of Figure 1, a schematic diagram of the balance system is shown. The procedure used with this apparatus consisted of evacuating the entire sampling and analytical train until a pressure of approximately one millimeter or less was obtained. The valve to the vacuum pump was then closed, and the valve in the sample line from the column was opened, permitting a sample of gas to flow into the system. The gases passed through a drying tube of calcium chloride. During the period when the system was under a vacuum, the valves in the leveling bottle arrangement, N, Q, and P, and in the

inclined manometer, R, (valve not shown) were kept closed. The absolute manometer, S, gave an indication of the pressure in the apparatus at all times. When the pressure reached atmospheric, the sample line was closed, and the valves on the inclined manometer and in the pressure adjustment system were opened. By using the leveling bottle and the rubber bellows for finer adjustment, the volume, and thus the pressure, of the gas in the apparatus was adjusted until the beam balanced. Mercury was used as the confining fluid. The pressure was read from the inclined manometer, and the temperature from a thermometer, T, inserted in one of the gas inlets to the balance shell, M, in Figure 1.

A great deal of difficulty was experienced in obtaining satisfactory performance of the balance. The principal trouble lay in the very delicate method used to suspend the beam. As shown in Figure 3, four brass ribbons, C, supported an aluminum platform, E, which in turn supported the beam. The ribbons were cut from 0.001-inch brass shim-stock to a width of 0.012 inches. Slippage of the ribbons, either in the slits in the aluminum platform, or between the clamps, K, used to hold the upper ends of the ribbons in place, changed the balance point considerably. Stretching of the ribbons had the same effect. As a result, it was found that any movement of the balance, as a whole, or shocks or

vibrations transmitted to the balance, caused a change in the balance point; this necessitated recalibration of the balance. To reduce movements and vibrations, the balance was placed on a platform which was mounted on one end of a piece of two-inch pipe; the other end of the pipe was securely fastened to the floor. Even then, vibrations induced by passing trucks and trains were sufficient to cause a change in the balance point.

The mere shock produced when the pressure was changed rapidly, which caused the beam to swing and hit at both top and bottom, was sufficient to cause a change in the balance point. Therefore, considerable care had to be taken in evacuating the system and drawing a sample.

Another serious difficulty arose through the required sensitivity of the balance. The beam had to be sensitive enough so that the smallest measurable change in pressure caused a noticeable change in the balance position of the beam. This condition was attained by adjusting several nuts on the center post, until the center of gravity of the beam was such that the period of motion of the beam was five seconds or longer. This was an extremely fine adjustment and consumed considerable time. In the process of adjusting the balance or period of motion, the brass ribbons supporting the beam

were broken several times.

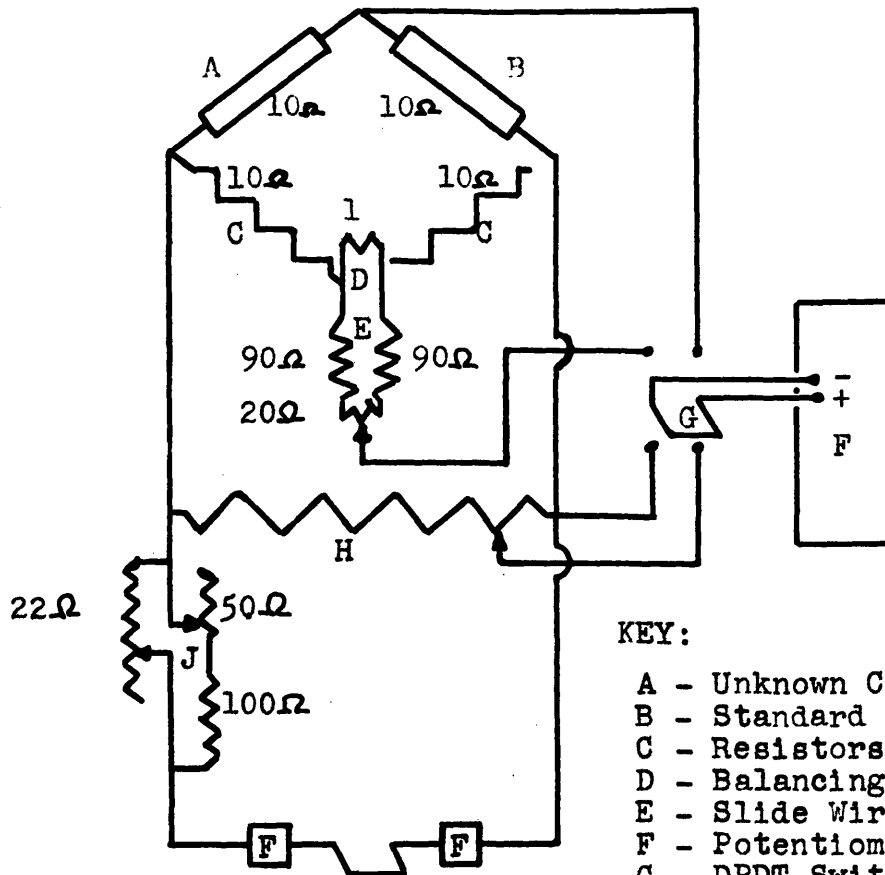
Due to the delicate nature of the instrument, the balance was generally calibrated with air after every three helium-air samples, in order to determine any change in the balance point.

b). Electric Analyzer

The second method of gas analysis used in this thesis utilizes the differences in the thermal conductivity of helium and air. The thermal conductivity of helium is about six times that of air (24).

A photograph of the apparatus is shown in Figure 6 and a schematic diagram in Figure A2. In Figure A2, two thermal conductivity cells, A and B, manufactured by Leeds and Northrup (Model No. 3284-F) were mounted in series in a Wheatstone Bridge circuit. The conductivity cells each consisted of a fine platinum filament enclosed in a glass jacket to which gases could be admitted; they were mounted in a constant temperature bath having a temperature of $37 \pm 0.1^\circ\text{C}$. The other two resistances, C, were wire wound on ceramic cores. The resistances of the cells and the two resistors were all about ten ohms. A one-ohm resistor, D, and the slide-wire, E, were employed to balance the circuit when dry air was admitted to both conductivity cells. All resistors used in the apparatus were greatly over-rated for power dissipation so as to reduce temperature

FIGURE A2
WIRING DIAGRAM: GAS ANALYZER



KEY:

- A - Unknown Cell
- B - Standard Cell
- C - Resistors
- D - Balancing Resistor
- E - Slide Wire
- F - Potentiometer
- G - DPDT Switch
- H - 1000 ohm Ayrton Shunt
- J - Voltage Regulator
- K - Two 6-Volt Batteries
- L - Lamp Bank
- M - Ammeter
- F - Fuse

110 Volt D.C. Line

effects. An emf of 5.00 volts was impressed across the bridge. The source of current was two six-volt storage batteries, K, connected in series and floated on the 110 volt D.C. line through a resistance bank, L. This arrangement gave a relatively constant voltage. Two slide wire resistors and a fixed resistor, J, regulated the voltage input to the bridge. The impressed voltage was measured by means of a Rubicon potentiometer, F, which measured the voltage drop across a 1:100 Ayrton shunt, H. The same potentiometer was used to read the unbalance of the bridge during analysis; a double-pole-double-throw switch, G, was used.

To operate the analyzer, the zero point was first checked by evacuating both cells, and then allowing air from the column to pass over drying tubes filled with Drierite (calcium sulfate) and into the cells. The impressed voltage was set at 5.00 volts and the potential between points "c" and "d" was then measured. During the course of the thesis, this bridge remained stable so that the potential between "c" and "d" never amounted to more than 0.2 millivolts when air was in both cells.

Once the zero point had been checked, cell B was sealed and cell A was evacuated; a vacuum gage indicated the pressure in the system. After evacuation of the cell and the line leading to the gas sample bottles, the line

between the vacuum pump and the cell was closed and a sample of gas displaced from a sample bottle into the cell by means of a mercury-filled leveling bottle attached to the bottom of the sample bottle. The pressure was adjusted to atmospheric by means of the leveling bottle, and the impressed voltage adjusted to 5.00 volts. Then the unbalance in the bridge between "c" and "d", due to the presence of the helium in cell A, was noted.

During analysis, cell A contains gas having a higher conductivity than the gas in cell B (pure air), and therefore the platinum wire in A will lose heat faster than the wire in B. Since the same current is flowing through both wires, this means that A will become cooler relative to B. The resistance of A will then drop relative to B, and hence a condition of unbalance in the bridge will be produced.

The bridge was calibrated by analyzing mixtures of helium and air of known composition. These samples were prepared by using the three gas bottles shown on the left side of the analysis table in Figure 6. The small bottle on the right was filled, under atmospheric pressure, with helium, which was then transferred to the middle bottle. The small bottle was then filled with air, under atmospheric pressure, to the same mercury level as with the helium. The air was forced into the middle

bottle, and then the resulting helium and air mixture was mixed by passing it back and forth between the middle bottle and the other large bottle on the left. After mixing, one-half of this gas was put into the small bottle and the other half analyzed. The remaining half was then diluted with an identical volume of air, mixed, half saved and the other half analyzed. By repeated addition of air and division into two parts, it was possible to cover a wide range of concentrations in the calibration. This method of subdivision produced samples of 50%, 25%, 12.5%, 6.25%, etc. helium concentration. A similar subdivision resulting in samples having helium concentrations of 33.3%, 16.67%, 8.33%, 4.17%, etc. was also employed.

The electric method for helium analysis provided rapid and trouble-free operation and was far superior to the gas density balance in use.

B. Derivations

1. Sampling Error in Down-Mixing Studies due to Bubbles

Let: Y = fraction of bed occupied by "lean" phase (bubbles)
 $1-Y$ = fraction of bed occupied by "dense" phase
 Z = fraction of total gas flowing up~~er~~ bubbles
 $1-Z$ = fraction of total gas flowing through dense phase
 Q_{A+H} = total gas rate, ft.³/min.
 Q_A = helium feed rate, ft.³/min.

Then: $Y Q_H$ = rate of helium injection into lean phase

$(1-Y)Q_H$ = rate of helium injection into dense phase

ZQ_{A+H} = total gas rate through lean phase

$(1-Z)Q_{A+H}$ = total gas rate through dense phase

$\frac{YQ_H}{ZQ_{A+H}}$ = helium concentration in lean phase

$\frac{(1-Y)Q_H}{(1-Z)Q_{A+H}}$ = helium concentration in dense phase

Assume fraction of normal sample drawn from lean phase = Y
 Assume fraction of normal sample drawn from dense phase = $(1-Y)$

Composition of normal sample = $C = \frac{Y(YQ_H)}{(ZQ_{A+H})} + \frac{(1-Y)(1-Y)Q_H}{(1-Z)Q_{A+H}}$

$$C = \frac{Q_H}{Q_{A+H}} \left[\frac{Y^2}{Z} + \frac{(1-Y)^2}{1-Z} \right]$$

$$C_o = \frac{Q_H}{Q_{A+H}} ; \text{ therefore, } \frac{C}{C_o} \text{ for normal sample} = \frac{Y^2}{Z} + \frac{(1-Y)^2}{1-Z}$$

$$\text{for } Z = Y ; \frac{C}{C_o} = Y + 1-Y = 1.0$$

2. Down-Mixing Derivation

u = gas velocity, ft./sec.
 x = distance below plane of injection
 C = concentration at x
 E = down-mixing coefficient
 n = ft.³ gas transferred/ft.²
 θ = time, sec.
 ϵ = fraction voids
 A = cross section area of bed
 L_1 = distance plane of injection to bottom of bed

Assume down-mixing is analogous to eddy mixing,

$$-\frac{dn}{d\theta} = E \frac{dC}{dx} \quad (1)$$

Assume steady state, and constant E
 Assume C , u , and ϵ constant at any x ,

Material Balance on differential section:

$$\text{Input; } uA\epsilon (C + dC) + EA\epsilon \left[\frac{dC}{dx} + \frac{d}{dx} \left(\frac{dC}{dx} \right) dx \right]$$

$$\text{Output; } uA\epsilon (C) + EA\epsilon \frac{dC}{dx}$$

Accumulation = 0

$$uA\epsilon dC + EA\epsilon \frac{d^2C}{dx^2} dx = 0 \quad (2)$$

rearranging,

$$\frac{d^2C}{dx^2} + \frac{u}{E} \frac{dC}{dx} = 0 \quad (3)$$

solving,

$$C = K_1 + K_2 \exp \left(-\frac{u}{E} x \right) \quad (4)$$

Boundary Conditions A

$$x = \infty, \quad C = 0, \quad K_1 = 0 \quad (5)$$

$$x = 0, \quad C = C_0, \quad K_2 = C_0 \quad (6)$$

$$\therefore \frac{C}{C_0} = \exp\left(-\frac{u}{E} x\right) \quad (7)$$

$$\ln \frac{C}{C_0} = -\frac{u}{E} x \quad (8)$$

$$\frac{d \ln \frac{C}{C_0}}{dx} = -\frac{u}{E} = \text{slope of } \ln \frac{C}{C_0} \text{ vs. } x \quad (8a)$$

Boundary Conditions B

$$x = L_1, \quad C = 0 \quad (9)$$

$$x = 0, \quad C = C_0 \quad (10)$$

Applying (10),

$$C_0 = K_1 + K_2 \quad (11)$$

Applying (9),

$$0 = K_1 + K_2 \exp\left(-\frac{uL_1}{E}\right) \quad (12)$$

$$\therefore C_0 = K_2 \left[1 - \exp\left(-\frac{uL_1}{E}\right)\right]$$

$$K_2 = \frac{C_0}{1 - \exp\left(-\frac{uL_1}{E}\right)} \quad (13)$$

$$K_1 = C_0 - \frac{C_0}{1 - \exp\left(-\frac{uL_1}{E}\right)} \quad (14)$$

$$C = C_0 - \frac{C_0}{1 - \exp\left(-\frac{uL_1}{E}\right)} + \frac{C_0 \exp\left(-\frac{u}{E} x\right)}{1 - \exp\left(-\frac{uL_1}{E}\right)}$$

$$\frac{C}{C_0} = \frac{\exp(-\frac{u}{E}x) - \exp(-\frac{uL_1}{E})}{1 - \exp(-\frac{uL_1}{E})} \quad (15)$$

$$\ln \frac{C}{C_0} = \ln \left[\frac{\exp(-\frac{ux}{E}) - \exp(-\frac{uL_1}{E})}{1 - \exp(-\frac{uL_1}{E})} \right] \quad (16)$$

$$\frac{d(\ln \frac{C}{C_0})}{dx} = \frac{1 - \exp(-\frac{uL_1}{E})}{\exp(-\frac{ux}{E}) - \exp(-\frac{uL_1}{E})} \cdot \frac{(-\frac{u}{E}) \exp(-\frac{ux}{E})}{1 - \exp(-\frac{uL_1}{E})}$$

$$\frac{d \ln \frac{C}{C_0}}{dx} = -\frac{u/E}{1 - \exp\left[-\frac{u}{E}(L_1 - x)\right]} \quad (17)$$

$$\text{at } x = 0, \quad C/C_0 = 1.0$$

$$\text{and the slope of } \ln \frac{C}{C_0} \text{ vs. } x = \frac{-\frac{u}{E}}{1 - \exp(-\frac{uL_1}{E})} \text{ at } x=0 \quad (17a)$$

For sufficiently large values of $\frac{u}{E}$, if L is large compared to x , (17) reduces to (8a) and if L is large (17a) reduces to (8a).

Thus, for samples taken at low values of x (compared to L), a plot of $\ln \frac{C}{C_0}$ vs. x may yield a straight line with slope = $-\frac{u}{E}$.

Inspection of (17), which is derived from the correct boundary condition, $C = 0$ at $x = L$, shows that as x

increases the slope should increase. Thus, if the data are to agree with the assumptions made, a plot of $\ln \frac{C}{C_0}$ vs. x should be concave downward.

If the data give a curved line, concave downward, the value of $\frac{u}{E}$ can be determined using (17a) and the slope at the point where $\frac{C}{C_0} = 1.0$.

Since u has been assumed constant, then $u = u_0$, where u_0 is the superficial velocity. In the application of these equations u_0 replaced u .

3. Probability Derivation of Significance of Residence-Time Data

In addition to the graphical approach used in the Discussion of Results, a probability concept can be applied in developing the significance of the residence-time data. In this section two proofs using a probability approach will be presented. The first is simplified and the second rigorous.

a) Simplified Derivation

Consider a bed of solids which is being fluidized by a succession of slugs of gas molecules. The probability function is defined as follows:

$$F\Delta(Q\theta/V\epsilon) = \text{the probability that a gas molecule} \quad (18)$$

$$\text{that has been in the bed for time} = \theta$$

$$\text{will have left the bed between } \theta \text{ and } \theta + \Delta\theta.$$

FIGURE A3
PROBABILITY DENSITY

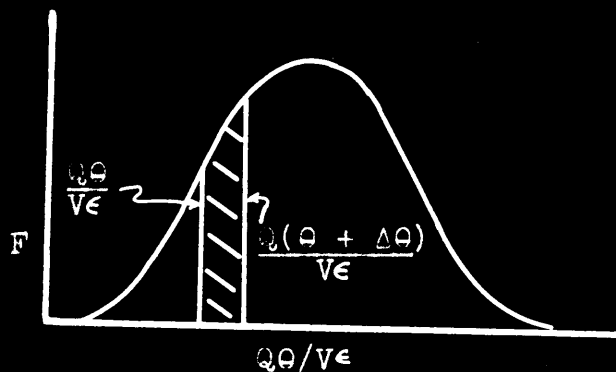


Figure A3 is presented as an aid to the visualization of this development and shows that F is a function $Q\theta/V\epsilon$. The shape of the curve is imaginary at this time, since the purpose of this discussion is to develop a method for determining the function P .

As the problem of gas flow in fluidized beds deals with large numbers of molecules, it follows from the definition (18) that:

$$F\Delta(Q\theta/V\epsilon) = \text{the fraction of a slug of gas having volume, } \Delta Q\theta/V\epsilon, \text{ that has been in the bed for time } = \theta \text{ that will have left the bed between } \theta \text{ and } \theta + \Delta\theta, \text{ i.e., that will have left in the slug, } \Delta Q\theta/V\epsilon, \text{ that leaves between } \theta \text{ and } \theta + \Delta\theta. \quad (19)$$

Therefore,

$$F\Delta(Q\theta/V\epsilon) = \text{the concentration of gas that has been in the bed for time } = \theta, \text{ in the slug } \Delta Q\theta/V\epsilon \text{ that leaves between } \theta \text{ and } \theta + \Delta\theta. \quad (20)$$

This assumes the flow rates of gas in and out of the bed are equal.

Summing,

$$\sum_0^{Q\theta/V\epsilon} F\Delta(Q\theta/V\epsilon) = \text{the concentration of gas, that entered the bed between } \theta = 0 \text{ and } \theta = \theta, \text{ in the gas leaving between } \theta \text{ and } \theta + \Delta\theta. \quad (21)$$

Allowing the size of the increments to go to zero,

$$\int_0^{Q\theta/V\epsilon} Fd(Q\theta/V\epsilon) = \text{the concentration of gas, that entered the bed between } \theta = 0 \text{ and } \theta = \theta, \text{ in the exit stream at time } \theta. \quad (22)$$

$$= X \text{ (by definition).}$$

Differentiating with respect to $Q\theta/V\epsilon$,

$$F = \frac{d(X)}{d(Q\theta/V\epsilon)} \quad (23)$$

F and X are functions of $Q\theta/V\epsilon$.

In the residence-time studies conducted in this thesis,

$$1 - C/C_0 = \text{the concentration of gas that entered the bed between } \theta = 0 \text{ and } \theta = \theta \text{ in the exit stream at } \theta.$$

$$= X$$

where θ , in the experiment, represents the time since fresh gas first entered the bed.

Thus,

$$F = - \frac{d(C/C_0)}{d(Q\theta/V\epsilon)} \quad (24)$$

Therefore, F can be determined as a function of $Q\theta/V\epsilon$, by taking the slope of the experimental curves at the desired values of $Q\theta/V\epsilon$. To repeat, F represents the probability that a gas molecule that has been in the bed for time equal to θ will leave the bed in the interval between θ and $\theta + d\theta$.

Referring to equation (19) it is evident that:

$$\int_0^{Q\theta/V\epsilon} Fd(Q\theta/V\epsilon) = \text{fraction of a differential slug,} \quad (25)$$

$d(Q\theta/V\epsilon)$, that entered at $\theta = 0$,
that will have left the bed by $\theta = \theta$.

and, therefore,

$$1 - C/C_0 = \text{the fraction of a differential slug,} \quad (26)$$

that entered the bed at $\theta = 0$, that
will have left the bed by $\theta = \theta$.

It follows that:

$$\int_{Q\theta/V\epsilon)_1}^{(Q\theta/V\epsilon)_2} Fd(Q\theta/V\epsilon) = X_2 - X_1 = (C/C_0)_1 - (C/C_0)_2 \quad (27)$$

= fraction of a slug of gas that
enters at time $\theta = 0$ that leaves the
bed between θ_1 and θ_2 .

and

$$C/C_0 \text{ at } Q\theta/V\epsilon = \text{the fraction of entering gas that} \quad (28)$$

remains for time = θ or longer.

b) Rigorous Derivation

Consider a bed of fluidized solids supported by a stream of gas.

$$F(Q\theta/V\epsilon)d(Q\theta/V\epsilon) \text{ is the probability that a gas mole-} \quad (29)$$

cule will leave the bed after it
has been in the bed at least θ time
but before it has been in the bed
for $\theta + d\theta$.

F is a probability function and is a function of $Q\theta/V\epsilon$; it will therefore be written as $F(Q\theta/V\epsilon)$.

A slug of gas of volume, $d(Q\theta/V\epsilon)$, enters at time t . It follows that the fraction of this slug which will leave in the interval between $t+\theta$ and $t+\theta+d\theta$ is

$$F\left(\frac{Q\theta}{V\epsilon}\right) d\left(\frac{Q\theta}{V\epsilon}\right) \quad (30)$$

The fraction of the slug which has left the bed up to time, γ , is:

$$\int_{\frac{Q\theta}{V\epsilon} = 0}^{\frac{Q\theta}{V\epsilon} = \frac{Q(\gamma-t)}{V\epsilon}} F\left(\frac{Q\theta}{V\epsilon}\right) d\left(\frac{Q\theta}{V\epsilon}\right) \quad (31)$$

The amount of the slug which has left up to time, γ , is then:

$$\int_{\frac{Q\theta}{V\epsilon} = 0}^{\frac{Q\theta}{V\epsilon} = \frac{Q(\gamma-t)}{V\epsilon}} F\left(\frac{Q\theta}{V\epsilon}\right) d\left(\frac{Q\theta}{V\epsilon}\right) d\left(\frac{Q\theta}{V\epsilon}\right) \quad (32)$$

The total amount of all the gas which entered between times $t = T$ and $t = \gamma$, which has left by time, γ , is then

$$\int_{\frac{Qt}{V\epsilon} = \frac{QT}{V\epsilon}}^{\frac{Qt}{V\epsilon} = \frac{Q\gamma}{V\epsilon}} \int_{\frac{Q\theta}{V\epsilon} = 0}^{\frac{Q\theta}{V\epsilon} = \frac{Q(\gamma-t)}{V\epsilon}} F\left(\frac{Q\theta}{V\epsilon}\right) d\left(\frac{Q\theta}{V\epsilon}\right) d\left(\frac{Qt}{V\epsilon}\right) \quad (33)$$

X is defined as the concentration in the exit stream of gas which has entered between T and γ . The total amount of this gas that has left by time, γ , is then

$$\int_{\frac{QT}{V\epsilon}}^{\frac{Q\gamma}{V\epsilon}} X d\left(\frac{Q\gamma}{V\epsilon}\right) \quad (34)$$

Thus (33) and (34) form an identity.

Differentiating both sides of the identity with respect to $(Q\gamma/V\epsilon)$, using Pierce (M2) No. 855 and 857:

$$X\left(\frac{Q\gamma}{V\epsilon}\right) = \int_{\frac{Qt}{V\epsilon} = \frac{QT}{V\epsilon}}^{\frac{Qt}{V\epsilon} = \frac{Q\gamma}{V\epsilon}} \left[\frac{d}{d\left(\frac{Q\gamma}{V\epsilon}\right)} \left(\frac{Q(\gamma-t)}{V\epsilon} F\left(\frac{Q\theta}{V\epsilon}\right) d\left(\frac{Q\theta}{V\epsilon}\right) \right) \right] d\left(\frac{Qt}{V\epsilon}\right)$$

$$\int_{\frac{Qt}{V\epsilon} = \frac{QT}{V\epsilon}}^{\frac{Qt}{V\epsilon} = \frac{Q\gamma}{V\epsilon}} F\left(\frac{Q(\gamma-t)}{V\epsilon}\right) d\left(\frac{Qt}{V\epsilon}\right) \quad (35)$$

Let $u = \gamma - t$; $t = \gamma - u$

$$du = -dt$$

$$X\left(\frac{Q\gamma}{V\epsilon}\right) = - \int_{\frac{Q(\gamma-T)}{V\epsilon}}^0 F\left(\frac{Qu}{V\epsilon}\right) d\left(\frac{Qu}{V\epsilon}\right) \quad (36)$$

Differentiating with respect to $(Q\gamma/V\epsilon)$

$$\frac{d X\left(\frac{Q\gamma}{V\epsilon}\right)}{d\left(\frac{Q\gamma}{V\epsilon}\right)} = F\left(\frac{Q(\gamma-T)}{V\epsilon}\right) \quad (37)$$

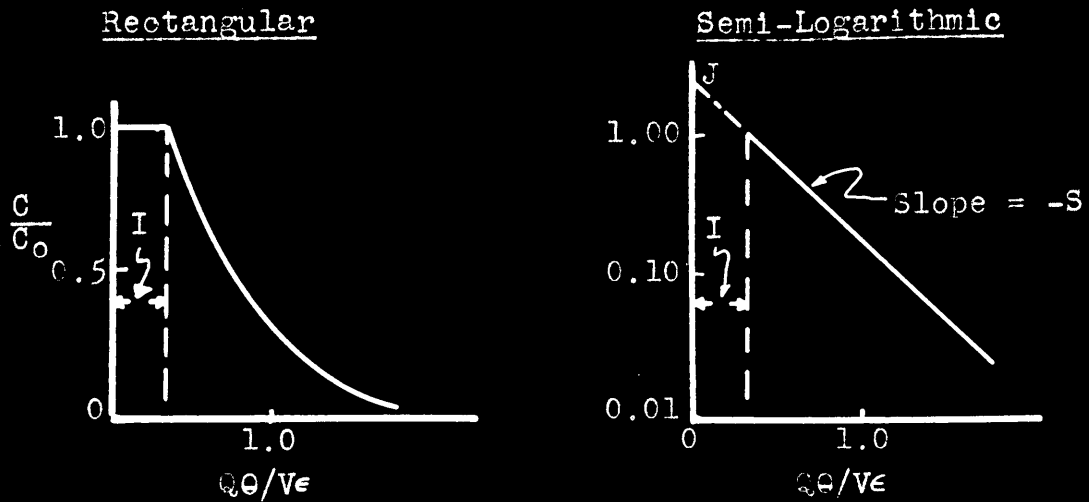
In the residence-time studies, T represents zero time, therefore γ represents the time in question after zero time, and

$$\frac{d X\left(\frac{Q\gamma}{V\epsilon}\right)}{d\left(\frac{Q\gamma}{V\epsilon}\right)} = F\left(\frac{Q\gamma}{V\epsilon}\right) \quad (38)$$

In the presentation of the experimental results in this thesis, the symbol θ replaces γ .

4. Semi-Logarithmic Plotting of Residence-Time Data

FIGURE A4



$$\ln \frac{C}{C_0} = J - S \left(\frac{Q_0}{V_0} \right) \quad (39)$$

or

$$\ln \frac{C}{C_0} = -S \left[\frac{Q_0}{V_0} - I \right] \quad (40)$$

then from (2) 40

$$\frac{C}{C_0} = \exp \left[-S \left(\frac{Q_0}{V_0} - I \right) \right] \quad (41)$$

$$\int_{\frac{Q_0}{V_0} = 0}^{\frac{Q_0}{V_0} = \infty} \frac{C}{C_0} d \left(\frac{Q_0}{V_0} \right) = 1.0 \quad (42)$$

Substituting (3) into (4)

$$\int_{\frac{Q\theta}{V\epsilon} = 0}^{\frac{Q\theta}{V\epsilon} = I} (1.0) d\left(\frac{Q\theta}{V\epsilon}\right) + \int_{\frac{Q\theta}{V\epsilon} = I}^{\frac{Q\theta}{V\epsilon} = \infty} \exp\left[-s\left(\frac{Q\theta}{V\epsilon} - I\right)\right] d\left(\frac{Q\theta}{V\epsilon}\right) = 1.0 \quad (43)$$

Integrating

$$I + \exp(sI) \int_I^{\infty} \exp\left[-s\left(\frac{Q\theta}{V\epsilon}\right)\right] d\left(\frac{Q\theta}{V\epsilon}\right) = 1.0 \quad (44)$$

$$I + \exp(sI) \frac{1}{-s} \left[\exp\left[-s\left(\frac{Q\theta}{V\epsilon}\right)\right] \right]_I^{\infty} = 1.0 \quad (45)$$

$$I + \frac{1}{s} = 1.0 \quad (46)$$

$$s = \frac{1}{1-I} \quad (47)$$

$$I = \frac{s-1}{s} \quad (48)$$

For piston flow $I = 1$, and $s = \infty$

For perfect mixing $I = 0$, and $s = 1$

B. Derivations (Cont'd)

5. Application of Back-Mixing Results to First Order Chemical Reaction

Let x = distance from bottom of bed
 C = concentration of reactants at x
 u_0 = superficial gas velocity
 A = cross section area of bed
 E = eddy diffusivity
 k = reaction rate constant

Neglect presence of solids and assume concentration and velocity constant at any cross section and that E is uniform throughout the bed. Assume a first order gas reaction occurring without change in volume. Assume steady state.

Material Balance on a Differential Section of Bed:

$$\text{Input} = u_0 A C - EA \frac{dC}{dx}$$

$$\text{Output} = u_0 A (C - dC) - EA \left[\frac{dC}{dx} - \frac{d}{dx} \left(\frac{dC}{dx} \right) dx \right]$$

$$\text{Accumulation} = -kAC \, dx$$

Equating: Input - Output = Accumulation

$$\frac{d^2C}{dx^2} - \frac{u_0}{E} \frac{dC}{dx} - \frac{k}{E} C = 0 \quad (49)$$

$$r = \frac{u_0 + \sqrt{u_0^2 + 4kE}}{2E}$$

$$C = A \exp \left[\frac{u_0}{2E} \left(1 + \sqrt{1 + \frac{4kE}{u_0^2}} \right) x \right] + B \exp \left[\frac{u_0}{2E} \left(1 - \sqrt{1 + \frac{4kE}{u_0^2}} \right) x \right] \quad (50)$$

$$\text{let } \sqrt{1 + \frac{4kE}{u_0^2}} = Y \quad (51)$$

$$C = B \exp \left[\frac{u_0}{2E} (1 - Y) x \right] \quad (52)$$

at $x = L$, $C = C_f$, where C_f = exit concentration of reactants

$$B = C_f \exp\left[-\frac{u_o L}{2E} (1-Y)\right] \quad (53)$$

Overall Material Balance:

$$u_o A (C_o - C_f) = k A \int_0^L C \, dx \quad (54)$$

$$C_o - C_f = \frac{k}{u_o} \int_0^L C \, dx \quad (55)$$

$$C_o - C_f = \frac{k}{u_o} \int_0^L C_f \exp\left[-\frac{u_o L}{2E} (1-Y)\right] \exp\left[\frac{u_o}{2E} (1-Y) x\right] dx \quad (56)$$

Integrating and rearranging,

$$C_o - C_f = \frac{k C_f}{\frac{u_o^2}{2E} \left[1 - \sqrt{1 + \frac{4kE}{u_o^2}}\right]} \left[1 - \exp\left[\frac{u_o L}{2E} \left(1 - \sqrt{1 + \frac{4kE}{u_o^2}}\right)\right]\right] \quad (57)$$

This equation (57) can be compared to the equation that would be obtained for the same assumptions in the absence of mixing and this is the usual first order equation.

$$C_f^* = C_o \exp(-k\theta) = C_o \exp\left(-\frac{kL}{u_o}\right) \quad (58)$$

where C_f^* = concentration of reactants leaving reactor for conditions of no gas mixing.

Equation (57) can be rewritten as

$$C_f = C_o \exp\left(-\frac{k'L}{u_o}\right) \quad (59)$$

where k' is the apparent reaction rate constant.

The ratio of the apparent reaction rate constant to the chemical reaction rate constant is given in Figure A5. The important criterion of the effect of mixing is the dimensionless group containing the product of the reaction rate constant and the mixing constant divided by the linear velocity squared. There is little effect on the reaction rate constant at low values of the dimensionless group, as this indicates either low mixing or a low reaction rate constant. In the first case, the effect of mixing would be expected to be low. In the second case, the effect is small because the low reaction rate constant implies that a long path of travel through the fluid bed would be necessary to make a significant difference in concentration, and thus even though mixing occurs it is not particularly serious, owing to the small concentration gradient.

The effect of such mixing on the reaction rate can also be shown as the effect on the fraction converted and the fraction unconverted. Figure A6 gives the ratio of the fraction converted with mixing to that without mixing and Figure A7 gives the corresponding ratio for the fraction unconverted. The most serious effect of mixing occurs when there is a significant concentration gradient -- i.e., when the conversion is high -- and the effect becomes small at low conversion.

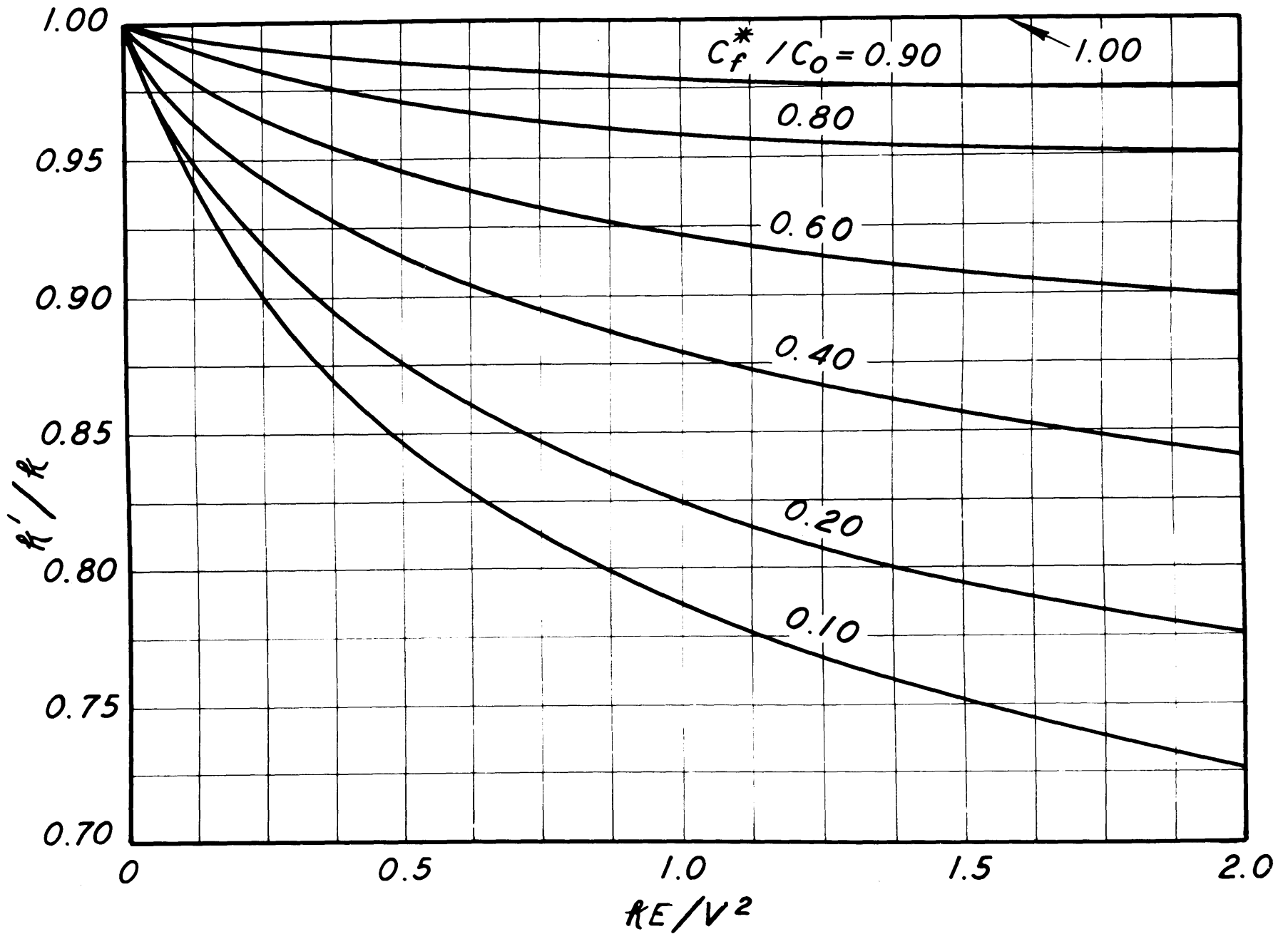


FIGURE A5 - EFFECT OF GAS MIXING ON FIRST ORDER CHEMICAL REACTION RATE CONSTANT

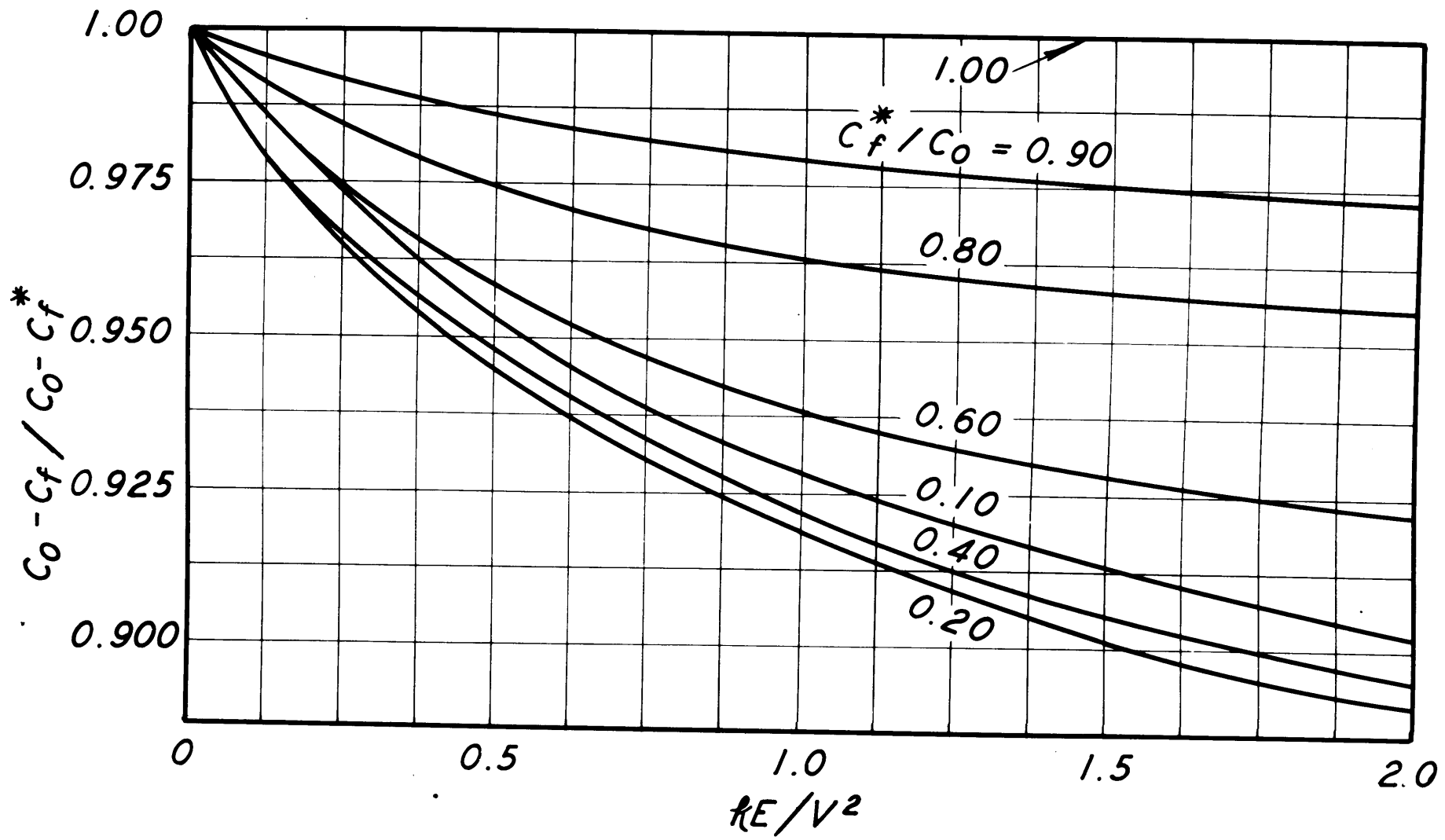


FIGURE A6 - EFFECT OF GAS MIXING ON FRACTION OF REACTANT CONVERTED IN FIRST ORDER REACTION

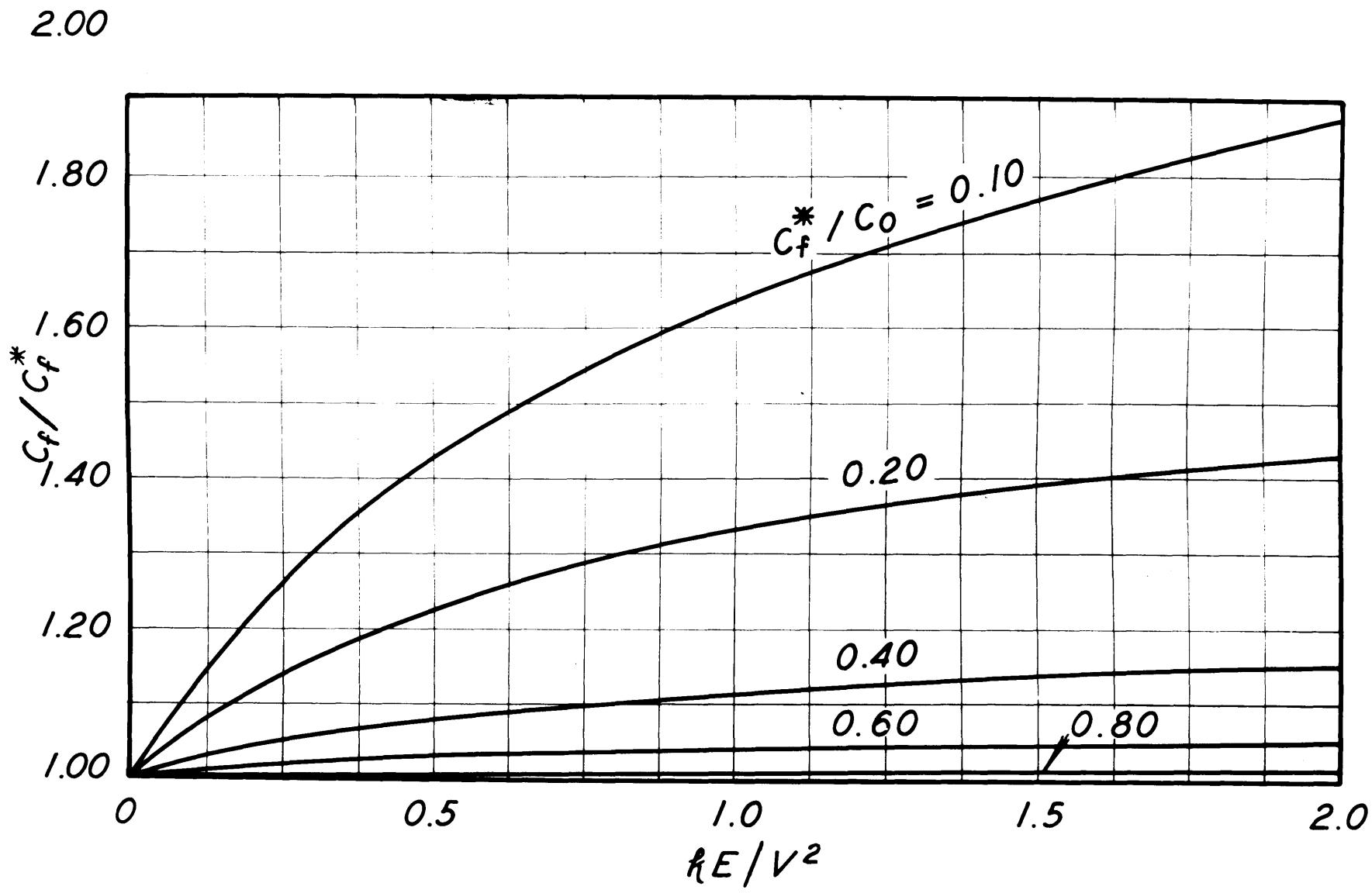


FIGURE A7 - EFFECT OF GAS MIXING ON FRACTION OF REACTANT UNCONVERTED IN FIRST ORDER REACTION

B. Derivations (Cont'd)

6. Application of Residence-Time Results to First Order Chemical Reaction

(a) Direct Derivation of Expression for Exit Composition for Piston Flow

Consider a differential slug of gas passing up through a fluidized bed; there is no mixing with other slugs. No change in volume.

n = mols of reactants in a differential slug
 $d(V\epsilon)$ at time θ

subscript o refers to entering conditions and
 f to exit

The first order expression is

$$-\frac{dn}{d\theta} = kn \quad \text{or} \quad -\frac{dn}{n} = kd\theta \quad (60)$$

$$Qd\theta = d(V\epsilon) \quad (61)$$

$$-\int_{n_o}^{n_f} \frac{dn}{n} = \int_0^{V\epsilon} \frac{kd(V\epsilon)}{Q} \quad (62)$$

$$\ln \frac{n_o}{n_f} = \frac{kV\epsilon}{Q} \quad (63)$$

$$\frac{n_f}{n_o} = \frac{C_f}{C_o} = \exp\left(-\frac{kV\epsilon}{Q}\right) \quad (64)$$

(b) Direct Derivation of Expression for Exit composition for Perfect Mixing

Balance around reactor:

Basis: unit time

Input = n_o

Output = $n_f + k_n$

$$n_o - n_f = k_n \quad (65)$$

$$C_f = \frac{n_f}{Q} ; \quad \theta = \frac{n}{V\epsilon} ; \quad n = \frac{n_f V\epsilon}{Q} \quad (66)$$

$$n_o - n_f = \frac{kV\epsilon}{Q} n_f \quad (67)$$

$$\frac{n_f}{n_o} = \frac{C_f}{C_o} = \frac{1}{1 + \frac{kV\epsilon}{Q}} \quad (68)$$

(c) Derivation of Residence-Time Expression for Perfect Mixing -- No Chemical Reaction

Tracer Balance Around Reactor:

Input = 0

Output = QC

Accumulation = $V\epsilon \frac{dC}{d\theta}$

$$\int_{C_o}^{C_f} \frac{dC}{C} = - \int_0^{\theta} \frac{Q}{V\epsilon} d\theta \quad (69)$$

Integrating

$$\frac{C_f}{C_o} = \exp\left(-\frac{Q\theta}{V\epsilon}\right) \quad (70)$$

(d) Derivation of Expression for Exit Composition for Perfect Mixing Using Probability Approach

Probability of a molecule remaining in

bed longer than $\theta = F = \exp\left(-\frac{Q\theta}{V\epsilon}\right) \quad (71)$

See section VII B.3. and equation (70).

Probability of a molecule remaining θ time
but leaving before $\theta + d\theta = Fd \left(\frac{Q\theta}{V\epsilon} \right) =$

$$\frac{Q}{V\epsilon} \exp\left(-\frac{Q\theta}{V\epsilon}\right) d\theta \quad (72)$$

assuming Q and $V\epsilon$ are constants

From first order expression

$$-\frac{dn}{d\theta} = kn \quad (60)$$

$$\frac{C}{C_0} = \exp(-k\theta) = \text{probability that a molecule will not react in time } \theta. \\ \text{See equation (64).}$$

The probability of a molecule reacting

$$\text{by time } \theta = 1 - \exp(-k\theta) \quad (74)$$

Combining the probability of a molecule remaining in the bed θ time and leaving in $\theta + d\theta$ and the probability of a molecule reacting by time θ should give the probability that a molecule in the exit stream will have reacted, i.e., the fraction of reacted molecules in the exit stream.

$$1 - \frac{C_f}{C_0} = \int_0^{\infty} \frac{Q}{V\epsilon} \exp\left(-\frac{Q\theta}{V\epsilon}\right) \left[1 - \exp(-k\theta)\right] d\theta \quad (75)$$

$$1 - \frac{C_f}{C_0} = 1 - \frac{Q/V\epsilon}{Q/V\epsilon + k} = 1 - \frac{1}{1 + \frac{V\epsilon k}{Q}} \quad (76)$$

This is the same as equation (68) derived directly for perfect mixing and therefore the method of multiplying probability times first order expression is verified.

(e) Derivation of Expression for Exit Composition Using Experimental Residence-Time Curves

In order to predict the effect of experimental residence-time curves on chemical reaction,

choose a reaction rate constant, k , and use the following equation

$$1 - \frac{C_f}{C_o} = \int_0^{\infty} [1 - \exp(-k\theta)] F d\left(\frac{Q\theta}{V\epsilon}\right) \quad (77)$$

where $-F$ is the slope of the residence-time curves obtained from gas mixing experiments.

The group $[1 - \exp(-k\theta)] F$ is plotted against $\frac{Q\theta}{V\epsilon}$ (Since F is obtained from slopes as a function of $Q\theta/V\epsilon$), and the value of $1 - \frac{C_f}{C_o}$ obtained by graphical integration.

If the residence-time curves are represented by

$$\frac{C}{C_o} = \exp\left[-s\left(\frac{Q\theta}{V\epsilon} - I\right)\right] \quad (78)$$

from $\frac{Q\theta}{V\epsilon} = I$ to $\frac{Q\theta}{V\epsilon} = \infty$

and by $\frac{C}{C_o} = 1.0$ (79)

from $\frac{Q\theta}{V\epsilon} = 0$ to $\frac{Q\theta}{V\epsilon} = I$

$$F = \frac{-d\left(\frac{C}{C_o}\right)}{d\left(\frac{Q\theta}{V\epsilon}\right)} = 0, \text{ from } 0 \text{ to } I \quad (80)$$

and $F = s \exp\left[-s\left(\frac{Q\theta}{V\epsilon} - I\right)\right]$, from I to ∞ (81)

Therefore equation (77) becomes

$$1 - \frac{C_f}{C_o} = s \int_I^{\infty} [1 - \exp(-k\theta)] \exp\left[-s\left(\frac{Q\theta}{V\epsilon} - I\right)\right] d\left(\frac{Q\theta}{V\epsilon}\right) \quad (82)$$

Integrating,

$$1 - \frac{C_f}{C_o} = 1 - \frac{s \exp\left(-\frac{kV\epsilon}{Q} I\right)}{s + \frac{kV\epsilon}{Q}} \quad (83)$$

Since $I = \frac{s-1}{s}$

$$1 - \frac{C_f}{C_o} = 1 - \frac{\exp\left(-\frac{V\epsilon k (S-1)}{QS}\right)}{1 + \frac{V\epsilon k}{QS}} \quad (84)$$

Equation (84) reduces to (64) for piston flow
($S = \infty$) and to (68) for perfect mixing ($S = 1$).

B. Derivations (Cont'd)

7. Application of Residence-Time Results to
Second Order Chemical Reaction

(a) Direct Derivation of Expression for Exit
Composition for Piston Flow

Consider a slug of gas flowing up through bed;
there is no mixing with other slugs and no change in
volume.

Let n = mols of reactants in the differential slug at
time θ

subscripts o and f refer to entering and exit
conditions

v = volume of differential slug, i.e., the volume
associated with the n_o mols.

The governing second order expression is

$$- \frac{dn}{d\theta} = kn \frac{n}{v} \quad (85)$$

$$d\theta = \frac{d(V\epsilon)}{Q} \quad (86)$$

$$- \int_{n_o}^{n_f} \frac{dn}{n^2} = \frac{k}{Qv} \int_0^{V\epsilon} d(V\epsilon) \quad (87)$$

$$\frac{1}{n_f} - \frac{1}{n_o} = \frac{kV\epsilon}{Qv} \quad (88)$$

$$\frac{n_f}{n_o} = \frac{C_f}{C_o} = \frac{1}{1 + \frac{kV\epsilon n_o}{Qv}} = \frac{1}{1 + \frac{kV\epsilon C_o}{Q}}$$

(b) Direct Derivation of Expression for Exit Composition for Perfect Mixing

Overall Balance on Reactants

n_o = mols reactants entering per unit time

n_f = mols reactants leaving per unit time

n = mols reactants in reactor at time θ

Q = total gas rate

Basis: unit time

Input = n_o

Output = $n_f + kn \frac{n}{V\epsilon}$

Accumulation = 0

$$n_o - n_f = kn \frac{n}{V\epsilon} \quad (90)$$

$$C_f = \frac{n_f}{Q} \quad \text{and} \quad C = \frac{n}{V\epsilon} \quad (91)$$

$$\text{for perfect mixing, } C_f = C \quad (92)$$

and

$$n = \frac{n_f V\epsilon}{Q} \quad (93)$$

Substitution in (90)

$$n_o - n_f = \frac{k n_f^2 V\epsilon}{Q^2} \quad (94)$$

Solving for n_f

$$n_f = \frac{-1 \pm \sqrt{1 + \frac{4k V\epsilon n_o}{Q^2}}}{\frac{2kV\epsilon}{Q^2}} \quad (95)$$

Only the positive root has physical significance (96)

$$\frac{n_f}{n_o} = \frac{C_f}{C_o} = \frac{-1 + \sqrt{1 + \frac{4kV\epsilon C_o}{Q}}}{\frac{2kV\epsilon C_o}{Q}} \quad (97)$$

(c) Derivation of Expression for Exit Composition Using Experimental Residence-Time Curves

In order to apply the residence-time results to second order reactions, it is necessary to know how the gas composition varies throughout the reactor. This is due to the n/v term in Equation (85).

The residence-time studies do not give information concerning the concentration gradients that may exist in fluid-beds, and therefore it is necessary to make an assumption concerning the nature of the gas flow through the beds. Therefore, it is assumed, for this derivation, that the entering gas flows through the bed in slugs which do not mix with other slugs. However, the gas molecules in these slugs have times of residence in the reactor conforming with the experimentally determined residence-time distributions.

This assumption should lead to an expression for the fraction converted that will be an upper limit on conversion for gas flow following the experimental residence-time distributions. Any mixing between successive slugs of entering gas would decrease the rate of reaction and hence the conversion for a given set of operating conditions.

The actual mechanism involved in this assumption is not stated, nor is it believed that there is no mixing between slugs. One mechanism that would give the experimental residence-time curves with no mixing is that of radial velocity gradient alone.

Since there is no mixing between slugs, the gas in any slug will follow the second order expression, Equation (89), and since

$$\frac{V\epsilon}{Q} = \theta_f = \text{time of contact} \quad (98)$$

$$1 - \frac{C}{C_0} = 1 - \frac{1}{1 + kC_0\theta} \quad (99)$$

= fraction converted by time θ

$$1 - \frac{C_f}{C_0} = \int_0^\infty F \left(1 - \frac{C}{C_0}\right) d\left(\frac{Q\theta}{V\epsilon}\right) \quad (100)$$

= fraction of entering slug of gas that is converted; refer to section VII B.6.(d).

$$F = 0, \text{ from } \frac{Q\theta}{V\epsilon} = 0 \text{ to } I \quad (101)$$

$$F = S \exp\left[-S\left(\frac{Q\theta}{V\epsilon} - I\right)\right], \text{ from } \frac{Q\theta}{V\epsilon} = I \text{ to } \infty \quad (102)$$

Substituting (99)(101) and (102) into (100),

$$1 - \frac{C_f}{C_0} = \int_I^\infty S \exp\left[-S\left(\frac{Q\theta}{V\epsilon} - I\right)\right] \left[1 - \frac{1}{1+kC_0\theta}\right] d\left(\frac{Q\theta}{V\epsilon}\right) \quad (103)$$

Integrating and using

$$I = \frac{S-1}{S} \quad (104)$$

$$1 - \frac{C_f}{C_0} = 1 - \frac{SQ}{V\epsilon k C_0} \exp\left[S\left(\frac{Q}{V\epsilon k C_0} + 1\right) - 1 \right] \int_S^\infty \frac{e^{-t} dt}{\frac{Q}{V\epsilon k C_0} + 1 - 1} \quad (105)$$

$$\text{where } t = \frac{SQ(1 + k C_0 \theta)}{V\epsilon k C_0} \quad (106)$$

Jahnke and Emde (11) tabulate values for the exponential integral,

$$- \text{Ei}(-x) = \int_x^{\infty} \frac{e^{-t}}{t} dt ; \quad \infty > x > 0 \quad (107)$$

Therefore the value of $1 - C_f/C_0$, which represents the fraction converted in a second order reaction under the assumed conditions, can be calculated for various flow conditions from (105) and (107).

For residence-times corresponding to the perfect mixing conditions, $S = 1$, and (105) reduces to

$$1 - \frac{C_f}{C_0} = 1 - \frac{Q}{V \epsilon k C_0} \exp\left(\frac{Q}{V \epsilon k C_0}\right) \int_{\frac{Q}{V \epsilon k C_0}}^{\infty} \frac{e^{-t}}{t} dt \quad (108)$$

This can be obtained directly using Equation (70).

For residence-times corresponding to piston flow conditions, $S = \infty$, and if the limit of (105) is taken as $S \rightarrow \infty$, Equation (89) is obtained showing that (105) fits both limits on S .

C = Concentration of Helium

$$(C)(4) + (1-x)(28.97) = M_M$$

$$C = 1.160 - \frac{M_M}{24.97} = 1.160 - \left[\frac{24.67 \pm 0.46\%}{24.97} \right]$$

$$C = 0.172 \pm 0.05 \quad (\pm 3\%)$$

Air Rate

R = Air differential manometer, in H₂O = 15.00 ± 0.10

P_{ST} = Static pressure manometer, in.Hg. = 12.70 ± 0.10

T = Air temperature, °R = 535 ± 1

Q $\sqrt{\frac{T}{P}}$ = Calibration reading = 15.0 ± 0.30

$$P = \text{Static pressure, in.Hg.} \quad \begin{array}{l} P_{ST} = 12.70 \pm 0.10 \\ \pi = 29.81 \pm 0.01 \\ P = \frac{42.51 \pm 0.11}{} \end{array}$$

$$\sqrt{\frac{T}{P}} = 3.55 \pm 2\%$$

$$Q_A = \frac{15.0 \pm 2\%}{3.55 \pm 0.2\%} = 4.23 \pm 0.09 \quad (\pm 2\%) \text{ ft.}^3/\text{min.}$$

air at 70°F. and 29.92 in.Hg.

Helium Rate

R = Helium differential manometer, in H₂O = 3.45 ± 0.10

P_{ST} = Helium static pressure manometer, in.Hg. = 12.00 ± 0.20

T = Helium temperature, °R = 533 ± 1

Q $\sqrt{\frac{MT}{P}}$ = Calibration reading = 3.29 ± 0.1

$$P = \text{Static pressure, in.Hg.;} \quad \begin{array}{l} P_{ST} = 12.00 \pm 0.20 \\ \pi = 29.81 \pm 0.01 \\ P = \frac{41.81 \pm 0.11}{} \end{array}$$

$$\sqrt{\frac{MT}{P}} = 7.14 \pm 0.36\%$$

$$Q_H = \frac{3.29 \pm 3\%}{7.14 \pm 0.4\%} = 0.461 \pm 0.016 \text{ (} \pm 3.4\% \text{) ft.}^3\text{/min.}$$

helium at 70°F. and 29.92 in.Hg.

$$Q_{A+H} = 4.69 \pm 0.11 \text{ (} \pm 2.3\% \text{) ft.}^3\text{/min.}$$

$$C_o = \text{Calculated Exit Concentration: } \frac{0.461 \pm 3.4\%}{4.69 \pm 2.3\%} = 0.099 \pm 0.006 \text{ (6\%)}$$

$$\frac{C}{C_o} = \frac{0.172 \pm 3\%}{0.099 \pm 6\%} = 1.74 \pm 0.15 \text{ (9\%)}$$

2. Residence-Time Studies

(a) Electric Analyzer

Gas Analysis

$$\begin{aligned} \text{Zero Sample} &= 62.4 \pm 0.1 \text{ millivolts} \\ 1 \text{ sec. " } &= 60.5 \pm 0.1 \text{ "} \end{aligned}$$

$$C_o = 62.4 \pm 0.1 \text{ mv} = (17.0 \pm 0.05) \% \text{ helium}$$

$$C = 60.5 \pm 0.1 \text{ mv} = (16.4 \pm 0.05) \% \text{ helium}$$

$$\frac{C}{C_o} = \frac{(16.4) \pm 0.3\%}{(17.0) \pm 0.3\%} = 0.965 \pm 0.006$$

(b) Air and helium rates for 3-inch column calculated in a manner similar to that of VII C 1.

(c) Air Rate from Rotameter - 4-1/2-inch Column

The rotameter calibration was expressed as cubic feet per minute at 29.92 inches of mercury and 70°F. To obtain the gas rate from the experimental conditions the following correction was applied.

$$Q_A = \text{CFM}(29.92 \text{ "Hg and } 70^\circ\text{F}) = \text{Calib. CFM} \sqrt{\frac{\pi + \text{PST}}{29.92}} \cdot \frac{530}{t_A + 460}$$

Calib. CFM = calibration reading for a given rotameter reading

π = atmospheric pressure, in. Hg.

P_{ST} = static pressure at rotameter, in. Hg.

t_A = temperature at rotameter, °F.

Run 7-35L-A

Rotameter reading = 5.0 ± 0.05

Calibration flow rate, $\text{ft.}^3/\text{min.} = 2.45 \pm 0.02$

$\pi = 29.95 \pm 0.01$ in. Hg.

$P_{ST} = 4.90 \pm 0.05$ in. Hg.

$t_A = 82.5 \pm 0.5$ °F.

$$Q_A = 2.45 \pm 1\% \sqrt{\frac{(34.85 \pm 0.2\%)(530)}{(29.92)(542.5 \pm 0.1\%)}}$$

$$Q_A = 2.61 \pm 0.03 (\pm 1\%) \text{ ft.}^3/\text{min. at } 70^\circ\text{F. and } 29.92 \text{ in. Hg.}$$

(d) Corrected Gas Rate

Run 7-37-A

$$Q_A = \text{ft.}^3/\text{min. air at } 70^\circ\text{F. and } 29.92 \text{ in. Hg.} = 1.17 \pm 2\%$$

$$T_A = \text{air temperature, } ^\circ\text{R} = 539 \pm 1$$

$$\pi = \text{barometric pressure, in. Hg.} = 30.00 \pm 0.01$$

$$P_{ST} = \text{static pressure at bottom of bed, in. Merriam Fluid, sp. gr.} = 2.95 = 14.15 \pm 0.1$$

$$P_{ave} = \text{average pressure in bed, in. Hg.} = \pi = 30.00 \pm 0.01$$

$$P_{ave} = \frac{(14.15 \pm 0.1)(2.95)}{(2)(13.5)} = \frac{1.55 \pm 0.01}{2} = 31.55 \pm 0.2$$

$$F = \frac{(539 \pm 1)(29.92)}{(530)(31.55 \pm 0.2)} = 0.96 \pm 0.2\%$$

$$Q = F Q_A = \text{ft.}^3/\text{min. air at } T_A \text{ and } P_{\text{ave}} =$$

$$1.12 \pm 0.02 (\pm 2\%)$$

$$u_o = \text{superficial velocity, ft./sec.} = \frac{Q}{(\pi/4)(D^2)(60)} =$$

$$0.38 \pm 0.008 (\pm 2\%)$$

(e) Void Volume - Glass Beads

$$\text{Charge weight} = 15 \text{ lb. } 15 \text{ oz. } \pm 1/2 \text{ oz.}$$

$$= 15.94 \pm 0.03 \text{ lb.}$$

$$\rho_s = \text{absolute density of glass beads, lb./ft.}^3 =$$

$$= 173 \pm 1\%$$

$$V = \text{volume of bed, ft.}^3 = \frac{\pi}{4} D^2 L = \frac{(\pi)(3)^2(37)}{(4)(12)(12)} =$$

$$= 0.151$$

$$V_e = \text{void volume of bed, ft.}^3 =$$

$$= 0.151 - \frac{15.94 \pm 0.2\%}{173 \pm 1\%} =$$

$$V_e = 0.059 \pm 0.001 (\pm 2\%)$$

$$\epsilon = \text{fraction voids} = \frac{0.059 \pm 2\%}{1.151} = 0.39 \pm 2\%$$

$$V_C = \text{volume of mixing space in cone, ft.}^3 = 0.0019$$

$$\theta = \text{time since helium turned off, sec.}$$

$$\theta^* = 1 \pm 0.2 \text{ sec.}$$

$$Q\theta^* = \frac{(1 \pm 20\%)(1.12 \pm 2\%)}{(60)} = 0.0187 \pm 0.0041 (\pm 22\%)$$

$$Q\theta = Q\theta^* - V_C = (0.0187 \pm 0.0041) - 0.0019 =$$

$$= 0.0168 \pm 0.0041 \text{ ft.}^3$$

$$\frac{Q\theta}{V_e} = \frac{0.0168 \pm 24\%}{0.059 \pm 2\%} = 0.29 \pm 0.08 (26\%)$$

$$\theta^* = 4 \pm 0.2 \text{ sec.}$$

$$Q\theta^* = \frac{(4 \pm 5\%)(1.12 \pm 2\%)}{60} = 0.0746 \pm 0.0052 (7\%) \text{ ft.}^3$$

$$Q\theta = 0.0746 \pm 0.0052 - 0.0019 = 0.0727 \pm 0.0052$$

$$\frac{Q\theta}{V_e} = \frac{0.0727 \pm 7\%}{0.059 \pm 2\%} = 1.24 \pm 0.11 (9\%)$$

(f) $\frac{Q\theta}{VE}$ for Microspheres from Plots of $\frac{C}{C_0}$ vs. $Q_A\theta$

$$\int_0^{\infty} \frac{C}{C_0} d(Q_{SC}\theta^*) = (\Sigma V)_{S.C.} = (VE)_{S.C.} + V_C \quad (1)$$

where $Q_{SC} = \text{ft.}^3 \text{ air/min. at } 70^\circ\text{F. and } 29.92 \text{ in.Hg.}$

$V_C = \text{volume of distributing cone}$

$V = \text{volume of bed, ft.}^3$

$VE = \text{void volume of bed, ft.}^3 = \text{volume of gas in bed}$

$\theta^* = \text{time since helium valve turned off.}$

$$\int_0^{\infty} \frac{C}{C_0} d(Q_{T.P.}\theta^*) = (\Sigma V)_{T.P.} = (VE)_{T.P.} + V_C \quad (2)$$

where $Q_{T.P.} = \text{ft.}^3 \text{ air/min. at temp. and pressure in bed.}$

$$\text{and since } Q_{T.P.} = Q_{S.C.} \left(\frac{T}{530} \right) \left(\frac{29.92}{\pi + \frac{P_{S.T.}}{2}} \right) = F \cdot T.P. Q_{S.C.} \quad (3)$$

where $T = \text{temperature of gas, } ^\circ\text{R.}$

$\pi = \text{barometric pressure, in. Hg.}$

$P_{S.T.} = \text{static pressure at base of bed, in. Hg.}$

$$(VE)_{T.P.} + V_C = \int_0^{\infty} \frac{C}{C_0} d(F_{T.P.} Q_{S.C.} \theta^*) = F \int_0^{\infty} \frac{C}{C_0} d(Q_{S.C.} \theta^*) \quad (4)$$

$$= F (VE)_{S.C.} + V_C \quad (5)$$

$$(VE)_{T.P.} = F(VE)_{S.C.} + V_C(F-1) \quad (6)$$

Since $F \approx 1$ and V_C small compared to (VE)
could drop $V_C(F-1)$ term and get

$$(VE)_{T.P.} = F(VE)_{S.C.} \quad (7)$$

Now, it is desired to plot $\frac{C}{C_0}$ vs. $\frac{Q_{T.P.}\theta}{(VE)_{T.P.}}$

where Θ = time since last of helium (or 1st air)
entered bottom of bed

$$\frac{Q_{T.P.} \Theta}{(V\epsilon)_{T.P.}} = \frac{Q_{T.P.} \Theta^* - V_C}{(V\epsilon)_{T.P.}} = \frac{F Q_{SC} \Theta^* - V_C}{F(V\epsilon)_{SC} + V_C(F-1)} \quad (8)$$

from (6) and where Θ = time since tracer
turned off corrected for V_C

$$= \frac{F Q_{SC} \Theta^* - V_C}{F[(\Sigma V)_{S.C.} - V_C] + V_C(F-1)} = \frac{F Q_{SC} \Theta^* - V_C}{F(\Sigma V)_{S.C.} - V_C}$$

Since $F \approx 1.0$ and V_C is small

$$= \frac{Q_{SC} \Theta^* - V_C}{(\Sigma V)_{S.C.} - V_C} = \frac{Q_{SC} \Theta}{(V\epsilon)_{S.C.}}$$

Therefore, to obtain $\frac{Q_{T.P.} \Theta}{(V\epsilon)_{T.P.}}$, plot $\frac{C}{C_0}$ against
the corresponding values of $Q_{S.C.} \Theta^*$, and integrate obtain-
ing $(\Sigma V)_{S.C.}$. Next subtract V_C from $(\Sigma V)_{S.C.}$ and from
all values of $Q_{S.C.} \Theta^*$. On dividing $(Q_{S.C.} - V_C)$ by
 $[(\Sigma V)_{S.C.} - V_C]$, $\frac{Q_{T.P.} \Theta}{(V\epsilon)_{T.P.}}$, or simply $\frac{Q\Theta}{V\epsilon}$, is obtained.
The original values of C/C_0 are now plotted vs. $Q\Theta/V\epsilon$.

3. Densities of Glass Beads

Number 7 Glass Beads

Graduate + Water + Beads	= 265.1 ± 0.1 gr	93.0 ± 0.1 cc
Graduate + Water	= 189.2 ± 0.1 gr	65.8 ± 0.1 cc
Beads	= 75.9 ± 0.2 gr	27.2 ± 0.2 cc
Sp. gr.	= $\frac{75.9 \pm 0.3\%}{27.2 \pm 0.7\%}$	= 2.78 ± 1%

$$\rho_s = (62.3)(2.78 \pm 1\%) = 173 \text{ lb./ft.}^3 \pm 1\%$$

Arithmetic average of several determinations
taken.

4. Calculation of Core and Annular Velocities from Back-Mixing Traverses

R = radius of column = 1.5 in.

R_C = radius of core, in.

C = concentration of helium in gas

u = average velocity of gas, ft./sec.

subscripts, A = annulus

C = core

o = superficial

Helium Balance

$$C_A u_A \frac{\pi}{144} (R^2 - R_C^2) = C_C u_C \frac{\pi R_C^2}{144}$$

Air Balance

$$\begin{aligned} (1 - C_C) u_C \frac{\pi R_C^2}{144} - (1 - C_A) u_A \frac{\pi}{144} (R^2 - R_C^2) &= \\ &= u_o \pi \frac{R^2}{144} \end{aligned}$$

Therefore:

$$u_A = \frac{2.25 u_o}{2.25 - R_C^2} \left[\frac{\left(\frac{C}{C_o}\right)_C}{\left(\frac{C}{C_o}\right)_A - \left(\frac{C}{C_o}\right)_C} \right]$$

$$u_C = u_A \frac{C_A}{C_C} \frac{2.25 - R_C^2}{R_C^2}$$

5. Calculation of Bed Densities, ρ_B

ρ_B = slope of static pressures plotted against distance from bottom of bed.

VIII. APPENDIX D. Summary of Data and Calculated Results

1. Back-Mixing Data - Table AI

Explanation of Headings

Sample No.: Samples numbered consecutively from No. 1

Solids: The following code is used in the table:

- A = No. 13 glass beads, mean diameter 0.0040 in. \pm 10%
- B = No. 7 glass beads, mean diameter 0.0178 in. \pm 10%
- C = Mixture of No. 6, 7, 9, 11, and 13 glass beads
- D = Microspheres less fines blown out at 1.5 ft./sec.
- E = Microspheres retained on 100 Tyler Mesh
- F = Microspheres through 150 Tyler Mesh
- G = Microspheres fines only
- M2 = Microspheres thru 150 Tyler Mesh, or 200 Tyler Mesh

V (ft./sec.): Superficial air velocity \pm 2%

C₀ (%): Final helium concentration calculated from orifice measurements

Position: First figure indicates vertical position of sample point in inches below injection level; second group indicates radius at which sample was drawn as follows:

- R0 center
- R1 0.566 in. north of center
- R2 0.980 in. north of center
- R3 1.27 in. north of center
- R4 1.45 in. north of center

C/C₀: Ratio of sample concentration as analyzed to concentration C₀. C₀ based on analyzed concentration of gas from cyclone at the top of the column.

Special Notations:

- v denotes sample selectively taken from voids
- s denotes sample selectively taken from solids
- x denotes sample not significant for any reason
- d denotes sample taken directly into analyzer cell

Sample No.:	Solids:	u_0 (ft./sec.):	C_0 (%):	Position:	C/C_0
1					
2	A	0.9	5.58	-2 -R3	1.69
3	A	0.9	5.27	-2 -R3	1.74
4	A	0.9	5.48	-2 -R2	1.31
5	A	0.9	5.5	-2 -R2	1.12
6	A	0.9	5.5	-2 -R1	1.83
7	A	0.9	5.5	-2 -R1	
8					
9	A	0.9	5.64	-2 R1	2.61
10	A	0.9	5.4	-2 R1	2.62
11	A	0.9	5.5	-2 R1	2.96
12	A	0.9	5.5	-2 R2	1.73
13	A	0.9	5.5	-2 R2	1.64
14	A	0.9	5.4	-2 R3	1.47
15	A	0.9	5.45	-2 R3	1.56
16	A	0.9	5.47	-2 R4	1.33
17	A	0.9	5.47	-2 R4	1.61
18	A	0.9	5.60	2 R3	0.99
19	A	0.9	5.65	2 -R2	0.96
20	A	0.9	5.64	2 -R1	1.04
21	A	0.9	5.65	2 R0	1.28
22	A	0.9			
23	A	0.9	5.68	top	
24	A	0.9	5.64	top	
25	A	0.9	5.74	-12 -R3	1.69
26	A	0.9	5.63	-12 -R2	1.69
27	A	0.9	5.72	-12 -R1	2.14
28	A	0.9	5.66	-12 R0	2.43
29	A	0.9	5.54	top	
30	A	0.9	5.43	top	
31	A	0.9	5.47	24 R0	0.99
32	A	0.9	5.84	24 R1	0.95
33	A	0.9	5.63	24 R2	0.98
34	A	0.9	5.65	24 R3	0.94
35	A	0.9	5.71	-11 R3	1.00
36	A	0.9	5.67	-11 R0	1.01
37	A	0.9	5.49	top	
38	A	0.9	5.74	-11 R1	1.00
39	A	0.9	5.56	-11 R2	0.99

Note: (1) Samples 1 through 28 were taken with helium injected through a single glass tube pointed upward
(2) Samples 29 through 39 were taken with helium injected beneath screen at the bottom of the column.

Sample No.:	Solids:	u_0 (ft./sec.):	C_0 (%):	Position:	C/C_0
40	A	0.9	5.40	-11 R2	1.77
41	A	0.9	5.54	-11 R3	1.51
42	A	0.9	5.51	-11 R4	1.52
43	A	0.9	5.54	-11 R1	1.90
44	A	0.9	5.62	-11 -R0	2.33
45	A	0.9	5.62	-11 -R1	2.03
46	A	0.9	5.62	-11 -R2	1.78
47	A	0.9	5.65	-11 -R3	1.69
48	A	0.9	5.47	-11 -R4 *	1.41
49	A	0.9	5.40	-11 -R2 *	1.62
50	A	0.9	5.60	-11 -R2 *	1.59
51	A	0.9	5.68	-11 -R1 *	2.03
52	A	0.9	5.80	-11 R2 *	1.49
53	A	0.9	5.80	top	
54	A	0.9	5.60	-11 R0	
55	A	0.9			
56	A	0.9			
57	A	0.9	5.70	top	
58	A	0.9	5.63	-11 R0	1.64
59	A	0.9	5.53	-11 -R1	1.91
60	A	0.9	5.51	-11 -R2	1.47
61	A	0.9	5.50	-11 -R3	1.46
62	A	0.9	5.50	-11 R1	1.96
63	A	0.9	5.50	-11 R2	1.41
64	A	0.9	5.50	-11 R3	1.49
65	A	0.9	5.50	-11 R4	1.46
66	A	0.9	5.57	top	
67	A	0.9	8.83	top	
68	A	0.9	8.97	-16 R4	1.20
69	A	0.9	9.00	-16 R3	1.11
70	A	0.9	8.93	-16 R2	1.19
71	A	0.9	9.00	-16 R1	1.16
72	A	0.9	8.75	-16 R0	1.19
73	A	0.9	8.75	-16 -R1	1.09
74	A	0.9	8.80	-16 -R2	1.10
75	A	0.9	8.80	-16 -R3	1.13
76	A	0.9	8.85	top	
77	A	0.9	9.00	top	
78	A	0.9	5.60	top	
79	A	0.9	5.60	top	

- Note: (1) Samples 40 through 54 were taken with helium injected through a single glass tube pointed upward
- (2) Samples 57 through 66 were taken with helium injected through a single glass tube pointed downward
- (3) Samples 67 through 77 taken with 12-point radial injection system
- (4) Samples 78, 79 with same injection as samples 40 through 54
- * (5) Samples 48 through 52 taken on an east-west diameter

Sample No.:	Solids:	u_0 (ft./sec.):	C_0 (%):	Position:	C/C_0
80	A	0.9	7.2	2 RO	1.28
81	A	0.9	6.9	2 R1	0.37
82	A	0.9	6.9	2 RO	0.33
83	A	0.9	7.8	2 R2	1.33
84	A	0.9	7.3	2 R3	1.16
85	A	0.9	7.7	2 R4	1.08
86	A	0.9	7.8	2 R1	1.31
87	A	0.9	6.3	4 RO	1.23
88	A	0.9	8.2	4 RO	1.20
89	A	0.9	8.3	4 R1	1.04
90	A	0.9	8.4	4 R2	0.89
91	A	0.9	8.4	4 R3	1.21
92	A	0.9	8.5	4 R4	1.97
93	A	0.9	8.5	4 R3	0.70
94	A	0.9	8.48	top	
95	A	0.9	8.7	4 R4	1.20
96	A	0.9	8.4	4 R2	0.73
97	A	0.9	8.5	4 R1	0.87
98	A	0.9	8.5	4 RO	1.17
99	A	0.9	8.5	4 RO	1.17
100	A	0.9	8.5	4v R1	0.77
101	A	0.9	8.5	4 R2	1.01
102	A	0.9	8.4	4 R3	0.86
103	A	0.9	8.5	4 R4	1.10
104	A	0.9	8.6	6 RO	0.76
105					
106	A	0.9	7.1	10 RO	0.82
107	A	0.9	7.2	8 RO	0.82
108	A	0.9	7.3	12 RO	0.80
109	A	0.9	8.1	14 RO	0.59
110	A	0.9	8.2	16 RO	0.36
111	A	0.9	8.2	18 RO	0.12
112	A	0.9	8.17	top	
113	A	0.9	8.4	2 RO	1.15
114	A	0.9	8.2	4 RO	1.07
115	A	0.9	8.2	6 RO	1.18
116	A	0.9	8.4	8 RO	0.96
117	A	0.9	8.4	10 RO	0.98
118	A	0.9	8.4	12 RO	0.67
119	A	0.9	8.4	14 RO	0.38
120	A	0.9	8.6	16 RO	0.36
121	A	0.9	8.6	18 RO	0.17
122	A	0.9	8.55	top	

Note: Samples 80 through 112 with 12-point injection, relative humidity of air to column 38 - 40%
Samples 113 through 122 with 12-point injection, R.H. 32 - 38%

Sample No.:	Solids:	u_0 (ft./sec.):	C_0 (%):	Position:	C/C_0
123	A	0.9	8.4	18 RO	0.145
124	A	0.9	8.4	16 RO	0.21
125	A	0.9	8.5	14 RO	0.19
126	A	0.9	8.6	12 RO	0.36
127	A	0.9	8.6	10 RO	0.46
128	A	0.9	8.6	8 RO	0.56
129	A	0.9	8.6	6 RO	0.95
130	A	0.9	8.4	4 RO	0.97
131	A	0.9	8.5	2 RO	1.24
132	A	0.9	8.47	top	
133	A	0.9	8.6	-11 RO	1.33
134	A	0.9	8.2	-11 RO	1.43
135	A	0.9	8.2	-11 R1	1.44
136	A	0.9	8.3	-11 R2	0.86
137	A	0.9	8.4	-11 R2	1.42
138	A	0.9	8.4	-11 R3	1.36
139	A	0.9	8.4	-11 R3	1.45
140	A	0.9	8.4	-11 R2	1.67
141	A	0.9	8.4	-11 R1	1.36
142	A	0.9	8.4	-11 RO	1.41
143	A	0.9	8.4	-16 RO	1.26
144	A	0.9	8.5	-16 R1	1.13
145	A	0.9	8.7	-16 R2	1.31
146	A	0.9	8.4	-16 R3	1.32
147	A	0.9	8.47	top	
148	A	0.9	5.6	-11 R1	2.04
149	A	0.9	5.7	-11 R1	1.92
150	A	0.9	5.7	-11 R1	2.13
151	A	0.9	5.8	-11 R1	2.18
152	A	0.9	5.7	-11 R1	2.38
153	A	0.9	5.7	-11 R1	2.30
154	A	0.9	5.7	-11 R1	2.13
155	A	0.9	5.70	top	
156	A	0.9	5.55	top	
157	A	0.9	5.59	top	1.01
158	A	0.9	5.59	top	0.98

- Note: (1) Samples 123 through 147 with 12-point injection; R.H. 58 - 64%
(2) Samples 148 through 158 with single glass injection tube (upward)
(3) Samples 148 through 154 taken at widely varying speeds of sampling
(4) Samples 157 through 158 taken by drawing the gas through a tube which was submerged in glass beads in order to look for any "barrier diffusion effect". The test was negative, and no difference in concentration was so obtained.

Sample No.:	Solids:	u_0 (ft./sec.):	C_0 (%):	Position:	C/C_0
159	A	0.9	5.67	-11 R2	2.36
160	A	0.9	5.67	-11 R2	2.43
161	A	0.9	5.67	-11 R2	2.14
162	A	0.9	5.67	-11 R2	2.21
163	A	0.9	5.67	-11 R2	1.34 V
164	A	0.9	5.67	-11 R2	1.50 S
165	A	0.9	5.67	-11 R2	3.15 S
166	A	0.9	5.67	-11 R2	1.32 V
167	A	0.9	5.6	-11 R2	2.04 S
168	A	0.9	5.6	-11 R4	0.92 V
169	A	0.9	5.70	top	
170	A	0.9	5.6	-11 -R4	0.80 V
171	A	0.9	7.8	6 RO	0.80
172	A	0.9	7.8	6 RO	0.93
173	A	0.9	7.8	6 RO	1.06
174	A	0.9	7.8	6 RO	0.82
175	A	0.9	7.9	6 RO	0.84
176	A	0.9	6.1	6 RO	1.31
177	A	0.9	6.0	6 RO	1.28
178	A	0.9	6.1	6 R1	1.37
179	A	0.9	6.0	6 R1	1.34
180	A	0.9	6.0	6 R2	1.56
181	A	0.9	6.0	6 R2	1.62
182	A	0.9	6.0	6 R3	1.43
183	A	0.9	6.2	6 R4	1.43
184	A	0.9	6.2	6 R4	1.41
185	A	0.9	6.2	6 R3	1.30
186	A	0.9	6.2	top	
187	A	0.9	7.9	8 RO	1.37
188	A	0.9	7.5	10 RO	1.27
189	A	0.9	7.5	12 RO	1.15
190	A	0.9	7.5	14 RO	0.52
191	A	0.9	7.6	14 RO	0.36
192	A	0.9	7.4	16 RO	0.088
193	A	0.9	7.8	18 RO	0.025
194	A	0.9	7.8	-11 RO	1.49
195	A	0.9	7.8	-11 R1	1.40
196	A	0.9	7.4	-11 R2	1.86
197	A	0.9	7.5	-11 R3	1.61
198	A	0.9	7.5	-11 R4	1.97

- Note: (1) Samples 159 through 162 taken at varying sampling speeds using single point glass injection tube
(2) Samples 163 through 170 with single point glass injection tube. Samples marked V taken selectively from voids, marked S from solids.
(3) Samples 171 through 175 with 12-point injection system
(4) Samples 176 through 198 with 8-point injection at wall of column.

Sample No.:	Solids:	u_0 (ft./sec.):	C_0 (%):	Position:	C/C_0
199	A	0.9	7.6	-11 R3	1.30
200	A	0.9	7.7	top	
201	A	0.9	7.75	-11 R3	1.17
202	A	0.9	7.85	-11 -R1	1.37
203	A	0.9	7.85	-11 -R3	1.63
204	A	0.9	7.93	top	
205	A	0.9	7.8	6 R3	0.87
206	A	0.9	7.95	6 R3	0.56 vx
207	A	0.9	7.8	6 R3	0.53
208	A	0.9	7.7	6 R3	0.48
209	A	0.9	7.55	6 R3	0.77
210	A	0.9	7.5	6 R3	1.12
211	A	0.9	7.8	6 R3	0.83
212	A	0.9	7.7	6 RO	1.20
213	A	0.9	7.7	6 RO	1.01
214	A	0.9	7.7	6 RO	0.62
215	A	0.9	7.8	6 RO	1.20
216	A	0.9	7.8	6 RO	0.85
217	A	0.9	7.9	6 RO	1.04
218	A	0.9	7.9	6 RO	0.86
219	A	0.9	7.75	6 RO	0.63 vx
220	A	0.9	7.8	6 RO	1.20 sx
221	A	0.9	7.8	6 RO	1.14 sx
222	A	0.9	7.9	6 RO	1.14 vx
223	A	0.9	7.9	6 RO	1.11 vx
224	A	0.9	7.9	14 RO	0.43
225	A	0.9	7.9	14 RO	0.68
226	A	0.9	7.8	14 RO	0.56
227	A	0.9	7.7	14 RO	0.43
228	A	0.9	7.75	14 RO	0.49
229	A	0.9	7.8	14 RO	0.45 vx
230	A	0.9	7.9	14 RO	0.45 vx
231	A	0.9	7.9	14 RO	0.32 sx
232	A	0.9	8.0	14 RO	0.37 sx
233	A	0.9	7.9	16 RO	0.27
234	A	0.9	7.5	18 RO	0.21
235	A	0.9	7.6	12 RO	0.50
236	A	0.9	7.6	10 RO	0.69
237	A	0.9	7.6	8 RO	0.91
238	A	0.9	7.61	top	

Note: (1) All samples from 204 on taken with 12-point injection
(2) Samples 199 through 203 with 8-point injection at wall

Sample No.:	Solids:	u_0 (ft./sec.):	C_0 (%):	Position:		C/C_0
239	A	0.9	6.25	6	RO	0.62
240	A	0.9	6.3	6	R1	0.67
241	A	0.9	6.35	6	R2	0.47
242	A	0.9	6.05	6	R3	0.32
243	A	0.9	6.1	6	R4	0.57
244	A	0.9	6.1	6	R3	0.58
245	A	0.9	6.1	14	RO	0.15
246	A	0.9	6.1	14	R1	0.12
247	A	0.9	6.2	14	R2	0.10
248	A	0.9	6.2	14	R3	0.12
249	A	0.9	6.25	14	R4	0.17
250	A	0.6	7.8	14	RO	0.075
251	A	0.6	7.8	14	R1	0.094
252	A	0.6	7.8	14	R2	0.064
253	A	0.6	7.8	14	R3	0.048
254	A	0.6	7.8	14	R4	0.090
255	A	0.6	7.8	14	R1	0.086
256	A	0.6	7.8	14	RO	0.105
257	A	0.6	7.8	14	RO	0.114
258	A	0.6	7.8	16	RO	0.0
259	A	0.6	7.8	16	RO	0
260	A	0.6	7.8	12	RO	0.25
261	A	0.6	7.8	10	RO	0.44
262	A	0.6	7.8	8	RO	0.67
263	A	0.6	7.8	6	RO	0.78
264	A	0.6	7.8	12	RO	0.23
265	A	0.6	7.8	15	RO	0
266	A	0.6	7.8	15	RO	0
267	A	0.6	7.8	14	RO	0.075
268	A	0.6	7.8	4	RO	0.99
269	A	0.6	7.8	10	RO	0.37 vx
270	A	0.6	7.8	-10	RO	0.46 vx
271	A	0.6	7.8	10	RO	0.62 vx
272	A	0.6	7.8	10	RO	0.36 sx
273	A	0.6	7.8	10	RO	0.61 s
274	A	0.6	7.8	10	RO	0.56 s
275	A	0.6	7.8	10	RO	0.19 v
276	A	0.6	7.8	10	RO	0.22 v
277	A	0.6	7.8	10	RO	0.18 v
278	A	0.6	7.8	10	RO	0.78 s
279	A	0.6	7.8	10	RO	0.40 s
280	A	0.6	7.8	10	RO	0.53 s
281	A	0.6	7.8	10	RO	0.75 s
282	A	0.6	7.8	10	RO	0.73 s
283	A	0.6	7.8	10	RO	0.39 s
284	A	0.6	7.8	10	RO	0.16 v

Sample No.:	Solids:	u_0 (ft./sec.):	C_0 (%):	Position:	c/c_0
285	A	0.6			
286					
287					
288					
289	A	0.6	7.9	10 RO	0.38
290	A	0.6	8.0	10 RO	0.18 ▽
291	A	0.6	8.0	12 RO	0.17
292	A	0.6	7.9	14 RO	0.126
293	A	0.6	7.9	8 RO	0.63
294	A	0.6	7.9	6 RO	0.88
295	A	0.6	7.9	4 RO	1.10
296	A	0.6	8.0	12 RO	0.18
297	A	0.6	8.12	top	
298	A	0.4	10.4	12 RO	0.004
299	A	0.4	9.85	10 RO	0.078
300	A	0.4	10.0	8 RO	0.15
301	A	0.4	10.0	6 RO	0.49
302	A	0.4	10.0	4 RO	0.77
303	A	0.4	10.2	4 RO	0.84
304	A	0.4	10.2	6 RO	0.43
305	A	0.4	10.4	6 RO	0.47
306	A	0.4	10.4	8 RO	0.30
307	A	0.4	10.6	10 RO	0.047
308	A	0.4	10.2	10 RO	0.085
309	A	0.4	10.2	8 RO	0.26
310	A	0.4	10.4	8 RO	0.24
311	A	0.4	10.5	top	
312	A	0.4	10.7	7 RO	0.39
313	A	0.4	9.9	5 RO	0.55
314	A	0.4	10.0	5 RO	0.37 ▽
315	A	0.4	10.2	5 RO	0.27 ▽
316	A	0.4	10.1	top	
317	A	1.2	4.75	4 RO	1.20
318	A	1.2	4.95	6 RO	1.17
319	A	1.2	4.95	8 RO	0.91
320	A	1.2	4.97	10 RO	0.98
321	A	1.2	4.96	10 RO	0.81
322	A	1.2	5.05	12 RO	0.71
323	A	1.2	5.01	14 RO	0.51
324	A	1.2	5.02	16 RO	0.36
325	A	1.2	4.90	10 RO	0.65 ▽
326	A	1.2	4.90	10 RO	0.95 s

Note: Samples 285 through 288 discarded because humidity was excessively high and bed appeared "wet".

Sample No:	Solids:	u_0 (ft./sec.):	C_0 (%):	Position:	C/C_0
327	A	1.6	3.83	10 RO	0.67 v
328	A	1.6	3.92	10 RO	0.96 s
329	A	1.6	3.92	10 RO	0.95
330	A	1.6	3.97	10 RO	0.69
331	A	1.6	3.88	top	
332	A	1.6	3.88	10 RO	0.22 v
333	B	1.56	3.15	top	
334	B	1.56	3.21	-11 RO	0.95
335	B	1.56	3.20	-11 R1	1.15
336	B	1.56	3.20	-11 R2	1.06
337	B	1.56	3.25	-11 R3	0.87
338	B	1.56	3.28	-11 RO	0.98 s
339	B	1.56	3.26	4 RO	0.098
340	B	1.56	3.28	4 RO	0.084s
341	B	1.56	3.29	4 RO	0.135
342	D	0.4	11.0	-11 RO	1.01
343	D	0.4	10.8	-11 R1	1.06
344	D	0.4	10.3	-11 R2	1.06
345	D	0.4	10.8	-11 R3	1.03
346	D	0.4	10.8	top	
347	D	0.4	10.8	-6 RO	1.19
348	D	0.4	10.9	-6 R1	1.11
349	D	0.4	10.8	-6 R2	1.09
350	D	0.4	10.8	-6 R3	1.06
351	D	0.4	10.8	-6 R4	1.05
352	D	0.4	10.8	top	
353	D	0.4	10.5	4 RO	0.68
354	D	0.4	10.7	6 RO	0.60
355	D	0.4	10.7	8 RO	0.47
356	D	0.4	10.7	10 RO	0.36
357	D	0.4	10.8	12 RO	0.30
358	D	0.4	10.8	14 RO	0.23
359	D	0.4	10.8	16 RO	0.18
360	D	0.4	10.9	18 RO	0.19
361	D	0.4	10.1	6 RO	0.67
362	D	0.4	10.2	6 R1	0.715
363	D	0.4	10.3	6 R2	0.87
364	D	0.4	10.3	6 R3	1.21
365	D	0.4	10.3	6 R4	1.40
366	D	0.4	10.3	6 RO	0.65
367	D	0.4	10.3	12 RO	0.26
368	D	0.4	10.3	12 RO	0.26
369	D	0.4			
370					

Note: Samples 333 through 341 with No. 7 glass beads; the bed did not appear fluidized with these beads, and samples were discontinued.

Sample No.:	Solids:	u_0 (ft./sec.):	C_0 (%):	Position:		c/c_0
371	D	0.4	10.3	12	R0	0.26
372	D	0.4	10.3	12	R1	0.28
373	D	0.4	10.3	12	R2	0.59
374	D	0.4	10.3	12	R3	0.77
375	D	0.4	10.3	12	R4	0.52
376	D	0.4	10.3	12	P4	0.51
377	D	0.4	10.3	12	R3	0.36 d
378	D	0.4	10.3	12	R3	0.49 d
379	D	0.4	10.3	12	R2	0.45 d
380	D	0.4	10.3	12	R2	0.38 d
380 A	D	0.4	10.3	12	R2	0.31 d
381	D	0.4	10.3	12	R2	0.40
382	D	0.4	10.3	12	R0	0.37 d
383	D	0.4	10.3	12	R0	0.25 d
384	D	0.4	10.3	12	R0	0.36 d
385	D	0.6	7.4	-11	R0	1.09
386	D	0.6	7.4	-11	R0	1.06
387	D	0.6	7.4	-11	R0	1.07
388	D	0.6	7.4	-11	R1	1.06
389	D	0.6	7.4	-11	R2	1.10
390	D	0.6	7.4	-11	R3	1.06
391	D	0.6	7.4	-11	R4	1.04
392	D	0.6	7.4	top		
393	D	0.6	7.4	4	R0	0.82
394	D	0.6	7.4	6	R0	0.60
395	D	0.6	7.4	6	R1	0.63
396	D	0.6	7.4	6	R2	0.81
397	D	0.6	7.4	6	R3	0.79
398	D	0.6	7.4	6	R4	0.84
399	D	0.6	7.4	8	R0	0.50
400	D	0.6	7.4	10	R0	0.29
401	D	0.6	7.4	12	R0	0.22
402	D	0.6	7.4	12	R1	0.27
403	D	0.6	7.4	12	R2	0.44
404	D	0.6	7.4	12	R3	0.50
405	D	0.6	7.4	12	R4	0.47
406	D	0.6	7.4	14	R0	0.146
407	D	0.6	7.4	16	R0	0.134
408	D	0.6	7.4	12	R4	0.38

Note: Samples marked "d" were taken directly into the analyzing cell and did not give steady readings; for this reason they must be considered unreliable.

Sample No.:	Solids:	u_0 (ft./sec.):	C_0 (%):	Position:	C/C_0
409	D	0.9	5.45	-11 R0	1.04
410	D	0.9	5.45	-11 R1	1.07
411	D	0.9	5.45	-11 R2	1.02
412	D	0.9	5.45	-11 R3	1.07
413	D	0.9	5.45	-11 R4	1.02
414	D	0.9	5.45	top	
415	D	0.9	5.45	4 R0	0.51
416	D	0.9	5.45	8 R0	0.35
417	D	0.9	5.45	10 R0	0.33
418	D	0.9	5.45	12 R0	0.21
419	D	0.9	5.45	14 R0	0.162
420	D	0.9	5.45	16 R0	0.12
421	D	0.9	5.45	18 R0	0.088
422	D	0.9	5.45	top	
423	D	0.9	4.8	6 R0	0.43
424	D	0.9	4.8	6 R1	0.43
425	D	0.9	4.8	6 R2	0.70
426	D	0.9	4.8	6 R3	0.75
427	D	0.9	4.8	6 R4	0.73
428	D	0.9	4.8	top	
429	D	0.9	4.8	12 R0	0.26
430	D	0.9	4.8	12 R1	0.22
431	D	0.9	4.8	12 R2	0.37
432	D	0.9	4.8	12 R3	0.42
433	D	0.9	4.8	12 R4	0.36
434	D	0.9	4.8	12 R1	0.183
435	D	0.9	4.8	12 R1	0.29
436	D	0.9	4.8	top	
437	D	1.2	3.6	12 R0	0.149
438	D	1.2	3.6	12 R1	0.255
439	D	1.2	3.6	12 R2	0.24
440	D	1.2	3.6	12 R3	0.31
441	D	1.2	3.6	12 R4	0.46
442	D	1.2	3.6	12 R4	0.28
443	D	1.2	3.6	top	
444	D	1.2	3.6	-11 R0	1.08
445	D	1.2	3.6	-11 R1	1.05
446	D	1.2	3.6	-11 R2	1.09
447	D	1.2	3.6	-11 R3	1.03
448	D	1.2	3.6	-11 R4	1.08
449	D	1.2	3.6	4 R0	0.42
450	D	1.2	3.6	6 R0	0.34
451	D	1.2	3.6	6 R1	0.45
452	D	1.2	3.6	6 R2	0.46

Sample No.:	Solids:	u_0 (ft./sec.):	C_0 (%):	Position:	C/C_0
453	D	1.2	3.6	6 R3	0.61
454	D	1.2	3.6	6 R4	0.71
455	D	1.2	3.6	8 RO	0.295
456	D	1.2	3.6	10 RO	0.24
457	D	1.2	3.6	12 RO	0.27
458	D	1.2	3.6	12 RO	0.156
459	D	1.2	3.6	12 RO	0.170
460	D	1.2	3.6	12 R1	0.187
461	D	1.2	3.6	12 R2	0.30
462	D	1.2	3.6	12 R3	0.34
463	D	1.2	3.6	12 R4	0.38
464	D	1.2	3.6	14 RO	0.147
465	D	1.2	3.6	16 RO	0.110
466	D	1.2	3.6	top	
467	D	0.6	8.0	top	
468	D	0.6	8.0	16 RO	0.20
469	D	0.6	8.0	14 RO	0.20
470	D	0.6	8.0	12 RO	0.20
471	D	0.6	8.0	12 RO	0.27
472	D	0.6	8.0	10 RO	0.30
473	D	0.6	8.0	8 RO	0.345
474	D	0.6	8.0	6 RO	0.45
475	D	0.6	8.0	4 RO	0.63
476					
477	D	0.6	8.0	16 RO	0.157
478	D	0.6	8.0	18 RO	0.127
479	D	0.6	8.0	4 RO	0.69
480	D	0.6	8.0	6 RO	0.46
481	D	0.6	8.0	8 RO	0.44
482	D	0.6	8.0	10 RO	0.325
483	D	0.6	8.0	10 RO	0.44 ▽
484	D	0.6	8.0	10 RO	0.15 ▽
485	D	0.6	8.0	10 RO	0.10 ▽
486	D	0.6	8.0	10 RO	0.10
487	E	0.4	10.8	-11 RO	1.01
488	E	0.4	10.8	-11 R1	1.05
489	E	0.4	10.8	-11 R2	1.06
490	E	0.4	10.8	-11 R3	1.10
491	E	0.4	10.8	-11 R4	1.04
492	E	0.4	10.8	-11 R4	1.07
493	E	0.4	10.8	top	
494	E	0.4	10.8	10 RO	0 ▽
495	E	0.4	10.8	10 RO	0
496	E	0.4	10.8	6 RO	0.16
497	E	0.4	10.8	6 RO	0.14 ▽
498	E	0.4	10.8	6 RO	0.11 ▽

Sample No.:	Solids:	u_o (ft./sec.):	C_o (%):	Position:	C/C_o
499	E	0.4	10.8	6 RO	0.12
500	E	0.4	10.8	top	
501	E	0.4	10.8	6 RO	0.18
502	E	0.4	10.8	6 RO	0.16 s
503	E	0.4	10.8	5 RO	0.17
504	E	0.4	10.8	4 RO	0.66
505	E	0.4	10.8	4 RO	0.38
506	E	0.4	10.8	4 RO	0.40
507	E	0.4	10.8	5 RO	0.13
508	E	0.4	10.8	5 RO	0.25
509	E	0.4	10.8	7 RO	0.13
510	E	0.4	10.8	7 RO	0.13
511	E	0.4	10.8	8 RO	0.063
512	E	0.4	10.8	8 RO	0.067
513	E	0.4	10.8	8 RO	0.065
514	E	0.4	10.8	6 RO	0.11
515	E	0.4	10.8	6 RO	0.057
516	E	0.4	10.8	6 RO	0.12
517	E	0.4	10.8	6 RO	0.14
518	E	0.4	10.8	5 RO	0.14
519	E	0.4	10.8	4 RO	0.35
520	E	0.4	10.8	5 RO	0.36
521	E	0.4	10.8	6 RO	0.19
522	E	0.4	10.8	7 RO	0.10
523	E	0.4	10.8	8 RO	0.069
524	E	0.4	10.8	top	
525	E	0.6	8.3	-11 RO	1.01
526	E	0.6	8.3	-11 R1	1.00
527	E	0.6	8.3	-11 R2	1.03
528	E	0.6	8.3	-11 R3	1.09
529	E	0.6	8.3	-11 R4	1.12
530	E	0.6	8.3	top	
531	E	0.6	8.3	4 RO	0.55
532	E	0.6	8.3	5 RO	0.44
533	E	0.6	8.3	6 RO	0.26
534	E	0.6	8.3	7 RO	0.23
535	E	0.6	8.3	8 RO	0.19
536	E	0.6	8.3	9 RO	0.15
537	E	0.6	8.3	10 RO	0.094
538	E	0.6	8.3	4 RO	0.59
539	E	0.6	8.3	5 RO	0.47
540	E	0.6	8.3	6 RO	0.34
541	E	0.6	8.3	7 RO	0.25
542	E	0.6	8.3	8 RO	0.17
543	E	0.6	8.3	10 RO	0.13

Sample No:	Solids:	u_0 (ft./sec.):	C_0 (%):	Position:	C/C_0
544	E	0.9	5.8	-11 RO	1.10
545	E	0.9	5.8	- 11 R1	1.12
546	E	0.9	5.8	-11 R2	1.18
547	E	0.9	5.8	-11 R3	1.12
548	E	0.9	5.8	-11 R4	1.16
549	E	0.9	5.8	top	
550	E	0.9	5.8	6 RO	0.46 d
551	E	0.9	5.8	6 RO	0.37 d
552	E	0.9	5.8	6 RO	0.36 d
553	E	0.9	5.8	6 RO	0.30 d
554	E	0.9	5.8	6 RO	0.176 v
555	E	0.9	5.8	6 RO	0.26 v
556	E	0.9	5.8	6 RO	0.43
557	E	0.9	5.8	4 RO	0.60
558	E	0.9	5.8	5 RO	0.50
559	E	0.9	5.8	7 RO	0.33
560	E	0.9	5.8	8 RO	0.38
561	E	0.9	5.8	9 RO	0.27
562	E	0.9	5.8	10 RO	0.20
563	E	0.9	5.8	8 RO	0.30
564	E	0.9	5.8	12 RO	0.074
565	E	1.2	4.5	12 RO	0.23
566	E	1.2	4.5	10 RO	0.29
567	E	1.2	4.5	8 RO	0.34
568	E	1.2	4.5	6 RO	0.41
569	E	1.2	4.5	4 RO	0.50
570	E	1.2	4.5	14 RO	0.099
571	E	1.2	4.5	8 RO	0.30 v
572	E	1.2	4.5	8 RO	0.24 v
573	E	1.2	4.5	8 RO	0.32 s
574	E	1.2	4.5	-11 RO	1.13
575	E	1.2	4.5	-11 R1	1.16
576	E	1.2	4.5	-11 R2	1.21
577.	E	1.2	4.5	-11 R3	1.27
578	E	1.2	4.5	-11 R4	1.18
579	E	1.2	4.5	top	
580	E				
580	F	0.4	10.6	-11 RO	1.01
581	F	0.4	10.6	-11 R1	1.04
582	F	0.4	10.6	-11 R2	1.075
583	F	0.4	10.6	-11 R3	1.07
584	F	0.4	10.6	-11 R4	1.03
585	F	0.4	10.6	top	
586	F	0.4	10.6	4 RO	0.84
587	F	0.4	10.6	6 RO	0.725
588	F	0.4	10.6	8 RO	0.505
589	F	0.4	10.6	10 RO	0.43
590	F	0.4	10.6	12 RO	0.31
591	F	0.4	10.6	14 RO	0.26

Sample No.:	Solids:	u_0 (ft./sec.):	C_0 (%):	Position:		C/C_0
592	F	0.4	10.6	16	RO	0.245
593	F	0.4	10.6	18	RO	0.177
594	F	0.6	7.3	-11	RO	1.065
595	F	0.6	7.3	-11	R1	1.015
596	F	0.6	7.3	-11	R2	1.045
597	F	0.6	7.3	-11	R3	1.025
598	F	0.6	7.3	-11	R4	1.035
599	F	0.6	7.3	top		
600	F	0.6	7.3	4	RO	0.68
601	F	0.6	7.3	6	RO	0.545
602	F	0.6	7.3	8	RO	0.50
603	F	0.6	7.3	10	RO	0.33
604	F	0.6	7.3	12	RO	0.37
605	F	0.6	7.3	14	RO	0.22
606	F	0.6	7.3	16	RO	0.23
607	F	0.6	7.3	18	RO	0.167
608	F	0.9	5.1	-11	RO	1.05
609	F	0.9	5.1	-11	R1	1.10
610	F	0.9	5.1	-11	R2	1.08
611	F	0.9	5.1	-11	R3	1.05
612	F	0.9	5.1	-11	R4	1.03
613	F	0.9	5.1	top		
614	F	0.9	5.1	4	RO	0.63
615	F	0.9	5.1	6	RO	0.47
616	F	0.9	5.1	8	RO	0.38
617	F	0.9	5.1	10	RO	0.31
618	F	0.9	5.1	12	RO	0.25
619	F	0.9	5.1	14	RO	0.18
620	F	0.9	5.1	16	RO	0.16
621	F	0.9	5.1	18	RO	0.15
622	F	1.2	3.8	-11	RO	1.05
623	F	1.2	3.8	-11	R1	1.04
624	F	1.2	3.8	-11	R2	1.08
625	F	1.2	3.8	-11	R3	1.08
626	F	1.2	3.8	-11	R4	1.08
627	F	1.2	3.8	top		
628	F	1.2	3.8	4	RO	0.58
629	F	1.2	3.8	6	RO	0.465
630	F	1.2	3.8	8	RO	0.345
631	F	1.2	3.8	10	RO	0.345
632	F	1.2	3.8	12	RO	0.265
633	F	1.2	3.8	14	RO	0.195
634	F	1.2	3.8	16	RO	0.16
635	F	1.2	3.8	18	RO	0.12
636	F	1.2	3.8	18	RO	0.12

Sample No.: Solids: u_0 (ft./sec.): C_0 (%): Position: C/C_0

637 Sample No. 637 through 713 were taken with microspheres fines only, but it was afterwards found the sample tube has been leaking - ie. drawing air - and so all of these samples were discarded and the runs repeated.

714	F	0.9	5.0	4	RO	0.56
715	F	0.9	5.0	6	RO	0.52
716	F	0.9	5.0	8	RO	0.356
717	F	0.9	5.0	10	RO	0.30
718	F	0.9	5.0	14	RO	0.184
719	F	0.9	5.0	top		
720	F	0.9	7.3	14	RO	0.23
721	F	0.9	7.3	16	RO	0.153
722	F	0.9	7.3	12	RO	0.24
723	F	0.9	7.3	10 _n	RO	0.32
724	F	0.9	7.3	8	RO	0.335
725	F	0.9	7.3	6	RO	0.41
726	F	0.9	7.3	4	RO	0.45
727	F	0.9	7.3	6	RO	0.44
728	F	0.9	7.3	8	RO	0.36
729	F	0.9	7.3	10	RO	0.264
730	F	0.9	7.3	12	RO	0.21
731	F	0.9	7.3	14	RO	0.195
732	F	0.9	7.3	16	RO	0.165
733	F	0.9	7.3	18	RO	0.087
734	F	0.9	7.3	top		
735	F	0.9	3.5	4	RO	0.52
736	F	0.9	3.5	6	RO	0.42
737	F	0.9	3.5	8	RO	0.38
738	F	0.9	3.5	10	RO	0.34
739	F	0.9	3.5	12	RO	0.23
740	F	0.9	3.5	14	RO	0.205
741	F	0.9	3.5	4	RO	0.59
742	F	0.9	3.5	6	RO	0.42
743	F	0.9	3.5	8	RO	0.40
744	F	0.9	3.5	10	RO	0.305
745	F	0.9	3.5	top		
746	F	0.9	10.1	8	RO	0.29
747	F	0.9	10.1	8	RO	0.28
748	F	0.9	10.1	14	RO	0.155
749	F	0.9	10.1	14	RO	0.18
750	F	0.9	10.1	top		

Sample No.:	Solids:	u_0 (ft./sec.):	C_0 (%):	Position:	c/c_0
751	G	0.4	10.5	-11 RO	0.98
752	G	0.4	10.6	-11 R2	0.97
753	G	0.4	10.6	-11 R3	0.97
754	G	0.4	10.6	top	
755	G	0.4	10.6	4 RO	0.29
756	G	0.4	10.6	5 RO	0.24
757	G	0.4	10.6	6 RO	0.172
758	G	0.4	10.6	7 RO	0.171
759	G	0.4	10.6	8 RO	0.127
760	G	0.4	10.6	9 RO	0.104
761	G	0.4	10.6	10 RO	0.086
762	G	0.6	6.9	4 RO	0.23
763	G	0.6	6.9	5 RO	0.195
764	G	0.6	6.9	6 RO	0.14
765	G	0.6	6.9	7 RO	0.12
766	G	0.6	6.9	8 RO	0.105
767	G	0.6	6.9	9 RO	0.084
768	G	0.6	6.9	top	
769	G	0.9	7.65	9 RO	0.082
770	G	0.9	7.65	4 RO	0.25
771	G	0.9	7.65	5 RO	0.20
772	G	0.9	7.65	6 RO	0.144
773	G	0.9	7.65	7 RO	0.115
774	G	0.9	7.65	8 RO	0.088
775	G	0.9	7.65	4 RO	0.22
776	G	0.9	7.65	5 RO	0.193
777	G	0.9	7.65	6 RO	0.137
778	G	0.9	7.65	7 RO	0.106
779	G	0.9	7.65	8 RO	0.085
780	G	0.9	7.65	9 RO	0.075
781	G	0.9	7.65	-11 RO	0.98
782	G	0.9	7.65	-11 R2	0.99
783	G	0.9	7.65	-11 R3	0.98
784	G	0.9	7.65	top	

Sample No:	Solids:	u_0 (ft./sec.):	C_0 (%):	Position:	C/C_0
785	F	0.6	7.3	top	
786	F	0.6	7.3	4 RO	0.66
787	F	0.6	7.3	4 RO	0.71
788	F	0.6	7.3	2 RO	0.74
789	F	0.6	7.3	1 RO	0.79
790	F	0.6	7.3	1 R1	1.12
791	F	0.6	7.3	1 R2	1.50
792	F	0.6	7.3	1 R4	1.89
793	F	0.6	7.3	1 -R1	0.92
794	F	0.6	7.3	1 -R2	1.09
795	F	0.6	7.3	1 -R3	1.49
796	F	0.6	7.3	1 -R4	1.60
797	F	0.6	7.3	12 RO	0.26
798	F	0.6	7.3	12 RO	0.33
799	F	0.6	7.3	12 RO	0.28
800	F	0.6	7.3	top	
801	F	0.6	7.6	top	
802	F	0.6	7.6	12 RO	0.37
803	F	0.6	7.6	12 RO	0.27
804	F	0.6	7.6	12 R1	0.38
805	F	0.6	7.6	12 R1	0.34
806	F	0.6	7.6	12 R2	0.435
807	F	0.6	7.6	12 R2	0.46
808	F	0.6	7.6	12 R3	0.45
809	F	0.6	7.6	12 R3	0.435
810	F	0.6	7.6	top	
811	F	0.6	7.6	12 R4	0.42
812	F	0.6	7.6	12 RO	0.27
813	F	0.6	7.6	6 RO	0.56
814	F	0.6	7.6	6 R1	0.66
815	F	0.6	7.6	6 R2	0.67
816	F	0.6	7.6	6 R3	0.69
817	F	0.6	7.6	6 R4	0.79
818	F	0.9	5.2	6 R4	0.73
819	F	0.9	5.2	6 R3	0.80
820	F	0.9	5.2	6 R2	0.63
821	F	0.9	5.2	6 R1	0.74
822	F	0.9	5.2	6 RO	0.60
823	F	0.9	5.2	6 R2	0.76

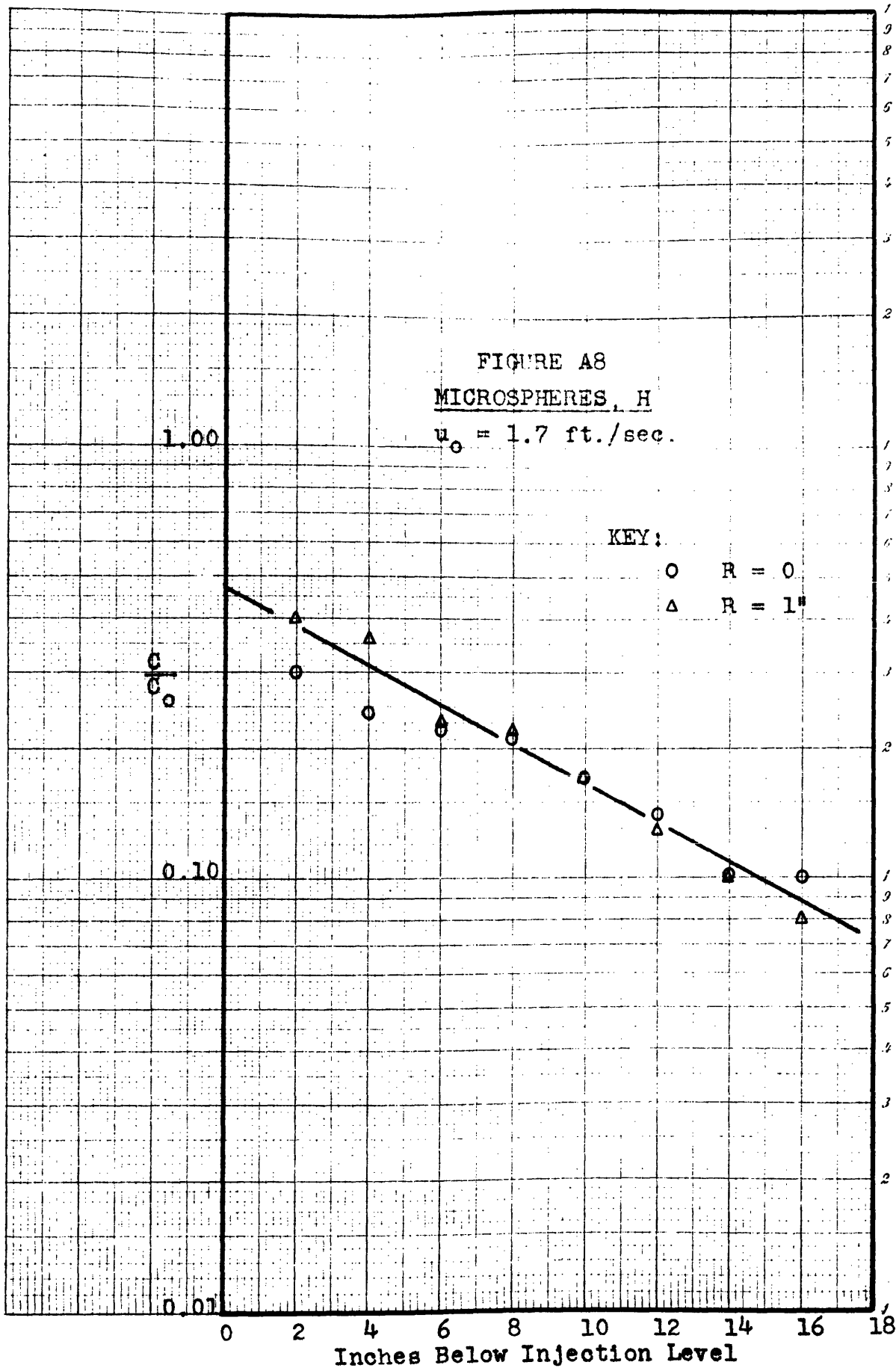
Solids:	u_0 (ft./sec.):	C_0 (%):	Position:	C/C_0
M2	0.4	11.2	-12 RO	1.10
M2	0.4	11.2	-12 1/4	1.13
M2	0.4	11.2	-12 3/4	1.10
M2	0.4	11.2	-12 1 1/4	1.09
M2	0.4	11.2	-12 1 3/4	1.09
M2	0.4	11.2	-12 2 1/4	1.12
M2	0.4	11.2	-12 -1 1/4	1.16
M2	0.4	11.2	3 -1 3/4	1.36
M2	0.4	11.2	3 -3/4	1.07
M2	0.4	11.2	3 RO	1.01
M2	0.4	11.2	3 1/4	1.04
M2	0.4	11.2	3 3/4	0.98
M2	0.4	11.2	3 1 1/4	1.15
M2	0.4	11.2	3 1 3/4	1.31
M2	0.4	11.2	3 2 1/4	1.31

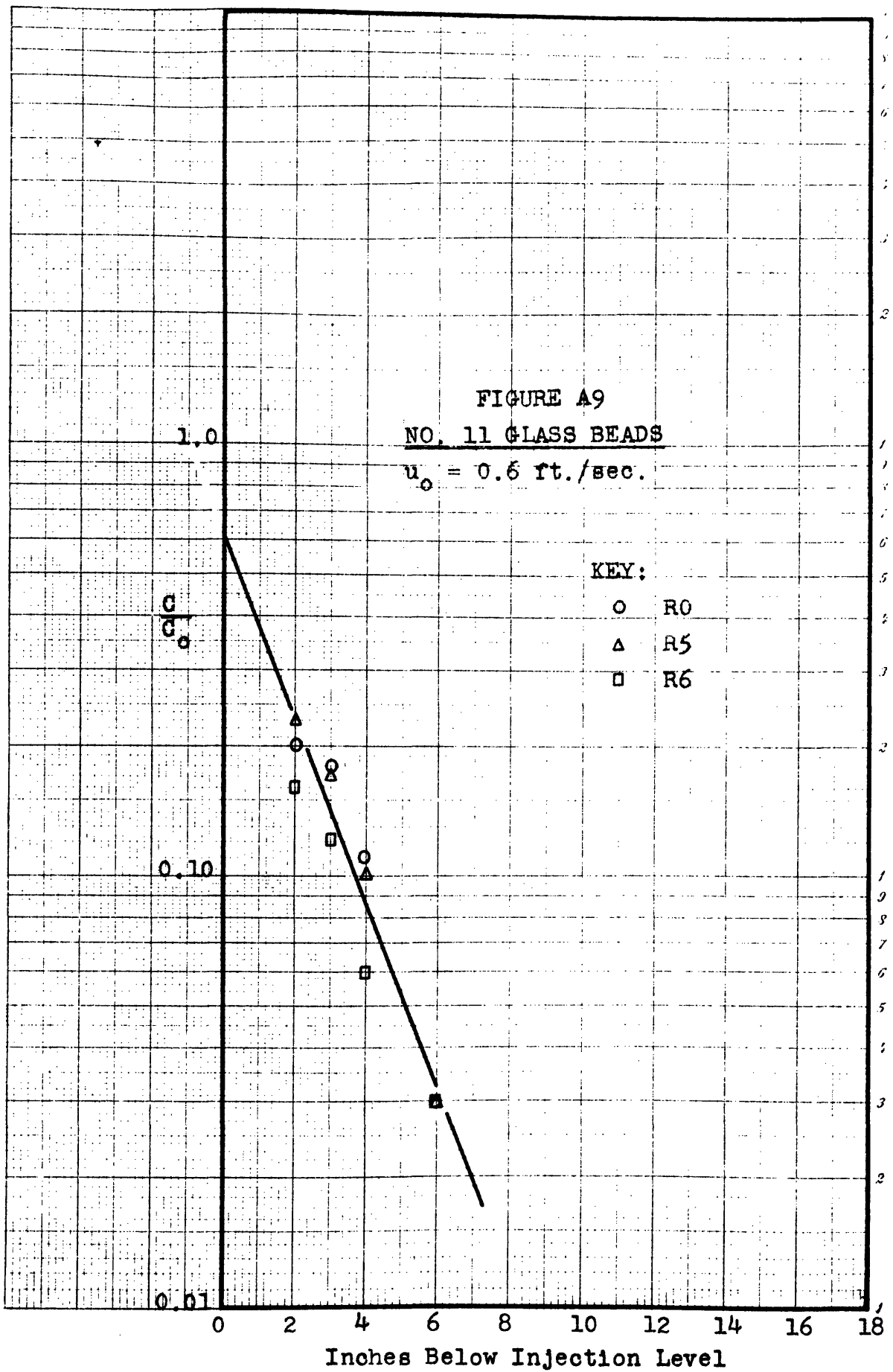
Note: These are the only steady state samples taken in the 4 1/2-inch column. All other samples listed in this table (preceding pages) were obtained in 3-inch column.

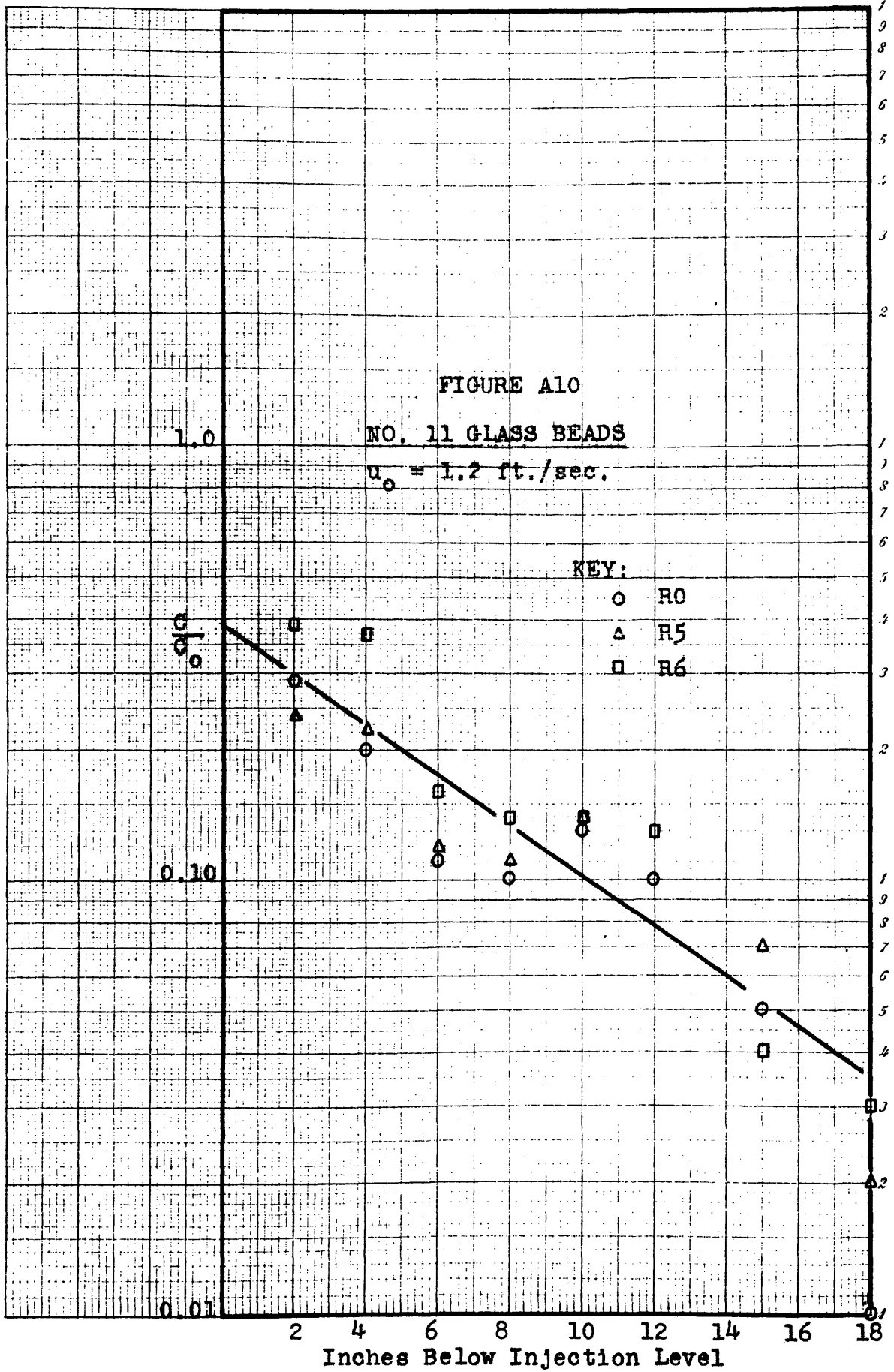
D. Summary of Data and Calculated Values (Cont'd.)

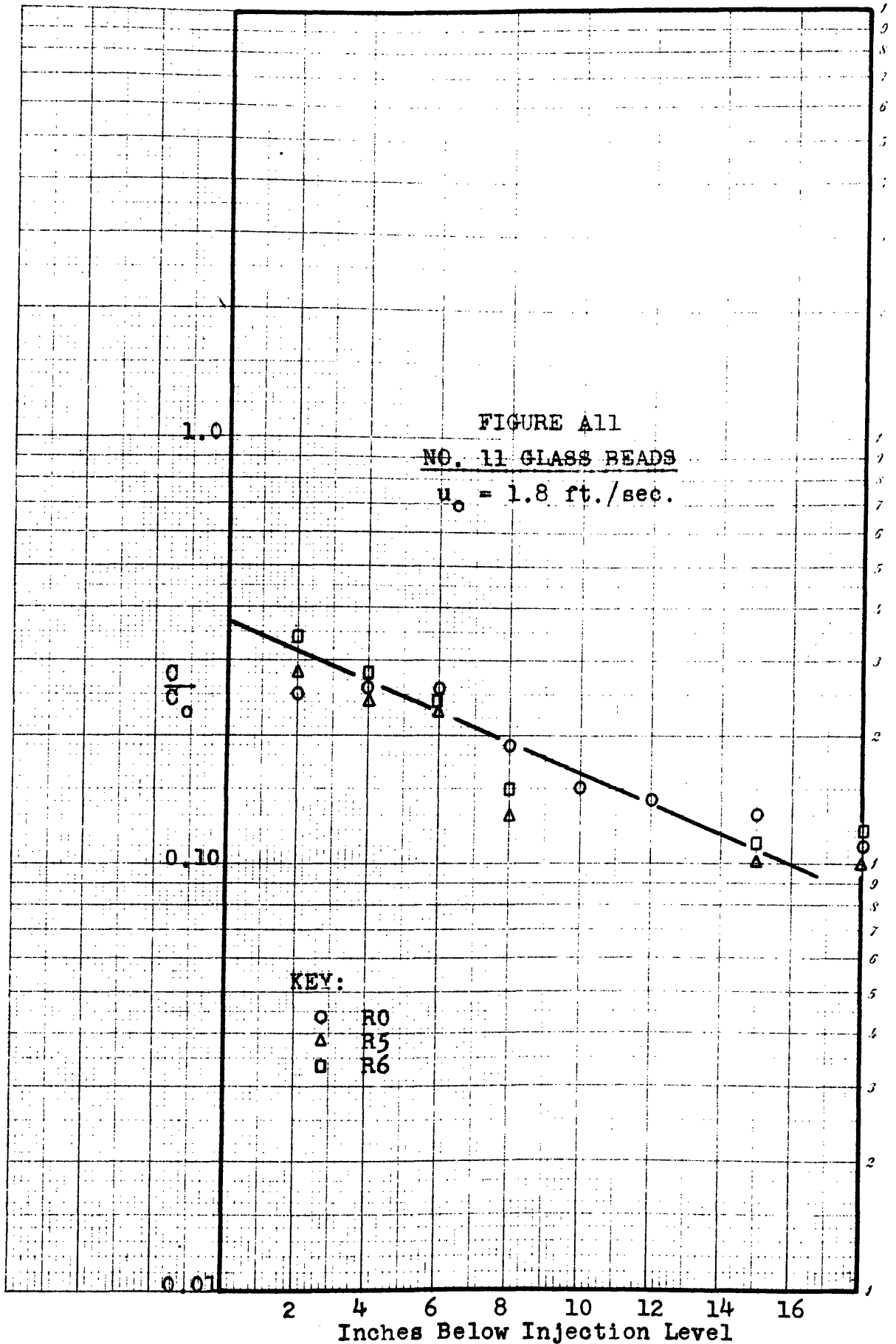
2. Back-Mixing Data - Semi-logarithmic Plots

Figures A8 through A12 made with single point injection. Figures A13 through A30 made with 12-point injection.









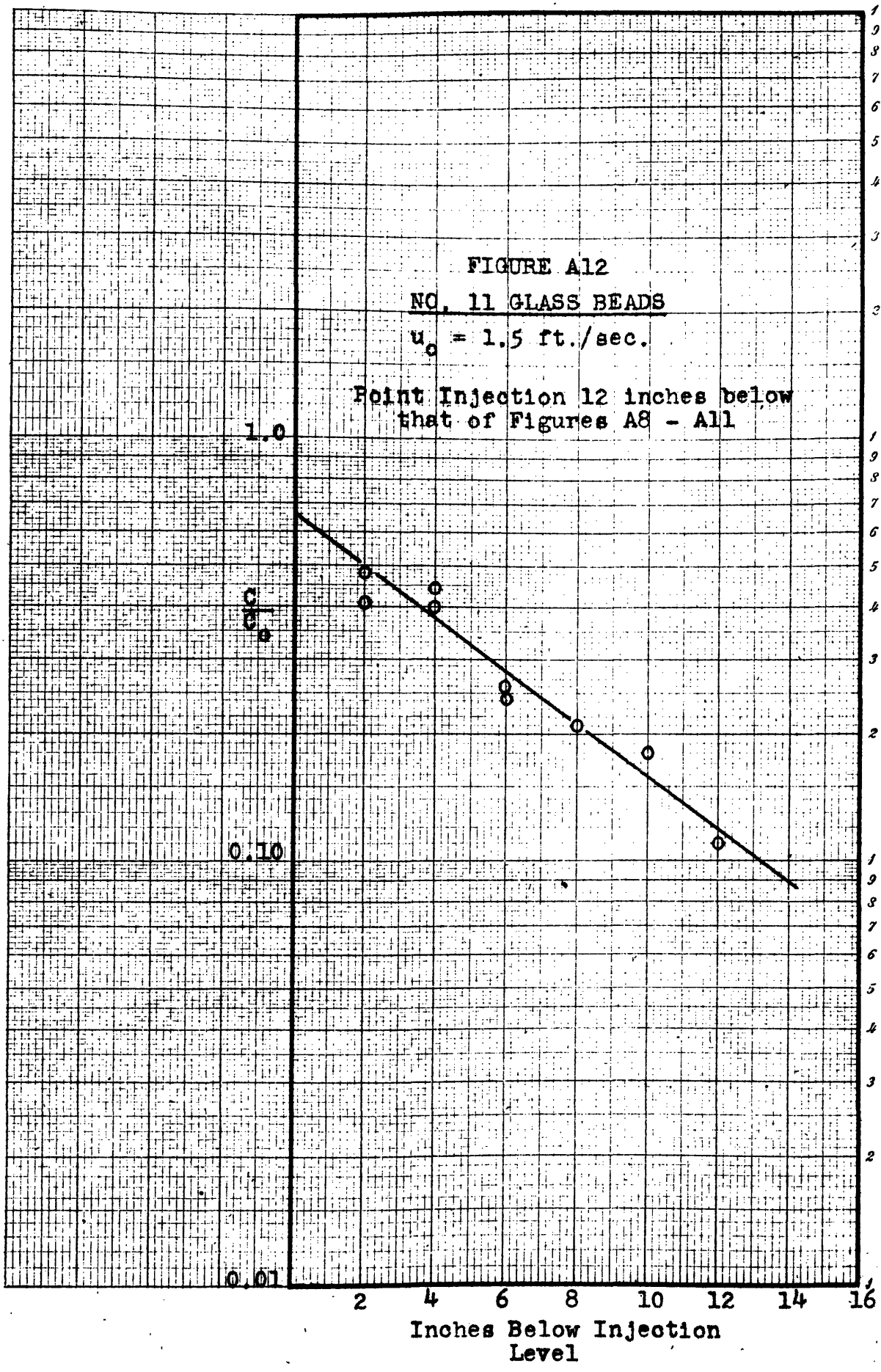


FIGURE A13

NO. 13 GLASS BEADS

KEY: ○ 0.4 FT./SEC.

△ 0.6 FT./SEC.

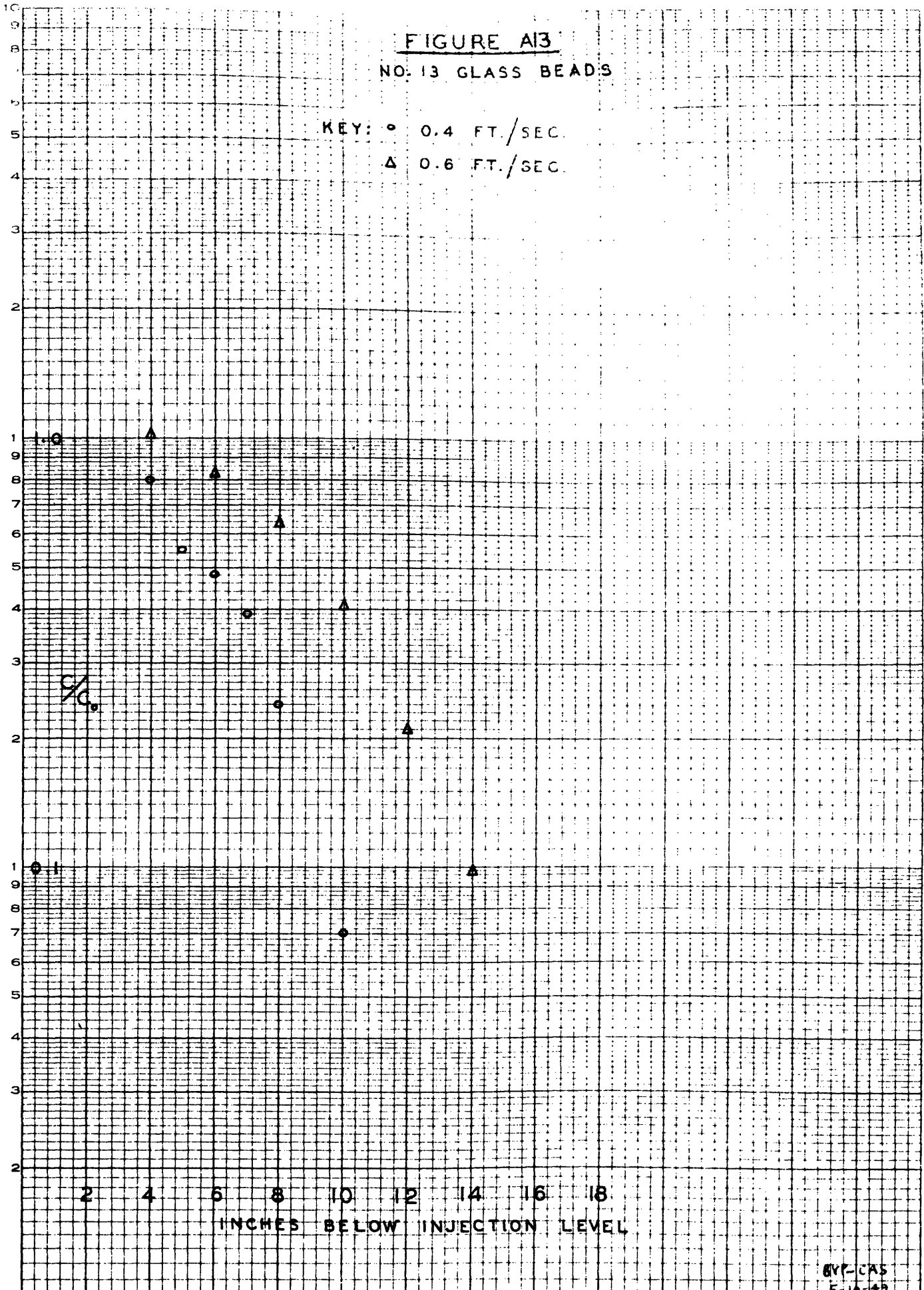


FIGURE A14

NO. 13 GLASS BEADS

KEY: □ 0.9 FT./SEC.
● 1.2 FT./SEC.

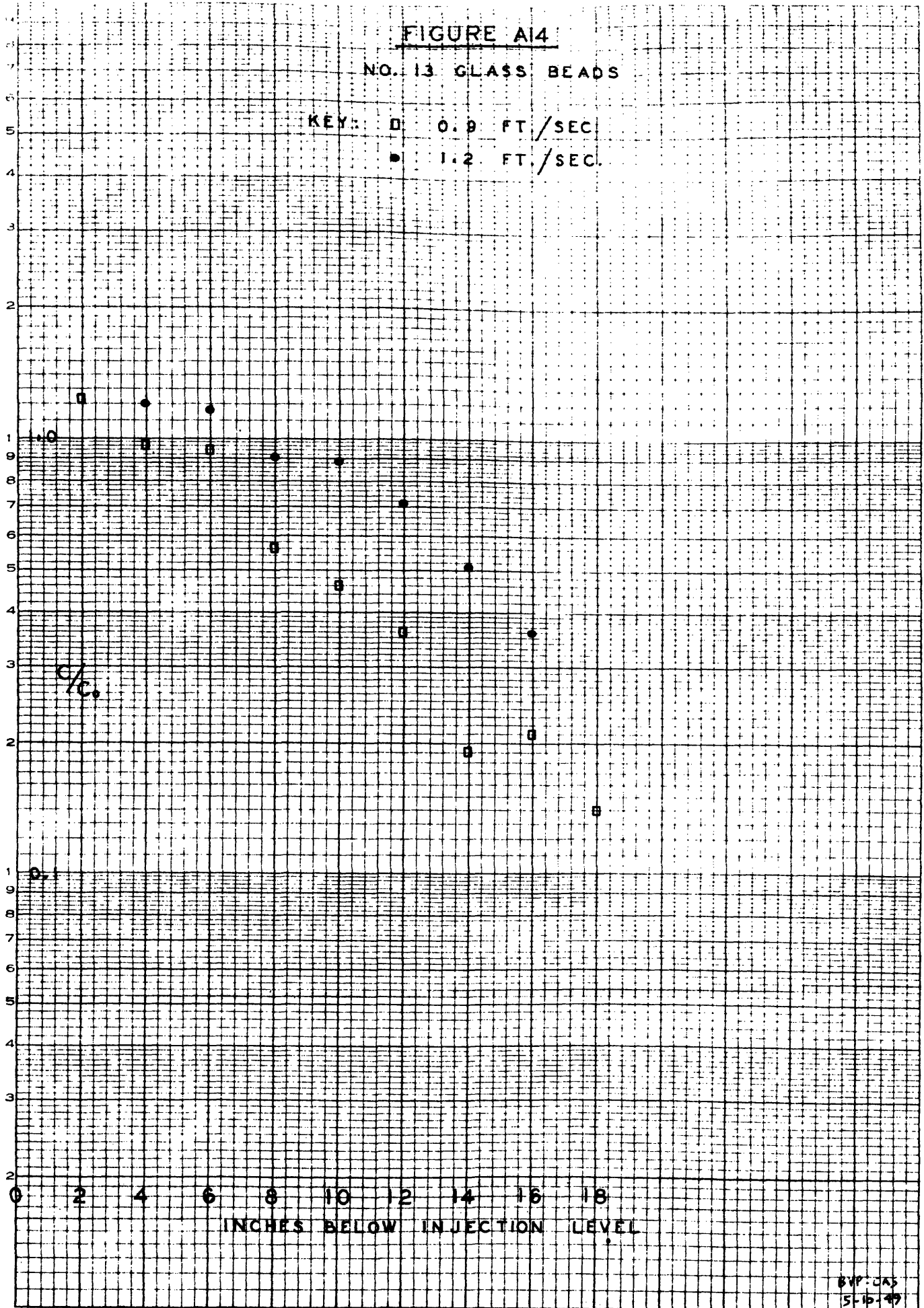
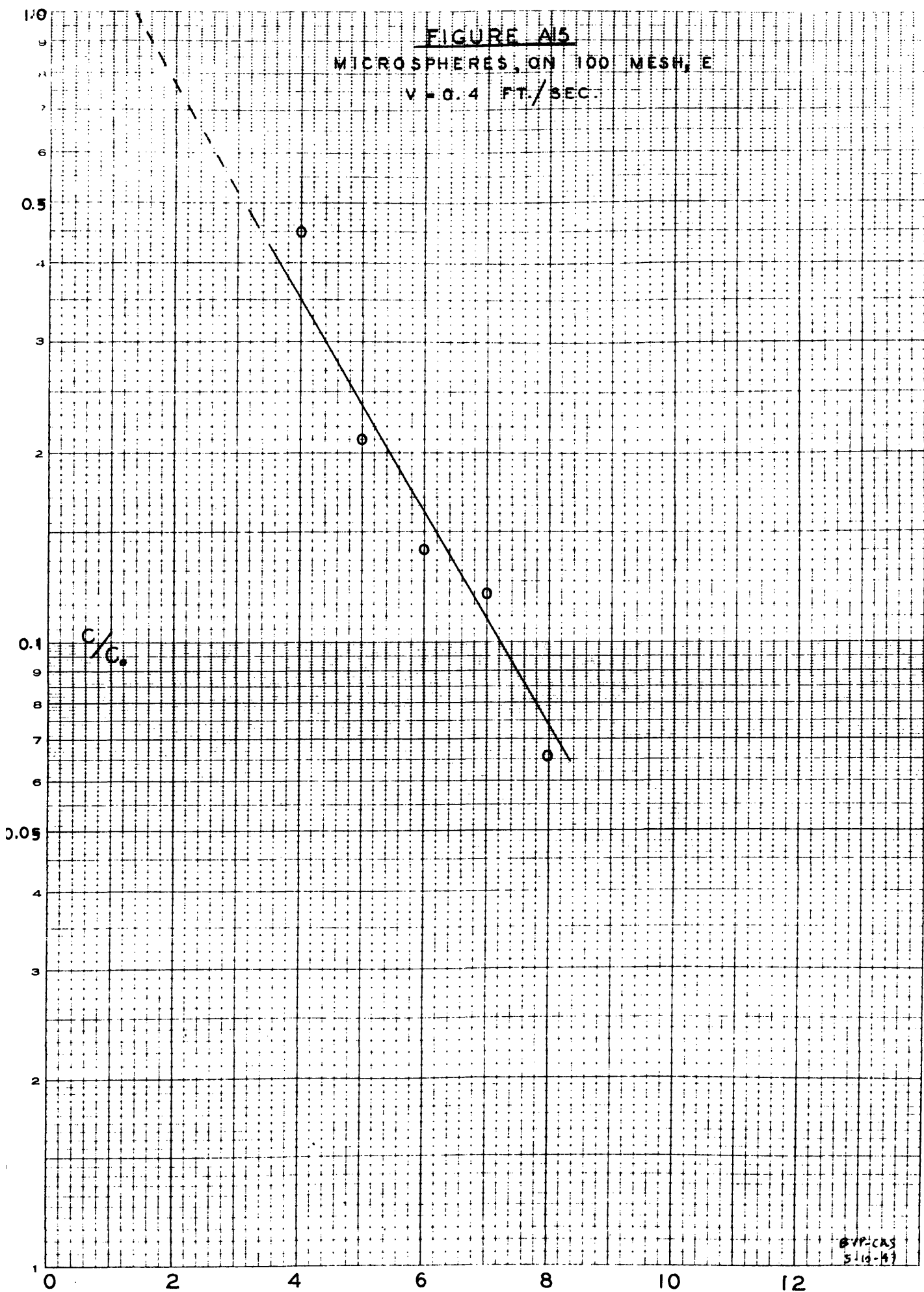


FIGURE A15

MICROSPHERES, ON 100 MESH, E

V = 0.4 FT./SEC.

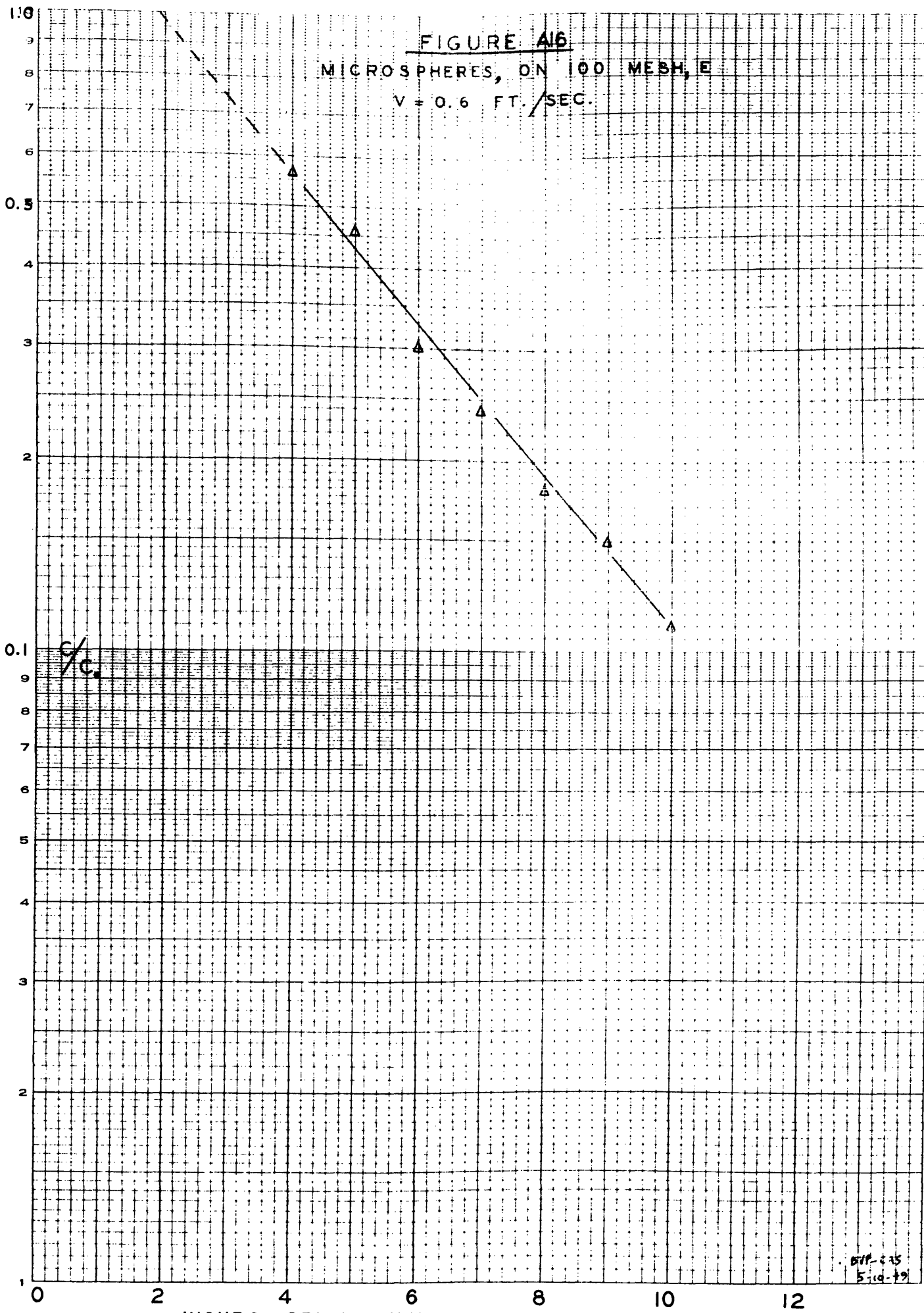


GVP: CAS
514-47

FIGURE A16

MICROSPHERES, ON 100 MESH, E

V = 0.6 FT./SEC.



511-235
5-10-79

FIGURE A7

MICROSPHERES, ON 100 MESH, E

V = 0.9 FT./SEC.

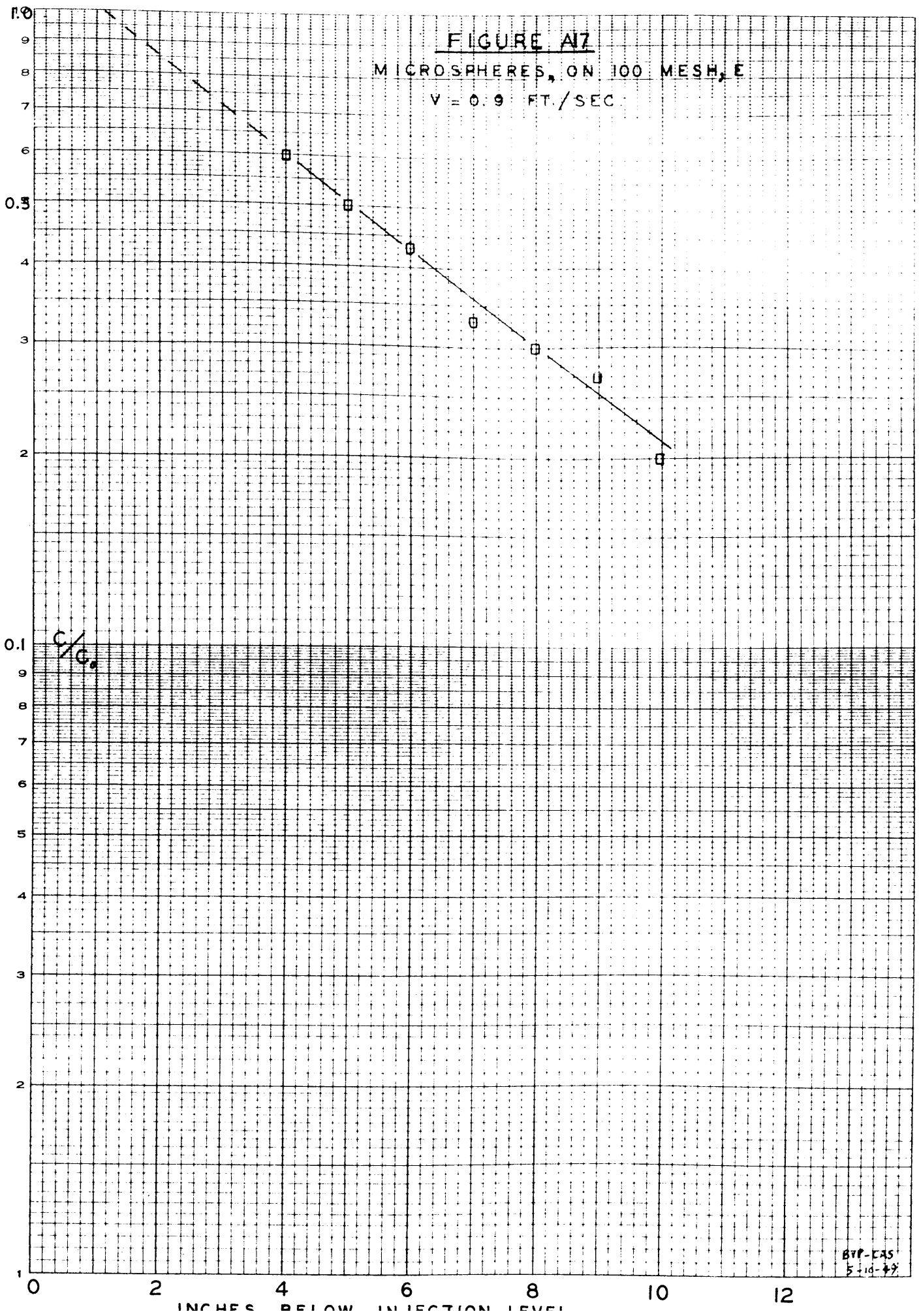


FIGURE A8

MICROSPHERES, ON 100 MESH, E

V = 1.2 FT/SEC.

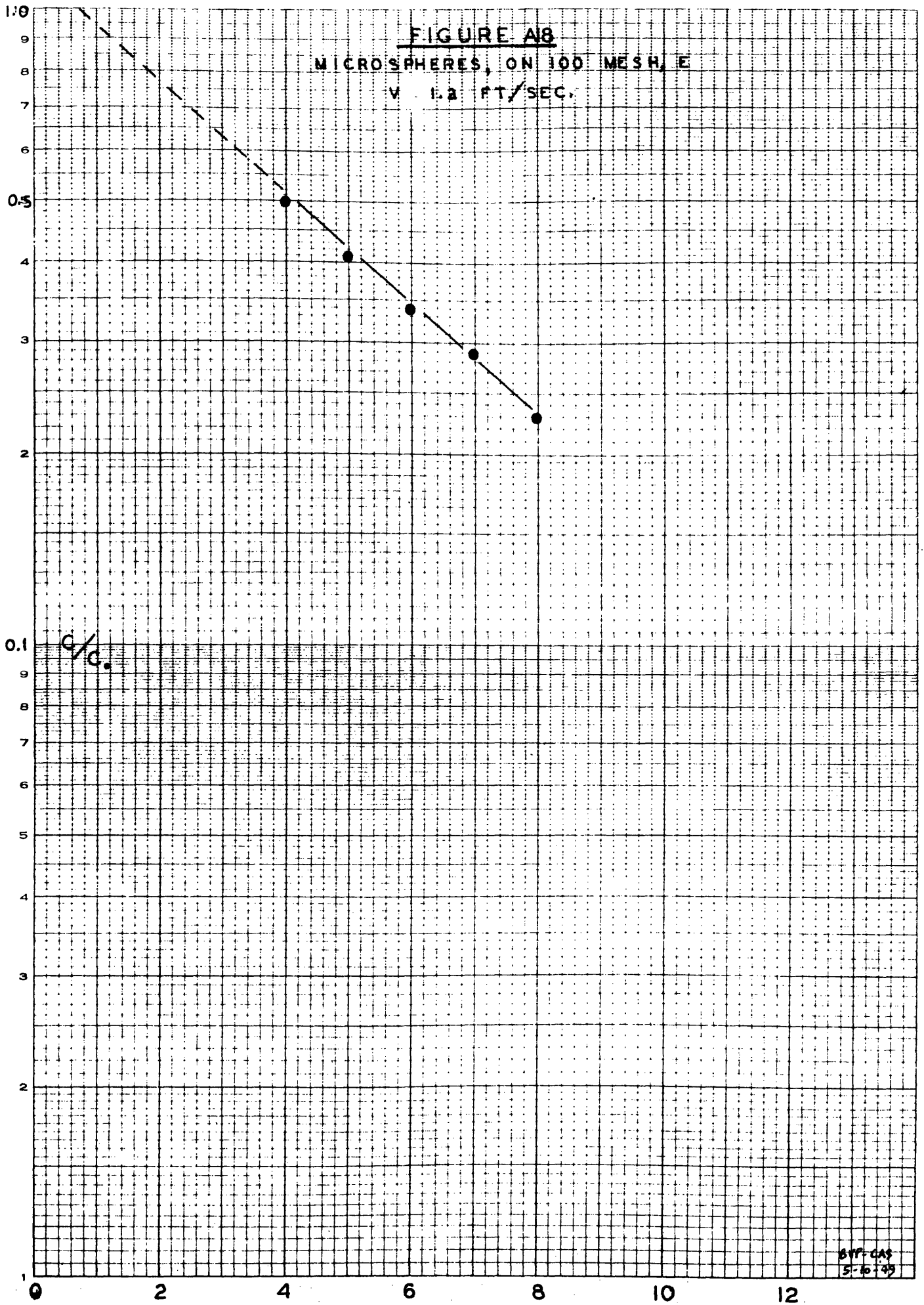


FIGURE A10
MICROSPHERES (LESS FINES), D
V = 0.4 FT./SEC.

(+ - SAMPLES AT R2)

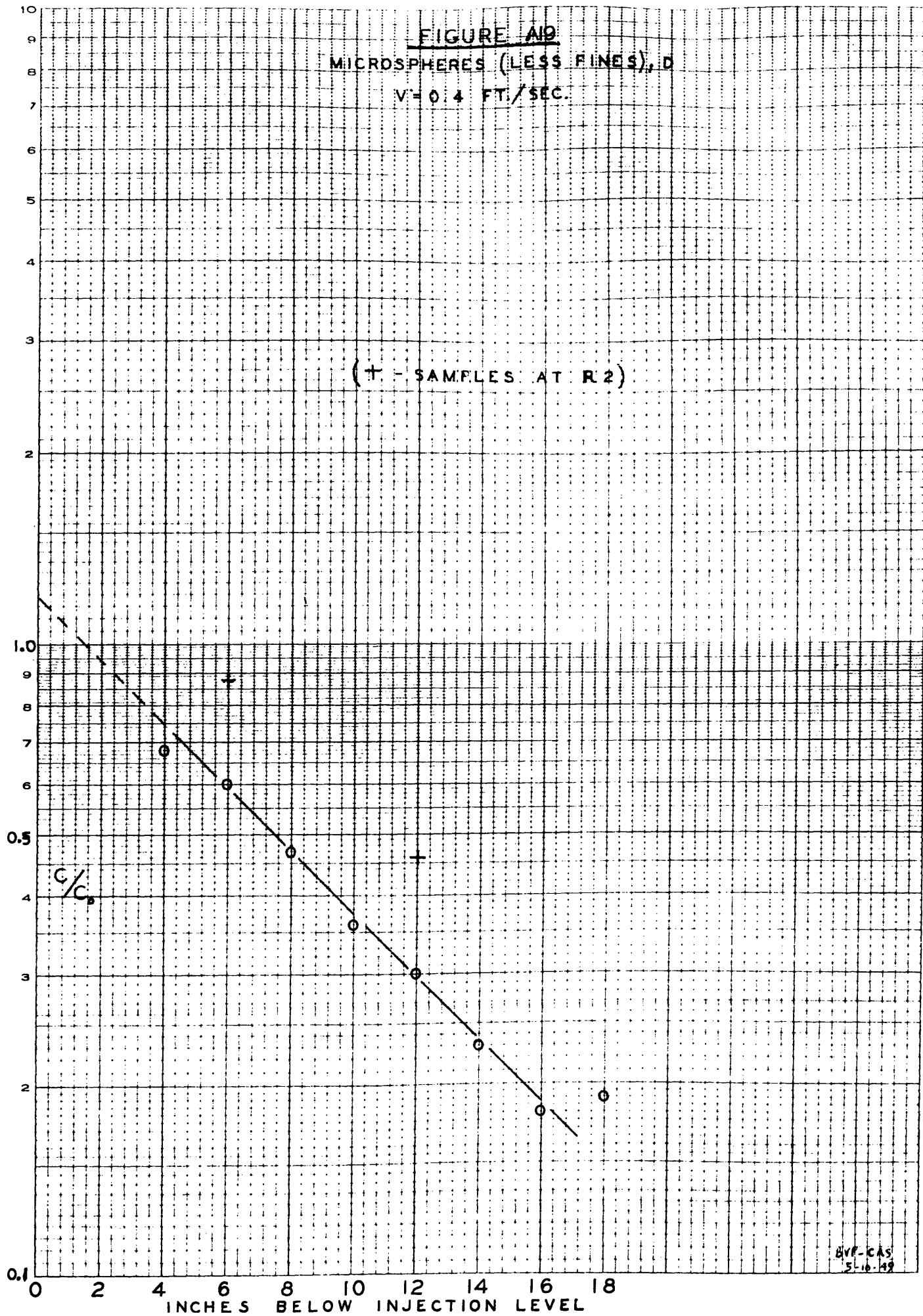


FIGURE A20
MICROSPHERES (LESS FINES), D
V = 0.6 FT./SEC.

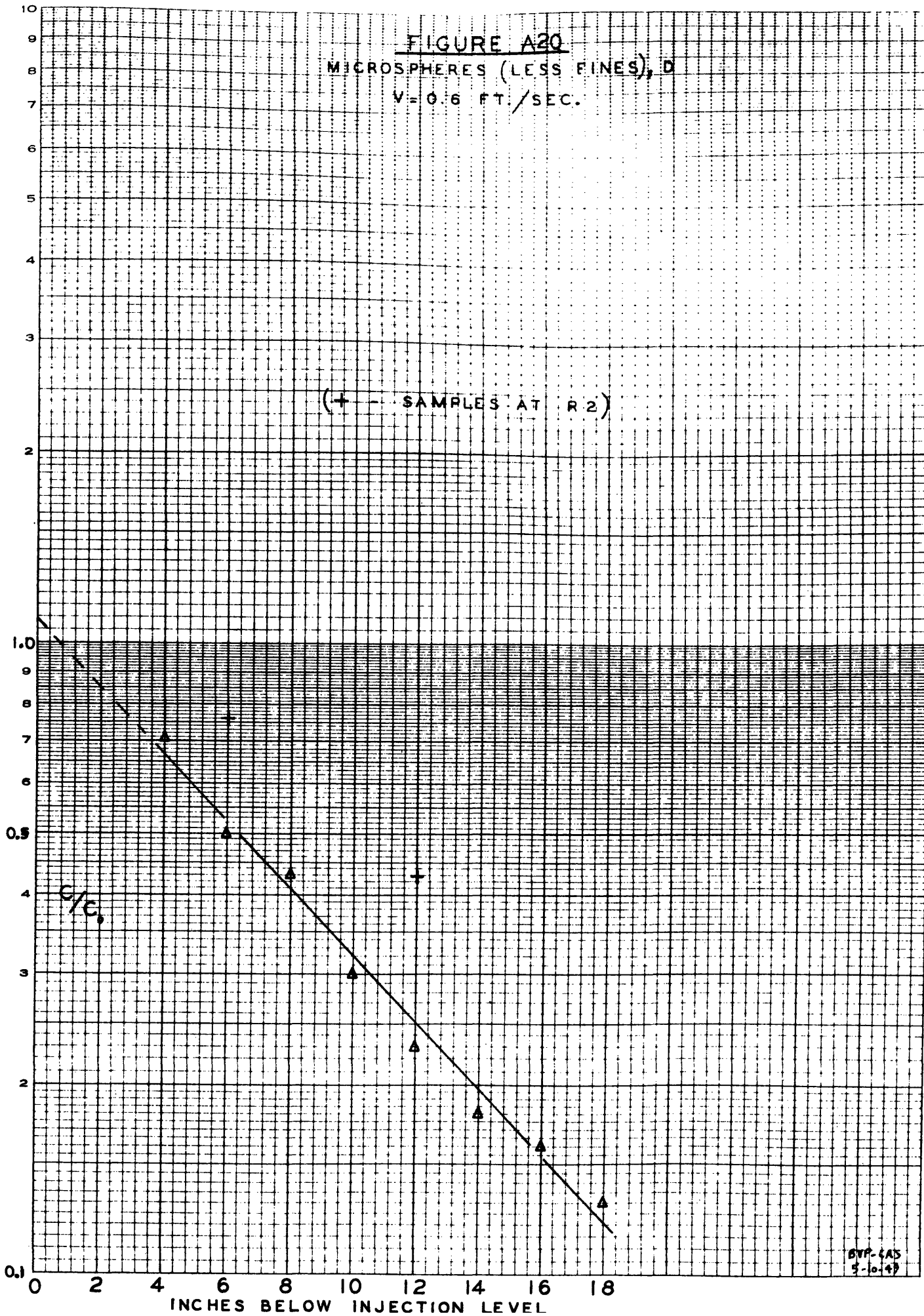


FIGURE A2
 MICROSPHERES (LESS FINES), ϕ

(+ - SAMPLES AT R2)

V = 0.9 FT./SEC.

+ V = 1.2 FT./SEC.

C/C_0

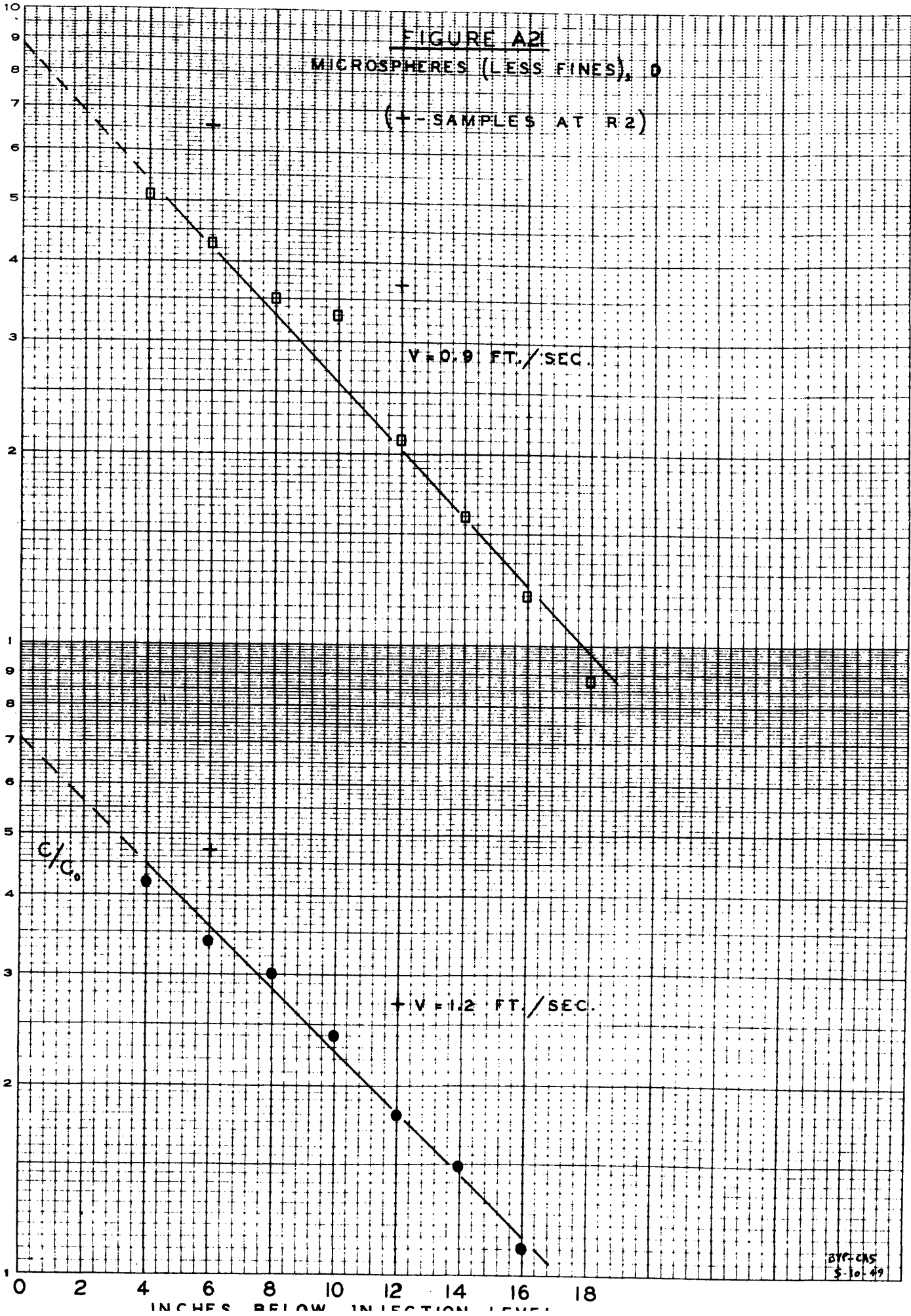


FIGURE A22
MICROSPHERES THROUGH 150 MESH (LESS FINES), F
V = 0.4 FT./SEC.

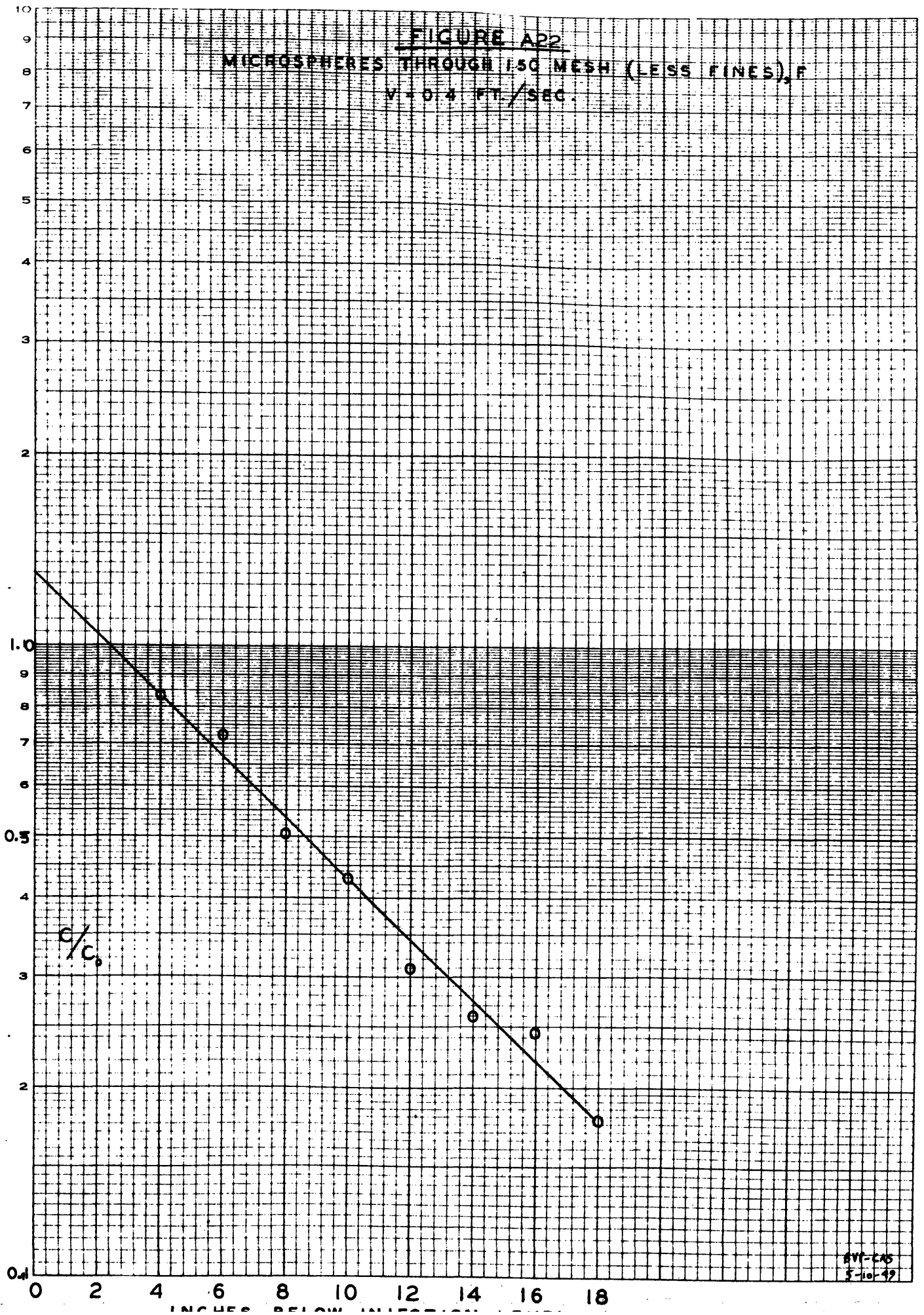


FIGURE A23

MICROSPHERES THROUGH 150 MESH (LESS FINES), P

V = 0.6 FT./SEC

▲ ADDITIONAL SAMPLES NOT USED FOR LINE

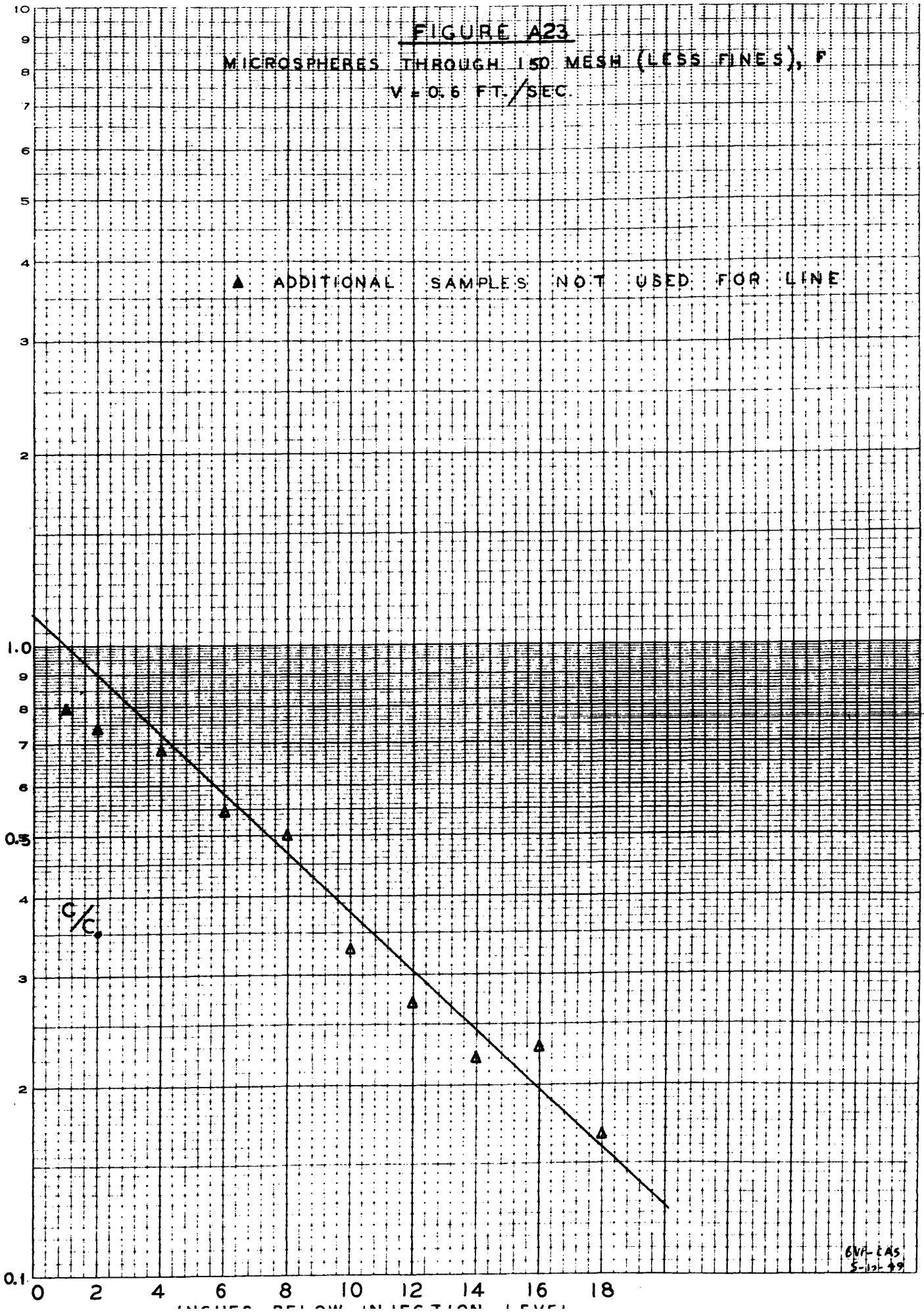


FIGURE A21

MICROSPHERES THROUGH 150 MESH (LESS FINES), F

$V = 0.9 \text{ FT/SEC}$

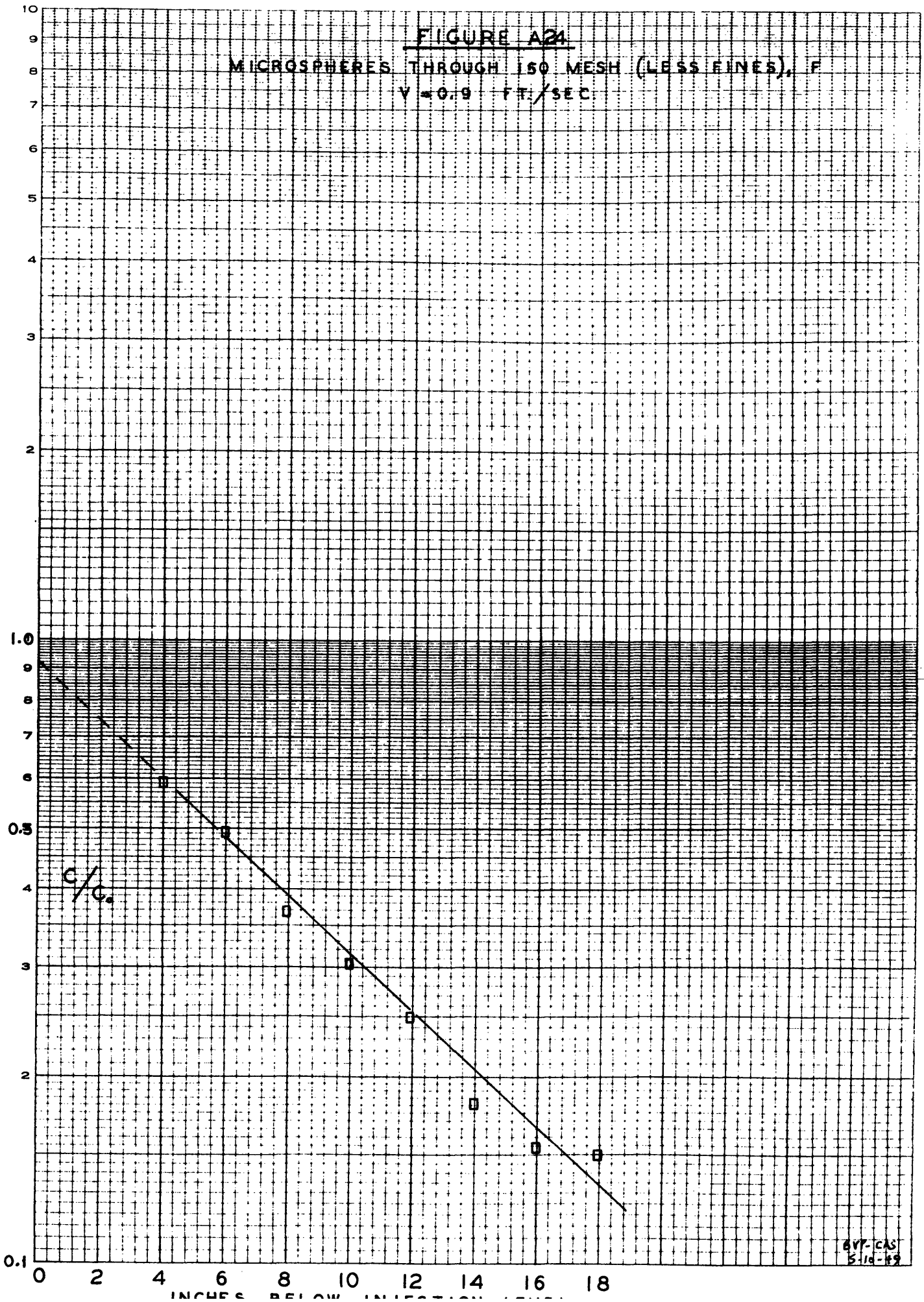


FIGURE A25

MICROSPHERES THROUGH 150 MESH (LESS FINES), F

V = 11.2 FT./SEC.

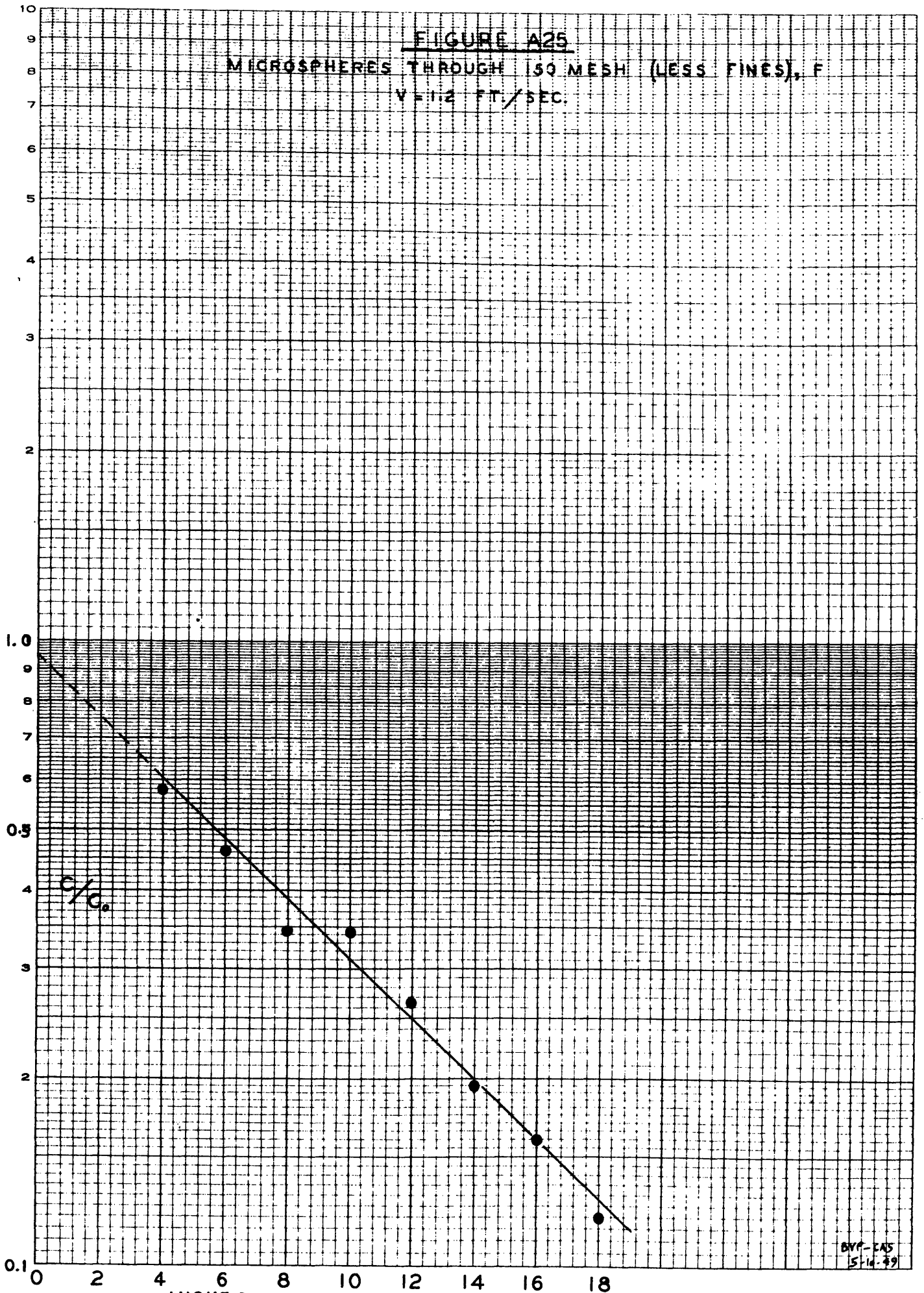


FIGURE A26
MICROSPHERES THROUGH 150 MESH (LESS FINES), F
V = 0.9 FT./SEC.

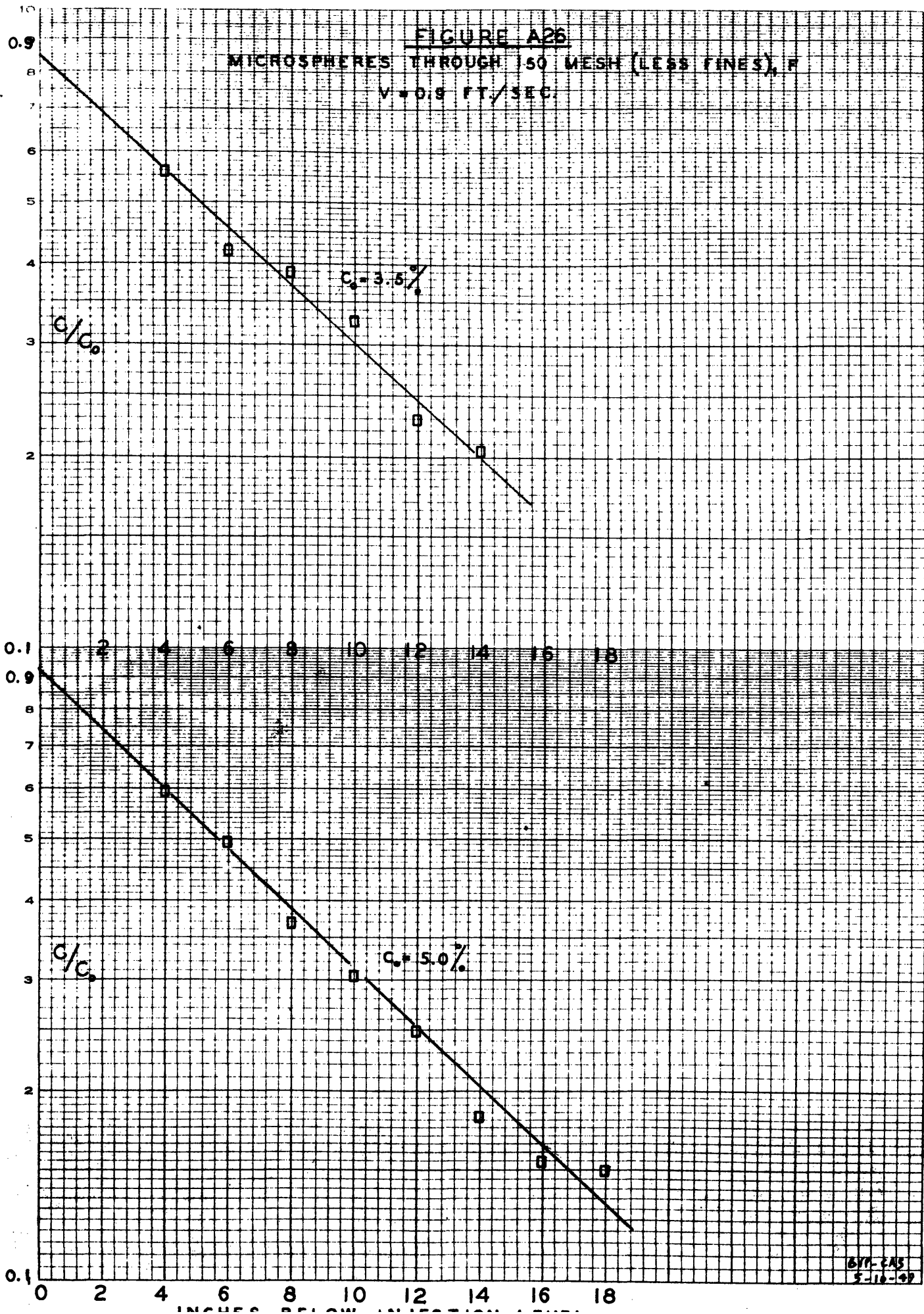


FIGURE A27

MICROSPHERES THROUGH 150 MESH (LESS FINES), F

V = 0.9 FT./SEC.

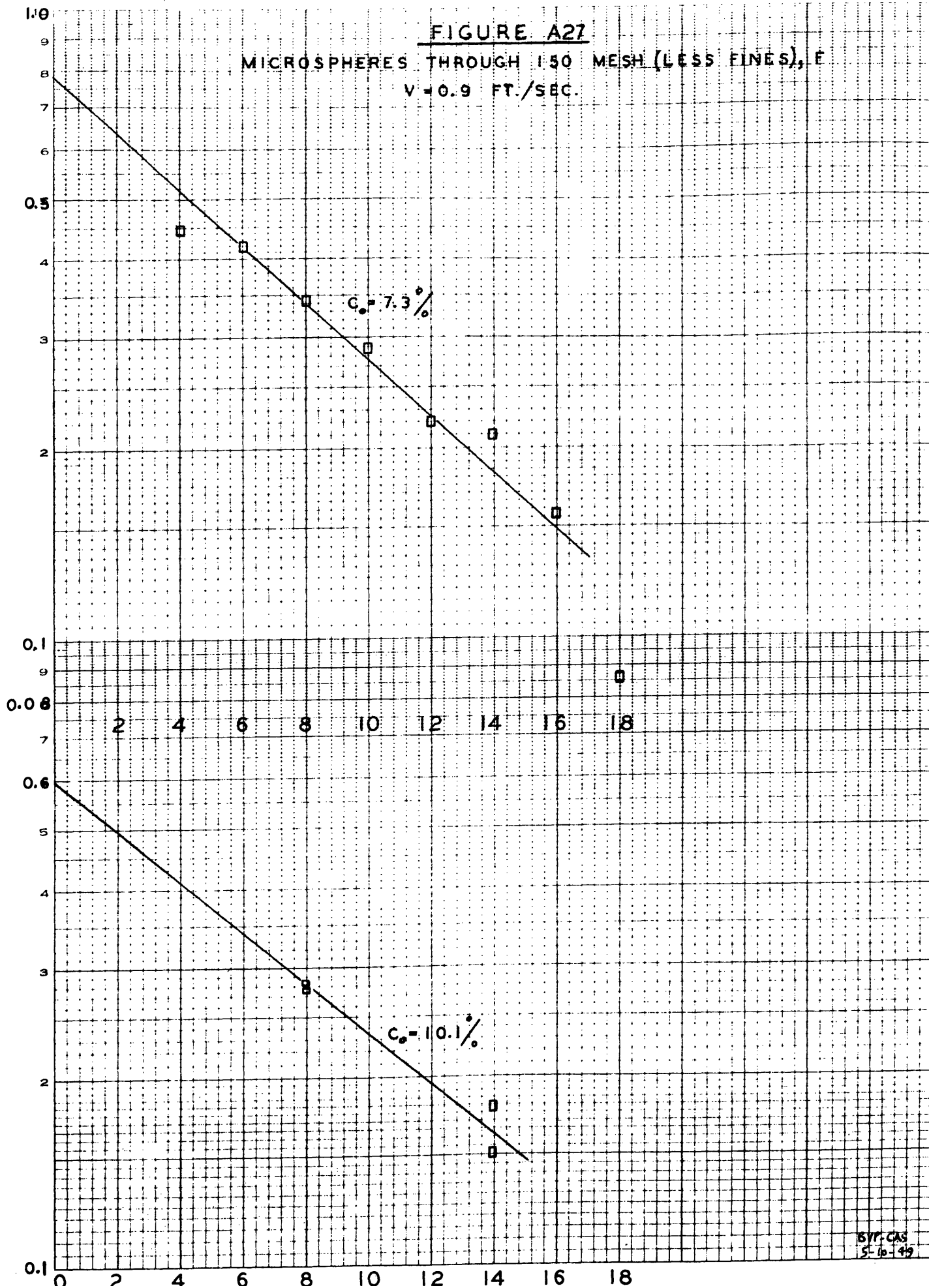


FIGURE A2B

MICROSPHERES, FINES ONLY, G

V = 0.4 FT./SEC.

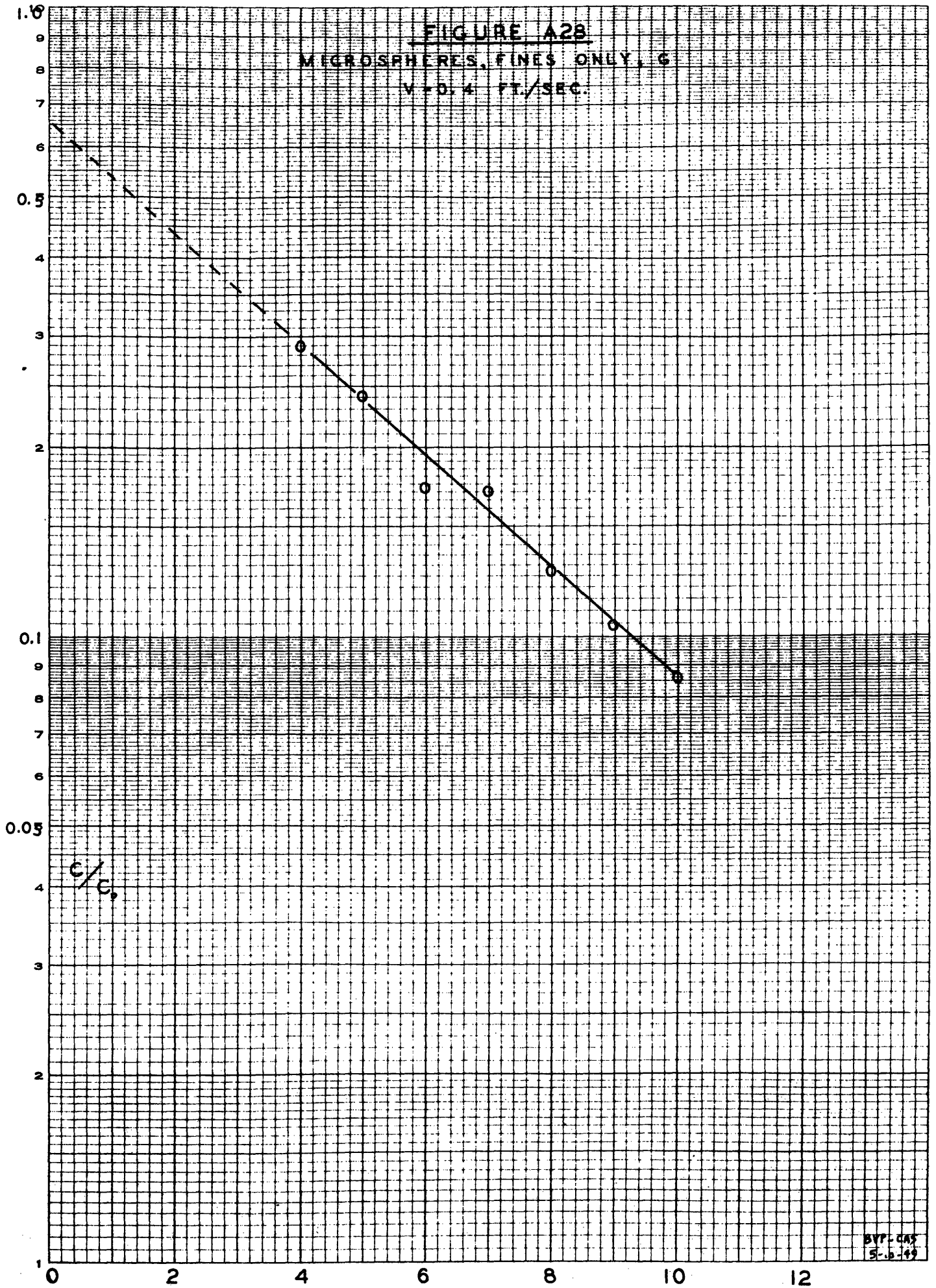


FIGURE A29

MICROSPHERES, FINES ONLY, G

V = 0.3 FT./SEC.

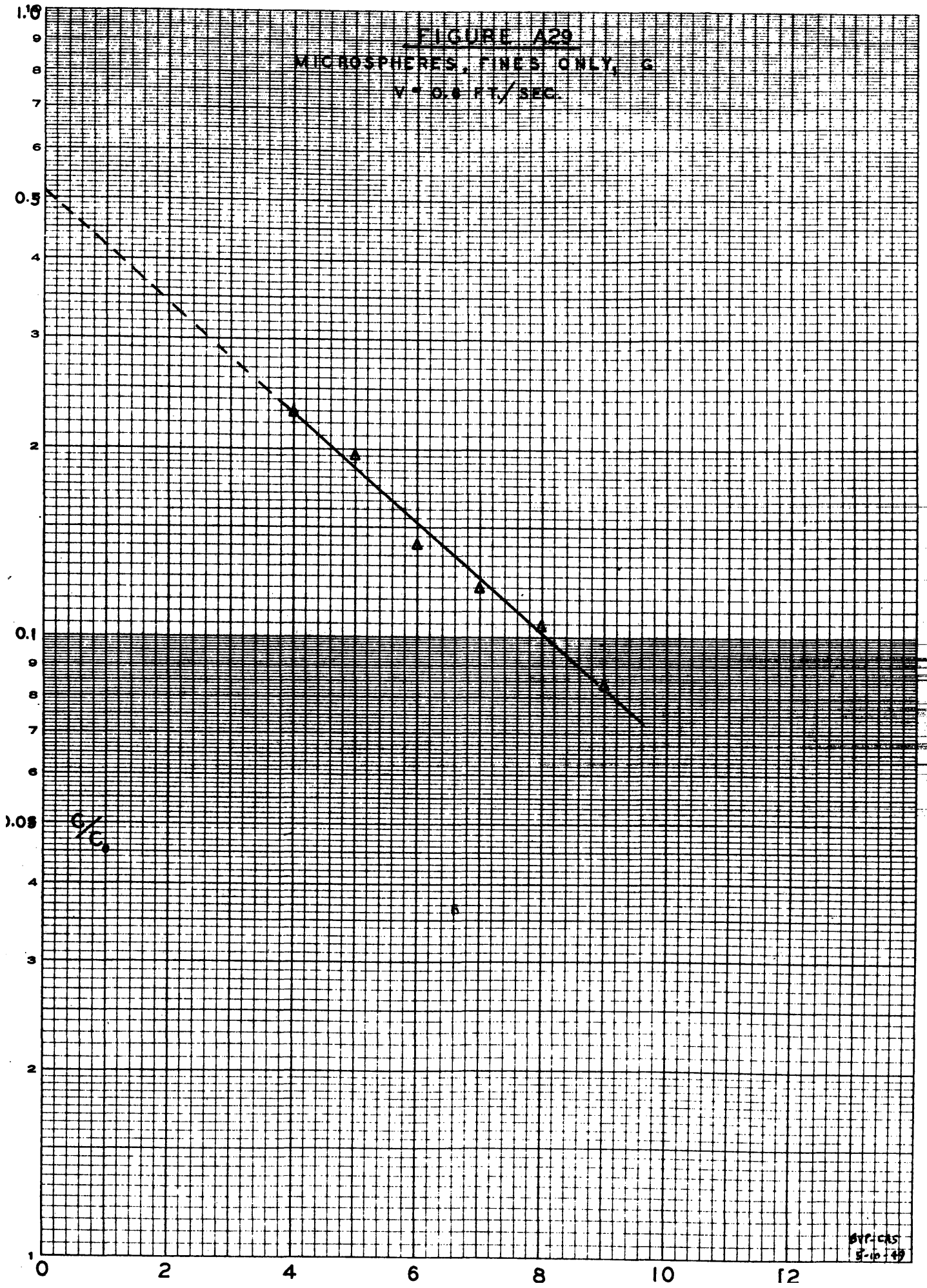
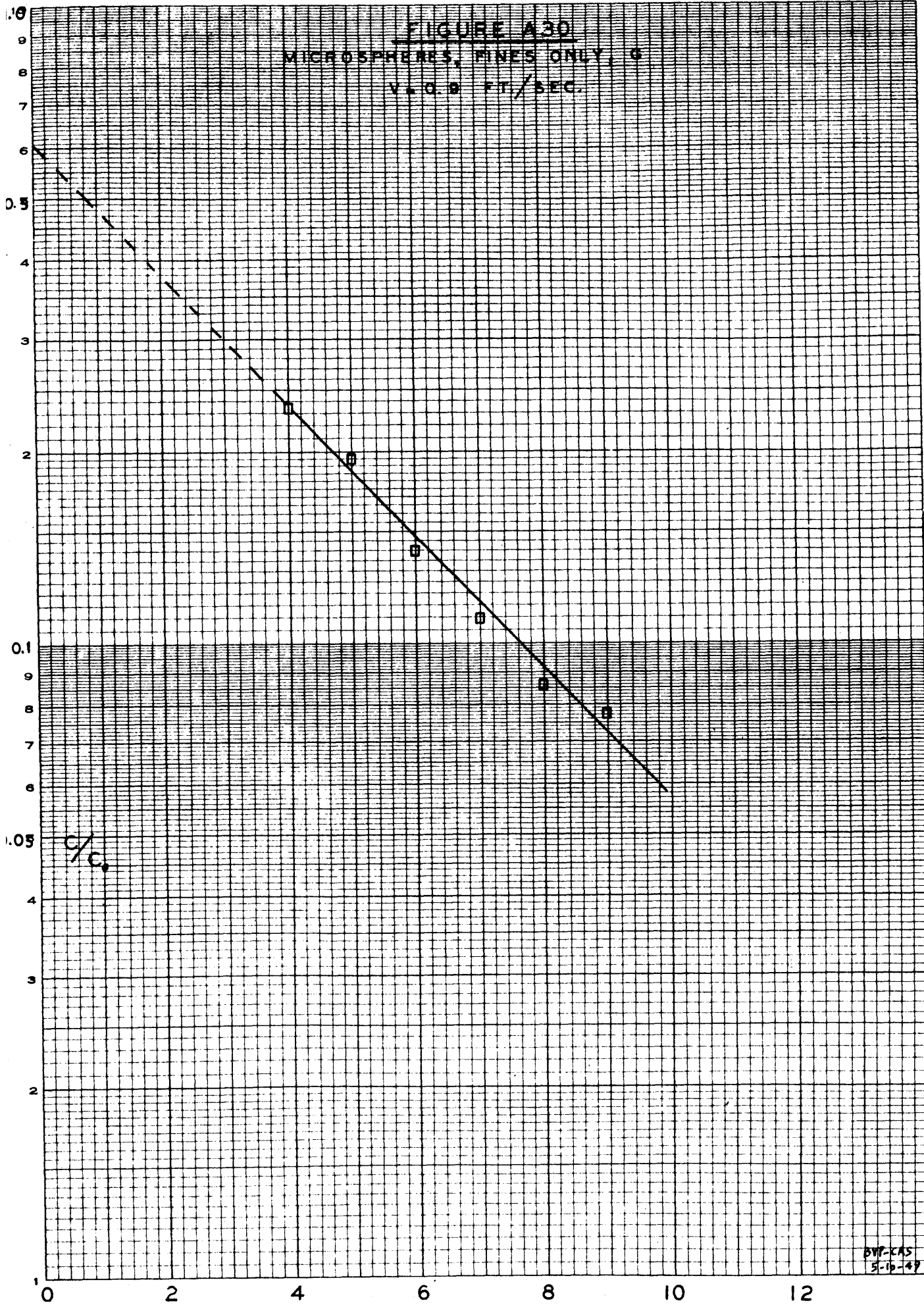


FIGURE A30

MICROSPHERES, FINES ONLY, ϕ

V. O. D. FT./SEC.



VIII. APPENDIX D. Summary of Data and Calculated Results (Contd)

3. Solids Concentration

TABLE AII

Height above bottom of column, feet:-	Pressure - Inches Water Gage						
	0	1	2	3	4	5	6
<u>Microspheres less fines:</u>							
0.4 ft./sec.	27.1	21.5	16.5	11.5	6.2	1.7	0.2
0.6 ft./sec.	23.8	18.4	13.5	8.85	4.45	0.65	0.22
0.9 ft./sec.	23.6	18.3	13.9	9.43	5.35	1.9	0.55
1.2 ft./sec.	21.0	15.8	11.4	7.53	3.70	1.40	0.60
<u>Microspheres on 100:</u>							
0.4 ft./sec.	30.7	24.6	19.2	13.4	8.05	0.26	0.17
0.9 ft./sec.	24.3	18.6	14.2	9.75	4.85	1.25	0.50
1.2 ft./sec.	22.8	17.6	12.7	8.80	4.00	1.40	0.85
<u>Microspheres thro' 140:</u>							
0.4 ft./sec.	24.6	18.4	13.9	8.8	3.05	0.15	0.15
0.6 ft./sec.	20.9	15.2	10.5	5.77	1.25	0.30	0.25
0.9 ft./sec.	22.6	17.2	12.5	8.25	3.75	0.80	0.40
1.2 ft./sec.	21.0	16.1	11.2	7.20	3.25	1.10	0.75
<u>Microspheres, fines only:</u>							
0.4 ft./sec.	17.0	13.4	11.65	7.45	4.37	1.52	0.50
0.6 ft./sec.	15.2	11.8	9.00	6.2	3.6	1.0	0.3
0.9 ft./sec.	11.6	8.55	6.5	4.13	2.05	0.7	0.5
<u>Microspheres, H:</u>							
1.7 ft./sec.	20.60	15.79	11.92	7.89	4.07	1.68	0.89
<u>No. 11 Glass Beads:</u>							
0.6 ft./sec.	72.78	57.47	43.84	28.53	14.28	3.28	0.12
0.9 ft./sec.	61.66	46.64	34.81	22.33	9.03	2.33	0.10
1.2 ft./sec.	57.35	42.60	29.85	19.97	7.94	2.16	0.18
1.8 ft./sec.	54.07	40.15	29.26	20.33	10.06	4.60	1.42
1.5 ft./sec.	50.03	35.2	22.0	--	3.85	1.10	0.95
<u>No. 13 Glass Beads</u>							
0.4 ft./sec.	70.9	57.1	44.0	30.3	12.3	3.10	0.20
0.6 ft./sec.	62.5	48.7	35.1	19.0	7.70	0.70	0.15
0.9 ft./sec.	53.8	41.9	26.8	14.5	3.05	0.50	0.35

FIGURE A31
PRESSURE GRADIENTS
MICROSPHERES, H

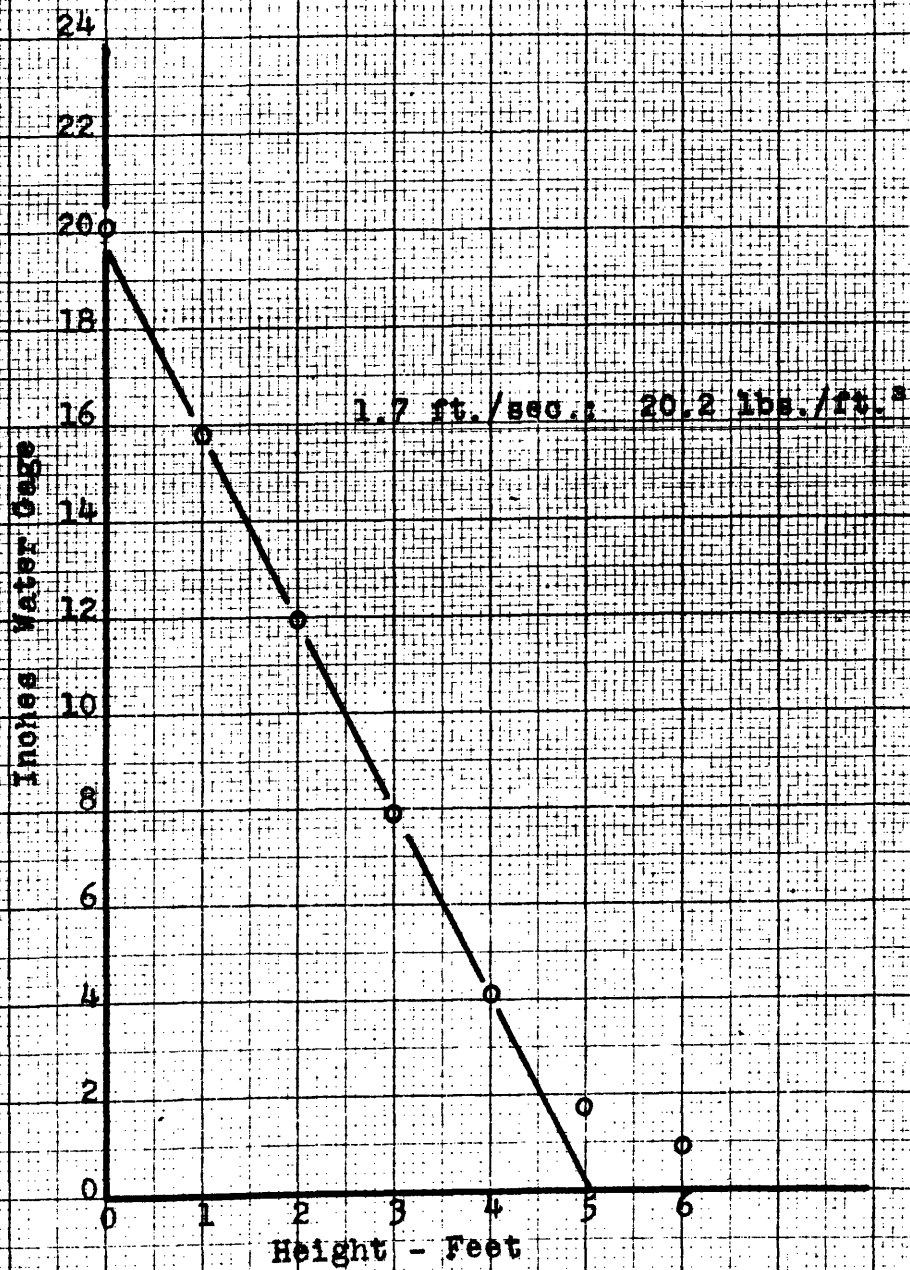


FIGURE A32
PRESSURE GRADIENTS
NO. 11 GLASS BEADS

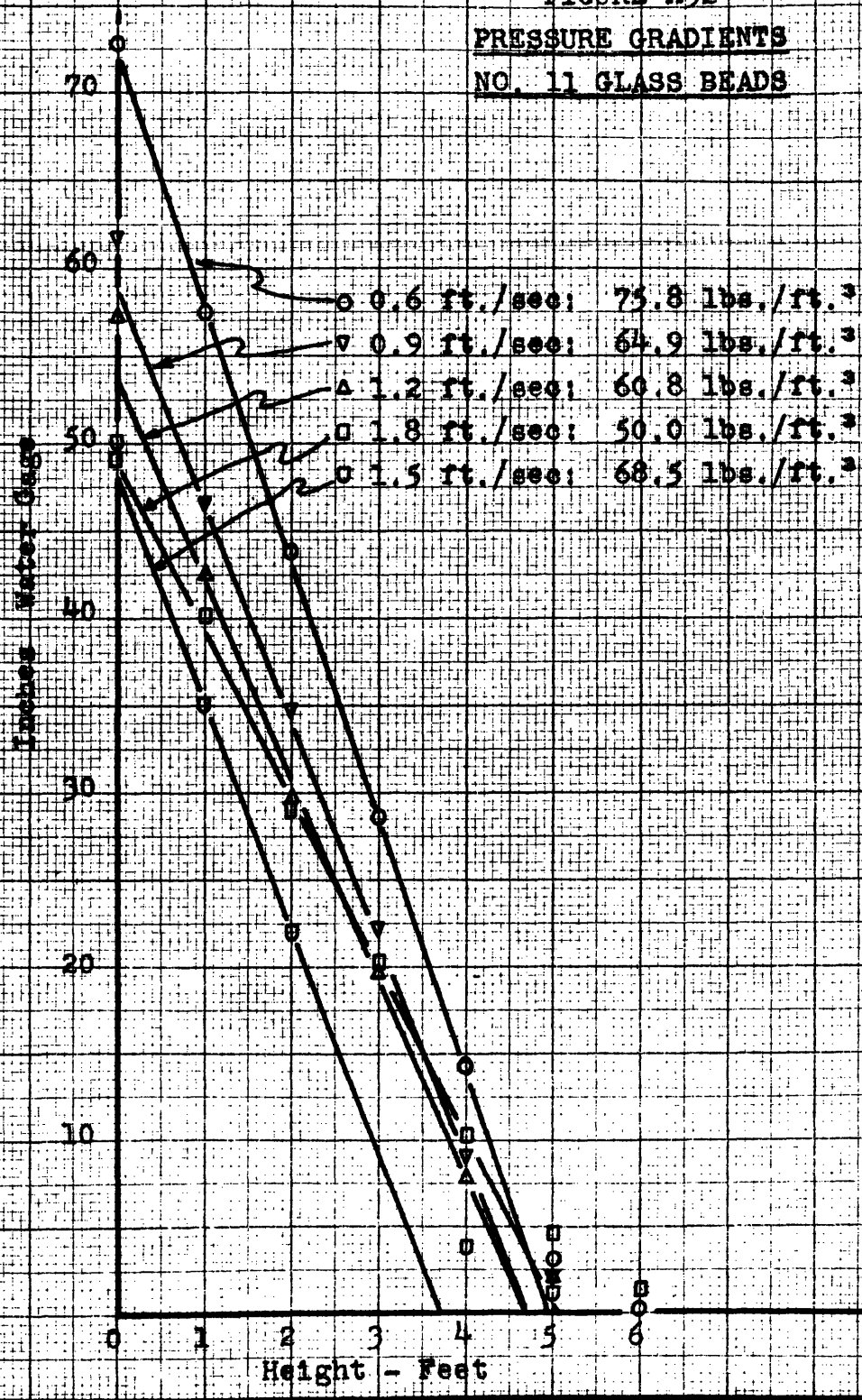


FIGURE A33
PRESSURE GRADIENTS
NO. 13 GLASS BEADS

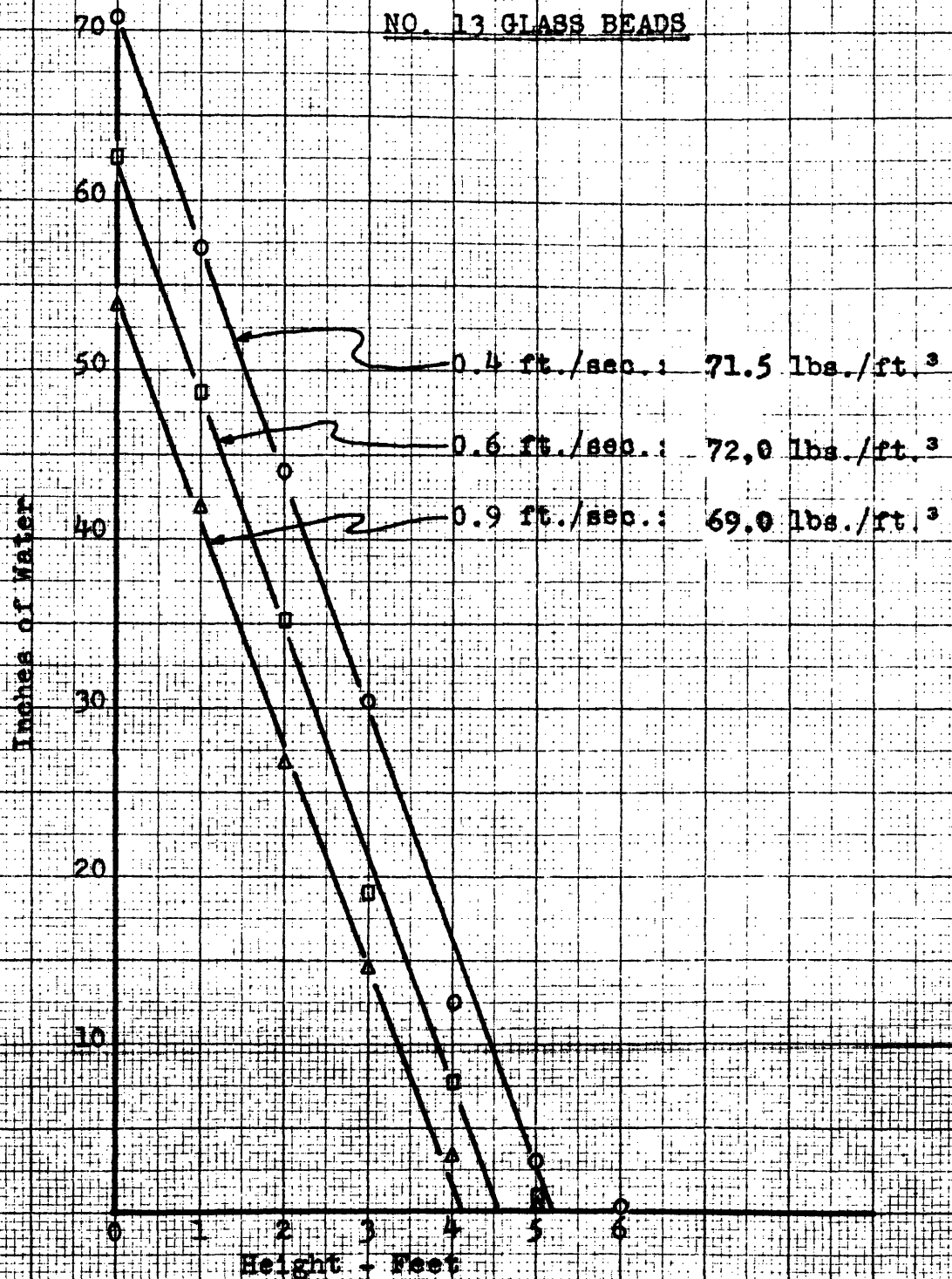


FIGURE A34

PRESSURE GRADIENTS
MICROSPHERES (LESS FINES), D

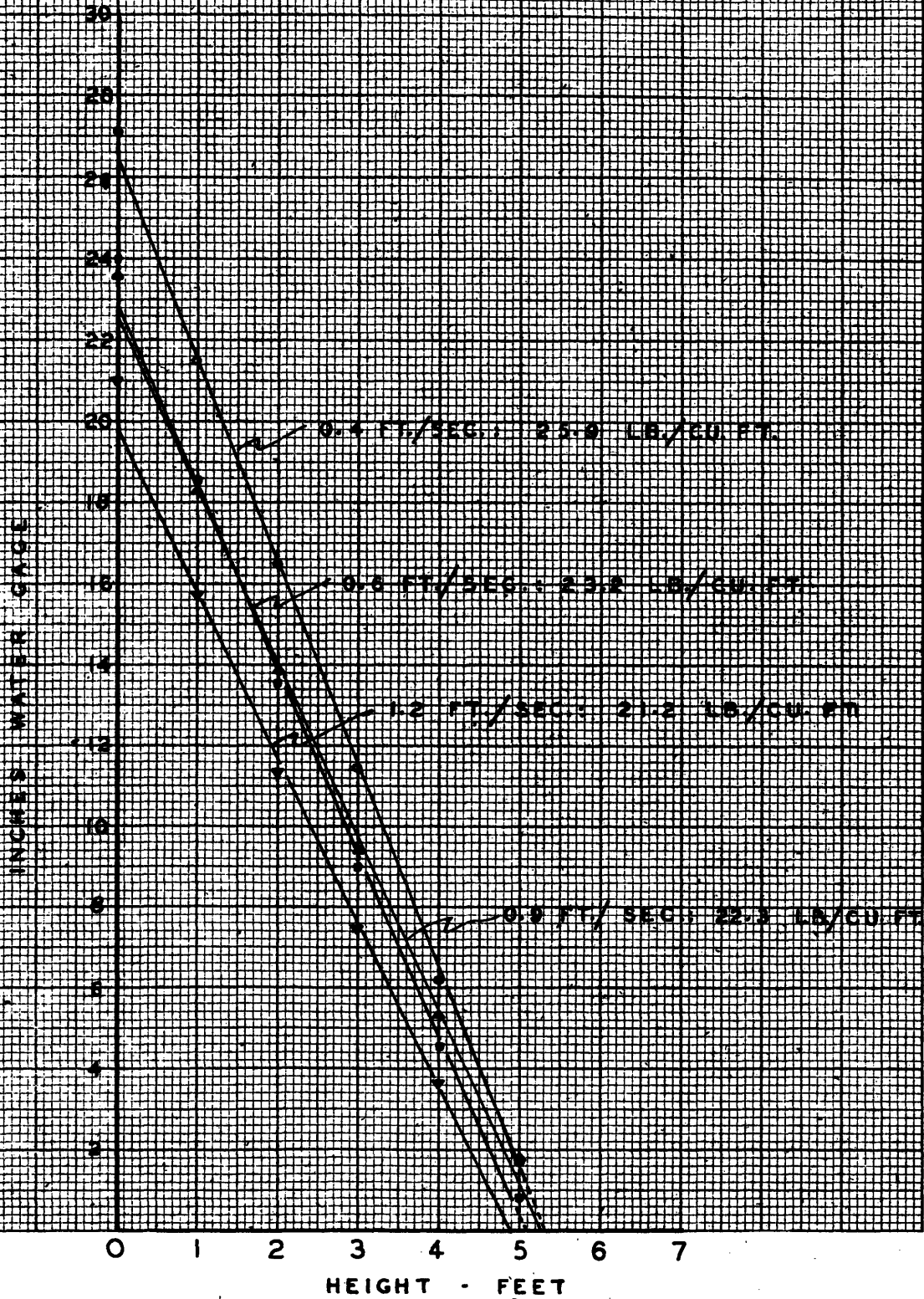


FIGURE A35

PRESSURE GRADIENTS
MICROSPHERES, ON 100 MESH, E

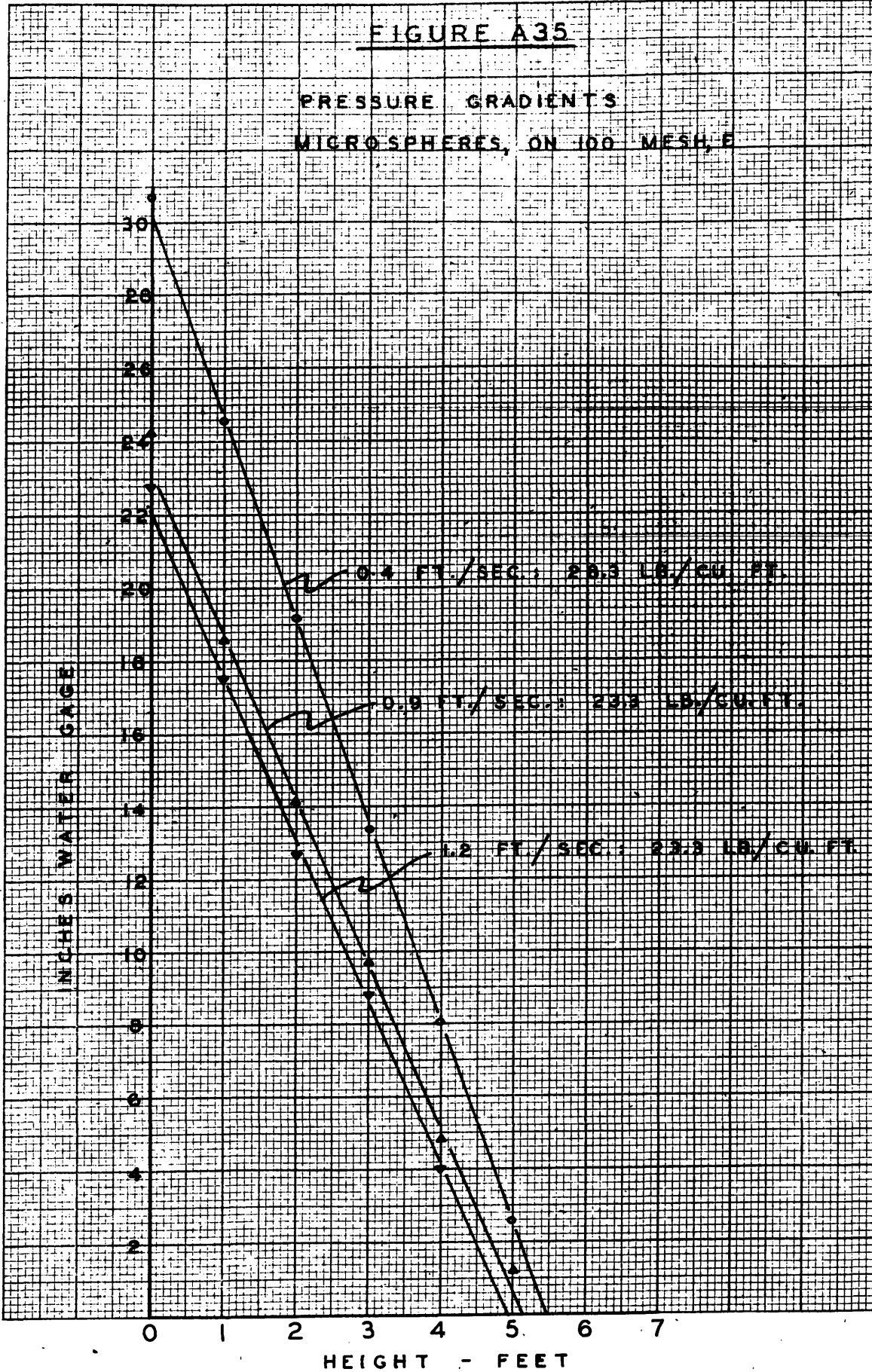


FIGURE A36

PRESSURE GRADIENTS
MICROSPHERES, THROUGH 150 MESH, F

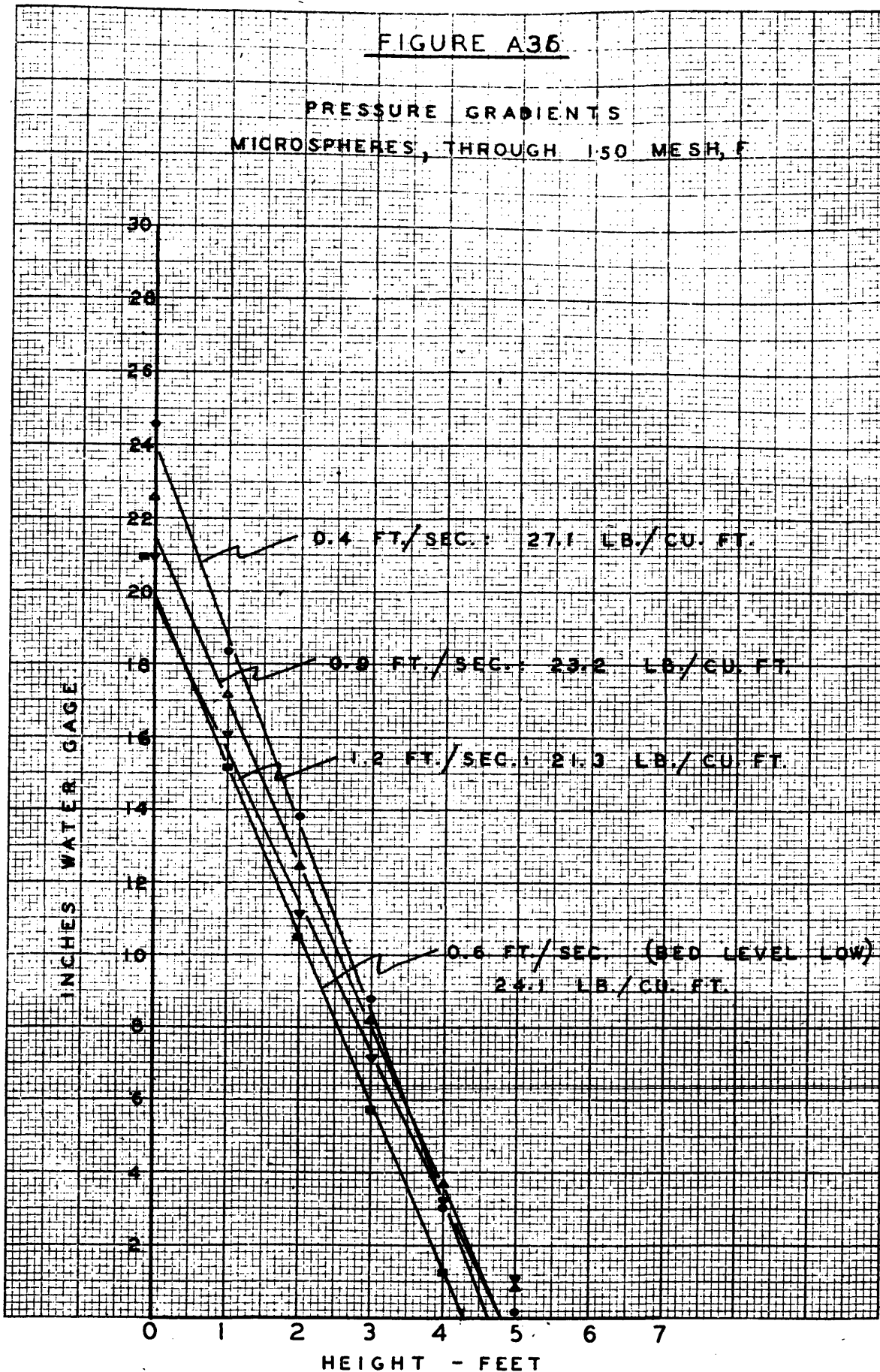
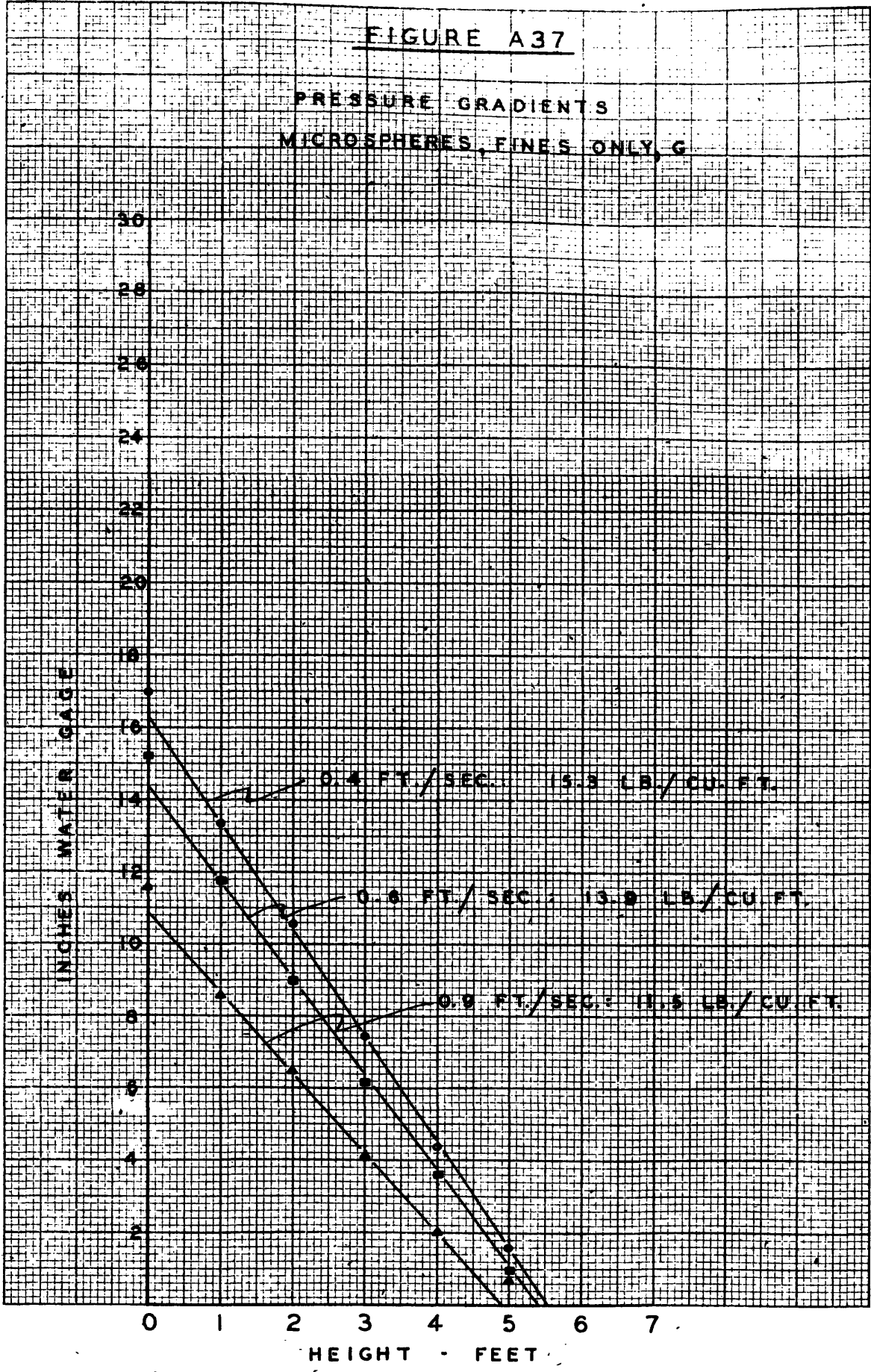


FIGURE A37

PRESSURE GRADIENTS
MICROSPHERES, FINES ONLY, G



VII APPENDIX D. Summary of Data and Calculated Values
(Continued)

4. Residence-Time Data

θ^* corrected for volume of mixing chamber, V_G ,

to give θ

<u>Column</u>	<u>V_G</u> <u>ft.³</u>
3-inch I.D.	0.0019
4-1/2-inch I.D.	0.0144

TABLE AIII

Residence Time Data

Run	Charge lb.	θ^* sec.	Q	$\frac{Q\theta}{VZ}$	C	$\frac{C}{C_0}$	Comments			
7-37-A	15.94	1	1.12	0.29	16.4	0.96	Fixed Bed			
		2		0.61	16.1	0.95				
		3		0.92	11.0	0.65				
		4		1.24	0.5	0.029				
		0		0	17.0	1.00				
		1.5	1.12	0.45	17.4	1.01				
		2.5		0.76	16.6	0.96				
		3.5		1.09	13.15	0.18				
		0		0	17.3	1.00				
		1		1.12	0.29	14.6		0.97		
		2	0.61		15.3	1.01				
		3	0.92		10.4	0.69				
		4	1.24		0.96	0.064				
		0	1.12		0	15.1		1.00		
		1.5		0.45	16.9	0.98				
		2.5		0.76	16.0	0.92				
		3.5		1.09	4.9	0.28				
		0		0	17.3	1.00				
		7-37-C	14.25	1	2.24	0.51		19.8	0.99	Bubbling Lowest Static Pressure in- creased when air rate in- creased. Not fluidized.
				2.2		1.16		4.0	0.20	
3	1.60			0		0				
4	2.14			0		0				
5	2.68			0		0				
0	2.24			0	20.0	1.00				
1.5				0.78	17.6	0.88				
2.5				1.33	0.62	0.03				
3.5				1.86	0	0				
4.5				2.41	0	0				
0	0	20.0	1.00							
7-37-D	12.53	1	2.76	0.57	21.3	0.96	Small slugs of gas			
		2		1.15	2.9	0.13				
		3		1.73	0	0				
		4		2.31	0	0				
		0		0	22.1	1.00				
		0.5	2.76	0.27	22.0	1.02				
		1.5		0.85	18.3	0.85				
		2.5		1.44	1.3	0.06				
		0		0	21.5	1.00				

TABLE AIII (CONTINUED)

Run	Charge lb.	t^* sec.	Q	$\frac{Q_0}{\sqrt{t}}$	C	$\frac{C}{C_0}$	Comments			
7-37-E	11.66	1	3.36	0.65	17.9	0.85	Slugging at bottom			
		2		1.31	3.85	0.18				
		3		1.99	0	0				
		4		2.65	0	0				
		0		0	21.0	1.00				
		1.5	3.36	0.32	20.3	0.95	Channelling at top			
		2.5		0.98	6.85	0.32				
		3.5		1.65	0.8	0.037				
		0		0	21.4	1.00				
		7-37-F	10.34	0.8	3.86	0.55	19.0	0.87	Slugging	
2	1.39			3.05		0.14				
3	2.11			0		0				
4	2.82			0		0				
0	0			21.8		1.00				
0.5	3.86			0.34	20.6	0.95				
1.5				1.04	7.5	0.35				
2.5				1.75	0.5	0.02				
0				0	21.6	1.00				
9-37-A	13.0			1	1.08	0.22	17.7	0.97		
		2	0.46	17.0		0.93				
		3	0.70	16.0		0.88				
		4	0.95	11.1		0.61				
		5	1.19	3.8		0.21				
		6	1.43	0.64		0.035				
		7	1.68	0		0				
		8	1.92	0		0				
		0	0	18.2		1.00				
		13.0	1.10	1		1.10	0.22	17.2		0.96
	2			0.47	16.9		0.94			
	3			0.71	15.6		0.87			
	4			1.00	13.4		0.75			
	5			1.21	1.3		0.073			
	6			1.46	0.6		0.03			
	0			0	17.9		1.00			
	1			1.10	0.22		17.4	0.93	Large Bubbles	
	2				0.47		16.4	0.98		
	3.5				0.84		12.0	0.64		
	4.5	1.07	7.2		0.38					
6	1.46	2.75	0.15							
7	1.71	0.9	0.048							
0	0	18.8	1.00							

TABLE AIII (CONTINUED)

Run	Charge lb.	θ^* sec.	Q	$\frac{Q\theta}{V\epsilon}$	C	$\frac{C}{C_0}$	Comments	
9-37-B	10.68	2	1.66	0.61	16.8	0.90		
		3		0.92	8.1	0.43		
		4		1.24	4.8	0.26		
		5		1.55	0.66	0.035		
		6		1.87	+0.0	+0.0		
		7		2.19	0.0	0.0		
		9		2.81	0.0	0.0		
		12		3.76	0.0	0.0		
		0		0.0	18.8	1.00		
		10.94		1	1.66	0.30	18.3	1.03
	2	0.62	14.4	0.81				
	3	0.95	14.0	0.79				
	4	1.27	2.4	0.14				
	6	1.92	0.4	0.022				
	0	0.0	17.8	1.00				
	2.5	0.81	10.8	0.59				
	3.5	1.11	4.5	0.24				
	0	0.0	18.4	1.00				
	10.94	1	1.69	0.30		18.4	1.00	
	2	0.62		18.8	1.03			
3	0.95	7.1		0.39				
4	1.27	4.2		0.23				
6	1.92	0.0		0.0				
0	0.0	18.3		1.00				
2.5	0.79	14.2		0.78				
3.5	1.11	5.8		0.32				
0	0.0	18.2		1.00				
9-37-C	8.75	1		2.27	0.36	17.9	0.98	
		2	0.75		14.3	0.78		
		3	1.12		3.7	0.20		
		4	1.51		0.91	0.05		
		0	0		18.3	1.00		
		0.5	0.17		19.0	1.00		
		1.5	0.54		18.0	0.95		
		2.5	0.93		9.6	0.51		
		0	0		19.0	1.00		
		1	2.28		0.36	18.3	1.00	
		2			0.75	13.8	0.75	
		3			1.13	3.5	0.19	
		4			1.51	0.78	0.042	
		5			1.90	0	0	
		0			0	18.4	1.00	
		1.5			0.55	16.5	0.91	
		2.5			0.94	5.9	0.33	
0	0	18.1		1.00				

TABLE AIII (CONTINUED)

Run	Charge lb.	Q [*] sec.	Q	$\frac{Q_0}{V\epsilon}$	C	$\frac{C}{C_0}$	Comments		
11-37-A	9.44	1	1.14	0.19	17.5	1.02	Some slugging Considerable solid falling through slugs		
		2		0.41	15.4	0.89			
		3		0.62	13.4	0.78			
		4		0.83	10.5	0.61			
		5		1.05	6.9	0.40			
		6		1.25	4.5	0.26			
		7		1.46	3.15	0.18			
		8		1.68	2.25	0.13			
		0	0	17.2	1.00				
		2	1.14	0.41	16.5	0.95			
		4		0.83	8.2	0.47			
		6		1.25	4.7	0.27			
		8		1.68	1.68	0.10			
		10		2.10	0.7	0.04			
		14		2.53	0	0			
		16		2.96	0	0			
		18		3.38	0	0			
		0	0	17.4	1.00				
		11-37-B	7.78	1	1.72	0.27	16.9	1.00	
				2		0.55	10.5	0.62	
3	0.84			9.1		0.54			
4	1.13			3.9		0.23			
5	1.41			2.9		0.17			
6	1.70			1.25		0.074			
7	1.99			0.68		0.04			
9	2.55			+0		+0			
0	0			16.8	1.00				
1	1.71			0.26	17.5	1.00			
2				0.56	14.0	0.80			
3				0.84	10.7	0.61			
4				1.13	5.6	0.32			
5				1.42	2.4	0.14			
6				1.72	1.2	0.068			
7				2.01	1.0	0.057			
9				2.58	0.5	0.028			
0	0			17.5	1.00				
11-37-C	6.66			1	2.29	0.34	19.5	0.99	Violent action; slugging at bottom. Channelling at top.
				2		0.69	16.2	0.82	
		3	1.05	5.5		0.28			
		4	1.40	4.1		0.21			
		5	1.76	1.45		0.074			
		6	2.12	0.76		0.039			
		7	2.48	0.5		0.025			
		8	2.83	0		0			
		0	0	19.7		1.00			

TABLE AIII (CONTINUED)

Run	Charge lb.	θ^* sec.	Q	$\frac{Q\theta}{V}$	C	$\frac{C}{C_0}$	Comments		
13-37-A	9.06	2	1.13	0.39	14.6	0.84			
		3		0.60	13.2	0.76			
		4		0.80	8.0	0.46			
		5		1.01	5.9	0.34			
		6		1.22	4.3	0.25			
		7		1.43	2.9	0.17			
		9		1.85	1.0	0.058			
		12		2.48	0.6	0.035			
		0		0	17.3	1.00			
		2		1.14	0.39	15.6	0.93		
		3			0.60	10.0	0.60		
		4			0.80	7.2	0.43		
	5	1.01	4.6		0.27				
	6	1.22	3.8		0.23				
	7	1.43	3.5		0.21				
	9	1.85	2.4		0.14				
	12	2.48	0.73		0.043				
	0	0	16.8		1.00				
	2	1.14	0.39		16.2	0.99			
	3		0.60		11.6	0.71			
	4		0.80		7.1	0.43			
	5		1.01	5.6	0.34				
	6		1.22	4.4	0.27				
	7		1.43	2.7	0.16				
9	1.85		1.35	0.08					
12	2.48		0.66	0.04					
0	0		16.4	1.00					
13-37-B	7.56		1	1.74	0.27	16.9	1.00	Slugging	
			2		0.55	10.9	0.65		
			3		0.84	7.8	0.46		
		4	1.13		4.5	0.27			
		5	1.42		2.0	0.12			
		6	1.70		1.3	0.077			
		7	1.99		0.73	0.043			
		9	2.56		0	0			
		0	0		16.8	1.00			
		1	1.73		0.26	14.6	0.97		
		2			0.55	12.7	0.84		
		3			0.83	6.2	0.41		
	4	1.12		3.6	0.24				
	6	1.69		1.5	0.10				
	0	0		15.1	1.00				
	1.5	0.41		12.5	0.87				
	2.5	0.69		11.0	0.77				
	0	0		14.4	1.00				

TABLE AIII (CONTINUED)

Run	Charge lb.	θ^* sec.	Q	$\frac{Q\theta}{V_c}$	C	$\frac{C}{C_0}$	Comments		
13-37-C	6.62	1	2.32	0.34	18.5	1.0			
		2.2		0.77	8.6	0.47			
		3		1.06	4.9	0.27			
		4		1.42	1.9	0.10			
		5		1.78	1.2	0.065			
		6		2.14	0.76	0.041			
		7		2.51	0.4	0.022			
		8		2.87	0	0			
		0		0	18.4	1.00			
		1		2.32	0.34	17.9	0.96		
		2			0.70	10.8	0.58		
		3			1.06	4.4	0.24		
		4			1.42	2.0	0.11		
	5	1.78	1.3		0.07				
	6	2.14	0.88		0.047				
	7	2.51	0.52		0.028				
	8	2.87	0.53		0.028				
	0	0	18.7		1.00				
	1	2.36	0.35		17.0	0.93			
	2		0.70		11.1	0.61			
	3		1.07		5.5	0.30			
	4		1.43		3.2	0.18			
	7		2.51	0.66	0.036				
	0		0	18.2	1.00				
	1.5		0.52	13.6	0.72				
	2.5		0.89	10.2	0.54				
0	0		18.8	1.00					
13-37-D	6.12		1	2.94	0.42	18.3	0.93		
			2		0.86	5.8	0.29		
			3		1.30	2.6	0.13		
			4		1.74	1.6	0.081		
		5	2.18		0.88	0.045			
		6	2.62		0.51	0.026			
		7	3.06		+0	+0			
		8	3.50		0	0			
		0	0		19.7	1.00			
		1	2.94		0.42	18.2	1.00		
		2			0.85	7.2	0.39		
		3			1.29	4.4	0.24		
		4			1.73	1.5	0.082		
	6	2.60		0.50	0.027				
	0	0		18.3	1.00				
	1.5	0.63		13.8	0.74				
	2.5	1.07		5.3	0.28				
	0	0		18.7	1.00				
	5.94	5.94		1	2.94	0.42	18.2	1.00	
				2		0.85	7.2	0.39	
				3		1.29	4.4	0.24	
				4		1.73	1.5	0.082	
			6	2.60		0.50	0.027		
			0	0		18.3	1.00		
			1.5	0.63		13.8	0.74		
			2.5	1.07		5.3	0.28		
0			0	18.7		1.00			

TABLE AIII (CONTINUED)

Run	Charge lb.	t^* sec.	Q	$\frac{Q_0}{V_f}$	C	$\frac{C}{C_0}$	Comments
13-35L-A	21.75	0	2.60	0	18.7	1.00	
		1		0.17	18.4	0.98	
		3		0.65	11.7	0.63	
		6		1.39	5.75	0.31	
		9		2.12	2.5	0.13	
		12		2.85	1.18	0.063	
		15		3.60	0.58	0.031	
		18		4.33	0.40	0.021	
		21		5.07	+0	+0	
		0	2.60	0	17.8	1.00	
	1		0.17	17.8	1.00		
	2		0.42	16.5	0.93		
	3		0.65	12.2	0.69		
	4		0.90	7.7	0.43		
	5		1.15	5.6	0.31		
	6		1.39	4.2	0.24		
	8		1.88	3.0	0.17		
	10		2.38	1.75	0.098		
	0	21.5	2.56	0	19.0	1.00	Smooth Fluidization
	1		0.17	16.7	0.88		
	3		0.65	12.1	0.64		
6		1.36	5.2	0.27			
9		2.08	2.39	0.13			
12		2.79	1.23	0.065			
15		3.52	0.56	0.03			
18		4.23	0.4	0.02			
21		4.95	+0	+0			
0	21.5	2.56	0	19.1	1.00		
1		0.17	19.3	1.01			
2		0.40	17.9	0.94			
3		0.65	14.9	0.78			
4		0.88	8.4	0.44			
5		1.12	7.0	0.37			
6		1.36	5.05	0.26			
8		1.84	3.25	0.17			
10		2.31	1.95	0.10			
0	21.25	2.54	0	18.3	1.00		
1		0.16	18.6	1.02			
3		0.62	12.6	0.69			
6		1.33	4.85	0.27			
9		2.01	2.33	0.13			
12		2.74	1.02	0.056			
15		3.44	0.5	0.027			
18		4.15	+0	+0			
21		4.88	0	0			

TABLE AIII (CONTINUED)

Run	Charge lb.	θ^* sec.	Q	$\frac{Q\theta}{V_c}$	C	$\frac{C}{C_0}$	Comments		
13-35L-A	21.25	0	2.54	0	18.3	1.00			
		1		0.16	19.0	1.04			
		2		0.39	17.1	0.94			
		3		0.62	10.3	0.56			
		4		0.86	8.0	0.44			
		5		1.01	6.2	0.34			
		6		1.33	4.8	0.26			
		7		1.56	3.55	0.19			
		8		1.79	2.6	0.14			
13-35L-B	19.75	0	4.03	0	17.8	1.00	A.S.S. added some static present		
		1		0.28	17.2	0.97			
		2		0.63	13.1	0.74			
		3		0.98	7.3	0.41			
		6		2.04	2.38	0.13			
		9		3.09	0.93	0.052			
		12		4.13	+0	+0			
		15		5.20	0	0			
		0		4.03	0	17.8		1.00	
		0.5	0.10		17.6	0.99			
		1.5	0.46		15.4	0.87			
		2.5	0.80		8.2	0.46			
		3.5	1.16		4.35	0.24			
		5	1.68		2.36	0.13			
		6.1	2.07		1.61	0.09			
		7	2.39		1.09	0.061			
		9	3.09		0.68	0.038			
		13-35L-C	17.5		0	5.21	0	18.0	1.00
				1	0.35		17.1	0.95	
2	0.78			9.9	0.55				
3	1.20			4.55	0.25				
4	1.63			2.75	0.15				
6	2.47			1.26	0.07				
8	3.32			0.52	0.029				
10	4.24			+0	+0				
12	5.02			0	0				
0	5.23			0	17.6	1.00			
0.5				0.15	17.2	0.98			
1.5				0.57	13.5	0.77			
2.5				1.00	4.7	0.27			
3.5				1.42	3.25	0.18			
5				2.09	1.61	0.092			
6				2.47	0.76	0.043			
7				2.90	0.62	0.035			
8				3.32	0.38	0.022			

TABLE AIII (CONTINUED)

Run	Charge lb.	Q^* sec.	Q	$\frac{Q\theta}{\sqrt{t}}$	C	$\frac{C}{C_0}$	Comments		
13-35L-D	15.81	0	6.66	0	17.1	1.00	Air humidified; stopped static R.H. = 50.5%		
		1		0.45	16.4	0.96			
		2		0.96	6.32	0.37			
		3		1.47	2.76	0.16			
		4		1.98	1.53	0.09			
		5		2.49	0.91	0.053			
		6		3.00	0.66	0.039			
		7		3.51	0.45	0.026			
		8	4.02	$\pm 0.36 \pm$	0.02				
		0	6.65	0	17.0	1.00	R.H. = 54%		
		0.5		0.20	17.1	1.01			
		1.5		0.70	9.9	0.58			
		2.5		1.22	4.2	0.25			
		3.5		1.72	1.82	0.11			
		5		2.49	1.14	0.067			
		6		3.00	0.73	0.043			
		7		3.51	0.60	0.035			
		8	4.01	$\pm 0.36 \pm$	0.02				
		15-35L-A	20.94	0	2.91	0	18.5	1.00	
				1		0.19	18.1	0.98	
2	0.46			14.5		0.78			
3	0.73			8.6		0.46			
4	1.00			6.4		0.35			
5	1.27			4.6		0.25			
8	2.08			2.3		0.12			
12	3.15			0.98		0.05			
0	2.91			0	18.3	1.00			
2.5				0.60	13.0	0.71			
4				1.00	7.5	0.41			
6				1.54	4.1	0.22			
8				2.08	2.46	0.13			
12				3.15	1.04	0.057			
15				3.96	0.52	0.028			
18				4.76	0.4	0.022			
20	5.31	+0	+0						

TABLE AIII (CONTINUED)

Run	Charge lb.	Q* sec.	Q	$\frac{Q\theta}{V\epsilon}$	C	$\frac{C}{C_0}$	Comments
15-35L-B	19.69	0	4.02	0	18.8	1.00	
		1		0.28	18.3	0.97	
		3		0.98	6.8	0.36	
		6		2.04	2.46	0.13	
		9		3.10	0.93	0.049	
		12		4.16	0.38	0.020	
		15		5.21	0	0	
		18		6.28	0	0	
		0		4.02	0	18.6	1.00
		1	0.28		17.0	0.92	
		2	0.63		12.8	0.69	
		3	0.98		7.0	0.38	
		4	1.34		4.73	0.25	
		5	1.69		2.86	0.15	
		6	2.04		2.10	0.11	
		7	2.40		1.35	0.073	
		8	2.75		1.0	0.054	
		15-35L-D	17.69	0	6.66	0	17.6
1	0.49			13.5		0.77	
2	1.02			5.13		0.29	
3	1.57			2.92		0.17	
4	2.12			2.17		0.12	
5	2.66			1.09		0.062	
6	3.21			0.88		0.050	
7	3.75			0.51	0.029		
0	6.66			0	17.8	1.00	
0.5				0.21	17.0	0.96	
1.5				0.75	7.9	0.44	
2.5				1.30	5.0	0.28	
4				2.12	2.0	0.11	
6				3.21	0.73	0.04	
7				3.75	0.45	0.025	
8		4.30	+0	+0			
10	5.40	0	0				

Note: 15-35L-C not reported since the two runs made did not agree in timing. Probably one (or both) zero times off.

TABLE AIII (CONTINUED)

Run	Charge lb.	θ^* sec.	Q	$\frac{Q\theta}{\sqrt{t}}$	C	$\frac{C}{C_0}$	Comments
7-35L-A	32.25	1	2.58	0.21	15.9	0.96	Fixed Bed
		2		0.53	15.9	0.96	
		3		0.85	12.3	0.75	
		4		1.16	1.02	0.062	
		5		1.48	0	0	
		0		0	16.5	1.00	
		0	2.58	0	16.2	1.00	
		1		0.21	16.5	0.96	
		2		0.53	15.8	0.98	
		3		0.85	9.9	0.61	
	4		1.16	1.06	0.065		
	5		1.48	0.5	0.03		
	2.5	2.58	0.68	15.7	0.96		
	3.5		1.00	3.4	0.21		
	0		0	16.3	1.00		
	33.19	0	2.53	0	17.5	1.00	
		2		0.55	17.6	1.00	
		3		0.87	16.0	0.91	
		4		1.20	1.35	0.08	
		5		1.52	0	0	
6			1.84	0	0		
0		2.53	0	17.3	1.00		
0.5			0.06	17.6	1.02		
1.5			0.38	17.0	0.98		
2.5			0.71	16.8	0.97		
3.5		1.02	3.88	0.22			
4.5		1.36 \pm 0.3	\pm 0.017				
5.5		1.69	0	0			
53.25	0	2.53	0	13.1	1.00		
	1		0.23	12.5	0.96		
	2		0.58	12.6	0.96		
	3		0.91	9.1	0.69		
	4		1.24	0.66	0.05		
	5		1.58	0	0		
	6		1.91	0	0		
	0	2.45	0	13.6	1.00		
	0.5		0.06	13.2	0.97		
	1.5		0.38	12.9	0.95		
	2.5		0.70	13.3	0.98		
	3.5		1.02	3.66	0.27		
	4.5		1.35	0	0		
	0	2.47	0	13.7	1.00		
	1		0.22	13.2	0.96		
2		0.54	13.2	0.96			
3		0.86	11.2	0.82			
4		1.17	0.96	0.07			
5		1.51	0	0			

TABLE AIII (CONTINUED)

Run	Charge lb.	Q^* sec.	Q	$\frac{QO}{\sqrt{F}}$	C	$\frac{C}{C_0}$	Comments	
M2-70-A	5.94	0	1.13	0	17.0	1.00	Smooth fluidization	
		2		0.16	17.1	1.00		
		4		0.32	16.5	0.97		
		6		0.49	14.4	0.85		
		8		0.66	11.8	0.69		
		10		0.82	9.1	0.54		
		15		1.24	5.2	0.31		
		20		1.65	2.5	0.15		
		25		2.07	1.23	0.072		
		0		1.13	0	17.1		1.00
		3			0.24	16.5		0.96
		5			0.41	15.0		0.88
		7			0.57	12.5		0.73
		8			0.66	10.7		0.63
		9			0.74	9.6		0.56
11	0.90	7.9	0.46					
13	1.07	5.9	0.34					
15	1.24	4.55	0.27					
M2-70-C	5.25	0	2.32		0	18.2	1.00	
		1		0.15	18.3	1.00		
		3		0.47	16.1	0.88		
		6		0.95	8.2	0.45		
		9		1.43	3.7	0.20		
		12		1.91	1.7	0.093		
		15		2.39	0.78	0.043		
		18		2.87	+ 0	+0		
		21		3.35	0	0		
		0		2.32	0	18.2	1.00	
		1.5			0.23	18.0	0.99	
		2.5			0.39	16.6	0.91	
		3.5			0.55	12.9	0.71	
		4.5			0.71	10.7	0.59	
		6			0.95	7.3	0.40	
7	1.11	5.0	0.27					
8	1.27	4.2	0.23					
9.1	1.45	2.88	0.16					
M3-70-A	6.12	0	1.16	0	16.7	1.00		
		2		0.16	16.7	1.00		
		4		0.33	15.9	0.95		
		6		0.50	13.3	0.80		
		8		0.67	11.2	0.67		
		10		0.82	8.7	0.52		
		15		1.26	5.0	0.30		
		20		1.64	2.28	0.14		
		27		2.28	0.85	0.051		

Note: M2-70-B not reported since the two runs made did not agree in timing.

TABLE AIII (CONTINUED)

Run	Charge lb.	θ^* sec.	Q	$\frac{Q\theta}{V\epsilon}$	C	$\frac{C}{C_0}$	Comments			
M3-70-A	6.12	0	1.16	0	16.6	1.00				
		2.5		0.20	16.6	1.00				
		3.5		0.29	16.5	0.99				
		4.5		0.37	15.4	0.93				
		5.5		0.45	14.0	0.84				
		6.5		0.54	12.5	0.75				
		8		0.67	10.5	0.63				
		9		0.75	9.4	0.57				
		10		0.82	8.2	0.49				
		M3-70-B	5.69	0	1.71	0	15.9	1.00	Slugging	
2				0.23	15.9	1.00				
4				0.47	13.6	0.86				
6				0.71	9.4	0.59				
8				0.95	7.0	0.44				
10				1.19	3.9	0.25				
15				1.79	2.0	0.13				
20				2.39	0.71	0.045				
25				2.98	0.4	0.025				
0	1.71			0	16.3	1.00				
2.5				0.29	15.6	0.96				
3.5				0.41	13.6	0.83				
4.5				0.53	12.0	0.74				
6				0.71	9.8	0.60				
7				0.83	8.3	0.51				
8				0.95	6.76	0.41				
9				1.07	5.7	0.35				
10				1.19	4.15	0.25				
D-37-A	3.75			1	1.18	0.15	15.6	0.97		
				3		0.48	11.2	0.70		
		6		0.47	6.4	0.40				
		9		1.46	3.5	0.22				
		12		1.95	1.8	0.11				
		15		2.44	1.0	0.062				
		18		2.94	0.6	0.037				
		24		3.91	0.45	0.028				
		0		0	16.0	1.00				
		1	1.18	0.15	15.1	0.96				
		3		0.48	11.4	0.72				
		5		0.80	7.8	0.49				
		7		1.13	4.8	0.30				
		15		2.44	1.0	0.063				
		18		2.96	0.5	0.032				
		29.5		4.81	0	0				
0		0	15.8	1.00						

TABLE AIII (CONTINUED)

Run	Charge lb.	θ^* sec.	Q	$\frac{Q\theta}{\sqrt{t}}$	C	$\frac{C}{C_0}$	Comments			
D-37-B	3.38	1	1.80	0.22	16.4	1.00				
		3		0.69	9.1	0.55				
		6		1.38	4.2	0.26				
		9		2.09	1.64	0.10				
		12		2.78	0.6	0.037				
		15		3.48	+0	0				
		18		4.18	0	0				
		21		4.89	0	0				
		0		0	16.4	1.00				
		2		1.80	0.45	10.8	0.72			
		4	0.90		5.8	0.39				
		6	1.37		3.7	0.25				
		10	2.30		1.5	0.10				
		0	0		15.0	1.00				
		1.5	0.33		10.0	0.83				
		2.5	0.56		7.9	0.65				
		0	0		12.1	1.00				
		D-37-C	3.12		1	2.44	0.26	16.0	0.94	Violent action; some slugging
					2		0.54	10.6	0.62	
				3	0.82		7.9	0.46		
4	1.09			4.9	0.29					
5	1.37			3.3	0.19					
6	1.65			2.15	0.13					
9	2.48			1.1	0.065					
12	3.31			1.0	0.059					
0	0			17.0	1.00					
1	2.44			0.26	15.3		0.96			
2				0.54	10.2	0.64				
3				0.82	6.4	0.40				
4				1.09	4.1	0.26				
6				1.65	2.15	0.13				
12				3.31	0.73	0.046				
15				4.13	0	0				
0				0	16.0	1.00				
D-37-D				2.94	1	2.91	0.39	13.2	0.72	
					2		0.80	8.4	0.46	
	3				1.21		6.3	0.34		
	4	1.62	4.1		0.22					
	5	2.02	2.6		0.14					
	6	2.43	1.5		0.082					
	9	3.66	0.54		0.029					
	12	4.89	0		0					
	0	0	18.4		1.00					

TABLE AIII (CONTINUED)

Run	Charge lb.	Q* sec.	Q	$\frac{Q_0}{\sqrt{E}}$	C	$\frac{C}{C_0}$	Comments	
D-37-D	2.94	1	2.91	0.39	12.5	0.68		
		2		0.80	7.6	0.41		
		3		1.21	6.1	0.33		
		4		1.62	3.0	0.16		
		9		3.66	0.5	0.027		
		0		0	18.4	1.00		
F-37-A	3.88	1	1.18	0.15	16.4	0.98		
		3		0.48	12.5	0.75		
		6		0.98	6.7	0.40		
		9		1.47	3.7	0.22		
		12		1.96	1.6	0.096		
		15		2.46	0.95	0.057		
		18	2.96	0.5	0.030			
		21	3.46	0.0	0.00			
		0	0	16.7	1.00			
		1	1.18	0.15	16.4	0.98		
		2		0.31	15.4	0.92		
		3		0.48	11.6	0.69		
		4		0.64	9.9	0.59		
		5		0.81	8.3	0.50		
		6		0.98	6.4	0.38		
		10		1.63	3.2	0.19		
		18		2.96	0.84	0.05		
		0		0	16.7	1.00		
		F-37-B		3.50	1	1.77	0.23	14.6
2	0.48				12.5		0.75	
3	0.73				7.5		0.45	
4	0.99				5.8		0.35	
6	1.49		3.9		0.23			
9	2.25		1.6		0.096			
12	3.00		0.75		0.045			
15	3.76		0.5		0.03			
0	0		16.7		1.00			
1	1.77		0.23		15.0	0.91		
2			0.48		11.0	0.67		
3			0.73		7.5	0.45		
4			0.99		5.9	0.36		
6			1.49		3.2	0.19		
9			2.25		1.4	0.085		
12			3.00		0.66	0.04		
15			3.76		0.45	0.027		
0			0		16.5	1.00		

TABLE AIII (CONTINUED)

Run	Charge lb.	Q* sec.	Q	$\frac{Q_0}{V\epsilon}$	C	$\frac{C}{C_0}$	Comments		
F-37-C	3.19	1	2.41	0.32	15.8	0.86			
		2		0.66	10.4	0.57			
		3		0.99	6.1	0.33			
		4		1.33	3.7	0.20			
		5		1.67	2.75	0.15			
		6		2.00	1.75	0.095			
		9		3.02	0.78	0.042			
		12		4.03	0.45	0.024			
		0	0	18.4	1.00				
		1	2.41	0.32	17.0	0.92			
		2		0.66	11.0	0.60			
		3		0.99	6.4	0.35			
		4		1.33	4.5	0.24			
		5		1.67	3.4	0.18			
		6		2.00	2.2	0.12			
		9		3.02	0.78	0.042			
		12		4.03	0.40	0.022			
		0	0.0	18.5	1.00				
		F-37-D	2.88	1	3.01	0.44	11.1	0.65	
				2		0.91	6.0	0.35	
3	1.37			4.0		0.23			
4	1.84			2.3		0.13			
6	2.76			1.1		0.064			
9	4.15			0.5		0.029			
12	5.55			0.0		0.00			
0	2.99			0		17.2	1.00		
1				0.44	14.2	0.77			
2				0.91	6.5	0.35			
3				1.37	4.6	0.25			
4				1.82	2.9	0.16			
5				2.28	1.85	0.10			
6				2.74	1.00	0.054			
9				4.12	+0.0	+0.0			
12	4.56			0.0	0.0				
0	0	18.4	1.00						
M2-37-A	3.12	0	1.18	0	16.5	1.00	Smooth Fluidization		
		1		0.14	16.4	0.99			
		3		0.44	11.8	0.72			
		6		0.90	6.70	0.41			
		9		1.36	3.82	0.23			
		12		1.82	2.28	0.14			
		15		2.28	1.48	0.072			
		18		2.74	0.69	0.042			
		21		3.20	0.51	0.031			

TABLE AIII (CONTINUED)

Run	Charge lb.	Q* sec.	Q	$\frac{QQ}{\sqrt{C}}$	C	$\frac{C}{C_0}$	Comments		
M2-37-A	3.12	0	1.18	0	16.5	1.00			
		1		0.14	15.8	0.96			
		2		0.29	14.7	0.89			
		3		0.44	12.2	0.74			
		4		0.60	9.61	0.58			
		5		0.75	8.37	0.51			
		6		0.90	6.85	0.42			
		9		1.36	4.20	0.25			
		12		1.82	2.64	0.16			
		M2-37-B		2.94	0	1.81	0	17.2	1.00
1	0.21		16.5		0.96				
2.9	0.62		10.0		0.58				
6	1.31		4.64		0.27				
9	1.97		2.00		0.12				
15	3.30		0.51		0.029				
18	3.96		+0.0		+0.00				
21	4.61		0.0		0.00				
0	1.81		0		17.1		1.00		
0.5			0.10		17.1		1.00		
2			0.43		13.4	0.78			
3			0.65		10.5	0.61			
4			0.87		7.30	0.43			
6			1.31		3.96	0.23			
7			1.53		2.63	0.15			
9			1.97		1.49	0.087			
12			2.63		0.76	0.044			
M2-37-C			2.75		0	2.37	0	18.3	1.00
	1				0.28		16.6	0.91	
	2				0.58		11.0	0.60	
	3				0.87		7.43	0.41	
	6	1.76		2.90	0.16				
	9	2.64		0.84	0.046				
	12	3.53		+0.0	+0.00				
	15	4.41		0.0	0.00				
	18	5.30		0.0	0.00				
	0	2.37		0	17.7		1.00		
	0.5			0.14	17.7	1.00			
	1.5			0.43	15.2	0.86			
	2.5			0.73	9.10	0.51			
	4			1.17	5.21	0.29			
	5			1.46	3.45	0.19			
	6			1.76	2.64	0.15			
	7	2.06		1.95	0.11				
9	2.64	1.10	0.062						

TABLE AIII (CONTINUED)

Run	Charge lb.	Q*	Q	$\frac{QO}{V}$	C	$\frac{C}{C_0}$	Comments		
M3-37-A	3.19	0	1.18	0	16.5	1.00	No slugging; some large bubbles about 3" long		
		1		0.14	16.6	1.01			
		3		0.45	13.4	0.81			
		6		0.91	7.30	0.44			
		9		1.37	3.77	0.23			
		12		1.84	1.90	0.12			
		15		2.30	1.02	0.062			
		18		2.76	0.54	0.033			
		21		3.23	+0.0	+0.00			
		0		1.18	0	16.5		1.00	
		1	0.14		16.4	0.99			
		2	0.29		15.5	0.94			
		3	0.45		13.0	0.79			
		4	0.60		10.9	0.66			
		5	0.76		9.2	0.56			
		6	0.91		7.55	0.46			
		8	1.22		4.55	0.28			
		10	1.53		2.83	0.17			
		M3-37-B	2.94		0	1.77	0	17.2	1.00
				1	0.21		16.9	0.98	
				2	0.44		14.8	0.86	
3	0.66			10.9	0.63				
6	1.34			4.18	0.24				
9	2.02			1.47	0.085				
12	2.70			0.58	0.034				
15	3.38			0.0	0.00				
18	4.06			0.0	0.00				
0	1.77			0	17.2		1.00		
1				0.21	16.9	0.98			
2				0.44	14.6	0.85			
3				0.66	9.5	0.55			
4				0.89	6.48	0.38			
5				1.12	5.10	0.30			
6				1.34	3.75	0.22			
7				1.57	2.90	0.17			
8	1.80	2.33	0.14						
M3-37-C	2.75	0	2.36	0	17.6	1.00	Slugging		
		1		0.28	17.1	0.97			
		2		0.58	13.7	0.78			
		3		0.87	8.0	0.45			
		4		1.17	4.28	0.24			
		6		1.76	2.1	0.12			
		8		2.35	1.14	0.065			
		10		2.94	0.58	0.033			
		12		3.53	+0.0	+0.00			

TABLE AIII (CONTINUED)

Run	Charge lb.	Q*	Q	$\frac{QQ}{V\epsilon}$	C	$\frac{C}{C_0}$	Comments
M3-37-C	2.75	0	2.36	0	17.6	1.00	
		1.5		0.43	14.4	0.82	
		2.5		0.73	8.1	0.46	
		3.5		1.02	5.61	0.32	
		5		1.46	3.1	0.18	
		6		1.76	2.0	0.11	
		7		2.05	1.43	0.081	
		8		2.35	1.05	0.060	
		9		2.64	0.78	0.044	
M4-37-A	3.12	0	1.23	0	16.4	1.00	Slugging
		1		0.14	16.2	0.99	
		3		0.46	13.2	0.80	
		6		0.94	7.7	0.47	
		9		1.41	3.73	0.23	
		12		1.89	1.57	0.096	
		15		2.36	0.73	0.045	
		18		2.84	+0.0	+0.00	
		21		3.32	0.0	0.00	
		0	1.23	0	16.5	1.00	
		1		0.14	16.4	0.99	
		2		0.30	15.9	0.96	
		3		0.46	13.4	0.81	
		4		0.62	9.5	0.58	
		5		0.78	8.5	0.52	
		6		0.94	7.2	0.44	
		8		1.26	4.7	0.28	
		10		1.57	2.88	0.17	
		M4-37-B		2.81	0	1.71	
1	0.21		15.9		0.96		
2	0.44		14.7		0.89		
3	0.67		9.75		0.59		
4	0.91		7.62		0.47		
6	1.37		3.71		0.23		
9	2.06		1.30		0.078		
12	2.74		0.50		0.031		
15	3.43		0.0		0.00		
0	1.77		0		16.5	1.00	
1			0.21		16.4	0.99	
2			0.44		13.0	0.79	
3			0.67		9.9	0.60	
4			0.91		6.86	0.42	
5			1.14		5.26	0.32	
6			1.37		4.00	0.24	
7		1.60	2.75	0.17			
8	1.83	1.73	0.11				

TABLE AIII (CONTINUED)

Run	Charge lb.	θ^* sec.	Q	$\frac{Q\theta}{VZ}$	C	$\frac{C}{C_0}$	Comments		
M2-35L-A	6.81	1	2.74	0.11	18.4	0.98			
		2		0.27	14.4	0.76			
		3		0.43	11.1	0.59			
		6		0.91	7.3	0.39			
		9		1.39	4.65	0.25			
		12		1.88	3.0	0.16			
		15		2.36	1.78	0.095			
		18		2.84	1.28	0.068			
		0		0	18.8	1.00			
		1	2.74	0.11	18.4	0.97			
		3		0.43	12.9	0.68			
		5		0.75	7.98	0.42			
		12		1.88	3.15	0.17			
		18		2.84	1.33	0.07			
		21		3.32	0.76	0.04			
		24		3.80	0.52	0.027			
		27		4.29	0.48	0.025			
		0		0	18.9	1.00			
		M2-35L-B	6.31	1	4.14	0.19	15.5	0.90	
				3		0.67	8.4	0.49	
				6		1.38	4.6	0.27	
				9		2.10	1.86	0.11	
				12		2.82	0.98	0.057	
				15		3.53	0.54	0.031	
				18		4.24	$\pm 0.03 \pm$	0.017	
				21		4.95	0.0	0.00	
				0		0	17.3	1.00	
1	4.14			0.19	17.8	0.89			
2				0.43	13.0	0.65			
3				0.67	9.5	0.47			
4				0.90	7.45	0.37			
5				1.14	5.6	0.28			
6				1.38	4.75	0.24			
10				2.34	1.97	0.098			
15				3.53	0.76	0.038			
0				0	20.0	1.00			
M2-35L-C	6.12			1	5.47	0.25	15.0	0.74	
				2		0.55	11.2	0.55	
				3		0.85	7.5	0.37	
				6		1.75	3.42	0.17	
				9		2.64	1.35	0.067	
				12		3.53	0.76	0.038	
				15		4.44	0.5	0.025	
				18		5.34	0.4	0.02	
				0		0	20.2	1.00	

TABLE AIII (CONTINUED)

Run	Charge lb.	Q* sec.	Q	$\frac{QQ}{\sqrt{C}}$	C	$\frac{C}{C_0}$	Comments		
M2-35L-C	6.12	0.5	5.47	0.10	19.5	0.97			
		2		0.55	11.5	0.57			
		3		0.85	8.2	0.41			
		4		1.15	5.6	0.28			
		5		1.44	4.3	0.21			
		6		1.75	3.4	0.17			
		7		2.04	2.5	0.12			
		8		2.34	1.8	0.09			
		0		0	20.2	1.00			
		M2-35L-D		5.75	1	6.83	0.38	13.7	0.66
3	1.25		5.2		0.25				
4	1.69		3.9		0.19				
6	2.56		1.89		0.09				
9	3.89		0.66		0.032				
12	5.18		+0.0		+0.00				
15	6.51		0.0		0.00				
0	0		20.8		1.00				
0.6	6.85		0.21		15.7		0.80		
2			0.82		8.0		0.41		
3			1.25		5.4	0.27			
4			1.69		3.5	0.18			
5			2.13		2.26	0.11			
6			2.56		1.54	0.08			
7			3.00		1.13	0.057			
8			3.43		0.84	0.043			
0			0		19.7	1.00			
M3-35L-A			7.00		1	2.64	0.096	19.6	1.00
	3				0.38		14.0	0.71	
	6				0.80		8.6	0.44	
	9	1.22		5.47	0.29				
	12	1.65		3.63	0.18				
	15	2.0		2.50	0.13				
	18	2.45		1.78	0.09				
	21	2.90		1.09	0.056				
	0	0		19.6	1.00				
	1	2.64		0.096	19.2		0.98		
	2			0.23	16.8	0.86			
	3			0.38	13.0	0.66			
	7			0.94	6.8	0.35			
	15			2.06	2.33	0.12			
	21			2.90	0.98	0.05			
	24			3.32	0.64	0.032			
	27			3.74	0.56	0.029			
	0			0	19.6	1.00			

TABLE AIII (CONTINUED)

Run	Charge lb.	Q* sec.	Q	$\frac{QQ}{VE}$	C	$\frac{C}{C_0}$	Comments	
M3-35L-A	7.06	0	2.64	0	19.7	1.00		
		1		0.10	18.4	0.93		
		3		0.37	13.8	0.70		
		6		0.80	7.8	0.40		
		9		1.22	4.7	0.24		
		12		1.64	3.2	0.16		
		15		2.07	2.0	0.10		
		18		2.52	1.3	0.066		
		0		2.64	0	19.5	1.00	
		2			0.24	17.5	0.90	
		4			0.52	12.0	0.62	
		6			0.80	7.5	0.38	
		12			1.65	3.89	0.20	
		18			2.52	1.68	0.086	
		24			3.35	0.93	0.048	
	30	4.18	0.69		0.035			
	M3-35L-B	5.88	1		3.94	0.18	16.7	0.91
			3	0.64		8.2	0.45	
			6	1.32		4.65	0.25	
			9	2.02		1.9	0.10	
			12	2.70		1.28	0.07	
15			3.39	0.68		0.037		
18			4.07	± 0.4		± 0.02		
21			4.80	± 0.0		± 0.0		
0			3.94	0		18.3	1.00	
1				0.18		16.8	0.92	
2				0.41		11.1	0.61	
3				0.64		9.3	0.51	
4				0.87		6.6	0.36	
5				1.10		5.2	0.29	
7				1.56		3.6	0.20	
9		2.02		2.32	0.13			
12		2.70		1.43	0.079			
0		6.38	0	18.2	1.00			
0			4.1	0	17.9	1.00		
3				0.67	9.6	0.54		
6				1.39	4.3	0.24		
9	2.12			2.3	0.13			
12	2.84			1.16	0.065			
15	3.56			0.64	0.036			
18	4.28			± 0.3	± 0.017			
21	5.01			0.0	0.00			

TABLE AIII (CONTINUED)

Run	Charge lb.	θ^* sec.	Q	$\frac{Q\theta}{\sqrt{z}}$	C	$\frac{C}{\sigma_0}$	Comments		
M3-35L-B	6.38	0	4.1	0	17.8	1.00			
		1		0.19	17.3	0.97			
		2		0.43	12.5	0.70			
		3		0.67	8.6	0.48			
		4		0.92	6.8	0.38			
		6		1.39	4.05	0.23			
		8		1.87	2.9	0.16			
		14		3.32	1.05	0.059			
		M3-35L-C		6.12	0	5.37	0	18.7	1.00
1	26		16.5		0.88				
3	88		7.35		0.39				
6	1.81		2.92		0.16				
9	2.74		1.19		0.06				
12	3.66		0.62		0.03				
15	4.59		+0.0		+0.00				
18	5.54		0.0		0.00				
0	5.37		0		18.9		1.00		
1			0.26		16.9	0.89			
2			0.57		11.0	0.58			
3			0.88		7.4	0.39			
4			1.19		5.78	0.31			
5			1.50		3.8	0.20			
6			1.81		2.89	0.15			
8			2.42		1.6	0.08			
M3-35L-D			5.62		0	6.82	0	18.3	1.00
	1				0.35		13.2	0.72	
	2	0.74		7.95	0.43				
	3	1.13		5.5	0.30				
	6	2.32		1.88	0.10				
	9	3.50		0.56	0.03				
	12	4.67		0.0	0.00				
	15	5.84		0.0	0.00				
	0	6.82		0	18.2		1.00		
	0.5			0.15	17.8	0.98			
	1.5			0.54	12.0	0.66			
	2.5			0.94	6.8	0.37			
	4			1.53	3.81	0.21			
	5			1.92	2.3	0.13			
	6			2.32	1.73	0.095			
	7			2.71	1.19	0.065			
8	3.10	1.1	0.06						

TABLE AIII (CONTINUED)

Run	Charge lb.	Q* sec.	Q	$\frac{Q_0}{V_e}$	C	$\frac{C}{C_0}$	Comments
13-35L-A R = + 1-5/8	22.25	0	2.52	0	19.1	1.00	4" Bubbles Slight static
		1		0.16	19.0	1.00	
		3		0.64	12.1	0.63	Radius Position + = North - = South
		6		1.36	5.8	0.30	
		9		2.08	2.29	0.12	
		12		2.80	1.1	0.058	
		15		3.52	0.64	0.03	
		18		4.24	+ 0.4	+ 0.02	
		21		4.95	+ 0.0	+ 0.0	
R = 0		0	2.52	0	18.8	1.00	To determine effect of radius of sampling
		1		0.16	18.8	1.00	
		3		0.64	14.1	0.75	
		6		1.36	5.5	0.29	
		9		2.08	1.9	0.10	
		12		2.80	1.05	0.06	
		15		3.52	0.3	+ 0.02	
		18		4.24	0.0	0.00	
		21		4.95	0.0	0.00	
R = 0		0	2.52	0	19.0	1.00	
		1		0.16	19.6	1.03	
		3		0.64	11.9	0.63	
		6		1.36	5.3	0.28	
		9		2.08	2.29	0.12	
		12		2.80	1.1	0.06	
		15		3.52	+ 0.4	+ 0.02	
		18		4.24	0.0	0.00	
		21		4.95	0.0	0.00	
R = + 1-5/8		0	2.51	0	18.3	1.00	
		1		0.16	18.3	1.00	
		3		0.64	9.7	0.53	
		6		1.36	4.9	0.26	
		9		2.07	1.92	0.10	
		12		2.79	0.78	0.04	
		15		3.51	+ 0.0	+ 0.00	
		18		4.22	0.0	0.00	
		21		4.95	0.0	0.00	
R = + 1-1/8		0	2.51	0	18.4	1.00	
		1		0.16	19.0	1.03	
		3		0.64	11.3	0.61	
		6		1.36	5.9	0.32	
		9		2.07	2.6	0.14	
		12		2.79	1.07	0.06	
		15		3.51	+ 0.4	+ 0.02	
		18		4.22	0.0	0.00	
		21		4.95	0.0	0.00	

TABLE AIII (CONTINUED)

Run	Charge lb.	Q* sec.	Q	$\frac{QQ}{V\epsilon}$	C	$\frac{C}{C_0}$	Comments
13-35L-A R = -1-5/8	22.25	0	2.51	0	18.2	1.00	
		1		0.16	18.4	1.01	
		3		0.64	13.0	0.72	
		6		1.36	5.47	0.30	
		9		2.07	1.8	0.10	
		12		2.79	0.73	0.04	
		15		3.51	+0.0	+0.00	
		18		4.22	0.0	0.00	
		13-35L-A $C_0 = 11.5\%$ $C_0 = 19.1\%$ $C_0 = 24.9\%$		21.69	0	2.59	0
1	0.17		11.4		0.99		
2	0.41		10.9		0.95		
3	0.64		7.7		0.67		
6	1.38		2.7		0.23		
9	2.10		1.29		0.11		
12	2.82		0.5		0.04		
15	3.54		0.0		0.00		
18	4.27		0.0		0.00		
	2.59		0	0	19.1	1.00	
			1	0.17	18.1	0.95	
			2	0.41	16.7	0.88	
			3	0.64	11.3	0.59	
			6	1.38	5.3	0.28	
			9	2.10	1.86	0.10	
			12	2.82	0.8	0.04	
			15	3.54	± 0.4	± 0.02	
			18	4.27	0.0	0.00	
	2.59	0	0	24.9	1.00		
		1	0.17	25.0	1.00		
		2	0.41	22.3	0.89		
		3	0.64	16.3	0.65		
		6	1.38	7.4	0.30		
		9	2.10	2.9	0.12		
		12	2.82	1.07	0.04		
		15	3.54	0.6	0.02		
		18	4.27	0.0	0.00		

TABLE AIII (CONTINUED)

Run	Charge lb.	θ^* sec.	Q	$\frac{Q\theta}{VZ}$	C	$\frac{C}{C_0}$	Comments
0-35L-A	0.0	0	2.68	0	18.4	1.00	No solids
		2		0.24	18.4	1.00	
		4		0.51	17.8	0.97	Re = 915
		6		0.79	16.1	0.88	
		7		0.92	13.5	0.73	
		8		1.07	3.91	0.21	
		9		1.20	+0.0	+0.00	
		10		1.35	0.0	0.00	
		0	2.68	0	18.4	1.00	
		2		0.24	18.6	1.01	
		3		0.37	18.3	1.00	
		4		0.51	18.1	0.98	
		5		0.65	16.8	0.91	
		6.5		0.86	15.2	0.83	
		7.5		1.00	8.1	0.44	
		8.5		1.14	0.7	0.04	
		9.5		1.27	0.0	0.00	

VII APPENDIX, D, Summary of Data and Calculated Values
(continued)

5. Semi-logarithmic Graphs of Residence-Time Data

The data of the residence-time studies are plotted on semi-logarithmic coordinates in Figures 47, 49, 51, and Figures A38 through A50 which follow.

FIGURE A38

RESIDENCE-TIME DATA: NO. 7 GLASS BEADS

Runs	u_0	S	I
○ 7-37-A	0.38	8 = 7.4	I = 0.87
△ 7-37-C	0.77		
□ 7-37-D	0.94	8 = 2.4	I = 0.56
▽ 7-37-E	1.14		
○ 7-37-F	1.32		

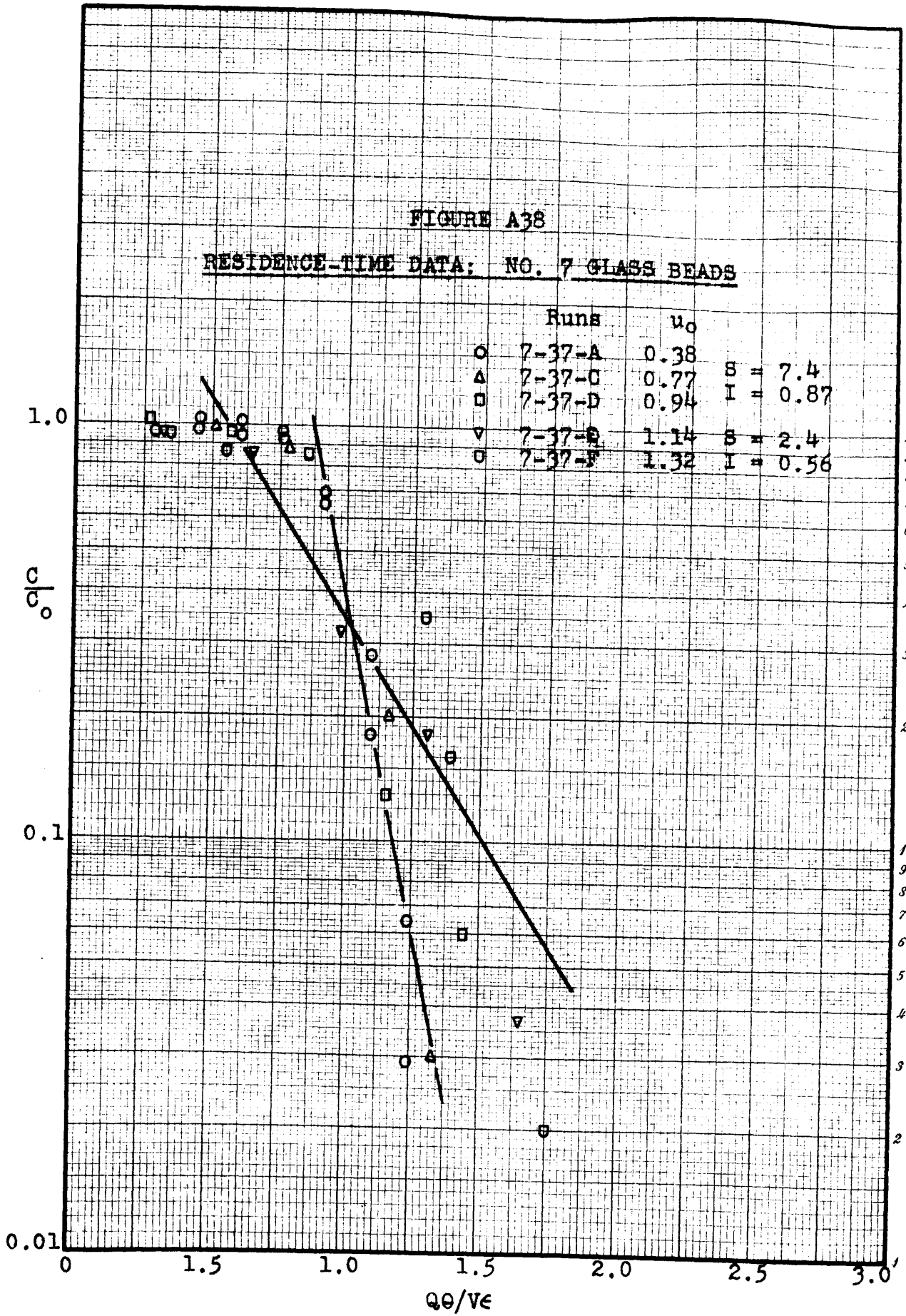


FIGURE A39

RESIDENCE TIME DATA: NO. 9 GLASS BEADS

Runs	u_0	$S =$	$I =$
○ 9-37-A	0.37	3.7	
▽ 9-37-B	0.57		0.77
△ 9-37-C	0.78		

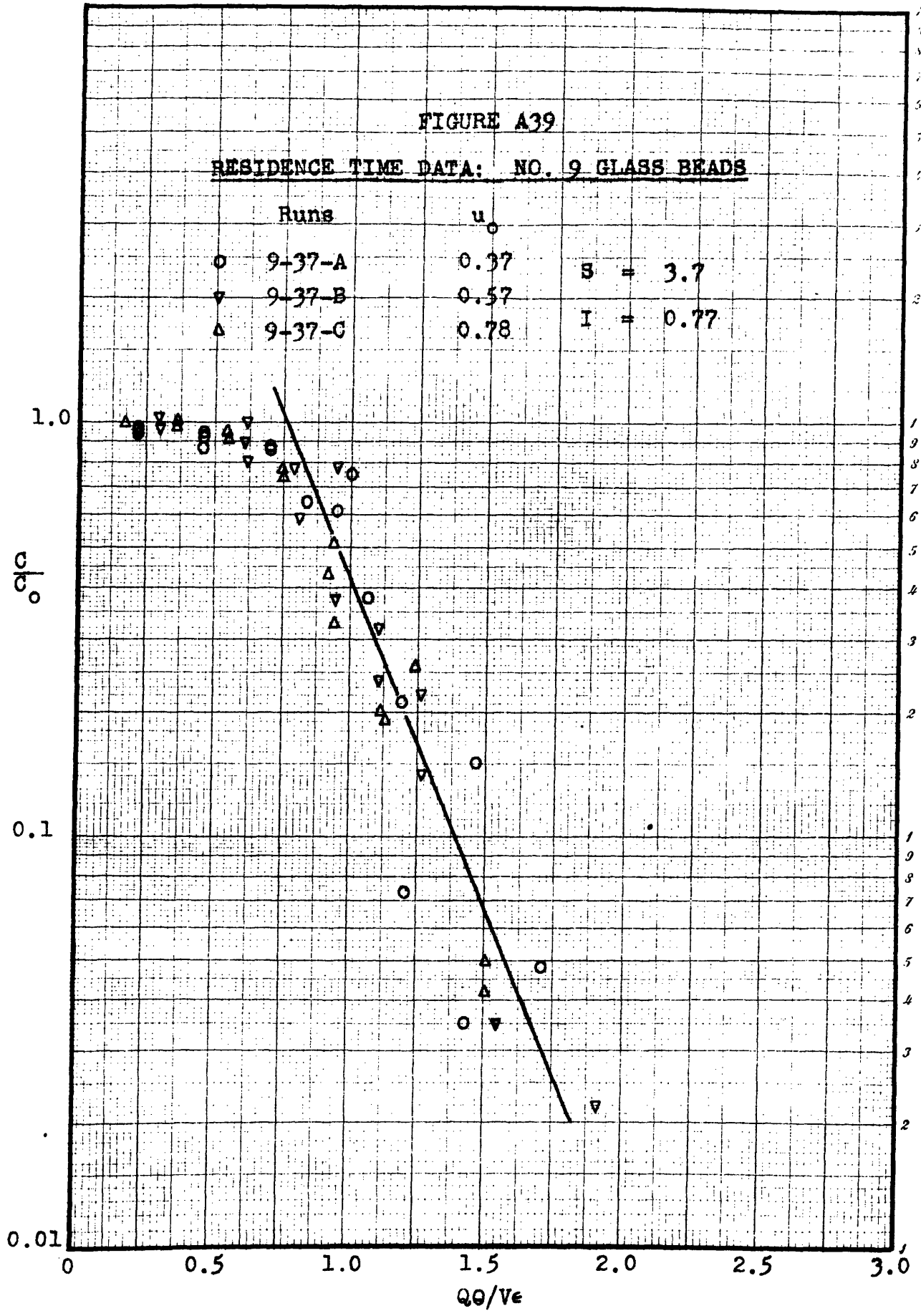


FIGURE A40

RESIDENCE-TIME DATA: NO. 11 GLASS BEADS

Runs	u_0	$S = 1.95$	$I = 0.48$
○ 11-37-A	0.39		
▽ 11-37-B	0.58		
△ 11-37-C	0.78		

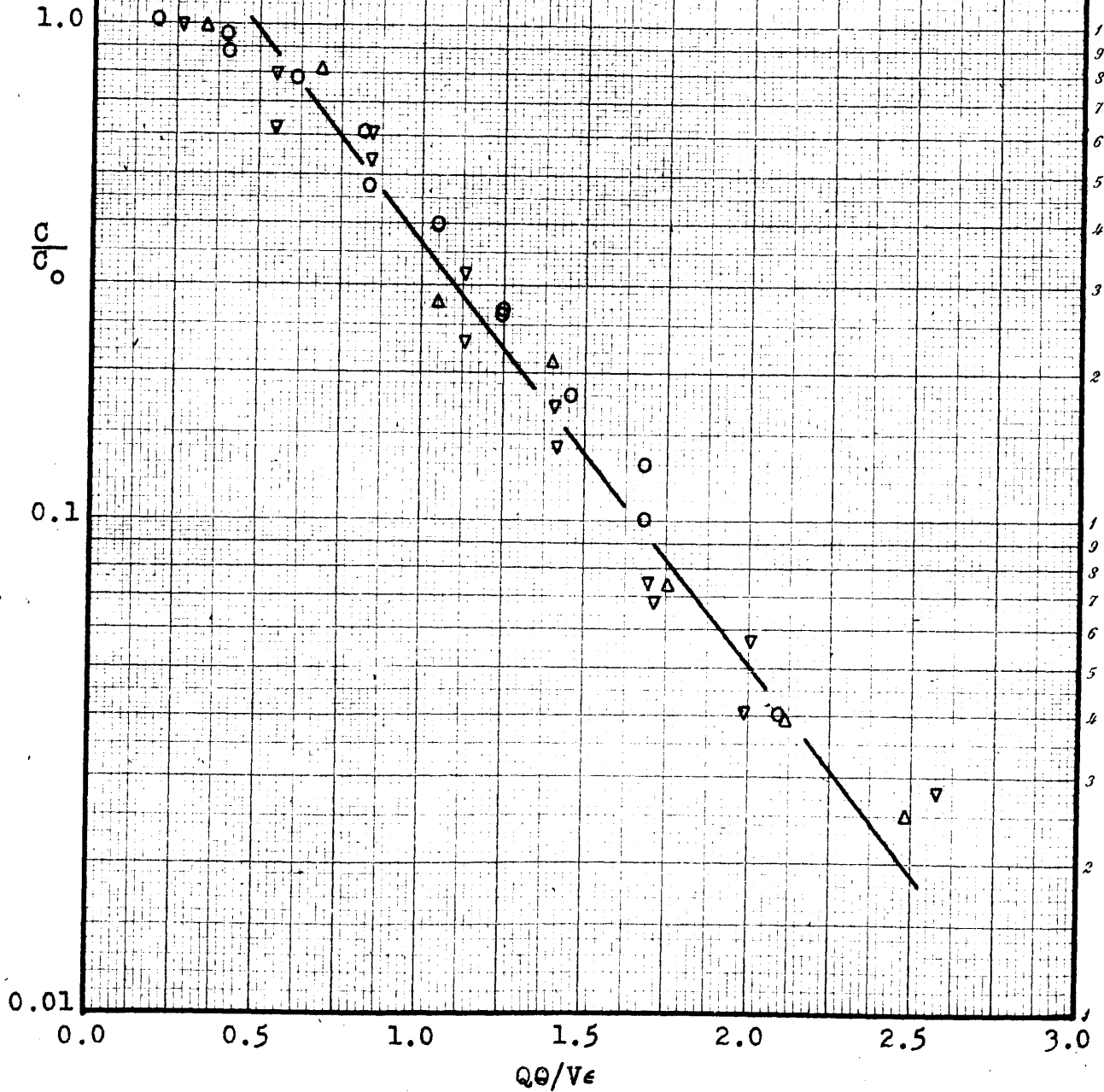


FIGURE A41

RESIDENCE-TIME DATA: NO. 13 GLASS BEADS

	Runs	u_0	
○	13-37-A	0.39	
▽	13-37-B	0.59	$S = 1.77$
△	13-37-C	0.79	$I = 0.38$
□	13-37-D	1.00	

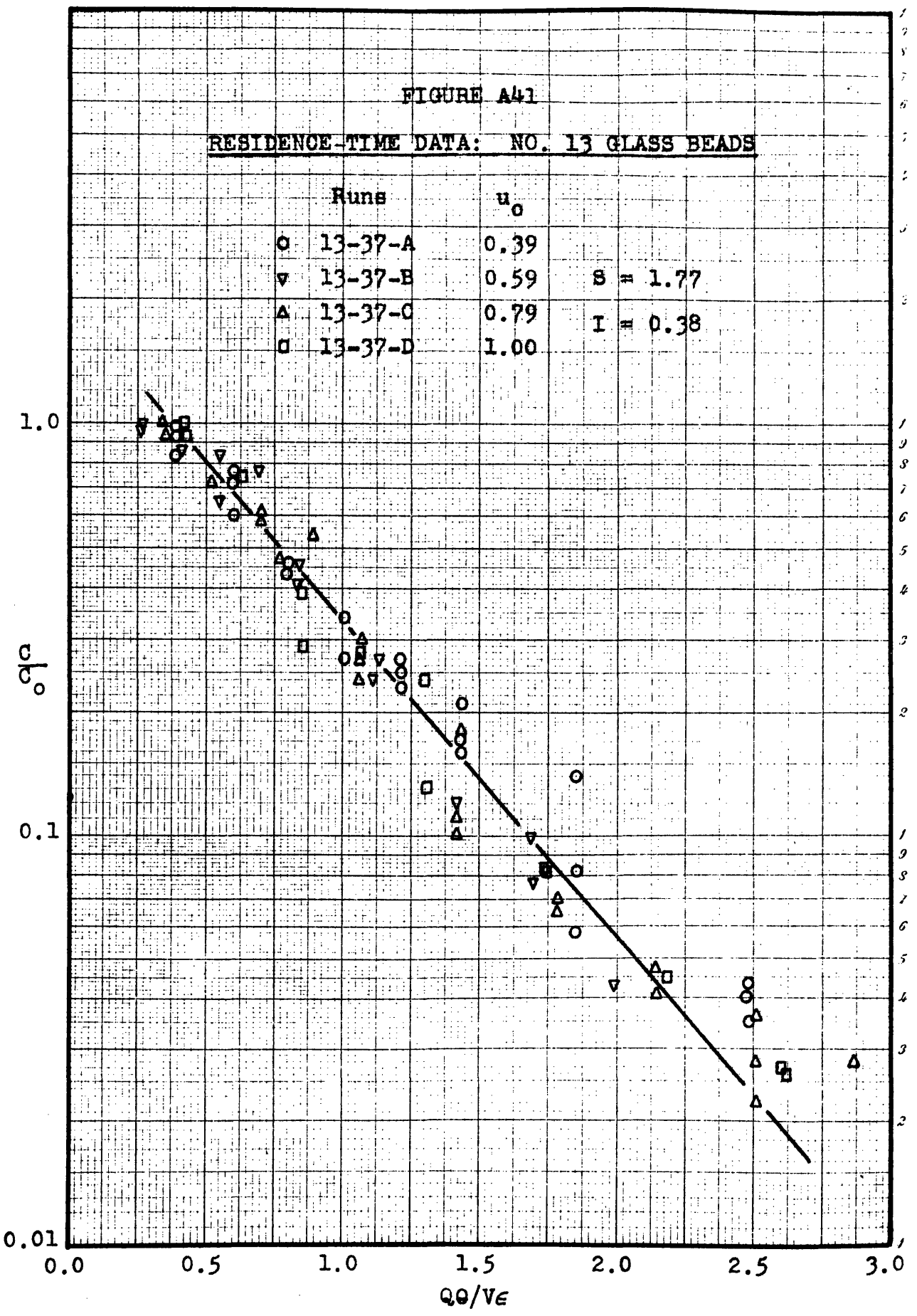


FIGURE A42

RESIDENCE-TIME DATA: NO.15 GLASS BEADS

Runs	u_o	
○ 15-35L-A	0.39	$S = 1.20$ $I = 0.22$
▽ 15-35L-B	0.61	
□ 15-35L-D	1.0	

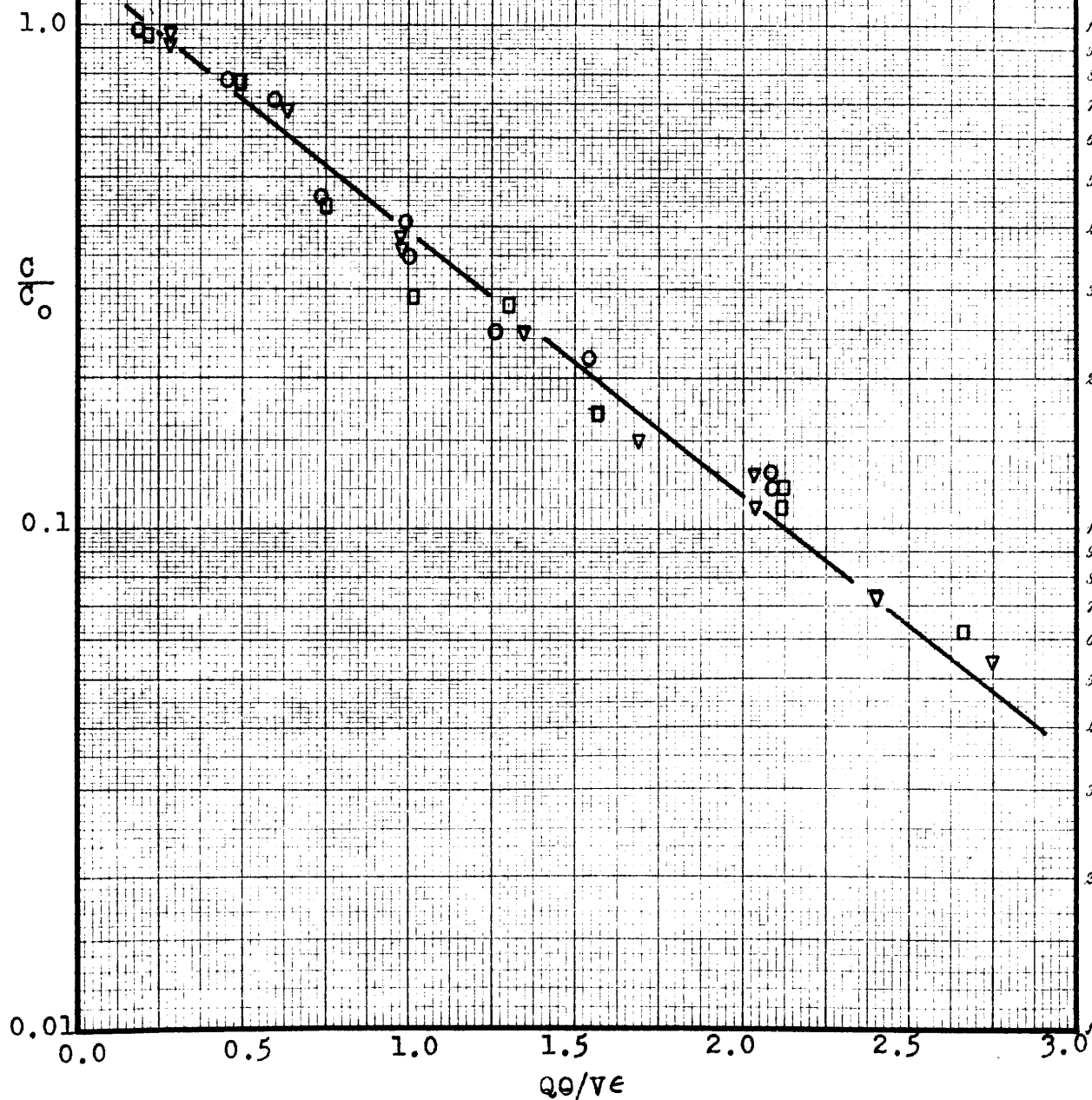


FIGURE A43

RESIDENCE-TIME DATA: NO. 13 GLASS BEADS

Runs	u_0	
○ 13-35L-A	0.39	
▽ 13-35L-B	0.61	$B = 1.15$
△ 13-35L-C	0.78	$I = 0.28$
□ 13-35L-D	1.0	

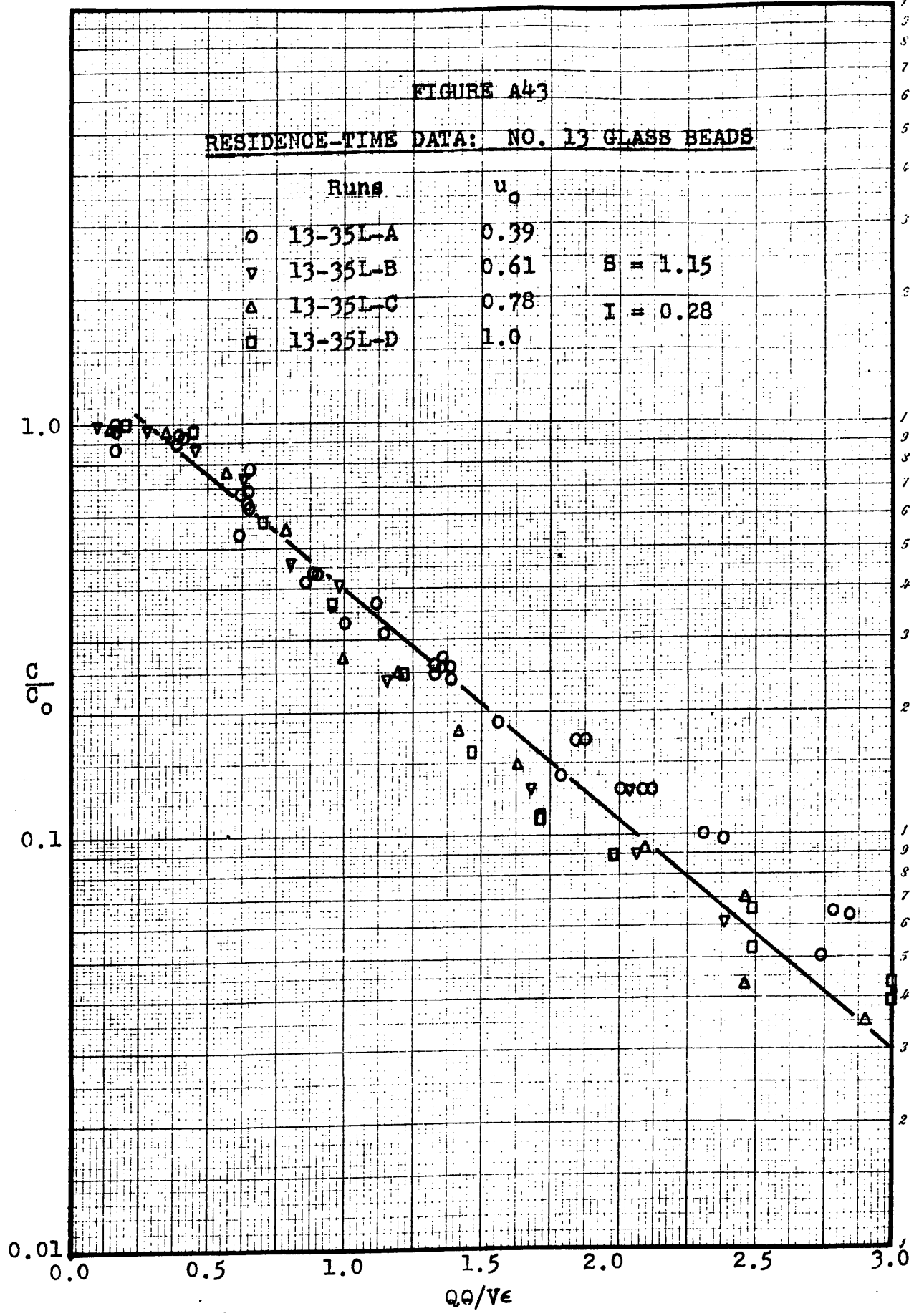


FIGURE A44

RESIDENCE-TIME DATA: MICROSPHERES, M3

Runs	u_0	$S =$	$I =$
○ M3-70-A	0.39	1.47	
▽ M3-70-B	0.58		0.36

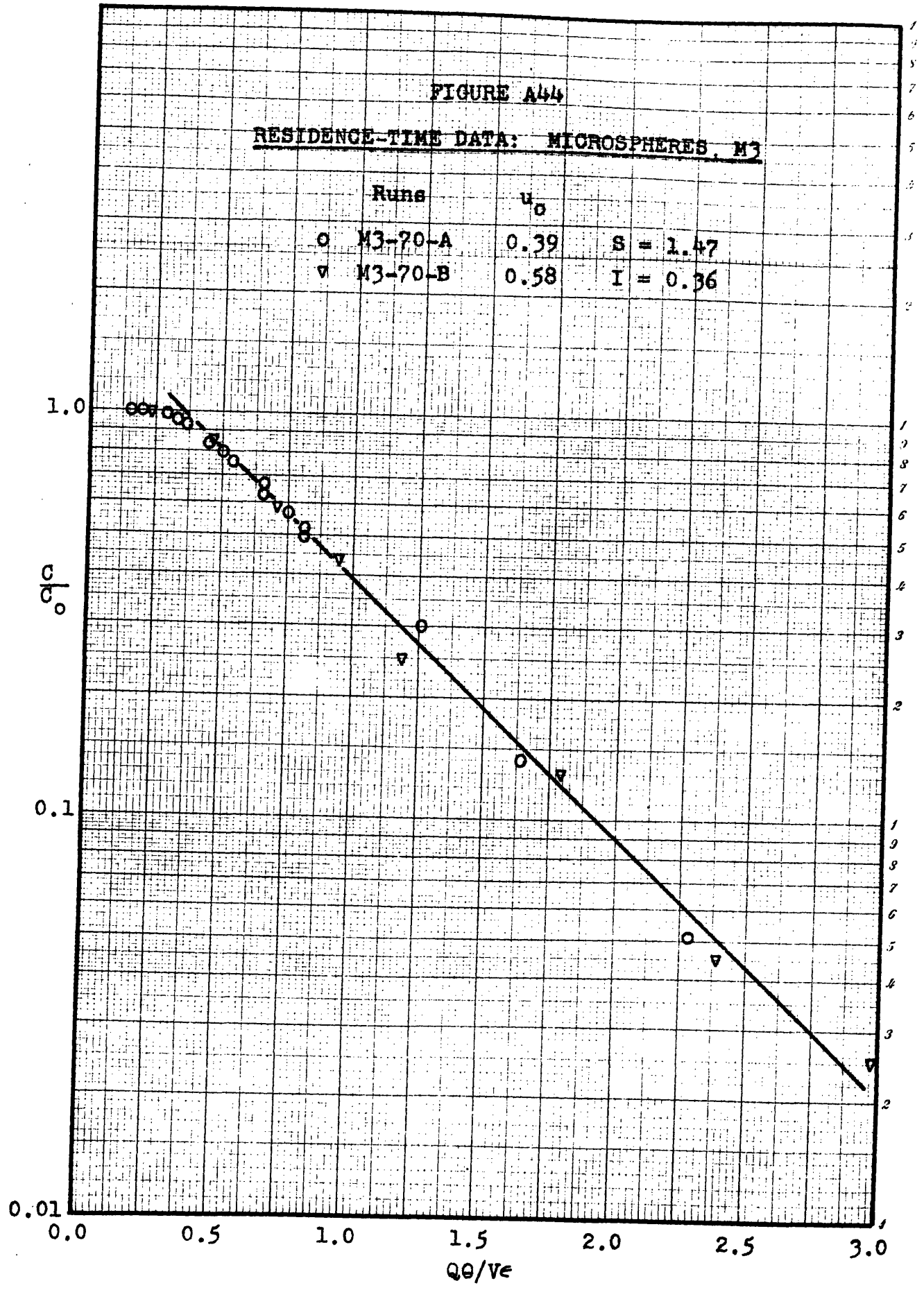


FIGURE A45

RESIDENCE-TIME DATA: MICROSPHERES, D

Runs	u_0	$S = 1.20$	$I = 0.15$
○ D-37-A	0.40		
▽ D-37-B	0.62		
△ D-37-C	0.83		
□ D-37-D	0.99		

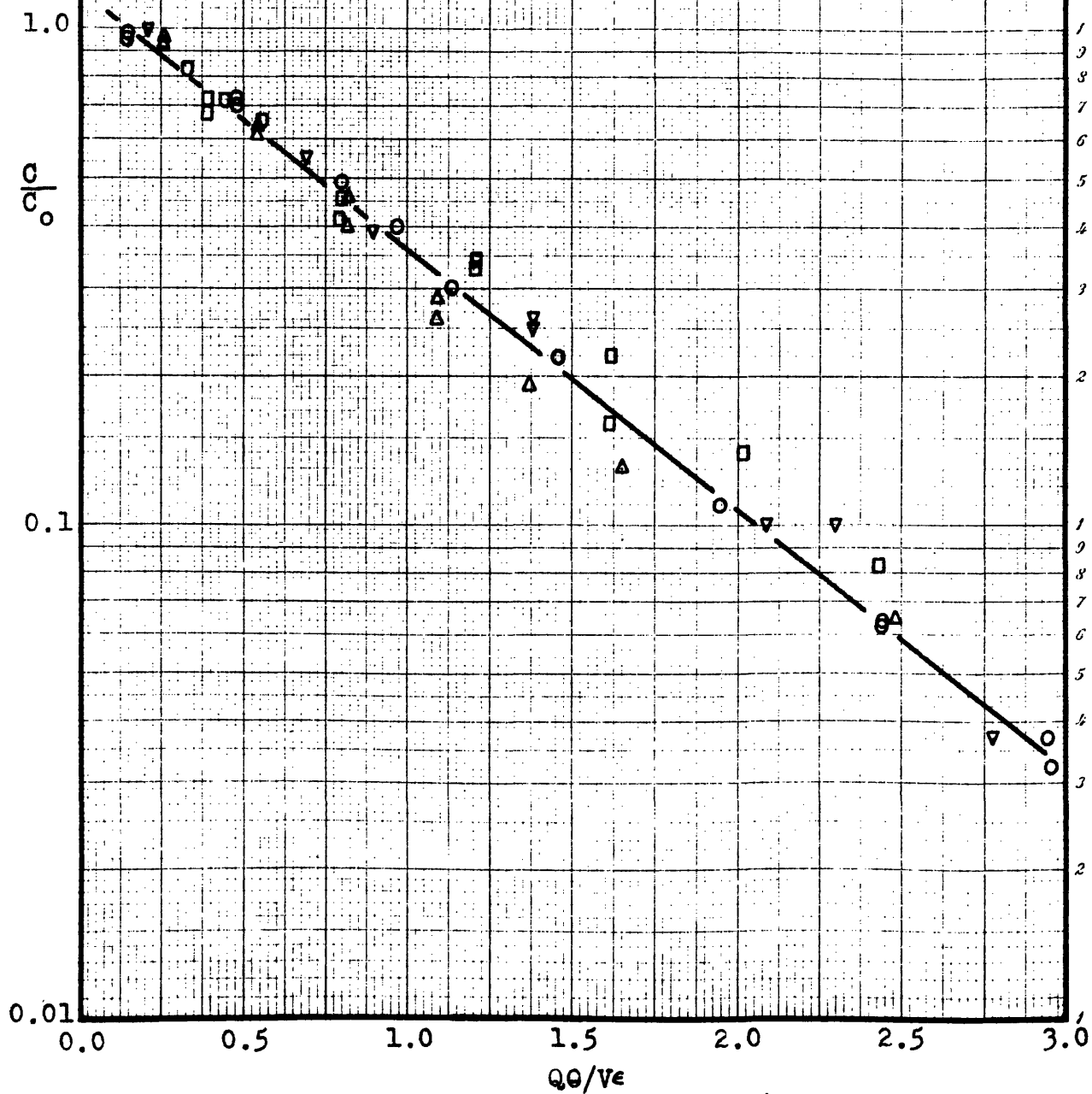


FIGURE A46

RESIDENCE-TIME DATA: MICROSPHERES, F

Runs	α_0	
○ F-37-A	0.40	
▽ F-37-B	0.61	S = 1.22
△ F-37-C	0.82	I = 0.16
□ F-37-D	1.02	

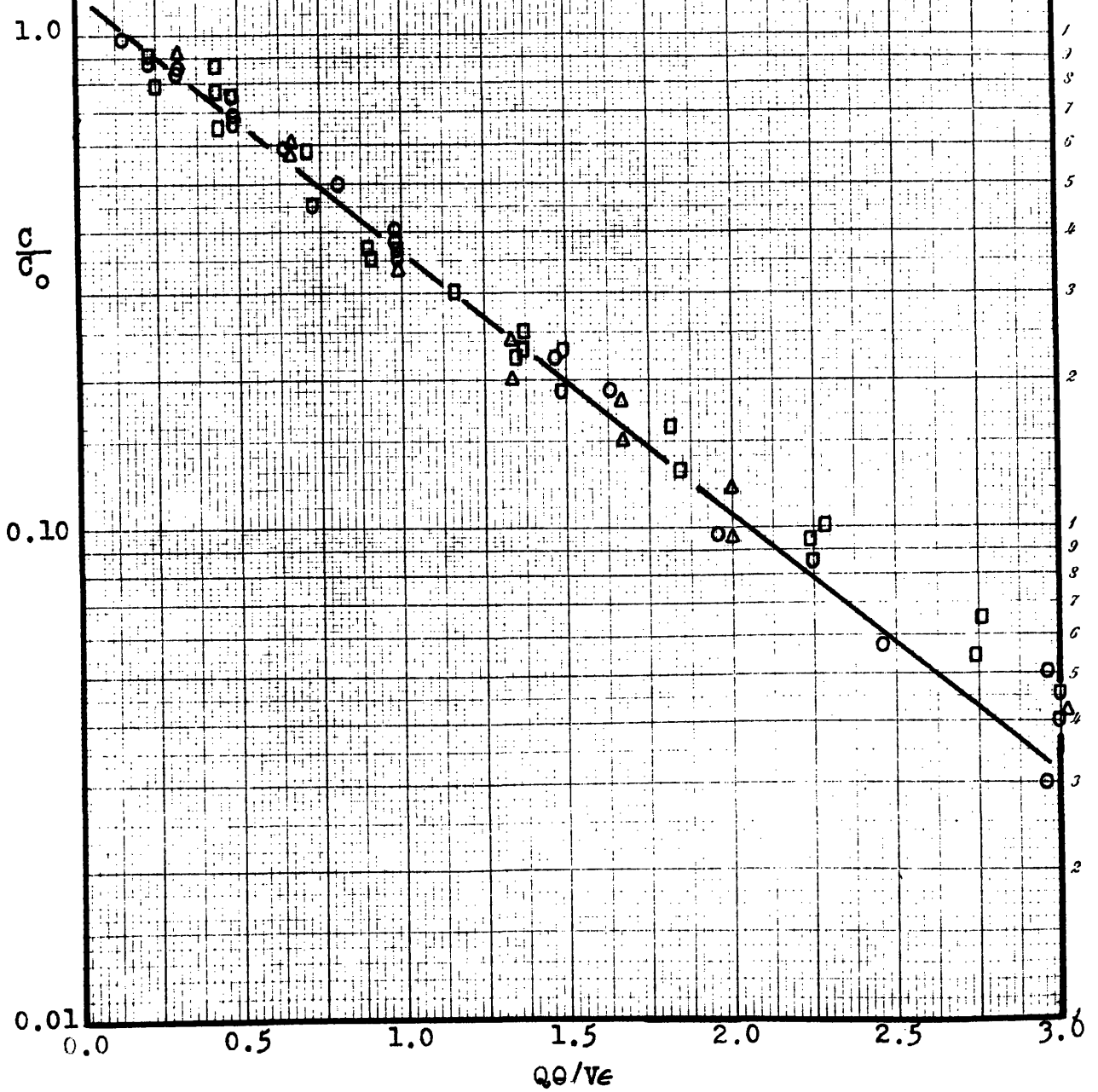


FIGURE A47

RESIDENCE TIME DATA: MICROSPHERES, M2

Runs	u_0	
○ M2-37-A	0.40	S = 1.25 I = 0.17
▽ M2-37-B	0.61	
△ M2-37-C	0.81	

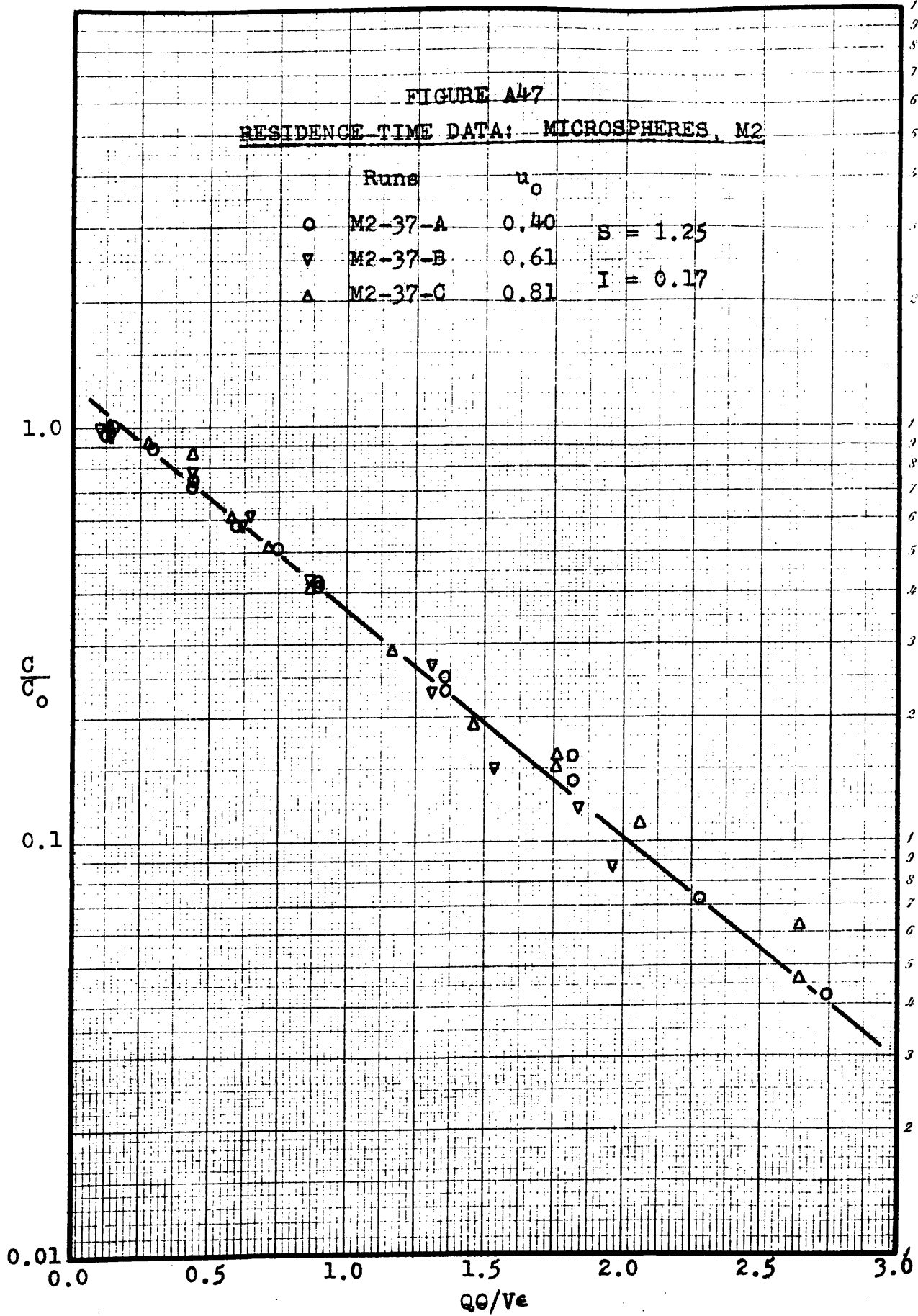


FIGURE A48

RESIDENCE-TIME DATA; MICROSPHERES, M3

Runs	u_0	$S = 1.32$	$I = 0.22$
○ M3-37-A	0.40		
▽ M3-37-B	0.60		
△ M3-37-C	0.81		

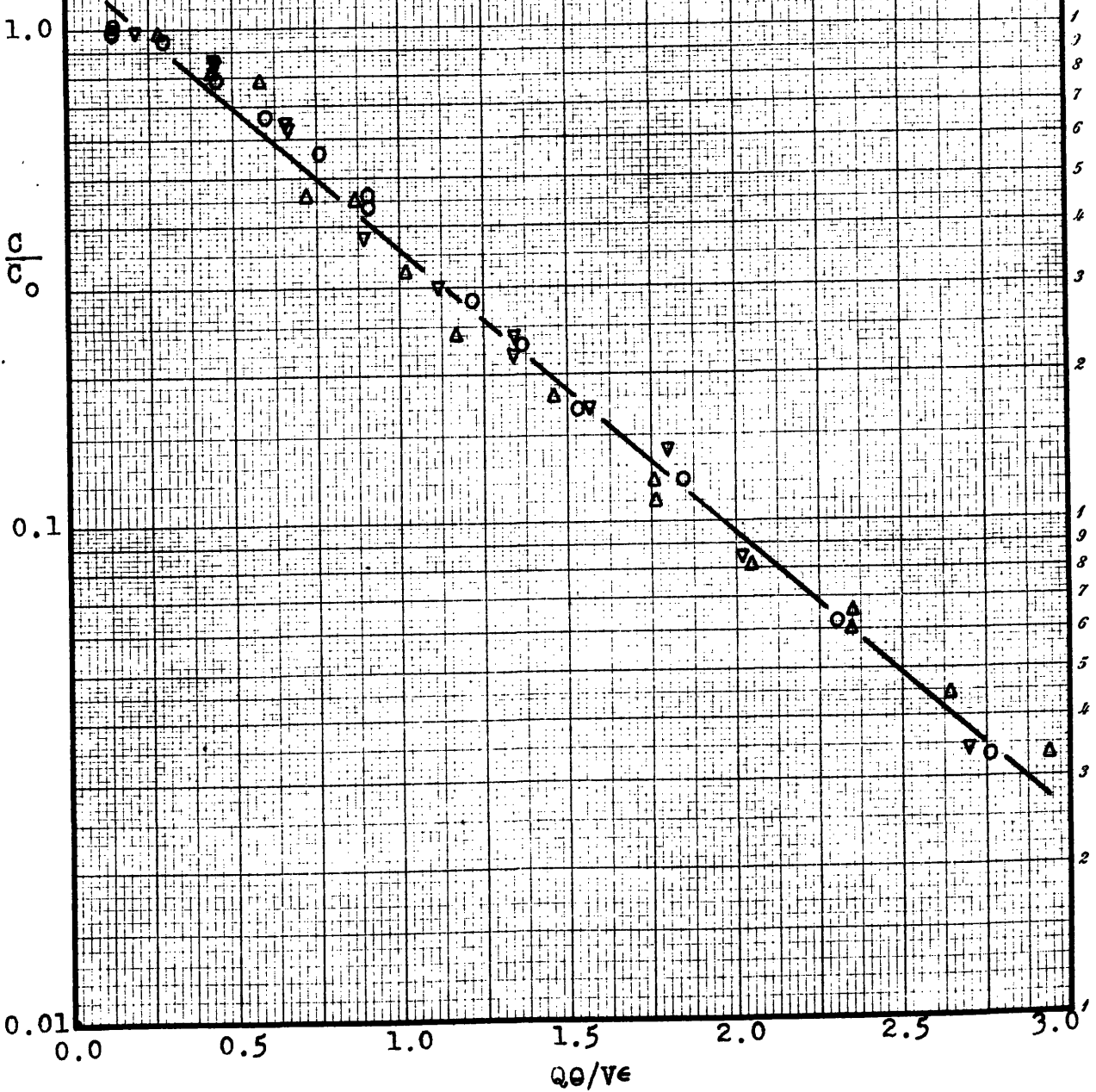


FIGURE A49

RESIDENCE-TIME DATA: MICROSPHERES, M4

Runs	u_0	
○ M4-37-A	0.42	$B = 1.44$
▽ M4-37-B	0.60	$I = 0.33$

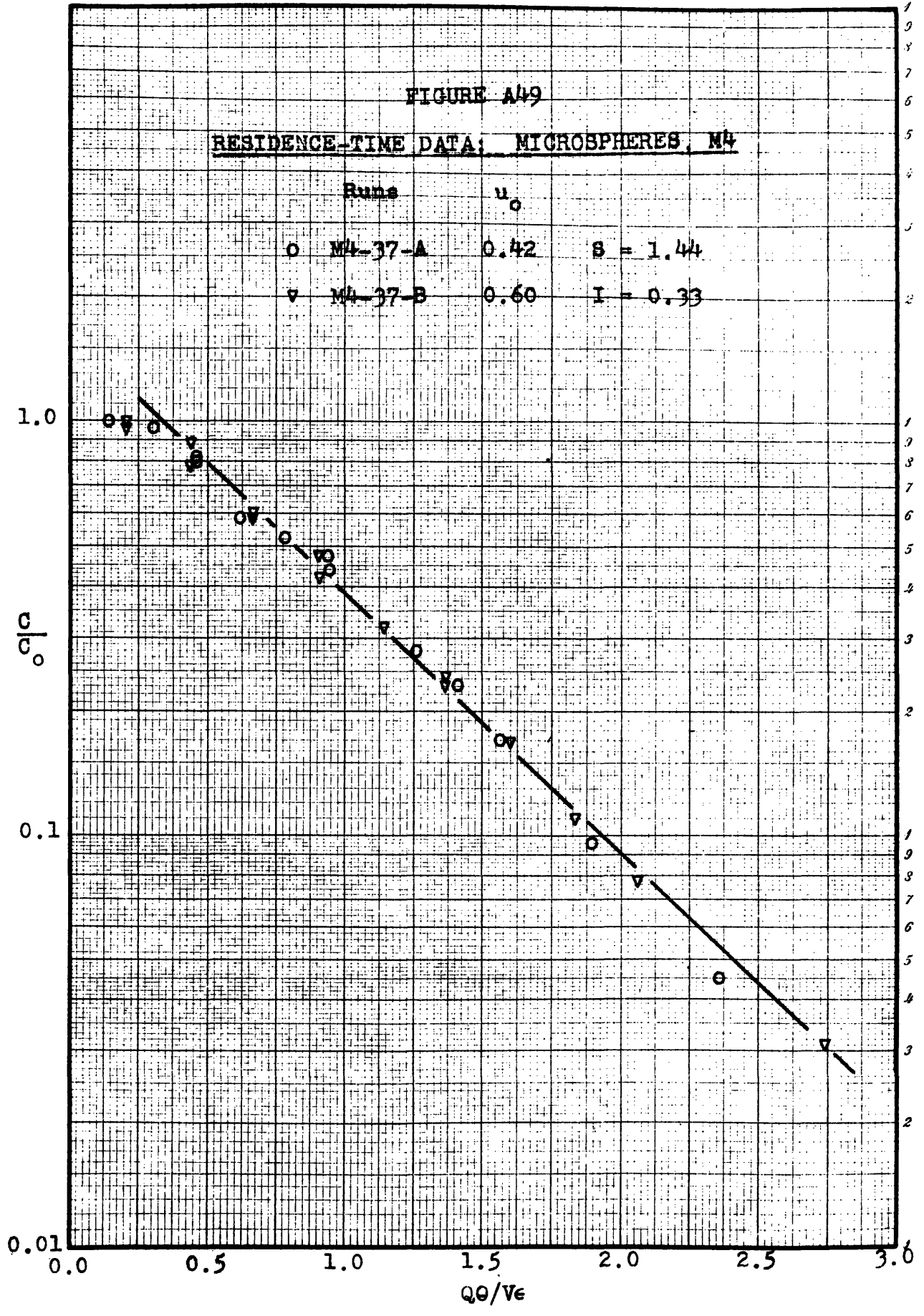
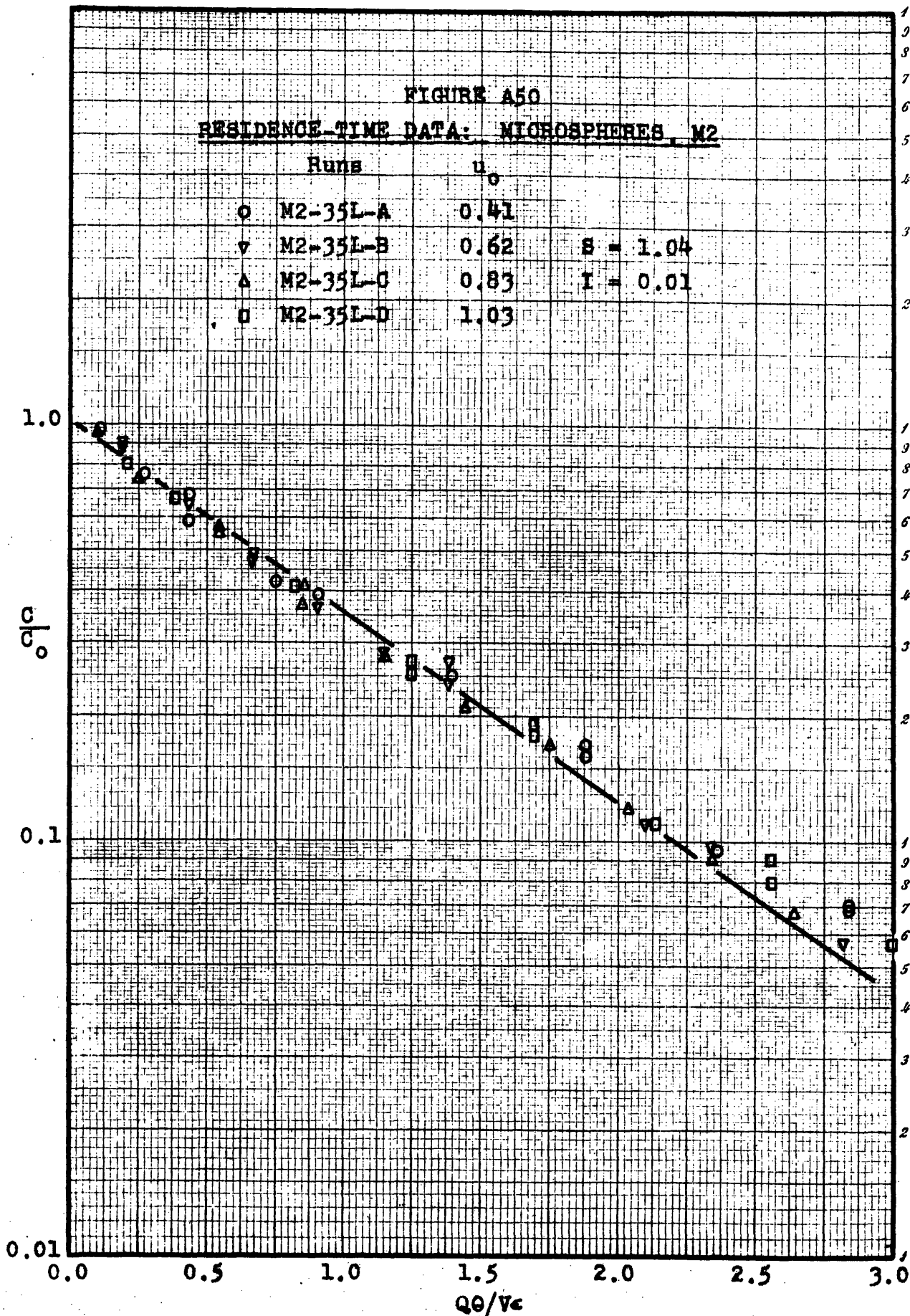


FIGURE A50

RESIDENCE-TIME DATA: MICROSPHERES, M2

Runs	u_0	
○ M2-35L-A	0.41	
▽ M2-35L-B	0.62	$S = 1.04$
△ M2-35L-C	0.83	$I = 0.01$
□ M2-35L-D	1.03	



E. Location of Original Data

The original data upon which this thesis is based may be found in notebooks on file with Prof. E. R. Gilliland at the Department of Chemical Engineering, Massachusetts Institute of Technology.

F. Nomenclature

- C concentration
- C_0 initial concentration
- C_f exit concentration
- C^* concentration of reactant for conditions of piston flow
- D diameter of bed
- D_p diameter of particle
- D_v molecular diffusivity
- E back-mixing eddy diffusivity
- E_m eddy diffusivity
- F probability density; $\int_M^N F d(Q\theta/V\epsilon) =$ fraction of entering gas which leaves between $Q\theta/V\epsilon = M$ and N
- I intercept of residence-time data on semi-logarithmic coordinates
- $J_D \frac{k_G p_{BM} M_M}{\mu \rho} \left(\frac{\mu_f}{\rho_D} \right)^{2/3}$
- k reaction rate constant
- k' apparent reaction rate constant
- k_G mass transfer coefficient, pressure units
- L height of bed
- M_M mean molecular weight of main fluid stream
- N_A mols of A transferred per unit area
- n quantity of material present at time θ
- p_{BM} log mean partial pressure of non-diffusing gas in film
- Q gas flow rate, ft.³/min.

- R radius; R0 = center; R1 = 0.566 inches; R2 = 0.980 inches; R3 = 1.27 inches; R4 = 1.45 inches; R5 = 1.10 inches; R6 = 1.43 inches.
- S negative of slope of residence-time data on semi-logarithmic coordinate
- u gas velocity, ft./sec.
- u_o superficial velocity
- u_M maximum velocity
- u_C core velocity
- u_A annular velocity
- V volume of bed, $\text{ft.}^3 = (\pi/4)D^2L$
- x distance
- ϵ fraction voids
- μ viscosity
- θ time, minutes; for residence-time studies, the time since "fresh" gas first entered bottom of bed
- θ^* time since helium valve was turned off
- ρ density, lbs./ft.^3
- ρ_B average solid concentration
- ρ_f density of fluid
- ρ_s absolute solid density

G. Literature Citations

1. Bart, R., Personal Communication (1950).
2. Bauer, W.C., "Characteristics of Fluidized Particles", Sc.D. Thesis, Chem. Eng., M.I.T., (1949).
3. Carlsmith, R.S. and Freund, G.A., "Mechanism of Solid Mixing in Batch Fluidization," S.M. Thesis, Chem. Eng., M.I.T. (1950).
4. Carman, P.C., Trans. Inst. Chem. Eng. (London), 15, Part 1, 150-156 (1937).
5. Chenault, B.R., "Solid Mixing in a Batch Fluidized Bed," S.M. Thesis, Chem. Eng., M.I.T. (1949).
6. Ciborowski, J.W., 10-90 Report, Chem. Eng., M.I.T. (1947).
7. Connors, J.A. and Fuchs, W.J., "Fine Particle-Air Mixtures under Vacuum," S.M. Thesis, Chem. Eng., M.I.T. (1944).
8. Goring, G.E., "Effect of Pressure on the Rate of Carbon Dioxide Reduction by High Temperature Coke in a Fluidized Bed," Sc.D. Thesis, Chem. Eng., M.I.T. (1949).
9. Hougen, O.A. and Watson, K.M., "Chemical Process Principles," Part III, 1005, 1006, John Wiley and Sons, Inc., New York, 1947.
10. "International Critical Tables", 1st ed., 3, 250, McGraw-Hill Book Co., Inc., New York, 1928.
11. Jahnke, E. and Emde, F., "Tables of Functions" 4th ed., 1-10, Dover Publications, New York, 1945.
12. Kennel, W.E., "A Study of Concentration Gradient in a Fluidized Powder Reactor," S.M. Thesis, Chem. Eng., M.I.T. (1947).
13. Kettenring, K.N., Manderfield, E.L., and Smith, J.M., Chem. Eng. Progress, 46, 139-145 (1950).
14. Kozeny, J., Ber. Wien Akad., 136a, 271, (1927).
15. Leva, M., Grummer, M., Weintraub, M., and Pollchik, M., Chem. Eng. Progress, 44, No. 7, 511-520 (1948).

16. Leva, M., Grummer, M., Weintraub, M., and Pollchik, M., Chem. Eng. Progress, 44, 8, 619-626 (1948).
17. Leva, M., Grummer, M., Weintraub, M., and Storch, H.H., Chem. Eng. Progress, 44, 9, 707-716 (1948).
18. Leva, M., Weintraub, M., and Grummer, M., Chem. Eng. Progress, 45, 563-572 (1949).
19. McBride, G.T., Jr., "Gasification of Carbon by Carbon Dioxide in a Fluidized Bed," Sc.D. Thesis, Chem. Eng., M.I.T. (1948).
20. Matheson, G.L., Herbst, W.A., and Holt, P.H., Ind. Eng. Chem., 41, 1099-1104 (1949).
21. Morse, R. D., Ind. Eng. Chem., 41, 1117-1124 (1949).
22. Parent, J.D., Yagol, N., and Steiner, C.S., Chem. Eng. Progress, 43, 429 (1947).
23. Paxton, R.R., "Low-Temperature Oxidation of Carbon", Sc. D. Thesis, Chem. Eng., M.I.T. (1949).
24. Perry, J. H., editor, "Chemical Engineers Handbook," 2d ed., 2079, McGraw-Hill Book Co., New York (1941).
25. Pierce, B.O., "A Short Table of Integrals" 3rd ed., Ginn and Co., Boston (1929).
26. Polack, J.A., "Radial Heat and Mass Transfer in Packed Beds," Sc. D. Thesis, Chem. Eng., M.I.T. (1948).
27. Potter, B.V., and Sleichner, C.A., "The Mixing of Gases in Fluidized Beds and Relation to Particle Size," S.M. Thesis, Chem. Eng., M.I.T. (1949).
28. Reed, W.A., "Studies in the Partial Oxidation of Methane with Metallic Oxides," Sc.D. Thesis, Chem. Eng., M.I.T. (1948)
29. Resnick, W. and White, R.R., Chem. Eng. Progress., 45, No. 6, 377-390 (1949).
30. Ryan, F.A., "The Use of X-Rays for Measuring Particle Concentration in a Fluidized Bed," S.M. Thesis, Chem. Eng., M.I.T. (1947).
31. Sherwood, T.K., and Reed, C.E., "Applied Mathematics in Chemical Engineering, 272-277, McGraw-Hill Book Co., Inc., New York (1939).

32. Sherwood, T.K. and Towle, W.L., Ind. Eng. Chem., 31, 457 (1939).
33. Sweeney, G.C., Jr., "The Effect of Velocity on Gas Mixing in a Fluidized Powder Reactor," S.M. Thesis, Chem. Eng., M.I.T. (1948).
34. Towle, W.L., "The Mixing of Gases in Turbulent Flow," Sc.D. Thesis, Chem. Eng., M.I.T. (1937).
35. Trilling, C.A., "Heat Transfer Characteristics of Beds of Fluidized Solids," Sc. D. Thesis, Chem. Eng., M.I.T. (1949).
36. Walker, S., "Flow Characteristics of Fluid-Fine Particles," S.M. Thesis, Chem. Eng., M.I.T. (1940).
37. Wilhelm, R.H. and Kwauk, M., Chem. Eng. Progress, 41, 201-218 (1948).
38. Wilson, H.A., Proc. Cambridge Phil. Soc., 12, 406 (1904).
39. Wu, P.C., "The Kinetics of the Reaction of Carbon with Carbon Dioxide," Sc.D. Thesis, Chem. Eng., M.I.T. (1949).

BIOGRAPHICAL NOTE

Edward Archibald Mason was born August 9, 1924, in Rochester, New York. While attending Monroe High School, he was a member of the Honor Work Group, which was an experiment in progressive education. In this experiment, no formal classes were held; the student was responsible for his own progress and was aided through weekly or bi-weekly discussions among the teacher and the eight or ten taking the particular course.

He attended the University of Rochester from 1942 until 1945, receiving the B.S. degree in Chemical Engineering. While there, he played intercollegiate basketball and tennis and was elected to Phi Beta Kappa and Tau Beta Pi. From 1943 to 1945, he was a member of the Naval College Training Program. Following this he served in the Pacific Area on a Navy transport.

After entering M.I.T. in June 1946, he received the S.M. degree in Chemical Engineering Practice in February, 1948. Since that time he has been engaged in the research leading to this thesis. The minor requirements were fulfilled in Business and Engineering Administration.

He has been a Research Assistant in Chemical

Engineering since August 1947, except for the period of September 1948 to June 1949 when he held a Charles A. Coffin Fellowship awarded by the General Electric Company. In addition, during the Fall term of 1949, he served as a full-time instructor in Chemical Engineering. He was elected to associate membership in Sigma Xi.

He is a junior member of the A.I.Ch.E. and a member of the A.C.S. He is co-author with Professor E. R. Gilliland of the paper "Gas and Solid Mixing in Fluidized Beds" (Ind. Eng. Chem. 41, 1191 (1949)).

He was married April 15, 1950, to Barbara Jean Earley.